Identification of host cell proteins involved in *Shigella flexneri* pathogenesis

MABEL YUEN TENG LUM, BSc (Hons)

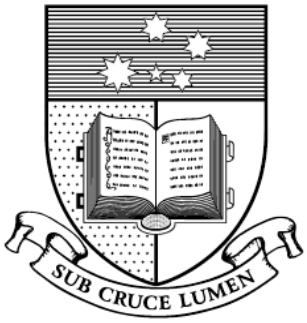

Submitted for the degree of Doctor of Philosophy

Discipline of Microbiology and Immunology,

School of Molecular and Biomedical Science, The University of Adelaide

ꕥ April 2014 ꕥ

∞ CONTENTS ∞

Abstract

Shigella flexneri is the etiological agent of bacillary dysentery (shigellosis). It is transmitted via the faecal-oral route and is a significant human pathogen due to the high morbidity among children <5 years in developing countries. The key pathogenic features of *Shigella* include cell death induction in myeloid immune cells and circumventing cell death in colonic epithelial cells, the site of bacterial infection. *Shigella* also interact with host proteins to initiate *de novo* actin synthesis to facilitate its intra- and intercellular spread to disseminate in the host.

In this thesis, the role of three host proteins: myosin IIA, dynamin II, and dynamin-related protein 1 (Drp1) during *Shigella* cell-to-cell spreading was examined. The myosin IIA specific kinase, myosin like chain kinase (MLCK), was previously shown to be important for *Shigella* plaque formation. Myosin IIA and MLCK have also been implicated in septin caging of non-motile *Shigella* which are targeted for degradation. Chemical inhibition and siRNA knockdown of myosin IIA reduced *Shigella* plaque formation. Curiously HeLa cells infected with *Shigella* mutants defective in cell-to-cell spreading have significantly reduced myosin IIA levels when quantified by immunofluorescence microscopy.

Dynamin II and Drp1 are members of the dynamin superfamily. Both proteins have self-assembly driven GTPase activation. Dynamin II is important for clathrin-mediated endocytosis and pinches the budding clathrin-coated vesicle, and Drp1 is essential for mitochondrial fission. It was hypothesized that *Shigella* protrusion formation into adjacent host cells resembles endocytic and exocytic processes, and components of these processes may facilitate *Shigella* dissemination. When dynamin II GTPase was inhibited with dynasore and dynamin II was knocked down with siRNA, *Shigella* cell-to-cell spreading was significantly reduced. The *in vivo* efficacy of dynasore was tested in a murine Sereny model. No significant reduction in inflammation was observed but mice were protected against weight loss during infection. Further experimentation suggested dynasore protected mice against cytotoxic effects from the three secretion system (TTSS) effectors expressed by *Shigella* during infection.

Drp1 was investigated in this thesis as dynasore also inhibits the GTPase of this mitochondrial fission protein. Mitochondrial fission is important in maintaining mitochondrial

dynamics and also in events downstream of intrinsic apoptosis and programmed necrosis pathways activation. Loss of mitochondrial function in *Shigella*-induced epithelial cell death has been reported previously. Hence the role of Drp1 in *Shigella* plaque formation and HeLa death was examined with the Drp1-specific inhibitor, Mdivi-1, and siRNA knockdown. HeLa cell death was significantly reduced; suggesting loss of mitochondrial function observed previously may now be attributed to Drp1 and subsequent Drp1-mediated mitochondrial fission. The impairment in *Shigella* cell-to-cell spreading in the absence of Drp1 suggests maintaining an intact mitochondrial network is essential for *Shigella* lateral spread since loss of Drp1 function would result in excessive mitochondrial fusion, leading to formation of net-like or perinuclear structures.

The outcomes of this thesis highlight the importance of host proteins during different stages of *Shigella* infection. By improving our understanding on the host and bacteria interaction, future work on novel approaches to prevent *Shigella* dissemination can be developed.

Declaration

I certify that this work contains no material which has been accepted for the award of any other degree or diploma in my name, in any university or other tertiary institution and, to the best of my knowledge and belief, contains no material previously published or written by another person, except where due reference has been made in the text. In addition, I certify that no part of this work will, in the future, be used in a submission in my name, for any other degree or diploma in any university or other tertiary institution without the prior approval of the University of Adelaide and where applicable, any partner institution responsible for the joint-award of this degree.

I give consent to this copy of my thesis when deposited in the University Library, being made available for loan and photocopying, subject to the provisions of the Copyright Act 1968.

The author acknowledges that copyright of published works contained within this thesis resides with the copyright holder(s) of those works.

I also give permission for the digital version of my thesis to be made available on the web, via the University's digital research repository, the Library Search and also through web search engines, unless permission has been granted by the University to restrict access for a period of time.

Adelaide, Australia, April 2014

_____

Mabel Yuen Teng Lum

Publications

Lum M, Attridge SR & Morona R (2013). Impact of dynasore an inhibitor of dynamin II on *Shigella flexneri* Infection. *PLoS One* 8, e84975.

Lum M & Morona R (2014). Dynamin-related protein Drp1 and mitochondria are important for *Shigella flexneri* infection. *Int J Med Microbiol* 304, 530-541.

Lum M & Morona R (2014). Myosin IIA is essential for *Shigella flexneri* cell-to-cell spread. *Pathog Dis*, DOI: 10.1111/2049-632X.12202.

Acknowledgements

First and foremost, I would like to thank the Australian Government for my scholarship.

I would like to thank my supervisor A/Prof Renato Morona for what has been a challenging project. Thank you for all the support and guidance over the past few years. I would also like to thank Luisa Van Den Bosch for the preliminary experiments and for imparting all her TC skills. I am grateful to Dr Stephen Attridge who was instrumental in setting up the animal model. I have enjoyed working with you. I would also like to thank members of the Morona laboratory for proof reading bits of my thesis, helpful suggestions, assistance with experiments, kind words of encouragement and putting up with my whinging.

Thank you to all my friends in the MLS building: Min, Pratiti, Donald, Rethish, Zarina, Alex, and Long, for always lending an ear. Also a big thank you to Donald, Min and Pratiti for the yummy cakes, desserts, snacks, dinner dates and shopping sprees. A shout-out to Paul who is my partner in crime in annoying Pratiti. To all my friends outside the lab, thank you all for your unwavering moral support. To my boss (and old friend) at AGRF, thank you for keeping me employed for so many years and for your many funny stories and words of encouragement when I needed them.

I would also like to thank my family who is very supportive in spite of not knowing what I actually do. To my sister in Adelaide, her husband and lovely children, thank you for always lending a hand and for silly times. A special thank you goes to my partner who is always there when I needed him. I look forward to a fun and exciting journey ahead with you!

Lastly I would like to dedicate this thesis to my late German teacher. I miss your passion for life and for learning. Thank you for always reminding me not to give up and that I can do better.

Abbreviations

~	approximately
aa	amino acids
ABM	actin-based motility
ADP	adenosine diphosphate
AJ(s)	adherens junction(s)
APC(s)	apical junctional complex(es)
ATP	adenosine triphosphate
ATPase	adenosine triphosphatase
BDM	2,3-butanedione monoxime
BSE	bundle signalling element
CFU	colony forming units
D0 / D1 / D2 / D3	day 0 / day 1 / day 2 / day 3
DCCR	DharmaFECT Cell Culture Reagent
DLP(s)	dynamin-like protein(s)
DLP1	dynamin-like protein 1 (alternate name for DNM1L/Drp1)
DNM1L	dynamin-1-like protein (alternate name for DLP1/Drp1)
DNM2	dynamin II gene
DMSO	dimethyl sulfoxide
Drp1	dynamin-related protein 1 (alternate name for DLP1/DNM1L)
GAPDH	glyceraldehyde 3-phosphate dehydrogenase
GED	GTPase effector domain
GTP	guanosine triphosphate
GTPase(s)	guanosine triphosphatase(s)
h	hour(s)
IF	immunofluorescence
IP	intraperitoneal
kDa	kilodaltons
LDH	lactate dehydrogenase
Lo	low myosin IIA protein levels
LPS	lipopolysaccharide

MEFs	mouse embryonic fibroblasts
Mdivi-1	*m*itochondrial *div*ision *i*nhibitor-*1*
MYH9	myosin, heavy chain 9, non-muscle gene (myosin IIA heavy chain gene)
min	minute(s)
MLCK	myosin light chain kinase
moi	multiplicity of infection
MOMP	mitochondrial outer membrane permeabilisation
myosin IIA / B / C	non-muscle myosin IIA / B / C
N-WASP	Neural Wiskott-Aldrich syndrome protein
NF-κB	nuclear factor-κB
NMP	*N*-methyl-2-pyrrolidone
NPF(s)	nucleation promoting factor(s)
OM	outer membrane
PEG / PEG300	polyethylene glycol 300
PGN	peptidoglycan
PH	pleckstrin homology
PMN(s)	polymorphonuclear cell(s)
PRD(s)	proline-rich domain(s)
PtK2	*Potorous tridactylis* kidney epithelial (cells)
R-LPS	rough LPS
ROS	reactive oxygen species
S-LPS	smooth LPS
siRNA	small interfering RNA
STS	staurosporine
t	time
TJ(s)	tight junction(s)
TTSS	type three secretion system
VP	virulence plasmid
VP^{-} / VP-	virulence plasmid-cured
WT	wild type

ꕥ Chapter 1 ꕥ

Introduction

Chapter 1: Introduction

1.1 *Shigella*

Shigella flexneri is the etiological agent of bacillary dysentery (shigellosis). It is transmitted via the faecal-oral route and is a significant human pathogen due to the high morbidity among children under the age of 5 years in developing countries. Over a period between 1990 - 2009, 125 million cases of shigellosis were recorded in Asia, of which ~14,000 were fatal (Bardhan *et al.*, 2010). The lack of a vaccine, an increase in multi-drug resistance and the absence of suitable small animal model to study the infection contribute to the persistence of shigellosis (Barry *et al.*, 2013). The four members in the *Shigell*a genus are *Shigella flexneri*, *Shigella boydii*, *Shigella sonnei* and *Shigella dysenteriae*. Each species is subdivided according to variations in the chemical structure of the O-antigen component of their lipopolysaccharide (LPS) (Simmons, 1993). The majority of *Shigella* deaths are attributed to the nineteen different serotypes of the *S. flexneri* species (Foster *et al.*, 2011; Levine *et al.*, 2007; Sun *et al.*, 2013). The most predominant serotype in developing countries are 1b, 2a, 3a, 4a and 6, whilst the most commonly isolated serotype in industrialised countries is 2a (Jennison & Verma, 2004; Levine *et al.*, 2007). *S. flexneri* serotype 2a is commonly studied and used in basic research (Jennison & Verma, 2004; Niyogi, 2005), and forms the basis of the work in this thesis.

The *S. flexneri* serotype 2a strain 2457T genome has been completely sequenced (Wei *et al.*, 2003). Comparative genomic analysis has shown that sequence divergence between *S. flexneri* and *Escherichia coli* (*E. coli*) K-12 is roughly 1.5% and hence *Shigella* is in fact a species of *E. coli* (Lan & Reeves, 2002). Key events during the convergent evolution of *Shigella* include acquisition of a large 200 kb virulence plasmid (VP), pathogenicity islands, and genes essential for modifying the LPS O-antigens, which accounts for the large variety in LPS serotypes (Buchrieser *et al.*, 2000; Ingersoll *et al.*, 2002; Jin *et al.*, 2002; Pupo *et al.*, 2000). Loss of catabolic genes, flagella and fimbriae also occurred, presumably to facilitate *Shigella* adaptation to an intracellular lifestyle (Al Mamun *et al.*, 1996; Ito *et al.*, 1991; Tominaga *et al.*, 2005; Yang *et al.*, 2005). In the absence of flagellar motility, *Shigella*

intracellular movement and cell-to-cell spread are facilitated by actin-based motility (ABM), which exploits host factors.

1.2 Pathogenesis

1.2.1 Overview

The key pathogenic features of *Shigella* infection include establishing an intracellular lifestyle as a means to evade immune activation, and exploitation of host factors to mediate lateral spreading. In the process, highly inflammatory conditions are provoked resulting in massive tissue destruction (Schroeder & Hilbi, 2008). Although the loss of tissue integrity is damaging, it allows the host to remove *Shigella*-infected cells. Unsurprisingly shigellae are able to counter such efforts by manipulating host signalling pathways to maintain a replicative niche (Ashida *et al.*, 2011b). The main features of *Shigella* pathogenesis are discussed below with emphasis on cell death induction and cell-to-cell spreading, which are explored in this thesis.

1.2.2 Initial stages of infection

Shigella are transmitted via the faecal-oral route through contaminated food and water. An infectious dose of 10 - 100 organisms is sufficient to establish symptomatic disease in humans due in part to *Shigella*'s resistance to stomach acid (DuPont *et al.*, 1989; Waterman & Small, 1996). In the jejunum, the action of the *S. flexneri* 2a Enterotoxins 1 and 2 (ShET1 and ShET2) leads to watery diarrhoea with loss of solutes (Fasano *et al.*, 1997; Nataro *et al.*, 1995). Shigellae then enter the colon, where the invasive phase of shigellosis takes place (Figure 1.1). At the colon, *Shigella* triggers its uptake into microfold (M) cells in the Peyer's patches and exploit the antigen sampling role of the M cells to achieve transcytosis (Figure 1.1A) (Man *et al.*, 2004; Sansonetti *et al.*, 1996; Wassef *et al.*, 1989). After shigellae are released into the underlying lymphoid follicles, the bacteria are engulfed by resident macrophages.

1.2.3 Induction of macrophage cell death

Shigellae evade macrophage immune surveillance by inducing macrophage cell death (Figure 1.1B). In early experiments, macrophage cell death subroutines observed during *Shigella*

infection included apoptosis and oncosis. These observations were based largely on microscopic observations (Nonaka *et al.*, 1999; Zychlinsky *et al.*, 1992; Zychlinsky *et al.*, 1996). However, it is now evident that cell death subroutines need to be characterised with biochemical and genetic studies, and not based on gross morphology alone (Galluzzi *et al.*, 2012). Collectively studies have shown that *Shigella* induce macrophage pyroptosis, which is mediated by IpaB, a type three secretion system (TTSS) effector encoded on the *Shigella* VP (Hilbi *et al.*, 1998; Senerovic *et al.*, 2012; Zychlinsky *et al.*, 1994). After oligomerising spontaneously, IpaB inserts into the macrophage plasma membrane. The internalised IpaB ion channels disrupt ion homeostasis within endosomal compartments (Senerovic *et al.*, 2012). The resulting endolysosomal leakage is followed by ICE protease-activating factor-dependent (IPAF/NLRC4) and apoptosis-associated speck-like protein containing caspase recruitment domain (ASC) inflammasome activation, and subsequent caspase-1-dependent processing of interleukin-1β (IL-1β) and interleukin-18 (IL-18), rapid plasma membrane rupture and nuclear condensation (Bergsbaken *et al.*, 2009; Fernandez-Prada *et al.*, 1997; Senerovic *et al.*, 2012; Suzuki *et al.*, 2007). IL-1β results in strong inflammatory responses and IL-18 magnifies innate immune responses (Sansonetti *et al.*, 2000). Consequently macrophage pyroptosis results in significant inflammation (Bergsbaken *et al.*, 2009).

Shigella also induces NLRP3 and ASC inflammasome dependent necrosis-like cell death in macrophages in a process termed pyronecrosis (Koterski *et al.*, 2005; Willingham *et al.*, 2007). Pyronecrosis is independent of caspase-1 and IL-1β but releases another proinflammatory factor, high-mobility group box 1 protein (HMGB1) (Willingham *et al.*, 2007). Macrophage cell death mediated by a lipid A-dependent (but caspase-1 and NLRC4 independent) pathway has also been reported (Suzuki *et al.*, 2005). The varied cell death subroutines reported may arise from the different experimental conditions used, such as the different cell types used, experimental conditions and different methods used to measure cell death. Nonetheless, it is evident macrophage cell death results in highly inflammatory conditions.

1.2.4 Enterocyte invasion and cell-to-cell spreading

Death of infected macrophages allows *Shigella* to escape into the submucosal tissue (Figure 1.1B). At the basolateral surface Shigallae gain access into the epithelial cells by injecting

various effector proteins, such as IpaA, IpaB, IpaC, IpgB1, IpgD and VirA via the TTSS Mxi/Spa. These effectors induce local reorganisation of actin and microtubulin cytoskeletal networks, dissociate the actin cytoskeleton from the plasma membrane and disrupt adhesion between cellular actin and the extracellular matrix (Schroeder & Hilbi, 2008). The resulting membrane ruffling engulfs the bacteria into a micropinocytic pocket and the bacterium is internalised (Figure 1.1C). *Shigella* disrupts the endocytic vacuole by releasing IpaB, IpaC and IpaD, escapes into the cytoplasm, and multiples (Figure 1.1D) (Bârzu *et al.*, 1997; High *et al.*, 1992; Picking *et al.*, 2005; Sansonetti *et al.*, 1986).

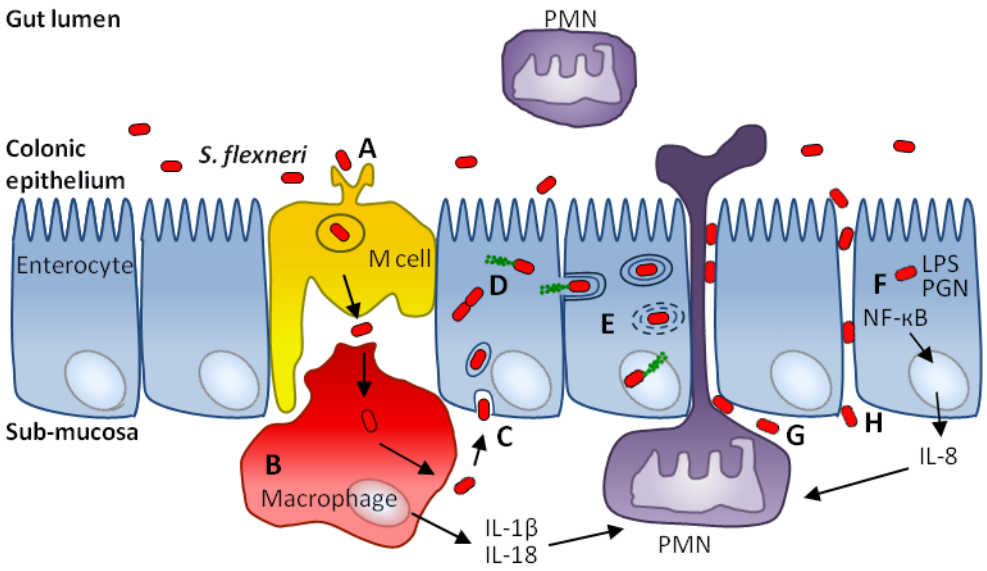

Figure 1.1 *Shigella flexneri* pathogenesis.

(A) Ingested *S. flexneri* reach the colon and exploit M cells to traverse the epithelial barrier. (B)Bacteria are transcytosed to the underlying lymphoid follicles and phagocytosed by resident macrophage. Shigellae induce macrophage pyroptosis and are released into the sub-mucosa. (C) Shigellae invade the apical surface of the enterocytes by triggering endocytosis. (D) Internalised bacteria escape the endocytic vacuole, replicate and initiate IcsA-dependent actin-based motility in the cytoplasm. (E) Motile bacteria form protrusions which are taken up by adjacent enterocytes. Escape from the double membrane vacuole allows *Shigella* to initiate a new cycle of replication, motility and cell-to-cell spread. (F) *Shigella* LPS and peptidoglycan (PGN) activate the host signalling pathways leading to NF-κB activation and promote the release of pro-inflammatory IL-8. The strong inflammation induced by shigellae in the sub-mucosa attracts and promotes migration of polymorphonuclear cells (PMNs) across the epithelium. (G) Migrating PMNs disrupts the integrity of the colonic epithelium, thus providing an additional pathway for bacterial entry into the sub-mucosa. (H) Additionally *S. flexneri* interferes with tight junctions to gain access into the sub-mucosa.

In the host cytosol, the *Shigella* IcsA (VirG) protein interacts with host proteins to initiate polymerisation of monomeric G-actin into filamentous F-actin in a process known as ABM. The polymerised F-actin, also known as actin tail or comet tail, generates a unidirectional force which propels the bacteria throughout the cytosol (Figure 1.1D) (Bernardini *et al.*, 1989; Goldberg, 2001; Lett *et al.*, 1989; Suzuki *et al.*, 1996; Suzuki *et al.*, 1998; Suzuki *et al.*, 2002). Shigellae are also propelled against the host plasma membrane, forming bacteria-containing protrusions that extend into the neighbouring enterocyte. In the adjacent cell, the protrusions are internalised and contained in a double membrane vacuole (Figure 1.1E) (Kadurugamuwa *et al.*, 1991; Prévost *et al.*, 1992). Lysis of the vacuole requires TTSS proteins: IpaB, IpaC, and IpaD (Schuch *et al.*, 1999). After escaping from the vacuole, *Shigella* is release into the cytoplasm, where it initiates replication, intra- and intercellular spreading (Figure 1.1E). The ability to mediate cell-to-cell spread is a key feature of shigellosis as it facilitates *Shigella* dissemination into uninfected enterocytes. The establishment on an intracellular lifestyle presumably shields the bacteria from immune detection. However the presence of the bacteria is also recognised by host proteins which upregulate signalling pathways to remove the infected cell (Ashida *et al.*, 2011b).

1.2.5 Innate immune responses

Invasion of the epithelial cells results in activation of host signalling pathways via the pro-inflammatory bacterial outer membrane (OM) components, through recognition by the host nucleotide-binding oligomerisation domain-containing protein 1 (Nod1, a peptidoglycan [PGN] sensor), which in turn activates the host nuclear factor-κB (NF-κB, PGN sensor) to upregulate production and release of IL-8 chemokine (Figure 1.1F) (Girardin *et al.*, 2003; Pedron *et al.*, 2003; Philpott *et al.*, 2000; Sansonetti *et al.*, 1999). IL-8 is a chemoattractant, which recruits polymorphonuclear cells (PMNs) to the site of infection (Singer & Sansonetti, 2004). Infiltration of PMNs disrupts the tight junctions (TJs) between the epithelial cells, destabilises the epithelium and creates a paracellular pathway for *Shigella* to gain access to the basolateral surface of the enterocytes (Figure 1.1G) (Perdomo *et al.*, 1994). Shigellae can also weaken the sealing of the epithelial cell TJs by altering TJ protein composition, thus providing an additional entry point to the basolateral surface (Figure 1.1G - H) (Sakaguchi *et al.*, 2002). The severe tissue damage resulting from the *Shigella* infection impairs adsorption

of water, nutrients, and solutes, which might account for the watery diarrhoea as well as the blood and mucus in stools typical of shigellosis.

Inflammatory conditions are initially required to facilitate bacterial entry into the basolateral surface, however shigellae are able to modulate immune responses post-invasion through the activities of TTSS effectors to dampen immune responses (Ashida *et al.*, 2011b; Carayol & Tran Van Nhieu, 2013). For instance, OspF, OspG, OspI, OspZ, IpaH, IpaH0722 and IpaH9.8 have been reported to counteract NF-κB activation. Δ*ospF*, Δ*ospG*, Δ*ipaH*, Δ*ipaH0722* and Δ*ipaH9.8* mutants also induce more severe inflammation in animal models compared to wild type (WT) *Shigella* (Arbibe *et al.*, 2007; Ashida *et al.*, 2007; Ashida *et al.*, 2010; Ashida *et al.*, 2013; Kim *et al.*, 2005; Okuda *et al.*, 2005; Sanada *et al.*, 2012; Zhang *et al.*, 2012).

IcsA-dependent ABM is central to *Shigella* pathogenesis as it facilitates motility and lateral spreading throughout the epithelial layer. Furthermore *Shigella* dissemination provokes highly inflammatory host responses leading to tissue destruction, typical of shigellosis. *Shigella* Δ*icsA* (Δ*virG*) mutants are highly attenuated in humans and animal models of shigellosis (Kotloff *et al.*, 1996; Kotloff *et al.*, 2002; Lett *et al.*, 1989; Lum *et al.*, 2013; Makino *et al.*, 1986; Sansonetti *et al.*, 1991).

1.2.6 Delay in epithelial cell death

Contrary to the resident macrophages, which are the first line of defence against *Shigella* bacteria, enterocytes are important as a replicative niche for *Shigella*. Eliminating infected enterocytes will prevent *Shigella* from propagating, and prevent further lateral spreading into uninfected cells (Ashida *et al.*, 2011a). To counter such efforts, *Shigella* are able to circumvent both apoptotic and necrotic cell death pathways. Apoptosis is a non-inflammatory programmed cell death which is activated by mitochondria and death receptor-mediated pathways characterised by caspase activation, DNA fragmentation, cell shrinkage, membrane blebbing and mitochondrial permeability (Lamkanfi & Dixit, 2010), whereas necrosis is characterised by nuclear swelling, membrane rupture and spillage of cellular contents into the environment resulting in inflammatory conditions. Other hallmarks of necrosis include the absence of caspase activation, reactive oxygen species (ROS) production, lysosomal

destabilisation, calpain release and ATP depletion (Golstein & Kroemer, 2007; Vandenabeele *et al.*, 2010).

It was initially observed that HeLa cells infected with *S. flexneri* strain M90T did not undergo cell death in spite of high bacterial loads in the cytosol (Mantis *et al.*, 1996). Furthermore no hallmarks of apoptosis or damage to the plasma membrane as measured with lactate dehydrogenase (LDH) release were observed 4 h post-invasion, suggesting HeLa cell death is either not activated or is suppressed (Mantis *et al.*, 1996). In latter studies, Spa15, a TTSS chaperone, which associates with MxiE, a TTSS transcriptional activator, was shown to inhibit apoptosis induced chemically by staurosporine (STS) by preventing caspase-3 activation (Clark & Maurelli, 2007; Faherty & Maurelli, 2009). IpaB incubation with HeLa cells also induced apoptosis, although the exact mechanism is not known (Senerovic *et al.*, 2012). In an *ex vivo* epithelial colonic cell model and in HeLa cells, *Shigella* infection triggered apoptosis via caspase-9 and caspase-3 activation (Lembo-Fazio *et al.*, 2011). Furthermore *gadd45a* (stress sensor growth arrest and DNA damage 45a), a stress-inducible gene, was also upregulated both *in vitro* and *ex vivo* (Lembo-Fazio *et al.*, 2011).

In other studies, *Shigella* infection in HeLa cells has been shown to induce an early genotoxic stress (Bergounioux *et al.*, 2012). The tumour suppressor protein, p53, an inducer of apoptosis, is normally stabilised during genotoxic response. However p53 is rapidly degraded by calpain, through degradation of the calpain protease inhibitor, calpastatin, by the *Shigella* VirA TTSS effector (Bergounioux *et al.*, 2012). Calpain activation inadvertently activates the necrosis pathway which restricts *Shigella* intracellular growth (Bergounioux *et al.*, 2012). In the colonic HCT116 cells, the slow degradation of p53 shifts the executing pathway from necrosis to apoptosis (Bergounioux *et al.*, 2012). In HaCat (immortalised keratinocytes) cells, the *Shigella* TTSS effector, OspC3, targets the p19 subunit of Caspase-4 to delay necrotic cell death (Kobayashi *et al.*, 2013). *In vivo* the Δ*ospC3* mutant exacerbates colonic inflammation in guinea pigs (Kobayashi *et al.*, 2013). In HeLa cells and mouse embryonic fibroblasts (MEFs), the pro-survival Nod1/NF-κB/Bcl-2 signalling pathway is activated to counteract the necrotic pathway mediated by Bnip3, a regulator of mitochondrial permeability transition during *Shigella* infection (Carneiro *et al.*, 2009).

Hence shigellae infection in epithelial cells can induce both apoptotic and necrotic cell death. Similar to macrophage cell death, various factors contribute to the different cell death

subroutines observed including specific epithelial cell type, and different experimental set ups such as the initial bacterial load and time of infection used. Regardless of the specific cell death pathways observed, it is evident *Shigella* bacteria are able to manipulate host signalling pathways to prolong epithelial cell survival. Some studies also point to the role of TTSS effectors during this process, thus extending the role of TTSS proteins during *Shigella* infection.

1.3 *Shigella* IcsA protein

1.3.1 Identification

Shigella intracellular movement and protrusion formation was initially observed microscopically within HeLa S3 and Henle epithelial monolayers (Ogawa *et al.*, 1968). Although the mechanism behind ABM was unknown at that time, it was observed that shigellae movement was initiated at a single pole and also at the pole from which new daughter cells emerged (Ogawa *et al.*, 1968). The genetic basis for *Shigella* motility was uncovered during transposon mutagenesis of the VP. Tn*5* insertions within an *Eco*RI - *Sal*I fragment, termed *virG* (*vir*ulence gene *G*), abolished cell-to-cell spreading *in vitro* and the mutants were also avirulent in the Sereny test (Makino *et al.*, 1986). The coding region of the 1,102 amino acids (aa) VirG protein was determined and the protein was shown to be surface exposed (Lett *et al.*, 1989). Concurrently Bernardini *et al.* (1989) identified the VirG protein as IcsA (*i*ntra- and inter*c*ellular *s*pread gene *A*) and reported for the first time that IcsA-mediated motility is dependent on polymerised host F-actin at one pole of the bacteria. Bernardini *et al.* (1989) also showed that *Shigella* motility is independent of myosin motors. In fact *Shigella* motility is based on actin treadmilling, which is discussed further in Section 1.4.1.

S. flexneri ABM has been studied in different model systems such as microscopy of infected tissue culture monolayers, *in vitro Xenopus* cell extracts and protein reconstitution systems (Egile *et al.*, 1999; Goldberg & Theriot, 1995; Loisel *et al.*, 1999). The ability to mediate ABM and subsequent cell-to-cell spread is a key feature of *Shigella* virulence. *Shigella* cell-to-cell spread can be measured using an *in vitro* plaque formation assay which detects and measures the area of dead cells after *S. flexneri* invasion of tissue culture

monolayers (Oaks *et al.*, 1985). Similarly the infectious focus assay is used to measure the area of bacterial spreading in confluent tissue culture monolayers following *Shigella* infection via immunofluorescence (IF) microscopy (Sansonetti *et al.*, 1994). The ability of *Shigella* strains to mediate ABM and intercellular spreading can be determined *in vivo* with the Sereny test, which evaluates the development of keratoconjunctivitis following *Shigella* infection of either guinea pig or mouse eyes (Murayama *et al.*, 1986; Sereny, 1957). Given that IcsA-mediated ABM is essential for *Shigella* cell-to-cell spread, these assays give indirect measures of IcsA and ABM efficiency. IcsA expression is essential and mutants lacking IcsA are non-motile. (Goldberg & Theriot, 1995). Heterologous expression of IcsA in closely related *E. coli* K-12 confers the ability to polymerise actin and exhibit ABM *in vitro* (Goldberg & Theriot, 1995; Kocks *et al.*, 1995).

1.3.2 Structural organisation

IcsA is a typical autotransporter and is composed of three distinct regions: an N-terminal signal sequence (aa 1 - 52), a central effector domain or α domain (aa 53 - 758), and a C-terminal translocation domain or β domain (aa 759 - 1102) (Suzuki *et al.*, 1995). The translocation of the IcsA polypeptide from the cytoplasm to the periplasm is directed by its unusually long signal sequence via the Sec pathway (Brandon *et al.*, 2003). In the periplasm, an intramolecular disulphide bridge is formed in the IcsA α domain (Brandon & Goldberg, 2001). The 80 kDa α domain is exported to the extracellular milieu when the 37 kDa β domain inserts itself into the OM via the BAM (β-barrel assembly machinery) complex (Jain & Goldberg, 2007; Suzuki *et al.*, 1995).

1.3.3 Polar localisation

IcsA is delivered predominantly to the old pole of the daughter cells whilst *S. flexneri* is still undergoing cell division and occurs in the cytoplasm prior to secretion across the cytoplasm (Brandon *et al.*, 2003; Charles *et al.*, 2001; Goldberg, 1994; Robbins *et al.*, 2001). Two IcsA polar determining regions ($IcsA_{1-104}$ and $IcsA_{506-620}$) in the α domain have been identified. Fusion of either region to GFP (green fluorescent protein) resulted in fluorescent detection at the polar regions of *S. flexneri* and *E. coli*. (Charles *et al.*, 2001). Insertion mutation studies at aa 532 and 563 of the IcsA α domain affected IcsA polar localisation, further supporting the role of the polar targeting region, $IcsA_{506-620}$ (May & Morona, 2008).

Recently YidC, a cytoplasmic membrane protein insertion chaperone, was shown to assist IcsA positioning at the cell pole within the *Shigella* cytoplasm independent of cell septation and cytokinesis proteins such as FtsQ (Gray *et al.*, 2014). This finding is consistent with the presently established notion that the information necessary for IcsA polar targeting is located in the bacterial cytoplasm or in the inner face of the cytoplasmic membrane. FtsQ, an essential protein for bacterial division, also facilitates IcsA targeting to the pole (Fixen *et al.*, 2012). Although FtsQ is a bitopic protein, its periplasmic domain alone was sufficient to direct IcsA polar targeting, suggesting for the first time that IcsA polarity can also be driven in other cellular compartments besides the cytoplasm (Fixen *et al.*, 2012). Expression of the normally polar *Bordetella pertussis* BrkA autotransporter in a VP-cured *S. flexneri* strain also resulted in BrkA polar localisation (Fixen *et al.*, 2012). Other than its role to recruit other divisional protein (FtsB and FtsL) during cytokinesis, the periplasmic domain of FtsQ has been speculated to remodel the PGN which occurs in conjunction with cell division, which may contribute to the establishment of autotransporter polarity (Fixen *et al.*, 2012).

The *Shigella* IcsP (SopA) protease cleaves IcsA at aa 758 and 759, releasing a ~95 kDa IcsA α domain into the culture supernatant (d'Hauteville *et al.*, 1996; Egile *et al.*, 1997; Fukuda *et al.*, 1995; Shere *et al.*, 1997; Steinhauer *et al.*, 1999). Recent data from our laboratory show that IcsP concentration is greater at the new daughter poles compared to the old poles, which may explain how IcsP contributes to the unipolar surface localisation of IcsA at the old poles (Tran *et al.*, 2013). To date, evidence to support IcsP's role in IcsA polar localisation and subsequent ABM is not convincing due to conflicting results arising from different cell lines and bacterial strains used in different studies (Egile *et al.*, 1997; Shere *et al.*, 1997). Unpublished data from our laboratory suggest Δ*icsP* mutants formed larger plaques (Tran, 2007) and are more virulent in a murine Sereny test.

Previously the *S. flexneri* VP-encoded ATP-diphosphohydrolase (apyrase, *phoN2*) was implicated in intercellular spreading and the Δ*phoN2* mutant was reported to have lost IcsA unipolarity (Santapaola *et al.*, 2006). The periplasmic apyrase enzyme depletes host ATP following invasion, a characteristic metabolic event following *S. flexneri* infection (Santapaola *et al.*, 2006). Apyrase is targeted to the *Shigella* old pole, however no direct interaction between apyrase and IcsA was observed (Santapaola *et al.*, 2006; Scribano *et al.*, 2014). Recent data suggest apyrase interacts with the periplasmic domain of OmpA, an OM

protein when it is in its 8-stranded β-barrel confirmation, whereby its pore is small and its large C-terminal domain is exposed into the periplasm (Scribano *et al.*, 2014). This confirmation represents a remarkably stable folding intermediate (Khalid *et al.*, 2008; Smith *et al.*, 2007; Zakharian & Reusch, 2005). Apyrase binding to the periplasmic domain of OmpA may act to stabilise OmpA in its folding intermediate and together with the shorter length LPS (short type O-antigen - Section 1.3.4) facilitate IcsA polar localisation (Scribano *et al.*, 2014). A possible role for OmpA in IcsA polarity and subsequent *Shigella* cell-to-cell spreading has been reported previously (Section 1.5.1) (Ambrosi *et al.*, 2012).

1.3.4 IcsA and LPS interaction

1.3.4.1 *S. flexneri* LPS

The OM of Gram-negative bacteria is an asymmetric bilayer containing mainly LPS in the outer leaflet (Kamio & Nikaido, 1976; Muhlradt & Golecki, 1975). LPS is composed of lipid A, core sugars and O-antigen polysaccharides (Nikaido, 2003). Complete LPS molecules are referred to as smooth LPS (S-LPS), while LPS molecules lacking O-antigens are referred to as rough LPS (R-LPS) (Figure 1.2). The lipid A component is anchored in the OM and the core sugar is assembled on the lipid A. O-antigen polysaccharide polymers of variable length is then attached to the core sugar unit. The O-antigen chain length is dependent on the Wzz polysaccharide co-polymerase family of proteins (Morona *et al.*, 2009). In *S. flexneri* 2a, the chromosomally encoded Wzz_{SF} regulates the polymerisation of short (S) type (12 - 17 O-antigen repeat units) LPS and the plasmid-borne Wzz_{pHS-2} mediates the polymerisation of very long (VL) type (>90 O-antigen repeat units) LPS (Hong & Payne, 1997; Morona *et al.*, 1995).

Expression of the VL-type O-antigen confers serum resistance, while the S-type O-antigen contributes to *Shigella* virulence by unmasking IcsA at the old cell pole (Hong & Payne, 1997; Morona *et al.*, 2003; Van Den Bosch *et al.*, 1997). The lipid A component of LPS is endotoxic (Ranallo *et al.*, 2012). A recent study has shown that during proliferation within epithelial cells, *Shigella* reduces the number of acyl chains (hypoacylated) within the lipid A component. Hypoacylated lipid A is less efficient at priming neutrophils (PMNs), thus reducing reactive oxygen species (ROS) production (Paciello *et al.*, 2013).

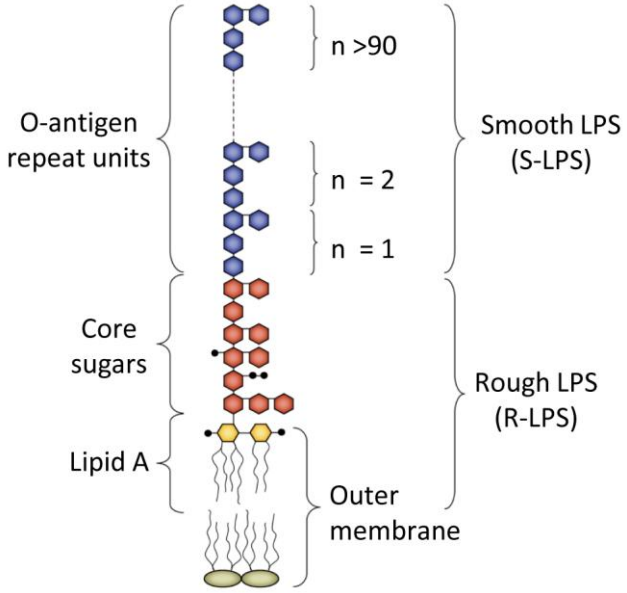

Figure 1.2 Structure of lipopolysaccharide (LPS).

LPS is composed of lipid A, core sugars, and O-antigen repeat units. The lipid A component is anchored in the OM and the core sugar is assembles on the lipid A. The O-antigen polysaccharide polymer of variable length is attached to the core sugar unit. Smooth LPS (S-LPS) has all three components and rough LPS (R-LPS) lacks the O-antigen units. Figure adapted from Grabowicz (2010), with permission from the author.

1.3.4.2 Role of LPS in IcsA polar localisation

The requirement for S-LPS during IcsA-dependent ABM and cell-to-cell spreading has been demonstrated through mutagenesis studies on genes involved in the LPS biogenesis pathway (*galU, rfe, rfb, rmlD, wecA* and *wzy*) (Hong & Payne, 1997; Okada *et al.*, 1991; Rajakumar *et al.*, 1994; Sandlin *et al.*, 1995; Sandlin *et al.*, 1996; Van Den Bosch *et al.*, 1997; Van Den Bosch & Morona, 2003). IcsA surface presentation at the *Shigella* and *E. coli* surface is unipolar in S-LPS strains. In R-LPS strains IcsA is detected on both the lateral and polar regions of the bacteria (Robbins *et al.*, 2001; Van Den Bosch *et al.*, 1997). It has been proposed that mutations in the LPS of the rough strains can alter the biophysical properties of the OM, such that the barrier to diffusion is reduced. This in turn increases IcsA migration from the pole to the lateral surface (Robbins *et al.*, 2001). Other studies have demonstrated that the LPS O-antigens function to mask IcsA expression at the lateral regions, thus reinforcing IcsA polar presentation (Morona *et al.*, 2003; Morona & Van Den Bosch, 2003).

Although loss of IcsA polarity is generally linked to impaired ABM and subsequent intercellular spreading, over-expression of non-cleavable IcsA in a S-LPS strain displayed IcsA localisation at the pole and on the lateral surface similar to R-LPS strains, but no impairment to ABM and cell-to-cell spread was observed (Van Den Bosch & Morona, 2003). Hence LPS O-antigens may have other undetermined roles in IcsA function.

1.4 Actin-based motility (ABM)

Shigella intracellular motility and cell-to-cell spread is a key feature allowing the bacteria to spread laterally to further its dissemination (Sansonetti *et al.*, 1994). ABM motility however is not unique to *Shigella*. Other pathogens such as *Listeria monocytogenes*, *Burkholderia pseudomallei*, *Mycobacterium marinum*, *Rickettsia spp.*, baculoviruses and vaccinia virus also exhibit ABM (Goldberg, 2001; Haglund & Welch, 2011; Welch & Way, 2013). *Listeria* is commonly used as a model system to study actin-based movements (Cossart & Toledo-Arana, 2008) and hence was included in some of the work carried out in this thesis. The major features of *Shigella* and *Listeria* ABM will be discussed below.

1.4.1 Actin treadmilling

Actin is the most abundant protein in the eukaryotic cell and exists either as monomeric globular G-actin or filamentous F-actin. It has a deep cleft which carries either an adenosine triphosphate (ATP) or adenosine diphosphate (ADP) and a Mg^{2+} ion (Pantaloni *et al.*, 2001; Qualmann & Kessels, 2002). Polymerised actin is essential for cellular functions as it allows the cell to respond to external stimuli by modulating the cell shape, extend protrusions or to engulf particles (Pantaloni *et al.*, 2001).

F-actin formation is initialised by the slow nucleation of a monomer, dimer and trimer; however further monomer addition stabilises the complex resulting in a rapid filament formation. ATP hydrolysis to ADP results in a conformational change of a tightly bound ADP product. ADP-bound actin has reduced affinity for the filament ends compared to ATP-bound actin. Furthermore monomer addition is greater at the barbed end, but is slower at the pointed end; thus contributing to F-actin polarity (Nicholson-Dykstra *et al.*, 2005; Qualmann & Kessels, 2002). In a steady state the rate of subunit addition at the barbed end is identical to the rate of depolymerisation at the pointed end, resulting in a net flow of monomers from one

end to the other in a process referred to as treadmilling (Qualmann & Kessels, 2002). Processes based on actin treadmilling such as lamellipodia formation and bacterial ABM are independent of myosin. The barbed end of the actin/comet tail is pushing the bacterium forward at the pole during ABM (Gouin *et al.*, 1999; Tilney & Portnoy, 1989; Tilney *et al.*, 1992) and in lamellipodia the barbed end is associated with the plasma membrane (Wang, 1985).

Exploitation of host actin cytoskeleton requires pathogens to express proteins which can either interact with actin, or mimic regulators that mediate or regulate actin polymerisation (Welch & Way, 2013). One of these protein classes is the actin-related protein-2/3 (Arp2/3) complex and its activators, the nucleation promoting factors (NPFs).

1.4.2 Arp2/3 complex

The Arp2/3 complex is a seven-subunit protein complex made up of Arp2, Arp3 and the remaining five subunits are actin-related protein complex-1 to -5 (ARPC1 - 5) (Goley & Welch, 2006; Welch *et al.*, 1997a). The Arp2/3 complex is a weak actin nucleator, but is activated when it binds to a NPF such as Neural Wiskott-Aldrich syndrome protein (N-WASP) or a NPF mimic (e.g. ActA of *Listeria*). NPF binding to the Arp2/3 complex results in a conformational change in Arp2 and Arp3 such that it mimics F-actin barbed ends to act as a template to nucleate and polymerise actin (Robinson *et al.*, 2001). The Arp2/3 complex also binds to the side of pre-existing filaments to polymerise a characteristic 70° angle Y-branching network (Mullins *et al.*, 1998).

1.4.3 Neural Wiskott-Aldrich syndrome protein (N-WASP)

The involvement of N-WASP NPF in *Shigella* ABM was initially described by Suzuki *et al.* (1998). Depletion of N-WASP from *Xenopus* egg extracts reduced F-actin tail formation, and this was restored upon addition of purified N-WASP protein (Suzuki *et al.*, 1998). Similarly *Shigella* does not exhibit movement in cells depleted of N-WASP or expressing dominant-negative variants of N-WASP (Lommel *et al.*, 2001; Snapper *et al.*, 2001; Suzuki *et al.*, 1998). Curiously even though IcsA can engage N-WASP, it cannot interact with other NPFs, such as the closely related Wiskott-Aldrich syndrome protein (WASP). Hence in macrophages where WASP expression is high and N-WASP expression is low, *Shigella* cannot exhibit ABM (Suzuki *et al.*, 2002).

Structurally N-WASP consists of a WASP homology 1 domain (WH1), which includes a pleckstrin homology (PH) domain and a calmodulin binding IQ motif; a basic domain; a GTPase binding domain/Cdc42 and Rac interactive binding (GBD/CRIB); a proline-rich domain (PRD); a verprolin-homology region (V)/WASP homology 2 domains (WH2); a cofilin-homology sequence (C); and a highly acidic region (A) at the C-terminal (Aspenström, 2005; Miki *et al.*, 1996; Miki & Takenawa, 2003; Mimuro *et al.*, 2000; Zettl & Way, 2002). N-WASP activity is primarily regulated through auto-inhibition via intramolecular interactions between the GBD/CRIB and VCA domains. The glycine-rich repeat (GRR) region of IcsA (aa 104 - 506), which includes eight GRRs and the subsequent 80 amino acids, activates N-WASP in the absence of host Cdc42 via interactions with the N-WASP PH domain and IQ motif (Suzuki *et al.*, 1996; Suzuki *et al.*, 1998). The N-WASP interacting regions have since been expanded and refined to IcsA aa 185 - 312, aa 330 - 382 and aa 508 - 730 (May & Morona, 2008; Teh & Morona, 2013).

IcsA activation of N-WASP is also dependent on other host signalling proteins and N-WASP co-factors such as Abl tyrosine kinase, Bruton's tyrosine kinase and Toca-1 (Burton *et al.*, 2005; Dragoi *et al.*, 2013; Leung *et al.*, 2008). However IcsA-mediated N-WASP activation is independent of other known N-WASP activating factors such as phosphatidylinositol (4,5) diphosphate, Cdc42, Rac, Wasp-interacting protein (WIP) and Nck, although WIP and Nck are both recruited to the *Shigella* actin tail (Moreau *et al.*, 2000).

1.4.4 *Shigella* ABM and comet tail

After escaping from the vacuole, *S. flexneri* is released into the host cytosol and ABM is initiated by IcsA through activation of the host N-WASP (Stevens *et al.*, 2006). Activation of the autoinhibited N-WASP by IcsA relieves the binding of the GBD/CRIB motif to the VCA region, thus exposing the VCA region to activate the Arp2/3 complex (Figure 1.3). In the *Shigella* comet tail, N-WASP is present at the bacterial pole and the Arp2/3 complex is located throughout the tail (Gouin *et al.*, 1999; Suzuki *et al.*, 1998).

The non-equilibrium state of actin treadmilling is maintained by actin depolymerisation factor (ADF)/cofilin, profilin, capping proteins and ATP. ADF accelerates depolymerisation at the pointed end to increase the concentration of free monomeric actin, thus promoting polymerisation at the barbed end, whilst profilin binds to ATP-monomeric actin (ATP-G-

actin) to enhance monomer addition at the barbed end (Pantaloni & Carlier, 1993). Capping proteins cap the barbed end to allow monomers from the pointed end to be added to newly synthesised filaments and ATP hydrolysis is important to provide energy for filament synthesis (Carlsson & Brown, 2006; Pantaloni *et al.*, 2001; Theriot, 2000).

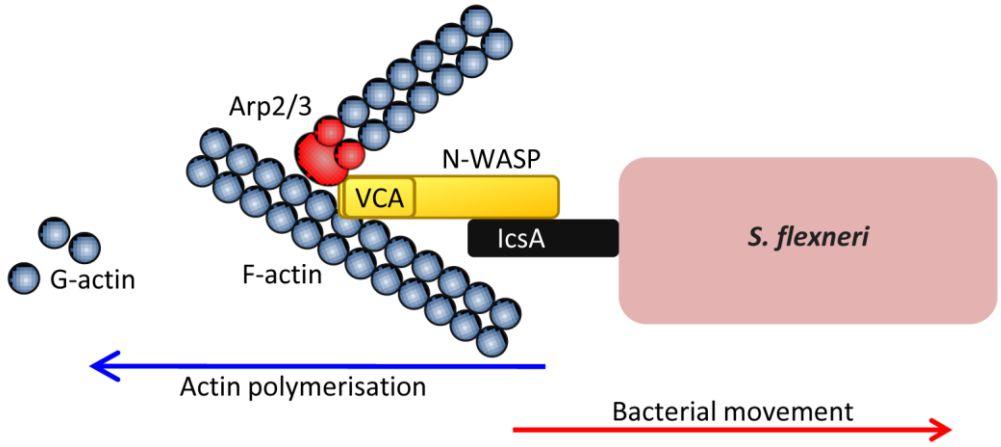

Figure 1.3 IcsA-mediated F-actin polymerisation.

The *S. flexneri* IcsA protein is localised to the old pole. Activation of the autoinhibited host N-WASP by IcsA exposes the N-WASP VCA region to activate the host Arp2/3 complex. N-WASP is a nucleation promoting factor (NPF). NPF binding to the Arp2/3 complex results in a conformational change in the Arp2 and Arp3 subunits such that it mimics F-actin barbed ends to act as a template to nucleate and polymerise monomeric G-actin to filamentous F-actin. The F-actin comet tail generates a propulsive force, which pushes the bacterium forward in the opposite direction.

Reconstitution of *Shigella* ABM in *in vitro* systems is dependent on G-actin, ATP, the Arp2/3 complex, N-WASP, cofilin/ADF, profilin and capping protein (Loisel *et al.*, 1999). Electron microscopy (EM) of myosin S1 decorated *Shigella* comet tails show that the tails are 5 - 15 μm in length (mean = 7 μm) with a mean width of 0.7 μm (Figure 1.4A). The individual filaments are between 0.1 - 1 μm. The filaments have a higher density at the bacterial pole and appeared more bundled at the end of the comet tail (Figure 1.4A) (Gouin *et al.*, 1999). The intracellular speed of *Shigella* is 3 - 26 μm/min depending on the host cell type (Gouin *et al.*, 1999; Shere *et al.*, 1997; Zeile *et al.*, 1996). In *Xenopus laevis* cytoplasmic extracts, *E. coli* expressing IcsA exhibits motility at the rate of 12.9 ± 7.8 μm/min (Goldberg & Theriot, 1995). In reconstituted protein systems, IcsA expressed in *E. coli* exhibited

maximal movement of 2.2 μm/min, suggesting that in a more complicated cellular context, other host factors might interact with the actin tail to allow *Shigella* to move more efficiently (Loisel *et al.*, 1999).

1.4.5 *L. monocytogenes* ABM and comet tail

Listeria has a similar intracellular lifecycle to *S. flexneri* and also forms comet tails (Figure 1.4). The ubiquitous Gram-positive bacterium infects humans and animals through ingestion of contaminated food, resulting in self-limiting gastroenteritis (Drevets & Bronze, 2008; Robinson *et al.*, 2001). In immunocompromised individuals, systemic infection causes further complications such as meningitis and encephalitis (listeriosis).

Listeria ABM is mediated by the chromosomally encoded *actA* gene (Kocks *et al.*, 1992). ActA is a 67 kDa protein and is structurally organised with a signal peptide followed by a WASP-like acidic domain (A), two WH2 domains, an Arp2/3 complex binding domain, a cofilin homology sequence (C), a phosphoinositide binding region (PI), four proline-rich repeats and a transmembrane anchor (Goldberg, 2001; Skoble *et al.*, 2000). The A, C, WH2 and Arp2/3 complex binding domains share significant homology with N-WASP and are essential for F-actin tail formation (Lasa *et al.*, 1997; Skoble *et al.*, 2000). ActA is a NPF mimic and can thus activate the Arp2/3 complex directly (Zalevsky *et al.*, 2001). Similar to IcsA, ActA is localised at the pole and is sufficient and necessary for pathogenesis (Kocks *et al.*, 1992; Smith *et al.*, 1995). Δ*actA* mutants are defective in actin nucleation *in vitro* and are also less virulent in mice (Brundage *et al.*, 1993). Expression of ActA in the non-pathogenic and non-motile *L. innocua* also conferred ABM in *Xenopus* cytoplasmic extracts (Kocks *et al.*, 1995).

Listeria bacteria form an actin cloud via interactions between its surface presented ActA and the Arp2/3 complex when the bacteria initially escape into the host cytoplasm (Tilney & Portnoy, 1989). Subsequent cell division and redistribution of ActA reorganises the actin cloud into an actin tail at the pole (Rafelski & Theriot, 2006). The 70° angle Y-branching network is also observed in *Listeria* actin tails (Cameron *et al.*, 2001). The Arp2/3 complex is located at the bacterial surface and throughout the actin tail (Welch *et al.*, 1997b). EM of myosin S1-decorated *Listeria* comet tails showed that they are 4 - 12 μm in length (mean = 5 μm) with a mean width of 1 μm. The length and density of the actin filaments are comparable

to the *Shigella* comet tail, although longer filaments (0.3 - 1.2 μm) are also observed along the sides of the bacterium (Figure 1.4D) (Gouin *et al.*, 1999). The intracellular speed of *Listeria* is 13 - 87 μm/min depending on the host cell type (Dabiri *et al.*, 1990; Gouin *et al.*, 1999).

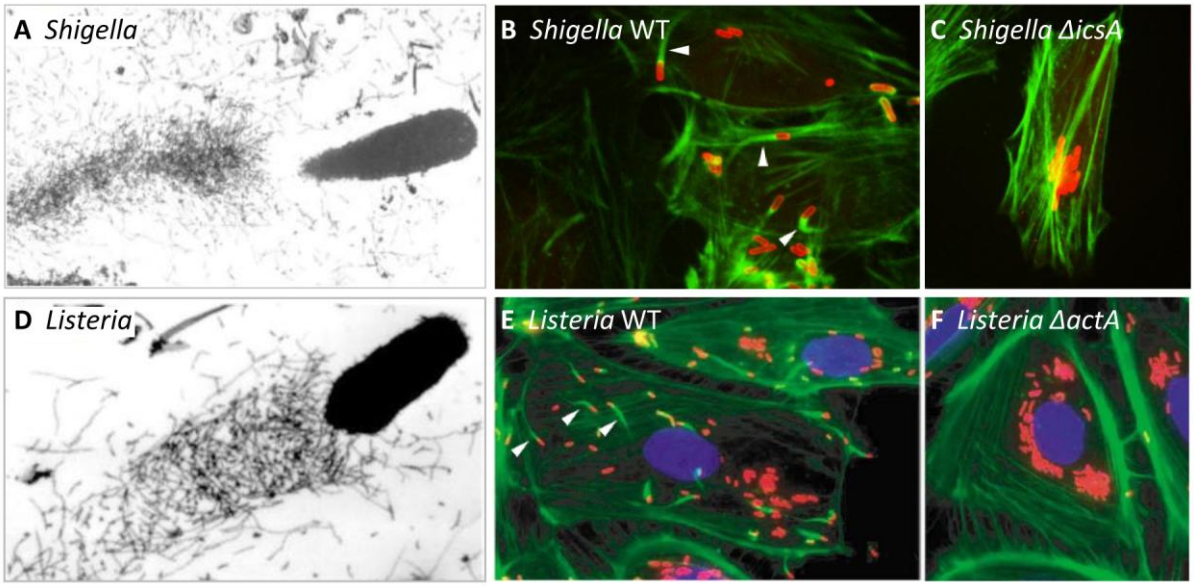

Figure 1.4 *Shigella* IcsA protein and *Listeria* ActA protein are essential for F-actin tails formation.

Post-invasion *Shigella* and *Listeria* initiate *de novo* F-actin tail polymerisation by exploiting host factors. The F-actin tails that are formed can be visualised with electron microscopy (EM) and immunofluorescence (IF) microscopy. (A) EM of *Shigella* actin tail analysed after myosin S1 decoration. (B) HeLa cells infected by *Shigella* wild type or (C) Δ*icsA* mutant. Infected cells were fixed and labelled with anti-O-antigen antibody to label *Shigella* bacteria (red) and FITC-phalloidin to label F-actin (green). Arrowheads indicate F-actin comet tails. (D) EM of *Listeria* actin tail analysed after myosin S1 decoration. (E) PtK2 (*Potorous tridactylis* kidney epithelial) cells infected by *Listeria* wild type or (F) Δ*actA* mutant. Infected cells were fixed and labelled with DAPI (blue) to visualise PtK2 and *Listeria* nuclei, anti-*Listeria* antibody (red) and FITC-phalloidin to label F-actin (green). Arrowheads indicate F-actin comet tails. IcsA- and ActA-mediated F-actin tail formation are essential for imparting motility to *Shigella* and *Listeria*, respectively. Mutant strains lacking these proteins do not form comet tails, are non-motile and appear as clumps inside infected host cells. Figures (A), (D), (E) and (F) reprinted from Current Opinion in Microbiology, 8, Gouin *et al.*, Actin-based motility of intracellular pathogens, 35-45, Copyright 2005, with permission from Elsevier. Figures (B) and (C) reprinted from Microbial Pathogenesis, 35, Van Den Bosch and Morona, The actin-based motility defect of a *Shigella flexneri rmlD* rough LPS mutant is not due to loss of IcsA polarity, 11-18, Copyright 2003, with permission from Elsevier.

1.5 *Shigella* cell-to-cell spreading

Cell-to-cell spreading is dependent on the bacteria's ability to initiate *de novo* F-actin tail polymerisation, followed by protrusion formation, uptake of bacteria-containing protrusion and finally lysis of the double membrane vacuole in the neighbouring cell (Figure 1.5). These processes are facilitated by both *Shigella* and host proteins, and will be discussed in the following sections.

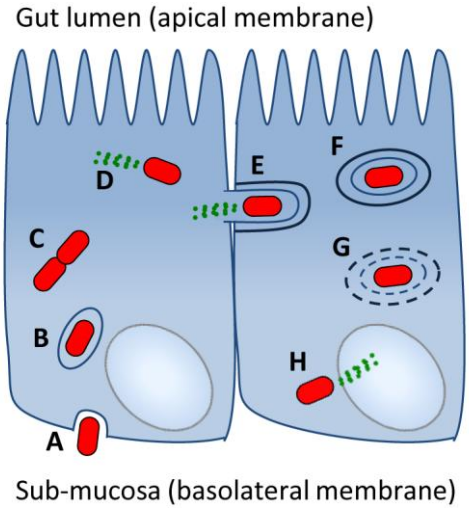

Figure 1.5 Key steps in *Shigella* cell-to-cell spreading.

(A) *Shigella* bacteria (red rods) initially invade the host colonic epithelium via the basolateral membrane. (B) After escaping from the vacuole, (C) Shigellae are released into the host cytoplasm to initiate replication. (D) *Shigella* IcsA protein interacts with host proteins to initiate F-actin tail formation (green trails) imparting motility to the bacteria. (E) Shigellae are propelled to the plasma membrane to form protrusions into the neighbouring cell. (F) The protrusion is taken up by the adjacent cell and the bacteria are contained in a double membrane vacuole. (G) After escaping from the vacuole, (H) *Shigella* are released into the cytoplasm and the infectious cycle is repeated. Steps (D) to (G) are essential for bacterial cell-to-cell spread and are dependent on bacterial and host factors. Inhibition of proteins essential for these steps impedes bacterial lateral movement.

1.5.1 Bacterial factors

Shigella cell-to-cell spreading is primarily dependent on IcsA as discussed earlier. However *Shigella* proteins involved in IcsA biogenesis (such as the IcsA specific protease, IcsP), proteins involved in LPS O-antigen biosynthesis and proteins involved in the lysis of the double membrane, resulting in the release of *Shigella* during protrusion formation (TTSS Ipa proteins) are also crucial.

Initially the uncharacterised VacJ lipoprotein (renamed MlaA) was thought to be involved in *Shigella* intercellular spreading, possibly by facilitating bacterial release from the double membrane vacuoles following protrusion formation (Suzuki *et al.*, 1994). However a recent study has shown that in *E. coli*, MlaA is part of an ATP-binding cassette (ABC) transport system which is hypothesized to be involved in actively preventing phospholipids of the inner leaflet of the OM from interfering with LPS expression and OM permeability (Malinverni & Silhavy, 2009). It has been suggested that the loss of MlaA may have disrupted the OM such that LPS localisation and subsequent IcsA expression is affected. A FACS (fluorescence activated cell sorter)-based method has also been developed to identify *S. flexneri* mutants defective in cell-to-cell spread. Besides factors associated with the LPS structure, ABM and the TTSS, no new *Shigella* factors were identified (Rathman *et al.*, 2000b).

Outer membrane protein A (OmpA) is a multifaceted major OM protein of *E. coli* and other Enterobacteriaceae family members (Krishnan & Prasadarao, 2012). OmpA is highly conserved among Gram-negative bacteria and is thought to play a key role in the structural integrity of the OM in conjunction with other bacterial components (Krishnan & Prasadarao, 2012). In rabbits challenged with virulent *S. flexneri* 2a, OmpA provided significant immunity (Pore *et al.*, 2009; Pore *et al.*, 2011). Further work has shown that OmpA activates both innate and adaptive immune responses, and is considered a good vaccine candidate as it is cross-reactive with other *Shigella* spp. (Pore *et al.*, 2011; Pore *et al.*, 2012; Pore & Chakrabarti, 2013). As mentioned earlier OmpA has been suggested to assist in IcsA polar localisation (Scribano *et al.*, 2014) (Section 1.3.3). Although the exact role of OmpA in this aspect remains unclear, Δ*ompA* mutants have significantly reduced protrusion and plaque formation in HeLa cells, while retaining the ability to form F-actin tails (Ambrosi *et al.*, 2012). While LPS biosynthesis was not affected, IcsA was detected on both the lateral and polar regions of the bacteria (Ambrosi *et al.*, 2012).

1.5.2 Host factors

1.5.2.1 Tight junction, adherens junction and gap junction proteins

Polarised colonic epithelium cells, the site of *Shigella* infection, is characterised by apical junctional complexes (APCs), consisting of tight junctions (TJs) and adherens junctions (AJs) at the most apical end. APCs are undercoated with a prominent network of actin-myosin II, also known as the actomyosin ring (Figure 1.6) (Miyoshi & Takai, 2005). Desmosomes are another form of adhesive contact between epithelial cells. They are found as intermittent spot adhesions along the lateral membrane and are anchored to intermediate filaments in the cytoplasm. These structures provide mechanical resilience to the epithelium, thus contributing to tissue homeostasis (Capaldo *et al.*, 2014). TJs at the apical end of the basolateral membrane are important in establishing cell polarity and providing a barrier between the epithelial cells to prevent diffusion of ions and macromolecules (Miyoshi & Takai, 2005). AJs are essential for initiating and stabilising cell-cell adhesion, actin cytoskeleton regulation, transcriptional regulation and intracellular signalling (Hartsock & Nelson, 2008). It has been proposed that TJs and AJs associate with the actin cytoskeleton, and hence formation and maturation of cell-cell contacts requires reorganisation of the actin cytoskeleton (Hartsock & Nelson, 2008).

Components of the AJs and TJs such as cadherin, vinculin, α-catenin, β-catenin and α-actinin are found at the actin tail of *Shigella* during protrusion formation (Kadurugamuwa *et al.*, 1991). Cadherin is important in cell-to-cell spread as it helps to maintain a tight association between the bacterium and the membrane of the protrusions (Figure 1.7) (Sansonetti *et al.*, 1994). *Shigella* invasion and dissemination is also dependent on ATP release by connexin 26 hemichannels (Tran Van Nhieu *et al.*, 2003). Connexin 26 is a gap junction protein with central pores which allow for the transfer of small signalling molecules with relatively low specificity. Adjacent gap junction proteins are coupled together chemically as well as electrically. Gap junctions have a narrow clearance of 2 - 4 nm between the two cells (Oshima, 2014). HeLa cells transfected with connexin 26 and infected with *S. flexneri* M90T had increased infectious foci area compared to untreated HeLa cells (Tran Van Nhieu *et al.*, 2003). No differences in *Listeria* cell-to-cell spreading was observed under similar experimental conditions, suggesting connexin involvement is specific to *Shigella* (Tran Van Nhieu *et al.*, 2003).

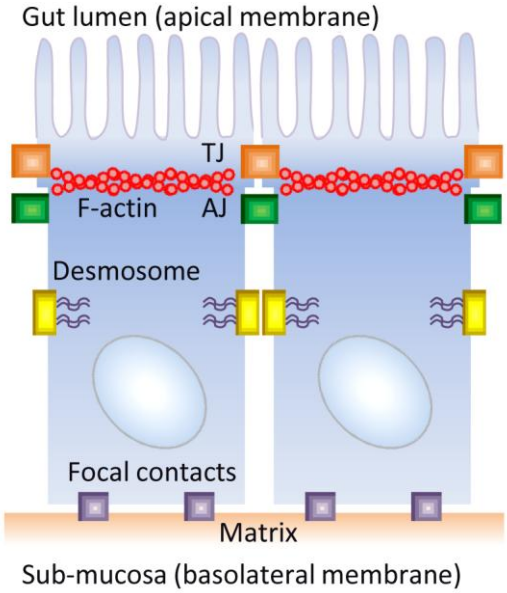

Figure 1.6 The structure of polarised epithelium cells.

Epithelial cells attach to adjacent cells via tight junctions (TJs, orange rectangles), adherens junctions (AJs, green rectangles) and desmosomes (yellow rectangles), and to the basement membrane by focal contacts (purple rectangles). The apical junctional complexes (AJCs), consisting of TJs and AJs are undercoated with a prominent network of F-actin and myosin (not shown), also known as an actomyosin ring. Desmosomes are undercoated with intermediate filaments and provide mechanical resilience to the epithelium, thus contributing to tissue homeostasis. TJs are important in establishing cell polarity and providing a barrier between the epithelial cells to prevent diffusion of ions and macromolecules. AJs are essential for initiating and stabilising cell-cell adhesion, actin cytoskeleton regulation, transcriptional regulation and intracellular signalling.

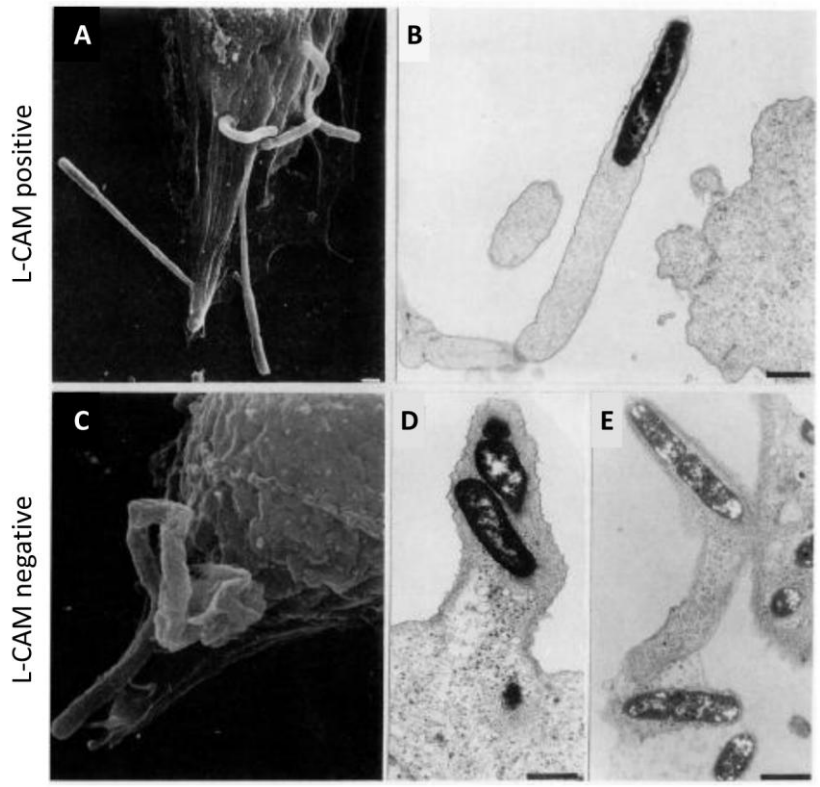

Figure 1.7 Host proteins are critical for efficient *Shigella* protrusion formation.

Efficient *Shigella* protrusion formation is dependent on host proteins, such as L-CAM, a component of adherens junctions (AJs). Transmitting electron microscope (TEM) and scanning electron microscope (SEM) images of (A - B) semi confluent L-CAM positive and (C - E) L-CAM negative cells infected with *S. flexneri* M90T. (A) In L-CAM positive cells, when observed with TEM, *Shigella* protrusions have straight cylindrical structures with a clear reduction in calibre behind the bacterial body, where the actin tail is located. (B) This was similarly observed with SEM. The bacterial surface is also tightly bound to the inner face of the host cell membrane, particularly at the tip of the protrusion. (C) In the absence of L-CAM, *Shigella* protrusions are flaccid, flatter in shape and do not show significant constriction behind the bacterial body. (D) The intimate interaction between the bacterial surface and the inner face of host cell membrane is also lost, and *Shigella* is surrounded by a thick layer of cytoplasmic material. (E) At late stages of protrusion formation *Shigella* is observed to be loosely interacting with the host cell membrane and losing contact with the actin material inside protrusions, and frequently display changes in orientation. Scale bar = 1 μm. Reprinted from Cell, 76, Sansonetti *et al.*, Cadherin expression is required for the spread of *Shigella flexneri* between epithelial cells, 829-839, Copyright 1994, with permission from Elsevier.

Myosin-X is an unconventional myosin and a component of AJs (Liu *et al.*, 2012). Knockdown of myosin-X resulted in shortened and thickened protrusion stalks which reduced the bacteria's ability to form plaques (Bishai *et al.*, 2012). Time-lapse microscopy confirmed that GFP-tagged myosin-X localised along the sides and the rear of the bacteria contained within protruding membranes, as well as at the F-actin tail immediate to the tip of bacteria (Bishai *et al.*, 2012). Myosin-X localisation however is not observed in *Shigella* found within the cytoplasm (Bishai *et al.*, 2012). Structurally myosin-X consists of a head domain with motor activity, a neck region followed by a large tail with PH domains (Liu *et al.*, 2012). It has been proposed that the myosin-X head domain binds to the actin filaments at the sides of the bacterium and the tail domain is linked to the inner leaflet of the protruding membrane. Movement of the myosin head is proposed to transport membrane towards the tip of the protrusion and as the protrusion elongates the base of the stalk progressively thins out as the filament content is pushed towards the protrusion tip (Bishai *et al.*, 2012). Even though ABM itself is independent of any motor activity, it appears that the forces generated by the myosin-X motor are required during protrusion formation. Curiously *Listeria* plaque formation was also affected when myosin-X was knockdown with RNAi, suggesting a fundamental role for myosin-X in bacterial cell-to-cell spread (Bishai *et al.*, 2012).

1.5.2.2 Myosin light chain kinase (MLCK)

In eukaryotic cells, the cortical tension is maintained by the actomyosin network (Pasternak *et al.*, 1989), which is important for various processes such as lamellipodia formation (Betapudi, 2010) and maintaining cell morphology (Eliott *et al.*, 1993; Even-Ram *et al.*, 2007; Wei & Adelstein, 2000). Thus for cell-to-cell spreading to occur, the tensions of the actomyosin ring have to be overcome as this may act to counter the pushing force generated via bacterial ABM (Rajabian *et al.*, 2009). MLCK regulates the cortical tension through phosphorylation of myosin II, which in turn activates the ATPase activity, filament formation and contractile activity of myosin II *in vitro* and *in vivo* (Conti *et al.*, 2008; Conti & Adelstein, 2008). The catalytic activity of MLCK is inhibited by ML-7, H-7 and wortmannin (Nakanishi *et al.*, 1992; Saitoh *et al.*, 1987), whilst myosin II can be inhibited by 2,3-butanedione monoxime (BDM) and (-)-blebbistatin (Ostap, 2002; Straight *et al.*, 2003).

MLCK was previously shown to be important for *Shigella* cell-to-cell spreading in polarised Caco-2 cells, and myosin II was also indirectly shown to play a role (Rathman *et al.*, 2000a). BDM treatment reduced *S. flexneri* intercellular spreading, as evident by a smaller foci of infection (24.3 ± 6.7 mm) compared to untreated Caco-2 cells (35.4 ± 6.4 mm) (Rathman *et al.*, 2000a). Addition of ML-7, H-7 and wortmannin to Caco-2 cells also reduced *Shigella*'s ability to disseminate, similar to an Δ*icsA* strain (Rathman *et al.*, 2000a). MLCK inhibition did not affect the integrity of the Caco-2 cell TJs but myosin IIA protein levels associated with the cytoskeleton were reduced as shown by Western immunoblotting (Rathman *et al.*, 2000a). Taken together this suggests that during intercellular spreading, MLCK increases myosin IIA association with the cytoskeleton, presumably to re-model the plasma membrane to allow protrusion formation to occur, although this remains to be investigated. Addition of (-)-blebbistatin, ML-7, H-7 and BDM to Caco-2 BBE1, Caco-2 and PtK2 cells, respectively, did not affect *Listeria* dissemination. Thus myosin IIA and MLCK involvement is specific for *Shigella* (Cramer & Mitchison, 1995; Rajabian *et al.*, 2009; Rathman *et al.*, 2000a).

1.5.2.3 Cytoplasmic factors

Similar to the Arp2/3 complex, formins initiate *de novo* actin polymerisation but can also cross-link actin filaments (Esue *et al.*, 2008). IF microscopy confirmed that Dia1 is localised to the actin tail and is present in the donor membrane surrounding the bacterium within the engulfed protrusion. It has been suggested that the switch to formin-mediated actin polymerisation remodels the cortical actin network such that the cortical actin is perpendicular to the plasma membrane and the forces generated by the parallel arrays of polymerised actin may facilitate protrusion formation (Heindl *et al.*, 2009). It remains unclear how *Shigella* is able to switch from Arp2/3 complex to formin-mediated actin polymerisation.

1.6 Host proteins examined in this study

1.6.1 Dynamin II

Dynamins are the founding members of a family of guanosine triphosphatases (GTPases) known as the dynamin-like proteins (DLPs), and are imporant for severing membrane-bound clathrin-coated vesicles during endocytosis. Endocytosis is important for many essential cellular processes such as mediating cellular uptake of nutrients, regulating protein concentrations in the plasma membrane and internalising activated receptors. Endocytosis is also used as a route of entry for some pathogens (Ferguson & De Camilli, 2012; McCluskey *et al.*, 2013). Dynamin II is a 96 kDa protein with an N-terminal guanosine triphosphatase (GTPase), a middle domain, a PH domain, a GTPase effector domain (GED) and a C-terminal proline-rich domain (PRD) (Figure 1.8A) (Kessels *et al.*, 2001; McNiven *et al.*, 2000; Muhlberg *et al.*, 1997). It is a cytoplasmic protein but can be membrane bound via interactions between its PH domain which binds phosphatidylinositol 4,5-bisphosphate [$PI(4,5)P_2$] and another region upstream of the PH domain which inserts into the lipid bilayer (Burger *et al.*, 2000). Three members of the family have been identified: dynamin I (neurons), dynamin II (ubiquitous), and dynamin III (brain, lung and testis). Multiple splice variants were also identified for all three dynamin isoforms (Cao *et al.*, 1998).

In its native state, dynamin is a dimer. The crystal structure of the dynamin I dimer (without the PRD) has been resolved and has a predicted three-dimensional hairpin-like folding structure (Figure 1.8A) (Faelber *et al.*, 2011; Ford *et al.*, 2011). In this configuration the GTPase domain is located in a helical bundle, known as the bundle signalling element (BSE) or neck (Chappie *et al.*, 2010; Low & Löwe, 2010), which is formed by three helices derived from sequences at the N-terminal and C-terminal sides of the G domain, and from the C-terminal region of the GED. The BSE is followed by a stalk made up of helices from the middle region and the N-terminal region of the GED (Chappie *et al.*, 2010; Chappie *et al.*, 2011; Faelber *et al.*, 2011; Ford *et al.*, 2011), and the foot of the stalk hairpin consists of the PH domain which binds to membranes (Figure 1.8A) (Ferguson *et al.*, 1994). The PRD, which is expected to be unfolded, protrudes at the boundary between the BSE and the GTPase domain, most likely away from the membrane, where it may interact with other proteins (Ferguson & De Camilli, 2012). The stalk of dynamin dimerises in a cross-like pattern to

form a dynamin dimer in which the two GTPase domains are oriented in opposite directions (Figure 1.8A) (Chappie *et al.*, 2010; Chappie *et al.*, 2011; Faelber *et al.*, 2011; Ford *et al.*, 2011). In the presence of guanosine triphosphate (GTP), helical dimerisation between adjacent dynamin molecules is thought to drive assembly-stimulated GTPase activity, resulting in constriction of the neck of clathrin-coated vesicles leading to scission and subsequent formation of endocytic vesicles (Figure 1.8B - C) (Chappie *et al.*, 2010; Faelber *et al.*, 2011; Ford *et al.*, 2011).

The GTPase activity of dynamin I, dynamin II and the mitochondrial dynamin, Drp1, are inhibited by dynasore, a non-competitive reversible inhibitor (Macia *et al.*, 2006). Dynasore has been shown to have protective effects in various animal models of non-infectious human diseases (Chen *et al.*, 2009; Gao *et al.*, 2013; Terada *et al.*, 2009). Dyngo4a, an analogue of dynasore has been developed and appear to be more potent compared to dynasore (Harper *et al.*, 2011; McCluskey *et al.*, 2013). During the course of this doctoral work, a study from Fukumatsu *et al.* (2012) reported that *Shigella* engulfment, but not protrusion formation into the neighbouring cell is triggered by phosphoinositide 3-kinase and is dependent upon dynamin II, Epsin-1 and clathrin which are essential components of the clathrin-mediated endocytic pathway (Fukumatsu *et al.*, 2012; McMahon & Boucrot, 2011). Furthermore *Shigella* preferentially translocate between TJs where three epithelial cells meet (tricellular junction) and this is dependent on the TJ protein, tricellulin (Fukumatsu *et al.*, 2012).

In contrast *Listeria* bacteria prefer to infect neighbouring cells at bicellular junctions, i.e the junctions where two cells meet. *Listeria* cell-to-cell spread is also less dependent on components of clathrin-mediated pathway (Fukumatsu *et al.*, 2012). This is not entirely surprising given that the secreted *Listeria* virulence protein InlC (internalin C) is able to alleviate host cell cortical tension. The mammalian Tuba and N-WASP proteins form a complex which generates cortical tension at apical junctions. However during *Listeria* infection, InlC interacts with Tuba, thus disrupting the Tuba-N-WASP interaction, presumably to relieve cortical tension (Rajabian *et al.*, 2009). As a consequence, the normally taut apical junctions become slack, likely due to reduced cortical tension, which in turn facilitates more efficient *Listeria* protrusion formation (Rajabian *et al.*, 2009).

Figure 1.8 Structure of dynamin and putative mechanism of dynamin-mediated membrane fission.

(A) Domain organisation of dynamin based on its three-dimensional structure, determined from crystallographic studies (numbers indicate amino acid position within the primary sequence of the human dynamin 1 xa splice variant). Regions that belong to the same folded module are shown in the same colour. The crystal structure of a dynamin dimer is shown below (without the PRDs, which are thought to be unfolded) and is colour-coded to match the linear domain representation. (B) Schematic representation of dynamin dimers and helical dynamin polymers around a tubular template in two different orientations (with 90° rotation between them). The colour-coding of the domains matches the colours in part (A) (without the PRDs, which are thought to project out of the polymerised helix). The approximate location of the bound nucleotide is highlighted in white circles. Dynamin polymerisation occurs as a result of interactions between the stalks of dynamin monomers (interface 2) and between stalk dimers (interfaces 1 and 3). The GTP-dependent dimerisation of G domains between adjacent rungs of the dynamin helix (highlighted by yellow stars in the longitudinal view of the helix), is thought to promote assembly-stimulated GTPase activity, resulting in membrane constriction and ultimately fission. (C) Schematic view of the key steps leading to dynamin-mediated membrane fission described in (B). BSE, Bundle signalling element; GED, GTPase effector domain; PH, pleckstrin homology domain; PRD, proline-rich domain. Figure adapted with permission from Macmillan Publishers Ltd: NATURE REVIEWS MOLECULAR CELL BIOLOGY, Ferguson SM & De Camilli P (2012). Dynamin, a membrane-remodelling GTPase. *Nat Rev Mol Cell Biol* 13, 75-88, Copyright 2012.

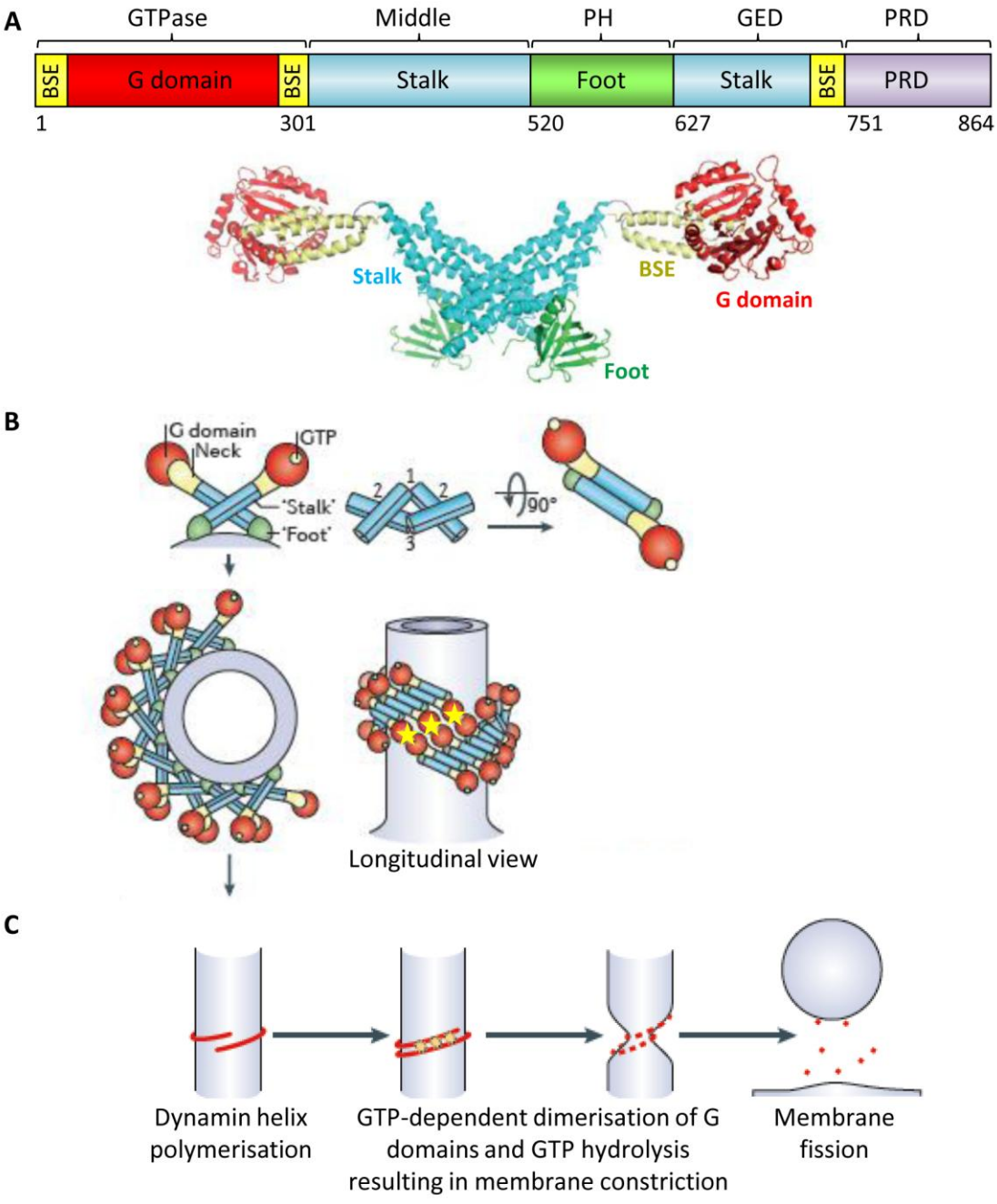
A
GTPase
Middle
PH
GED
PRD
BSE
G domain
BSE
Stalk
Foot
Stalk
BSE
PRD
1
301
520
627
751
864
Stalk
BSE
G domain
Foot
B
G domain
Neck
GTP
'Stalk'
'Foot'
1
2
2
3
90°
Longitudinal view
C
Dynamin helix polymerisation
GTP-dependent dimerisation of G domains and GTP hydrolysis resulting in membrane constriction
Membrane fission

1.6.2 Dynamin-related protein 1 (Drp1)

Mitochondria are important for many metabolic functions such as supplying cells with ATP generated by oxidative phosphorylation, catabolic and anabolic reactions, developmental processes and ageing. It is also an essential organelle in the activation of cell death pathways such as intrinsic apoptosis and programmed necrosis (Otera *et al.,* 2013). Mitochondria undergo fusion and fission depending on the demands of the cell (Bereiter-Hahn, 1990) and these are mediated by large GTPases. Inner mitochondrial membrane fusion is dependent on optic atrophy protein 1 (OPA1) (Olichon *et al.,* 2003) and outer mitochondrial membrane fusion is mediated by mitofusin 1 (MFN1) and 2 (MFN2) (Legros *et al.,* 2002). Dynamin-related protein 1 (Drp1), also known as dynamin-1-like protein (DNM1L) or dynamin-like protein 1 (DLP1), is key for fission (Smirnova *et al.*, 1998; Smirnova *et al.*, 2001). The loss of mitochondrial dynamics contributes to various neurodegenerative disorders such as Charcot-Marie-Tooth disease type 2a, Alzheimer's and Parkinson's diseases (Ranieri *et al.,* 2013).

Drp1 belongs to the same dynamin family of DLPs and has a similar protein domain organisation, structure and membrane severing activity (Ferguson & De Camilli, 2012). The 89 kDa protein has an N-terminal GTPase, a middle domain, a small B-insert and a C-terminal GED (Figure 1.9A) (Otera *et al.*, 2013). Drp1 lacks the PH and PRD domains of dynamin. The crystal structure of human Drp1 has been resolved and consists of a G domain, a BSE and a stalk. Similar to dynamin, Drp1 dimers form via interactions at the stalk (Figure 1.9A) (Fröhlich *et al.*, 2013). Drp1 dimers further assemble via a second previously unknown stalk interface to form a linear filament (Figure 1.9B) (Fröhlich *et al.*, 2013). Drp1 activity is regulated by various post-translational modifications (Otera *et al.*, 2013). Mitochondrial constriction is initially mediated by the endoplasmic reticulum and actin (Friedman *et al.*, 2011; Korobova *et al.*, 2013). Dimeric or tetrameric cytosolic Drp1 is then recruited to fission sites on the mitochondria to its receptor, Mff (Otera *et al.*, 2010). In the presence of GTP, Drp1 self-assembly stimulates GTP hydrolysis and formation of higher order structures as foci at the mitochondrial fission sites (Smirnova *et al.,* 2001). Oligomerised Drp1 wraps around the mitochondria and following GTP hydrolysis, the mitochondrial membrane is severed (Smirnova *et al.,* 2001). Drp1 assembly on the mitochondria can be inhibited by the small molecule inhibitor, *m*itochondrial *div*ision *i*nhibitor-*1* (Mdivi-1) (Figure 1.10), through interactions with an allosteric site which does not affect its GTPase activity (Cassidy-Stone *et*

al., 2008). Mdivi-1 has therapeutic effects in various animal models of non-infectious diseases (Ferrari *et al.*, 2011; Ong *et al.*, 2010; Tang *et al.*, 2013).

Mitochondrial fission is a key downstream event for intrinsic apoptosis and programmed necrosis signalling pathways (Figure 1.10) (Otera *et al.*, 2013). During apoptosis, pro-apoptotic Bax localises to the OM of the mitochondria and co-localises with Mfn2 and activates Drp1 at fission sites (Wasiak *et al.*, 2007). Following mitochondrial fragmentation, mitochondrial outer membrane permeabilisation (MOMP) and cristae reorganisation, cytochrome *c* is released and caspases are subsequently activated (Frank *et al.*, 2001). Upon programmed necrosis induction by tumour necrosis factor-α (TNF-α), receptor-interacting serine/threonine-protein kinase 1 (RIP1) and RIP3 interact with mixed lineage kinase domain-like protein (MLKL) (Wang *et al.*, 2012). The RIP1/RIP3/MLKL complex is translocated to the mitochondria to initially engage mitochondrial protein phosphatase long variant (PGAM5L) and subsequently PGAM short variant (PGAM5S) on the mitochondrial membrane. Drp1 GTPase activity is activated via dephosphorylation at Ser637, likely by both PGAM5L and PGAM5S *in situ* on the mitochondrial OM (Wang *et al.*, 2012). It is speculated Drp1 activation may cause mitochondrial fragmentation resulting in reduced ATP production, ROS generation or other downstream events (Wang *et al.*, 2012).

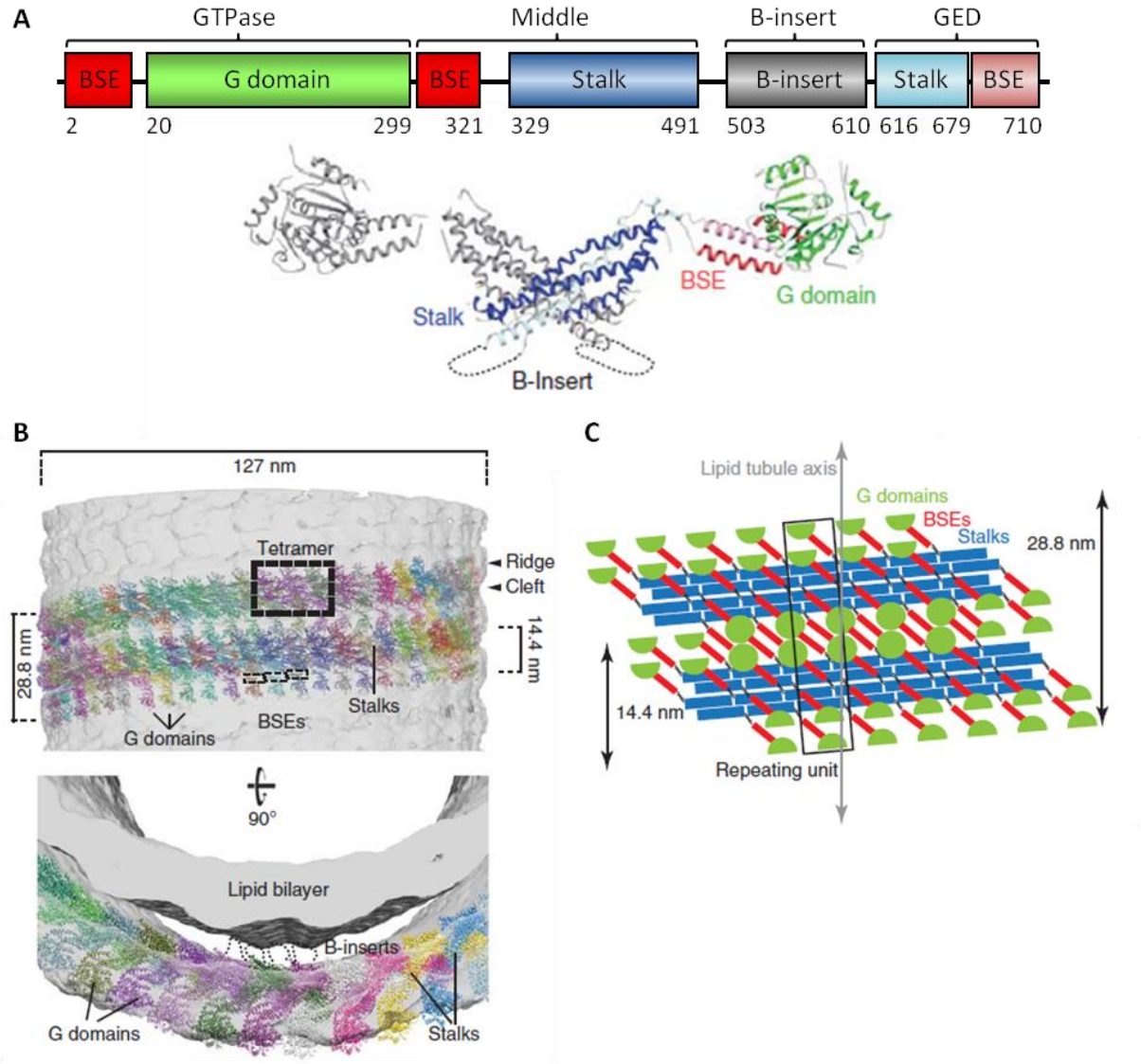

Figure 1.9 Structure of Drp1 and schematic model of Drp1 oligomer.

(A) Domain organisation of Drp1 based on its three-dimensional structure, determined from crystallographic studies. The first and last residue of each domain is labelled. The crystal structure of a Drp1 dimer shown is colour-coded to match the linear domain representation. Regions not resolved in the crystal structure, such as the B-insert, are indicated by dotted lines. (B - C) Structural model of Drp1 oligomer. (B) Drp1 tetramers were manually fitted into the EM reconstruction of yeast Drp1 homologue, Dnm1. In this model, the stalks of Drp1 are orientated tangentially to the lipid tubule, with the B-insert pointing towards the tubule. Oligomerisation of Drp1 into a filament proceeds via stalk interfaces 1, 2 and 3; similar to dynamin in Figure 1.8B. Additionally stalk interface 4 mediates the assembly of a double stalk filament. (C) Schematic illustration of Drp1 molecules in the oligomeric model. The repeating unit (boxed) contains eight Drp1 monomers. BSE, Bundle signalling element; GED, GTPase effector domain. Figure adapted and reprinted from Fröhlich *et al.*, EMBO J, Structural insights into oligomerization and mitochondrial remodelling of dynamin 1-like protein, 32, 1280-1292, Copyright 2013, with permission from John Wiley and Sons.

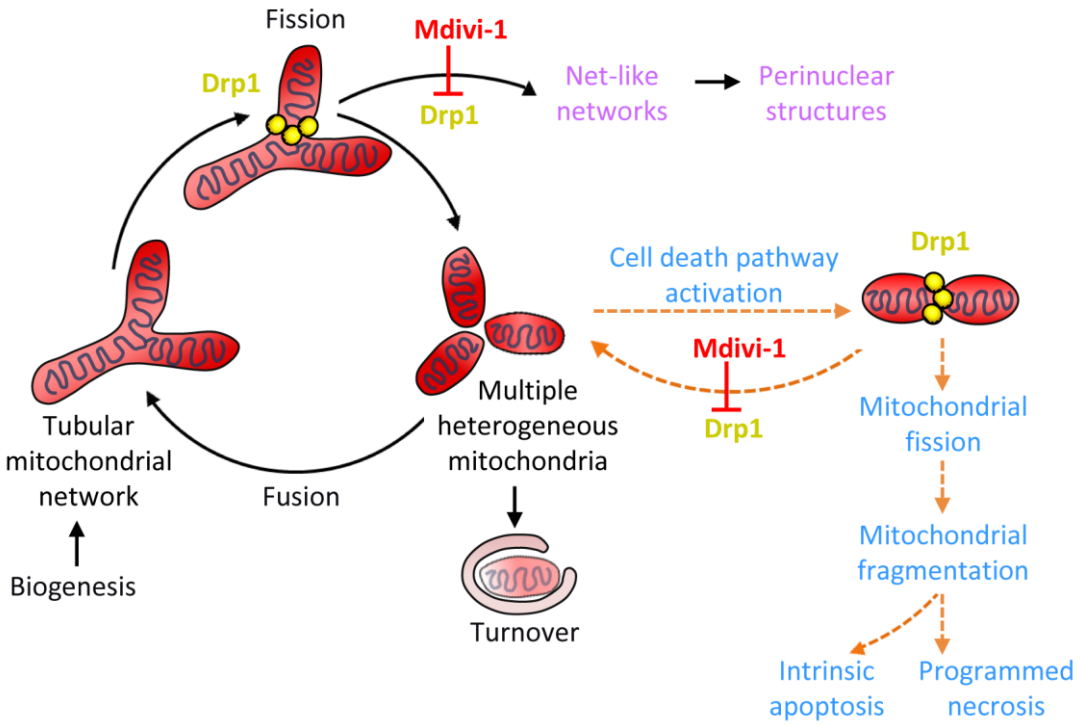

Figure 1.10 Mitochondrial dynamics during homeostasis and Drp1-mediated activation of cell death pathways.

Biogenesis of the mitochondria begins with growth and division of pre-existing organelles and ends with mitophagy (turnover) of damaged or surplus organelles. Mitochondria undergo frequent cycles of fusion and fission which allow the cell to generate multiple heterogeneous mitochondria or interconnected mitochondrial networks, depending on the physiological conditions. Mitochondrial fission is dependent on Drp1, which oligomerises on the mitochondrial outer membrane leading to membrane constriction, followed by GTP hydrolysis which severs the mitochondrial membrane. Drp1 assembly can be inhibited by *m*itochondrial *div*ision *i*nhibitor-*1* (Mdivi-1). Inhibition of Drp1 forms net-like mitochondrial networks, which can collapse into perinuclear structures. Mitochondrial fission is a key downstream event for intrinsic apoptosis and programmed necrosis. Following activation of intrinsic apoptosis, Drp1-mediated mitochondrial fragmentation facilitates mitochondrial outer membrane permeabilisation (MOMP) which results in cytochrome *c* release and subsequent caspase activation. In the case of programmed necrosis, it has been speculated mitochondrial fragmentation may result in reduced ATP production, reactive oxygen species (ROS) production or other downstream events (Wang *et al.*, 2012). Drp1 inhibition with Mdivi-1 reduces mitochondrial fragmentation under these conditions.

1.6.3 Myosin IIA

Non-muscle myosin II (myosin II) are hexamers composed of a pair of heavy chains, essential light chains and regulatory light chains (Figure 1.11). The heavy chains have a globular head region which can bind reversibly to actin filaments, followed by actin-activated ATP hydrolysis to convert chemical energy into mechanical force and movement. Myosin II plays diverse roles during development processes, intracellular transport, organelle localisation, signal transduction and tumour suppression (Conti *et al.*, 2008; Krendel & Mooseker, 2005).

Myosin II is regulated through phosphorylation of the 20 kDa regulatory light chain (MLC_{20}) at Ser19 by a number of kinases including myosin light chain kinase (MLCK) (Conti *et al.*, 2008). The catalytic activity of myosin II can be inhibited by BDM and (-)-blebbistatin (Ostap, 2002; Straight *et al.*, 2003). Phosphorylation of myosin II activates its ATPase activity, filament formation and contractile activity *in vitro* and *in vivo* (Conti & Adelstein, 2008). Mammalian cells express three myosin II isoforms, IIA, IIB and IIC. The corresponding heavy chains are encoded by *MYH9* (IIA), *MYH10* (IIB) and *MYH14* (IIC) (Heissler & Manstein, 2013). In spite of the high degree of similarity in sequence identity and structural conservation, myosin II isoforms differ in enzymatic properties and subcellular localisation (Conti *et al.*, 2008; Maupin *et al.*, 1994). They also have distinct and redundant roles depending on the specific cellular processes (Betapudi, 2010; Kelley *et al.*, 1996; Kolega, 1998; Wang *et al.*, 2011). As mentioned earlier in Section1.5.2.2, MLCK was previously shown to be important for *Shigella* cell-to-cell spreading and there is also some evidence for myosin II involvement (Rathman *et al.*, 2000a). Hence the role of myosin II during *Shigella* infection is investigated further in this doctoral work.

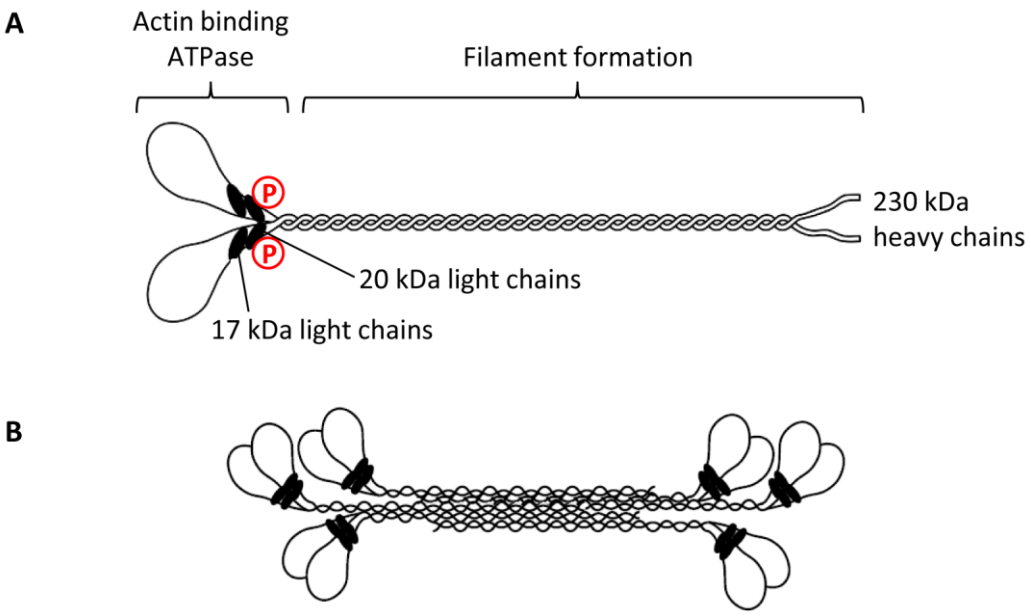

Figure 1.11 Myosin II

(A) Diagram of the non-muscle myosin II (myosin II) molecule showing the heavy chain dimer and two pairs of light chains. Phosphorylation of the 20 kDa regulatory light chain (MLC_{20}) by myosin light chain kinase (MLCK) activates the catalytic activity, filament formation and contractile activity of myosin II. (B) An example of a bipolar myosin II filament. Adapted with permission from Journal of Cell Science. Conti MA & Adelstein RS (2008). Nonmuscle myosin II moves in new directions. *J Cell Sci* 121, 11-18. Copyright 2008 The Company of Biologists Ltd.

1.7 Aims and hypotheses

To date little is known about the host cell factors which are important for *Shigella* infection, in particular in cell-to-cell spread, and host cell death as well as host survival. Further investigation into these aspects will improve our understanding of the *Shigella*-host interaction and in the long term, lead to novel therapeutic interventions.

This thesis investigated several hypotheses which were:

1. *Shigella* cell-to-cell spread is similar to endocytosis and/or exocytosis and is dependent on components important for these processes.
2. *Shigella* induces necrosis / non-apoptotic cell death during infection in HeLa cells.
3. *Shigella* induced-HeLa cell death requires involvement of specific host proteins.

The following aims investigated the hypotheses:

1. To investigate the role of the host proteins: dynamin II, Drp1 and myosin IIA in *S. flexneri* plaque formation and cell-to-cell spread.
2. To investigate the role of Drp1 and mitochondria during *Shigella*-induced HeLa cell death.
3. To investigate if administration of small chemical inhibitors targeted against dynamin II and Drp1 will ameliorate *Shigella*-induced keratoconjunctivitis in a mouse Sereny test.

☙ Chapter 2 ❧

Materials and Methods

Chapter 2: Materials and Methods

2.1 Chemicals, enzymes and reagents

2.1.1 Buffers and Reagents

All reagents were prepared with either RO water (Millipore) or MQ water (Millipore, 18.2 MΩ/cm).

2.1.2 Chemicals

The chemicals used in this study, their source and stock concentrations are listed in Table 2.1. Stock solutions were dissolved in dimethyl sulfoxide (DMSO) (D2650; Sigma-Aldrich) for *in vitro* studies. All chemicals were stored in the dark at -20°C; except ML-9, Necrox-2, Necrox-5 and necrosulfornamide, which were stored in the dark at 4°C. MitoTracker Red® CMXROS (M-7512; Invitrogen) was prepared as a 1 mM stock in DMSO and stored in the dark at -20°C. For *in vivo* studies, chemicals were dissolved in a formulation containing *N*-methyl-2-pyrrolidone (NMP/Pharmasolve; Ashland ISP) and polyethylene glycol 300 (PEG300; Sigma-Aldrich) (1 part NMP to 9 parts PEG300). Chemicals were prepared as a 22 mg/mL stock and was diluted 1/4 (5.5 mg/mL or 30mg/kg) with NMP/PEG before injection into mice.

2.1.3 Antibodies

The rabbit anti-GAPDH antibody (600-401-A33; Rockland Immunochemicals, Inc.), mouse anti-DLP1 antibody (611112; BD Biosciences), mouse anti-dynamin antibody (610245; BD Biosciences) and rabbit anti-Myosin IIA antibody (M8064; Sigma-Aldrich) were used at 1:3000, 1:100, 1:125 and 1:400 for Western immunoblotting, respectively. Horseradish peroxidase (HRP)-conjugated goat anti-mouse and anti-rabbit secondary antibodies (KPL) (1mg/mL) were used at 1:30,000. For immunofluorescence (IF) microscopy, all antibodies were diluted 1/100. Rabbit anti-active (cleaved) caspase-3 (AB3623) and rabbit anti-Myosin IIB (M7939) antibodies were purchased from Merck Milipore and Sigma-Aldrich, respectively. Rabbit polyclonal N-WASP antibody was prepared in the laboratory. Secondary antibodies (2 mg/mL; Molecular Probes) used were Alexa Fluor 594-conjugated donkey anti-

rabbit, Alex Fluor 594-conjugated donkey anti-mouse and Alexa Fluor 488-conjugated donkey anti-rabbit IgG.

2.1.4 Transfection

All siRNAs were purchased from Thermo Scientific and were prepared as a 5 µM stock with DEPC-treated water (AM9915G, Invitrogen). The ON-TARGETplus SMARTpool Human siRNAs used in this study were DNM2 (L004007-00-0005), DNM1L (L012092-00-0005) and MYH9 (L-007668-00-0005). Control siRNAs used were ON-TARGETplus Non-targeting Pool (D-001810-10-05) and siGLO Green Transfection Indicator (D-001630-01-05). DharmaFECT 3 Transfection Reagent (T-2003-03) and DharmaFECT Cell Culture Reagent (DCCR; B-004500-100) were also purchased from Thermo Scientific.

2.2 Bacterial strains, plasmids and growth conditions

2.2.1 Bacterial strains and plasmids

Bacterial strains (*E. coli*, *S. flexneri* and *L. monocytogenes*) and plasmids created and/or used in this study are detailed in Table 2.2. Virulence plasmid-cured (VP^{-}) derivative of WT *S. flexneri* strain was isolated on Congo Red agar as white colonies and re-streaked until pure (Morona & Van Den Bosch, 2003).

2.2.2 Growth media and conditions

Bacterial strains were maintained in a suspension of 30% (v/v) glycerol and 1% (w/v) peptone (Difco) in glass vials (Wheaton) for long-term storage at -80ºC. Bacterial strains were cultivated for 16 h at 37°C in Luria Bertani (LB) broth (10 g/L Bacto Tryptone Peptone [BD], 5 g/L yeast extract [Difco], 5 g/L NaCl). For *E. coli* growth on solid media, 15 g/L Bacto-agar (BD) was added to LB. In order to confirm the maintenance of the *Shigella* virulence plasmid, strains were grown on tryptic soy agar (TSA) (30 g/L Tryptic Soy Broth [BD], 15 g/L Bacto Agar [BD]) supplemented with 0.01% (w/v) Congo Red solution and incubated at 37ºC. Congo Red binds to proteins expressed from the virulence plasmid, thus imparting a deep red colour to the colonies. Conversely virulence-plasmid negative colonies appeared white. Where appropriate, Gentamicin (Gm), Kanamycin (Km) and Tetracycline (Tc) were added at 50 µg/mL and 10 µg/mL, respectively. For subcultures, Tc was added at 4 µg/mL. SOC (20

g/L tryptone [BD], 5 g/L yeast extract, 20 mM glucose, 8.6 mM NaCl, 2.5 mM KCl, 20 mM $MgSO_4$) was used to cultivate bacteria following electroporation.

2.3 Nucleic acid methods

2.3.1 Plasmid preparation

Plasmid DNA from bacterial cultures was isolated with the QIAprep spin miniprep kit (Qiagen) as per manufacturer's instructions.

2.3.2 Preparation of electrocompetent *E. coli* and *S. flexneri*

A 10 mL overnight culture of *S. flexneri* or *E. coli* was sub-cultured 1:20 in LB broth and grown for 2 h before centrifugation (13,000 rpm, 10 min, 4ºC, Eppendorf Centrifuge 5415R). Bacterial pellets were washed twice by resuspension in 1 mL of ice-cold MQ water and centrifuged as before. Bacteria were washed twice by resuspension in 1 mL of ice-cold 10% (v/v) glycerol and centrifuged as before. Washed pellets were resuspended in 100 µL of 10% (v/v) glycerol. 100 µL aliquots of the suspension were stored at -80ºC until required.

2.3.3 Electroporation

A 100 µL aliquot of electrocompetent cells was thawed on ice and an electroporation cuvette (2 mm electrode gap; Bio-Rad) was chilled. 1 µL of plasmid DNA (Section 2.3.1) and cells were electroporated (Bio-Rad Gene Pulser, 1.8 kV, 25 µF, Pulse Controller 200 Ω) in the cold cuvette, with resultant time constants of 4.4-5.0 msec. The cells were added to 1 mL of SOC (Section 2.2.2) and incubated with aeration for 1 h at 37ºC. The cells were pelleted by centrifugation (13,000 rpm, 1 min, RT, Eppendorf Centrifuge 5415R) and the supernatant was removed by gentle tapping into a waste container. The pellet was resuspended in the remaining 100 µL supernatant and was plated on LB agar with appropriate antibiotics (depending on the antibiotic resistance of the plasmid) and incubated for 16 h at 37ºC.

2.4 Protein techniques

2.4.1 Preparation of HeLa lysate extracts

Cell lysates of re-transfected HeLa cells in 12-well trays (Section 2.5.11.1) were extracted as described by Qualmann and Kelly (2000) with some modifications. The monolayers were washed with PBS for 15 - 20 min, dislodged with 110 µL 0.1% trypsin [w/v] in 0.02% [w/v] EDTA/PBS and resuspended in 190 µL PBS. The cells were centrifuged (3,500 rpm, 5 min, RT, Eppendorf 5415R) and the supernatant was discarded. The pellet was resuspended in 80 µL 0.1 % (v/v) Triton X-100 in lysis buffer A (10 mM Hepes pH 7.4, 150 mM NaCl, 1 mM EGTA, 0.1 mM $MgCl_2$) supplemented with protease inhibitors (5 µg/mL pepstatin, 10 µg/mL aprotinin, 10 µg/mL chymostatin, 1 mM PMSF). The cells were incubated for 30 min at 4 °C (ice bucket) to allow cell lysis. The lysed cells were ultracentrifuged (25,000 rpm, 30 min, 4°C, Beckman OptimaTM MAX-UP Ultracentrifuge). The supernatant was collected and mixed with 80 µL 2× Sample buffer (0.125 M Tris-HCl, pH 6.8, 4% [w/v] SDS, 20% [v/v] glycerol, 10% [v/v] β-mercaptoethanol, 0.04% [w/v] Bromophenol blue), and stored at -20°C.

2.4.2 SDS-PAGE

Samples for sodium dodecyl sulfate-polyacrylamide gel electrophoresis (SDS-PAGE) analysis were heated at 100ºC for 5 min prior to loading. The SDS-PAGE gel apparatus used was Bio-Rad Mini-Protean System III. SDS-PAGE was performed by electrophoresing samples through 12% (v/v) acrylamide gels in PAGE running buffer (0.025 M Tris-HCl, 0.2 M glycine, 0.1% [w/v] SDS) at 200 V for 1 h. Proteins were visualised by Western immunoblot analysis (Section 2.4.3). Benchmark^{TM} pre-stained standard (Invitrogen; 190 kDa, 120 kDa, 85 kDa, 60 kDa, 50 kDa, 40 kDa, 25 kDa, 20 kDa, 15 kDa, 10 kDa) was included to allow estimation of protein molecular mass.

2.4.3 Western transfer and detection

Proteins separated by SDS-PAGE (Section 2.4.2) were transferred to a membrane (Nitrobind 0.45 micron pure nitrocellulose [Bio-Rad]) for 2 h at 200 mA in transfer buffer (3.06 g/L Tris, 0.2 M glycine, 5% [v/v] methanol). The membrane was blocked for 1 h with 5% (w/v) skim

milk in TTBS (2.4 g/L Tris, 0.12 M NaCl, 0.05% [v/v] Tween 20 [Sigma]), followed by incubation with the desired primary antibody (Section 2.1.3) in 0.02% (w/v) skim milk in TTBS for 16 h. After three 10 min washes in TTBS, the membrane was incubated with HRP-conjugated goat anti-rabbit or a HRP-conjugated goat anti-mouse secondary antibodies (Biomediq DPC) in 0.02% (w/v) skim milk in TTBS for 2 h. The membrane was washed three times in TTBS, followed by three washes with TBS (2.4 g/L Tris, 120 mM NaCl). For detection of protein bands, the membrane was incubated with Chemiluminescent Peroxidase Substrate-3 (Sigma) for 5 min. Chemiluminescence was detected by exposure of the membrane to X-ray film (AGFA). The film was developed with the Curix 60 automatic X-ray film processor (AGFA).

2.5 Tissue culture

2.5.1 Growth and maintenance of HeLa monolayers

Human cervical cancer cell line, HeLa was grown and maintained in Minimum Essential Medium (MEM) (Gibco, catalogue #11095-080), supplemented with 10% (v/v) foetal calf serum (FCS), 100 U/mL penicillin/streptomycin in 0.85% (v/v) saline and 2 mM L-glutamine (replaced every 7 days). HeLa cells were grown and maintained at 37°C in a humidified chamber with 5% CO_2.

2.5.2 Splitting and seeding HeLa cells

HeLa cells were grown to ~70 - 90% confluency in 75 cm^2 culture flasks (Corning) for long term maintenance. HeLa cells were seeded by washing the cells in PBS for 5-10 min, followed by incubation in 1.5 mL 0.1% (w/v) trypsin containing 0.02% (w/v) EDTA in PBS for 5 min. Dislodged cells were resuspended in 10 mL tissue culture media and 1 mL of cells were seeded into a new 75 cm^2 flask.

For tissue culture experiments, HeLa cells were split as above and diluted 1/5 in Trypan Blue (20 µL cells in 80 µL Trypan Blue) before counting in a haemocytometer (Weber). For plaque assay (*Shigella* and *Listeria*) (Section 2.5.4) and infectious focus assay (Section 2.5.5), 1.2×10^6 cells were seeded in each 9.6 cm^2 well in a 6-well tray (Corning) in 5 mL media/well to achieve confluent cells the next day. For invasion assay (Section 2.5.6),

MitoTrackerRed® CMXRos labelling (Section 2.5.7) and protrusion formation (Section 2.5.8), 8×10^4 cells were seeded on sterile round cover slips in each 2.0 cm^2 well in a 24-well tray (Corning) in 0.5 mL media/well to obtain semi-confluent cells the next day. For assay for growth of intracellular bacteria (Section 2.5.12), 8×10^4 cells were seeded in each 2.0 cm^2 well in a 24-well tray (Corning) in 0.5 mL media/well to obtain semi-confluent cells the next day. For lactate dehydrogenase (LDH) cytotoxicity assay (Section 2.5.9), 3×10^4 cells were seeded in each 0.32 cm^2 well in a 96-well tray (Corning) in 100 µL media/well to achieve confluent cells the next day for *Shigella* infection and 3.5×10^4 cells were seeded for *Listeria* infection. For reverse transfection (Section 2.5.10), 2.5×10^5 cells were seeded in each 3.2 cm^2 well in a 12-well tray (Corning) in 1.2 mL DCCR, DharmaFect 3 and siRNA mixture/well to achieve semi-confluent cells the next day.

2.5.3 Bacterial preparation for infection

Overnight cultures (16 h) were diluted 1:20 in 10 mL LB broth, and grown for 1.5 h at 37°C with aeration. For plaque assay (Section 2.5.4) and infectious focus assay (Section 2.5.5), the equivalent of 1×10^8 bacteria/mL was centrifuged (13,000 rpm, 1 min, RT, Eppendorf Centrifuge 5415R), resuspended in 1 mL of serum/antibiotic-free DMEM, and diluted 1:1000 in DMEM prior to infection. For invasion assay (Section 2.5.6), Mitotracker® Red CMXRos labelling (Section 2.5.7), protrusion formation (Section 2.5.8) and assay for growth of intracellular bacteria (Section 2.5.12), the equivalent of 1×10^9 bacteria/mL was centrifuged as above and resuspended in 1 mL of D-PBS (Dulbecco's PBS; PBS containing 0.1% [w/v] $CaCl_2$ and 0.1% [w/v] $MgCl_2$). For plaque assay and infectious focus assay using transfected cells (Sections 2.5.11.2 and 2.5.11.3, respectively), the equivalent of 1×10^8 bacteria/mL was centrifuged as above, resuspended in 1 mL of serum and antibiotic-free DMEM and diluted 1:100 in DMEM prior to infection. For LDH cytotoxicity assay using non-transfected (Section 2.5.9) and transfected cells (Section 2.5.11.5), the equivalent of 3×10^8 bacteria/mL was centrifuged as above and resuspended in 1 mL of PBS.

2.5.4 Plaque assay

Plaque assays were performed with HeLa cells as described previously by Oaks *et al.* (1985) with modifications. A confluent monolayer of cells in 6-well tray (Section 2.5.2) was washed twice with serum/antibiotic-free Dulbecco's modified Eagle medium (DMEM) prior to

inoculation with 0.25 mL of 1:1000 bacterial suspensions prepared in Section 2.5.3. Trays were incubated at 37°C, 5% CO_2 and were rocked gently every 15 min to spread the inoculum evenly across the well. At 90 min post-infection, the inoculum was carefully aspirated. 3 mL of the first overlay (DMEM, 5% [v/v] FCS, 20 µg/mL gentamicin, 0.5% agarose [w/v] [Seakem ME]) was added to each well. When applicable, 0.1 - 0.2 % DMSO (v/v) and specific chemicals were added and were swirled gently to ensure even distribution. The second overlay (DMEM, 5% [v/v] FCS, 20 µg/mL gentamicin, 0.5% agarose [w/v] [Seakem ME], 0.01% [w/v] Neutral Red [Sigma] in 1% [v/v] glacial acetic acid) was added 48 h post-infection and digital photo images were taken 6 h later.

2.5.5 Infectious focus assay

Shigella infectious focus analysis was carried out similar to the plaque assay with the following modifications. The monolayers were infected with strain MLRM107 expressing red fluorescent protein (mCherry). At 90 min post-infection, the inoculum was carefully aspirated. 3 mL of DMEM (phenol red-free) (31053-028; Life Technologies) supplemented with 1 mM sodium pyruvate, 5% (v/v) FCS, 20 µg/mL gentamicin and 2 mM IPTG (isopropyl β-D-1-thiogalactopyranoside) was added to each well. When applicable, 1 % (v/v) DMSO and specific chemicals were added and were swirled gently to ensure even distribution. 24 h later the infectious foci were examined by microscopy as described in Section 2.6.2.

2.5.6 Invasion assay and immunofluorescence (IF) microscopy

Invasion assay with *Shigella* strains was performed as described by Morona *et al.* (2003). Briefly, cells were grown to semi-confluence on 13 mm glass cover slips as described in Section 2.5.2, washed twice with D-PBS and once with antibiotic-free MEM containing 10% (v/v) FCS prior to bacterial infection. 40 µL of bacterial suspension (Section 2.5.3) was added into each well. Infected monolayers were centrifuged (2000 rpm, 7 min, RT, Heraeus Labofuge 400R Centrifuge) to allow bacteria attachment to the monolayers, followed by incubation at 37°C in a humidified 5% CO_2 incubator for 1 h. The infected cells were washed thrice with D-PBS and incubated with 0.5 mL MEM containing 40 µg/mL of gentamicin for a further 1.5 h. When applicable, specific chemicals and/or solvents were added and were swirled gently to ensure even distribution. HeLa cells were washed thrice with D-PBS, fixed

in 3.7% (v/v) formalin for 15 min, incubated with 50 mM NH_4Cl in D-PBS for 10 min, followed by permeabilisation with 0.1% (v/v) Triton X-100 for 5 min. After blocking with 10% (v/v) FCS in PBS, the infected cells were incubated at 37°C for 30 min with the desired primary antibody (Section 2.1.3). HeLa cells were washed thrice. The appropriate secondary antibody, either Alexa Fluor 594-conjugated donkey anti-rabbit or Alex 594-conjugated donkey anti-mouse (Molecular Probes); diluted 1:100 in PBS with 10% (v/v) FCS and Alexa Fluor 488-conjugated phalloidin (for F-actin staining) were added and incubated at 37°C for 1 h. After the incubation, the monolayers were washed thrice with PBS, incubated with 10 µg/mL 4',6'-diamidino-2-phenylindole (DAPI; Sigma) in MQ water (for bacteria and HeLa cell nuclei staining) for 1 min 25 sec at RT, followed by two washes with PBS and one wash with MQ water. The cover slips were mounted onto glass slides and examined by IF microscopy as described in Sections 2.6.1.1 and 2.6.2.

2.5.7 MitoTracker® Red CMXRos labelling

HeLa cells were seeded and infected as described in Section 2.5.6. The infected cells were washed thrice with D-PBS and incubated with 0.5 mL MEM containing 40 µg/mL of gentamicin for 2 h 55 min. The media was removed and replaced with pre-warmed 400 nM MitoTracker® Red CMXRos (Invitrogen) in 200 µL MEM, 40 µg/mL gentamicin for 35 min. HeLa cells were washed thrice with pre-warmed D-PBS, fixed in pre-warmed 3.7% (v/v) formalin for 15 min, followed by three washes with pre-warmed PBS. Bacteria and HeLa cell nuclei were stained with 10 µg/mL DAPI in MQ water for 1 min 25 sec at RT, followed by two washes with pre-warmed PBS and one wash with pre-warmed MQ water. The cover slips were mounted onto glass slides and examined by IF microscopy as described in Sections 2.6.1.1 and 2.6.2.

2.5.8 Protrusion formation

HeLa cells were seeded, infected and fixed as described in Section 2.5.6. HeLa cells were washed twice with 1× Annexin V binding buffer prepared in MQ water (99902; Biotium), mounted on glass slides with the same buffer and were examined with an Olympus IX-70 microscope with phase-contrast optics using a 40× oil immersion objective. Protrusion formation was defined as extensions of bacterial projection(s) (minimum of a full bacterial length) beyond the periphery of the HeLa cell.

2.5.9 Lactate dehydrogenase (LDH) cytotoxicity assay

HeLa cell death was assayed by measuring the release of LDH into the culture medium. Cells were grown to confluence in each 0.32cm^2 well in a 96-well tray (Corning) as described in Section 2.5.2 and were washed twice with PBS prior to bacterial infection. 50 µL of bacterial suspension in PBS (Section 2.5.3) and 50 µL phenol-red free DMEM (Life Technologies, catalogue #31053-028), 1 mM sodium pyruvate was added into each well. Infected monolayers were centrifuged (2000 rpm, 7 min, RT, Heraeus Labofuge 400R Centrifuge) to allow bacteria attachment to the monolayers, followed by incubation at 37°C in a humidified 5% CO_2 incubator for 1 h. The infected cells were washed thrice with PBS and incubated with 100 µL phenol-red free DMEM, 1 mM sodium pyruvate, 40 µg/mL of gentamicin for 4 h. When applicable, 1% (v/v) DMSO and specific chemicals were added and swirled gently to ensure even distribution. LDH activity was measured with the Cytotoxicity Detection Kit^{Plus} as per manufacturer's instructions (Roche). The percentage of LDH released was calculated with the following formula: ((experimental LDH release − spontaneous LDH release)/(maximal LDH − spontaneous LDH release)) × 100.

2.5.10 siRNA reverse transfection of HeLa cells

Reverse transfection of HeLa cells was carried out based on a method by Thermo Scientific. siRNA were prepared as a 5 µM stock and the final concentration was 50 nM. 12 µL siRNA was mixed gently with 6 µL DharmaFect 3 and 282 µL DCCR in a tube and was transferred to a single well (3.8 cm^2) in a 12-well tray (Tray 1) and was incubated for 40 min at RT. 2.5 × 10^5 HeLa cells in 0.9 mL MEM, 10% (v/v) FCS were added to each well, bringing the total volume to 1.2 mL. For HeLa cell lysate extract preparation (Section 2.5.11.1), plaque assay (Section 2.5.11.2) and infectious focus assay (Section 2.5.11.3), two wells were prepared for each siRNA. For invasion assay, IF microscopy and MitoTracker® Red CMXRos labelling (Section 2.5.11.4), and LDH assay (Section 2.11.5), one well was prepared for each siRNA. The tray was incubated overnight at 37°C, 5% CO_2. HeLa cells were re-transfected on day 2.

2.5.11 siRNA re-transfection for HeLa cell assays

2.5.11.1 HeLa cell lysate extracts for Western immunoblotting

For re-transfection on day 2, the siRNA:DharmaFect 3: DCCR mixture (Tray 2) was prepared as described in Section 2.5.10 in a 12-well tray. One well was prepared for each well of HeLa cells that were transfected on day 1. The HeLa cells that had been transfected the day before (Tray 1) were washed with PBS for 15 - 20 min, trypsinised (110 µL 0.1% [w/v] trypsin/0.02% [w/v] EDTA/PBS) for 5 min and resuspended in 190 µL MEM, 10% (v/v) FCS. This cell suspension and 600 µL MEM, 10% (v/v) FCS were added to the DCCR mixture in Tray 2, bringing the total volume to 1.2 mL. The tray was incubated overnight at 37°C, 5% CO_2. On day 3, HeLa cell lysate extracts were prepared as described in Section 2.4.1.

2.5.11.2 Plaque assay

For re-transfection on day 2, a single tube containing 12 µL siRNA was mixed gently with 6 µL DharmaFect 3 and 282 µL DCCR and was transferred to a single well (3.8 cm^2) in a 12-well tray (Tray 2) and was incubated for 40 min at RT. The HeLa cells from the two wells that had been transfected the day before (Tray 1) were washed with PBS for 15 - 20 min, trypsinised (110 µL 0.1% [w/v] trypsin/0.02% [w/v] EDTA/PBS) for 5 min and resuspended in 190 µL MEM, 10% (v/v) FCS. The trypsinised HeLa cells were combined with 300 µL MEM, 10% (v/v) FCS and were added to the DCCR mixture in Tray 2 bringing the total volume to 1.2 mL. The tray was incubated overnight at 37°C, 5% CO_2. On day 3, the media in the wells were replaced with fresh MEM, 10% (v/v) FCS. On day 4, plaque assay was carried out on confluent HeLa cells as described in Section 2.5.4 with the following modifications. 5 x 10^4 log phase bacteria in 150 µL DMEM were added to each well. The volume of the first overlay was reduced to 0.5 mL. On day 5, 0.5 mL of the second overlay was added and plaques were imaged 6 h later with a digital camera.

2.5.11.3 Infectious focus assay

Re-transfection was carried as per Section 2.5.11.2. Infectious focus assay was carried out on day 3 as described in Section 2.5.5 with the following modifications. 5 x 10^4 log phase bacteria expressing red fluorescent protein (mCherry) in 150 µL DMEM were added to each

well. 1 mL of DMEM (phenol red-free), 1 mM sodium pyruvate, 5% (v/v) FCS, 20 µg/mL gentamicin, 2 mM IPTG was added to each well to induce mCherry expression. The infectious foci were examined by microscopy as described in Section 2.6.2.

2.5.11.4 Invasion assay, IF microscopy and MitoTracker® Red CMXRos labelling

For re-transfection on day 2, a single tube containing 6 µL siRNA was mixed gently with 3 µL DharmaFect 3 and 141 µL DCCR and was transferred to a single 2.0 cm^2 well in a 24-well tray with sterile 13 mm glass cover slips (Tray 2) and was incubated for 40 min at RT. The HeLa cells from one well that had been transfected the day before (Tray 1) were washed with PBS for 15 - 20 min, trypsinised (110 µL 0.1% [w/v] trypsin/0.02% [w/v] EDTA/PBS) for 5 min and resuspended in 190 µL MEM, 10% (v/v) FCS, bringing the total volume to 300 µL. 240 µL of this cell suspension was combined with 210 µL MEM, 10% (v/v) FCS and were added to the DCCR mixture in Tray 2 bringing the total volume to 600 µL. The tray was incubated overnight at 37°C, 5% CO_2. On day 3, invasion assay and IF microscopy or MitoTracker® Red CMXRos labelling was carried out as described in Section 2.5.6 and Section 2.5.7, respectively.

2.5.11.5 LDH cytotoxicity assay

Re-transfection on day 2 was based on a method by Thermo Scientific. 1.8 µL DharmaFect 3 was diluted by adding 373.2 µL DCCR bringing the total volume to 375 µL. In three separate tubes, 100 µL diluted DharmaFect 3 and 0.25 µL siRNA stock solutions were mixed. 25 µL of the siRNA:DharmaFect 3 complex was transferred into triplicate 0.32cm^2 wells in a 96-well tray and was incubated for 40 min at RT. The HeLa cells from one well that had been transfected the day before (Tray 1) were washed with PBS for 15 - 20 min, trypsinised (110 µL 0.1% [w/v] trypsin/0.02% [w/v] EDTA/PBS) for 5 min and resuspended in 190 µL MEM, 10% (v/v) FCS, bringing the total volume to 300 µL. 500 µL MEM, 10% (v/v) FCS was added to the cell suspension, bringing the total volume to 800 µL. 100 µL of the cell suspension was added to each well containing the siRNA:DharmaFect 3 complex, bringing the total volume to 125 µL. The tray was incubated overnight at 37°C, 5% CO_2. On day 3, LDH cytotoxicity assay was carried out as described in Section 2.5.9.

2.5.12 Assay for growth of intracellular bacteria

The invasion efficiency of bacteria in the presence of specific inhibitors was measured with a gentamicin protection assay. Cells were grown to semi-confluence in each 2.0 cm^2 well in a 24-well tray (Corning) as described in Section 2.5.2, washed twice with D-PBS and once with antibiotic-free MEM containing 10% (v/v) FCS prior to bacterial infection. 40 µL of bacterial suspension (Section 2.5.3) was added into each well. Infected monolayers were centrifuged (2000 rpm, 7 min, RT, Heraeus Labofuge 400R Centrifuge) to allow bacteria attachment to the monolayers, followed by incubation at 37°C in a humidified 5% CO_2 incubator for 1 h. The infected cells were washed thrice with D-PBS and incubated with 0.5 mL MEM containing 40 µg/mL of gentamicin. For each condition, duplicate wells were prepared for each time point. When applicable, 1% (v/v) DMSO and specific chemicals were added and swirled gently to ensure even distribution. After 1, 2, 4 or 6 h incubation, the medium was removed; cells were washed four times with PBS. 500 µL 0.1% (v/v) Triton X-100 in PBS were added in each well to lyse the cells. The lysed cells were diluted 1/1000 with PBS and 50 µL of the bacterial solution was plated onto one half of a TSA agar plate and incubated overnight at 37°C. The number of viable bacteria was enumerated the next day.

2.6 Microscopy and imaging

2.6.1 Mounting medium

2.6.1.1 IF microscopy

Mowiol 4-88 for mounting medium was prepared by mixing 0.4 g of Mowiol 4-88 (Calbiochem), 1 g of glycine and 1 mL MQ water. This was incubated for 2 h at 56°C prior to the addition of 2 mL of 0.2 M Tris-HCl pH 8.5 and heating at 50°C for at least 10 min or more until it was dissolved. The mixture was centrifuged at 5000 × *g* for 15 min to remove any remaining solids and the supernatant was collected and stored at 4°C. A fresh stock of *ρ*-phenylenediamine (PPD; Sigma) was prepared each time at 25 mg/mL in ethanol. The stock was vortexed and centrifuged (13,000 rpm, 1 min, RT, Eppendorf 5417R) to remove undissolved PPD. The PPD solution was added to Mowiol 4-88 at a ratio of 1:5 (PPD:Mowiol). This mounting medium was vortexed and centrifuged (13,000 rpm, 1 min,

RT, Eppendorf 5417R) to remove any bubbles. Coverslips were mounted (cell-side down) onto glass slides with 4 μL of mounting medium and the edge was sealed with nail polish.

2.6.1.2 Protrusion formation

Coverslips were mounted (cell-side down) onto glass slides with 2.5 μL 1× Annexin V binding buffer and the edge was sealed with nail polish.

2.6.2 Microscopy

Microscopy was performed with an Olympus IX-70 microscope with phase-contrast optics and fluorescence imaging. The filter set used was DA/FI/TX-3X-A-OMF (Semrock). For the infectious focus assay, individual infectious focus was imaged with a 10× objective. IF images were taken with a 100× objective. For protrusion formation, cells were imaged with a 40× objective. Fluorescence and phase contrast images were false colour merged with the Metamorph software programme (Version 7.7.3.0, Molecular Devices).

2.6.2.1 Indirect quantification of protein levels by IF

Indirect immunofluorescence was quantified with Metamorph to determine protein levels in bacteria-infected HeLa cells compared to uninfected HeLa cells. Invasion assay and IF microscopy was carried out as described in Section 2.5.6. Cells were imaged with a 40× objective. In each image, the maximum fluorescence (100%) was determined by the mean fluorescence of uninfected HeLa cells (2 - 3 cells). Infected and uninfected cells were selected by tracing and the mean fluorescence of the outlined area was determined with Metamorph. HeLa cells exhibited two distinct immunofluorescence staining patterns (high and low) when infected compared to uninfected HeLa cells. In such instances, the HeLa cells were arbitrarily assigned into distinct populations, before the level of fluorescence of the infected cell was determined. The fluorescence of ≥100 infected cells for each category was measured for each experiment.

2.7 Animal studies

The use of animals in this study has been approved by the University of Adelaide Animal Ethics Committee (Project number: S-2012-90). All animals used were handled in compliance with the *Australian code of practice for the care and use of animals for scientific purposes, 7th edition (2004).*

2.7.1 Preparation of bacterial stocks for ocular infection

Bacterial broths were prepared by inoculating a loop of bacteria from the glycerol stock into pre-warmed 10 mL LB broth. A 1/8 dilution was also prepared in pre-warmed LB. After 7 h incubation at 37°C, the optical density (OD_{600}) and the concentration of the bacteria was determined; an OD_{600} reading between 0.6 - 1.0 is desirable. The estimate of the bacteria count was determined by multiplying the reading from the spectrophotometer by 0.6. Estimated 1×10^5, 3×10^4 and 1×10^4 bacteria in 100 µL LB was subsequently spread onto three separate LB agar plates and was incubated for 17 h at 37°C. On day 2, the LB agar plate with approximately 50% confluency was selected for harvesting bacteria. 5 mL of pre-warmed LB broth was added to the agar plate and the bacteria were gently resuspended into the LB broth with a sterile spreader. The LB agar plate was gently tilted and the top 2 mL was removed carefully with a pipette into a 10 mL yellow cap tube. The bacterial suspension was allowed to stand for 2 min at RT to allow for bacterial clumps to collect at the bottom of the tube. Subsequently 1.05 mL of the bacterial suspension was removed carefully from the top of the meniscus into a 1.5 mL reaction tube. 50 µL of the bacterial suspension was added to 950 µL LB broth and the OD_{600} was determined. The estimate of the bacteria count in 50 µL was determined by multiplying the reading from the spectrophotometer by 1.5. This approximation was multiplied by 20 to estimate bacteria count in 1 mL broth. The remaining 1 mL bacteria suspension was centrifuged (13,000 rpm, 2.5 min, RT, Eppendorf 5417R) and resuspended in an appropriate volume to achieve a concentration of 1×10^{11} bacteria/mL. 5 µL or the equivalent of 5×10^8 bacteria was used to infect the mice. A 1/20 dilution of the bacteria stock was diluted in pre-warmed LB to achieve the equivalent of 2.5×10^7 bacteria in 5 µL.

2.7.2 Ocular infection and intraperitoneal (IP) injections of Balb/c mice

6 - 8 weeks old (~20 - 22 g) male BALB/c mice were used. Under anaesthesia (Attane™ Isoflurane; Bomac), the left eye of the mice were treated with 2 × 2.5 µL of warm LB broth (control) and the right eye was infected with 2 × 2.5 µL of bacteria (approximately 5×10^8 or 2.5×10^7 bacteria) that was prepared in Section 2.7.1. Mice were given 100 µL intraperitoneal (IP) injections of NMP/PEG or drugs at specific time points. The mice were also weighed at the start (D0) and at the end of the experiment (D3). In later experiments, mice were weighed daily throughout the experiment (D1, D2, D3).

2.7.3 Scoring of ocular inflammation

Infected mice were scored daily in the morning or were scored each time when IP injections were administered. A score of 0 is defined as no infection. Mouse keratoconjunctival inflammation was defined as follows: a score of 1 is defined as mild keratoconjunctivitis where the eye lid is slightly swollen, a score of 2 is defined as mild keratoconjunctivitis where the eye is half closed, and a score of 3 is defined as fully developed keratoconjunctivitis where the eye is completely closed.

2.7.4 Sectioning and H&E staining of mice eyes and eye lids

For histopathological observation, the infected right eye and eye lids, and uninfected left eye and eye lids mice were removed and fixed in 4% (v/v) buffered formaldehyde overnight and embedded in paraffin. Sections were stained with hematoxylin plus eosin. Sectioning and staining were performed by the Ophthalmic Research Laboratories, Centre for Neurological Diseases, Adelaide, Australia.

2.8 Statistical analysis

Statistical analysis was carried out using GraphPad Prism 6. Results are expressed as means ± SEM of data obtained in independent experiments. Statistical differences between two groups were determined with a two-tailed unpaired *t*-test. Statistical differences between three or more groups were determined with a one-way ANOVA followed by Tukey's or Dunnett's multi comparison post hoc test. Statistical significance was set at $p < 0.05$.

Table 2.1 Chemicals used in this study

Chemical	Stock concentration	Source
(-)-Blebbistatin	50 mM	Merck Calbiochem (203391-1MG)
(+)-Blebbistatin	50 mM	Merck Calbiochem (203392-1MG)
Dynasore	80 mM	Exclusive Chemistry (EC-000.2052)
		Sigma-Aldrich (D7693-25MG)
		Abcam (ab120192)
IM-54	5 mM	Enzo Life Sciences (ALX-430137-M001)
Mdvi-1	50 mM	Sigma-Aldrich (M0199-25MG)
		Enzo Life Sciences (BML-CM127-0050)
ML-7	30 mM	Sigma-Aldrich (I2764-5MG)
ML-9	100 mM	Sigma-Aldrich (C1172-5MG)
Necrostatin-1	100 mM	Sigma-Aldrich (N9037)
Necrostatin-7	20 mM	Enzo Life Sciences (ALX-430-170-M00)
Necrosulfonamide	20 mM	Toronto Research Chemicals (N388600)
NecroX-2	5 mM	Enzo Life Sciences (ALX-430-166-M00)
NecroX-5	5 mM	Enzo Life Sciences (ALX-430-167-M00)
Staurosporine (STS)	10 mM	Biotium (00025)
Z-FA-fmk	20 mM	BD Biosciences (550411)
Z-VAD(OMe)-fmk	20 mM	Merck Calbiochem (627610-1MG)

Table 2.2 Plasmids and bacterial strains used in this study

Plasmid or strain	Description	Source
Plasmid		
pMP7604	Broad host range vector, pME6031 [*mCherry*; Tc^R]	(Lagendijk *et al.*, 2010)
pMP7605	Broad host range vector, pME6031 [*mCherry*; Gm^R]	(Lagendijk *et al.*, 2010)
pMP7607	Broad host range vector, pME6031 [*mCherry*; Km^R]	(Lagendijk *et al.*, 2010)
Strain		
***E. coli* K-12**		
DH5α	F^- φ80*lacZ*ΔM15 Δ(*lac*ZYA-*arg*F)U169 *rec*A1 *end*A1 *hsd*R17(rk^-, mk^+) *pho*A*sup*E44 *thi*-1 *gyr*A96 *rel*A1 λ-	GIBCO-BRL
MLRM101	DH5α [pMP7604; Tc^R] (I)	This study
MLRM102	DH5α [pMP7604; Tc^R] (II)	This study
MLRM103	DH5α [pMP7605; Gm^R] (I)	This study
MLRM104	DH5α [pMP7605; Gm^R] (II)	This study
MLRM105	DH5α [pMP7607; Km^R] (I)	This study
MLRM106	DH5α [pMP7607; Km^R] (II)	This study
L. monocytogenes		
DRDC8	Dairy isolate	(Francis & Thomas, 1996)
S. flexneri		
2457T	*S. flexneri* serotype 2a	Laboratory collection
MLRM107	2457T [pMP7604; Tc^R] (I)	This study
MLRM108	2457T [pMP7604; Tc^R] (II)	This study

(continued over page)

Table 2.2 Plasmids and bacterial strains used in this study *(continued)*

Plasmid or strain	Description	Source
Strain		
S. flexneri		
MLRM109	2457T [pMP7605; Gm^R] (I)	This study
MLRM110	2457T [pMP7605; Gm^R] (II)	This study
MLRM111	2457T [pMP7607; Km^R] (I)	This study
MLRM112	2457T [pMP7607; Km^R] (II)	This study
RMA723	2457T *rmlD*::Km^R	(Van Den Bosch *et al.*, 1997)
RMA2041	2457T Δ*icsA*::Tc^R	(Van Den Bosch & Morona, 2003)
RMA2043	2457T Δ*icsA*::Tc^R Δ*rmlD*::Km^R	(Van Den Bosch & Morona, 2003)
RMA2159	Virulence plasmid-cured 2457T	Laboratory collection

MANUSCRIPTS

ꕥ CHAPTER 3 ꕥ

IMPACT OF DYNASORE AN INHIBITOR OF DYNAMIN II ON *Shigella flexneri* INFECTION

Impact of dynasore an inhibitor of dynamin II on *Shigella flexneri* infection

Mabel Lum, Stephen R. Attridge and Renato Morona

School of Molecular and Biomedical Science, University of Adelaide, Adelaide, South Australia, Australia

Lum M, Attridge SR & Morona R (2013). Impact of dynasore an inhibitor of dynamin II on *Shigella flexneri* infection. *PLoS One* 8, e84975.

STATEMENT OF AUTHORSHIP

Title of Paper	Impact of dynasore an inhibitor of dynamin II on *Shigella flexneri* infection
Publication Status	○ Published ○ Accepted for Publication ○ Submitted for Publication ○ Publication Style
Publication Details	Lum M, Attridge SR & Morona R (2013). Impact of dynasore an inhibitor of dynamin II on *Shigella flexneri* infection. *PLoS One* 8, e84975.

Author Contributions

By signing the Statement of Authorship, each author certifies that their stated contribution to the publication is accurate and that permission is granted for the publication to be included in the candidate's thesis.

Name of Principal Author (Candidate)	Mabel YT Lum		
Contribution to the Paper	Performed all experiments, performed analysis on all samples, interpreted data, wrote manuscript and acted as corresponding author. Mouse Sereny test experiments, mouse Sereny test data analysis and mouse Sereny test data interpretation were carried out with Stephen R. Attridge.		
Signature		Date	

Name of Co-Author	Stephen R. Attridge		
Contribution to the Paper	Carried out mouse Sereny test experiments, mouse Sereny test data analysis and mouse Sereny test data interpretation with Mabel YT Lum and assisted in editing the paper.		
Signature		Date	15/04/14

Name of Co-Author	Renato Morona		
Contribution to the Paper	Supervised development of work, helped in data interpretation, helped to evaluate and edit the manuscript.		
Signature		Date	

Chapter 3: Impact of dynasore an inhibitor of dynamin II on *Shigella flexneri* infection

3.1 Abstract

Shigella flexneri remains a significant human pathogen due to high morbidity among children <5 years in developing countries. One of the key features of *Shigella* infection is the ability of the bacterium to initiate actin tail polymerisation to disseminate into neighbouring cells. Dynamin II is associated with the old pole of the bacteria that is associated with F-actin tail formation. Dynamin II inhibition with dynasore as well as siRNA knockdown significantly reduced *Shigella* cell-to-cell spreading *in vitro*. The ocular mouse Sereny model was used to determine if dynasore could delay the progression of *Shigella* infection *in vivo.* While dynasore did not reduce ocular inflammation, it did provide significant protection against weight loss. Therefore dynasore's effects *in vivo* are unlikely to be related to the inhibition of cell-to-cell spreading observed *in vitro*. We found that dynasore decreased *S. flexneri*-induced HeLa cell death *in vitro* which may explain the protective effect observed *in vivo*. These results suggest the administration of dynasore or a similar compound during *Shigella* infection could be a potential intervention strategy to alleviate disease symptoms.

3.2 Introduction

Shigella flexneri is the etiological agent of bacillary dysentery (shigellosis). It is transmitted via the faecal-oral route and is a significant human pathogen due to the high morbidity among children <5 years in developing countries. Over a period between 1990 - 2009, 125 million shigellosis cases were recorded in Asia, of which ~14,000 were fatal (Bardhan *et al.*, 2010). The lack of a vaccine, an increase in multi-drug resistance and the absence of suitable small animal model to study the infection contribute to the persistence of shigellosis (Barry *et al.*, 2013).

The pathogenic determinants of *S. flexneri* are mainly encoded on the large 200 kb virulence plasmid (VP) (Yang *et al.*, 2005). These proteins are involved in the type three secretion system (TTSS), the modulation of host immune responses, and the mediation of *Shigella* actin-based motility (ABM). *Shigella* bacteria invade the host intestinal epithelium via microfold cells and induce pyroptosis of the resident macrophages in the follicle associated epithelium through caspase-1 activation (Zychlinsky *et al.*, 1992). Caspase-1 activation releases interleukin-1β and interleukin-18, resulting in strong inflammatory responses and magnified innate responses, respectively (Sansonetti *et al.*, 2000). After *Shigella* bacteria are released into the basolateral compartment, *Shigella* bacteria invade enterocytes via the TTSS, followed by lysis of the endocytic vacuole and replication in the cytoplasm (Cossart & Sansonetti, 2004; Sansonetti *et al.*, 1986). The *Shigella* IcsA protein interacts with the host Neural Wiskott-Aldrich syndrome protein (N-WASP) and Arp2/3 complex to initiate F-actin nucleation and polymerisation, leading to ABM and intracellular spreading, and subsequently intercellular spreading via protrusions into adjacent cells. After escaping from the double membrane vacuole, subsequent cycles of infection are initiated (Schuch *et al.*, 1999).

Shigella ABM is dependent on both the 120 kDa outer membrane protein, IcsA (VirG), and the lipopolysaccharide (LPS) structure (Bernardini *et al.*, 1989; Lett *et al.*, 1989; Makino *et al.*, 1986). IcsA is necessary for pathogenesis as Δ*icsA* strains have greatly reduced virulence in human volunteers and in animal infection models (Kotloff *et al.*, 1996; Makino *et al.*, 1986; Sansonetti *et al.*, 1999). Smooth *Shigella* strains express the complete LPS molecule, i.e. the lipid A core, core oligosaccharide and O-antigen subunit. In rough strains

the O-antigen subunit is absent due to mutations in chromosomal genes encoding for LPS synthesis. Rough strains can invade epithelial cells and initiate ABM but have a defect in intercellular spreading (Hong & Payne, 1997; Okamura *et al.*, 1983).

Polarised colonic epithelium cells, the site of *Shigella* infection, are characterised by apical junctional complexes (APCs). APCs consist of tight junctions (TJs), adherens junctions (AJs) and desmosomes at the apical end, and are undercoated with a prominent network of actin-myosin II (actomyosin) ring (Miyoshi & Takai, 2005). Thus for cell-to-cell spreading to occur, the tensions of the actomyosin ring have to be overcome before disruption of the cellular contacts can take place (Rajabian *et al.*, 2009). Components of the AJs and TJs such as L-CAM, α-catenin, β-catenin, α-actinin and vinculin are found at the actin tail of *Shigella* during protrusion formation. L-CAM is important in cell-to-cell spread as it helps to maintain a tight association between the bacterium and the membrane of the protrusions (Kadurugamuwa *et al.*, 1991; Sansonetti *et al.*, 1994). Myosin-X is a component of adherens junctions but are not localised to the *Shigella* actin tail. Knockdown of myosin-X resulted in shortened and thickened protrusion stalks which reduced the bacteria's ability to form plaques (Bishai *et al.*, 2012). *Shigella* invasion and dissemination is also dependent on ATP release by connexin 26, and formins, Dia1 and Dia2 (Heindl *et al.*, 2009; Tran Van Nhieu *et al.*, 2003). Similar to the Arp2/3 complex, formins initiate *de novo* actin polymerisation but can also cross-link actin filaments (Esue *et al.*, 2008). Recent report suggests *Shigella* preferentially translocate between TJs where three epithelial cells meet, a process dependent on the TJ protein, tricellulin (Fukumatsu *et al.*, 2012). Bacteria engulfment, but not protrusion formation into the neighbouring cell is triggered by phosphoinositide 3-kinase and is dependent upon dynamin II, Epsin-1 and clathrin, which are essential components of the clathrin-mediated endocytic pathway (Fukumatsu *et al.*, 2012; McMahon & Boucrot, 2011).

Dynamin II is a 96 kDa protein with an N-terminal guanine triphosphatase (GTPase), a middle domain, a pleckstrin homology (PH) domain, a GTPase effector domain (GED) and a C-terminal proline-rich domain (PRD) (Kessels *et al.*, 2001; McNiven *et al.*, 2000; Muhlberg *et al.*, 1997). It is a cytoplasmic protein but can be membrane bound via interactions between its PH domain which binds phosphatidylinositol 4,5-bisphosphate [$PI(4,5)P_2$] and another region upstream of the PH domain which inserts into the lipid bilayer (Burger *et al.*, 2000). Three members of the family have been identified: dynamin I (neurons), dynamin II

(ubiquitous), and dynamin III (brain, lung and testis) (Cao *et al.*, 1998). Multiple splice variants were also identified for all three dynamin isoforms (Cao *et al.*, 1998). In its native state, dynamin is a dimer. In the presence of GTP, helical dimerisation between adjacent dynamin molecules is thought to drive assembly-stimulated GTPase activity, resulting in constriction of the neck of clathrin-coated vesicles leading to scission (Chappie *et al.*, 2010; Faelber *et al.*, 2011; Ford *et al.*, 2011). The GTPase activity of dynamin I, dynamin II and the mitochondrial dynamin, Drp1 are inhibited by dynasore, a non-competitive reversible inhibitor (Macia *et al.*, 2006). Dynasore has also been shown to have protective effects in various animal models of non-infectious human diseases (Chen *et al.*, 2009; Gao *et al.*, 2013; Terada *et al.*, 2009).

We hypothesized that *S. flexneri* movement from one cell to the next may depend on various components important for endocytosis and/or exocytosis. Hence we investigated the role of dynamin II in *S. flexneri* cell-to-cell spread. In this study dynamin II inhibition with dynasore as well as knockdown with dynamin II siRNA reduced *Shigella* plaque formation. We also investigated if dynamin II is important for *Listeria monocytogenes* cell-to-cell spreading and found that dynamin II inhibition with dynasore reduced *Listeria* plaque formation to a lesser extent. A murine Sereny test was used to determine if dynasore could prevent *Shigella*-induced keratoconjunctivitis. Infected mice treated with the dynasore carrier alone, NMP/PEG, developed a strong inflammatory response and lost significant body weight. Conversely infected mice treated with dynasore lost a significantly smaller portion of body weight but a strong inflammatory response was still observed. If dynasore was inhibiting cell-to-cell spreading, it is expected that the inflammatory response would be lessened. This prompted us to investigate the effect of dynasore on *S. flexneri*-infected HeLa cells in a cytotoxicity assay. Surprisingly at high dynasore concentrations (≥120 μM), HeLa cell death was significantly reduced, which may explain the protective effect observed *in vivo*.

3.3 Materials and methods

3.3.1 Bacterial strains and growth media

The strains and plasmids used in this study are listed in Table 3.1. *Escherichia coli* K-12 strain DH5α was used for routine cloning. All bacterial strains were routinely cultured in Luria Bertani (LB) broth and on LB agar. *S. flexneri* strains were grown from a Congo Red positive colony as described previously (Morona *et al.*, 2003). Bacteria were grown in media for 16 h with aeration, subcultured 1/20 and then grown to mid-exponential growth phase by incubation with aeration for 1.5 h at 37°C. Where appropriate, media were supplemented with tetracycline (4 or 10 μg/mL) or kanamycin (50 μg/mL).

3.3.2 DNA methods

Plasmid pMP7604 confers tetracycline resistant and expresses mCherry under the control of the *tac* promoter (Lagendijk *et al.*, 2010). mCherry expression was induced with 2 mM IPTG. Strain MLRM107 was constructed by electroporation of pMP7604 into 2457T and selected with LB agar supplemented with tetracycline. DNA manipulation, PCR, transformation and electroporation into *S. flexneri* were performed as described previously (Baker *et al.*, 1999; Morona *et al.*, 1995).

3.3.3 Chemicals and antibodies

Dynasore (EC-000.2052; Exclusive Chemistry, D7693-25MG; Sigma-Aldrich, ab120192; Abcam) was prepared as an 80 mM stock in dimethyl sulfoxide (DMSO) (D2650; Sigma-Aldrich) for *in vitro* studies. For *in vivo* studies, dynasore was dissolved in a formulation containing *N*-methyl-2-pyrrolidone (NMP/Pharmasolve; Ashland ISP) and polyethylene glycol 300 (PEG300; Sigma-Aldrich) (1 part NMP to 9 parts PEG300). Chemicals were prepared as a 22 mg/mL stock and diluted 1/4 (5.5 mg/mL) with NMP/PEG before injection into mice. Mouse anti-dynamin antibody (610245; BD Biosciences) was used at 1:125 for Western immunoblotting. Rabbit anti-GAPDH antibody (600-401-A33; Rockland Immunochemicals, Inc.) was used at 1:3000 for Western immunoblotting. For immunofluorescence (IF) microscopy, the anti-dynamin antibody, rabbit polyclonal anti-N-WASP (May & Morona, 2008), Alexa Fluor 488-conjugated donkey anti-rabbit and Alexa

594-conjugated donkey anti-mouse secondary antibody (Molecular Probes) were used at 1:100.

Table 3.1 Bacterial strains and plasmids

Strain or plasmid	Relevant characteristics[#]	Reference or source
Plasmid		
pMP7604	Broad host range vector, pME6031 [*mCherry*; Tc^R]	(Lagendijk *et al.*, 2010)
***E. coli* K-12**		
DH5α	F^- φ80*lac*ZΔM15 Δ(*lac*ZYA-*arg*F)U169 *rec*A1 *end*A1 *hsd*R17(rk^-, mk^+) *pho*A*sup*E44 *thi*-1 *gyr*A96 *rel*A1 λ-	Gibco-BRL
S. flexneri		
2457T	*S. flexneri* 2a wild type	Laboratory collection
MLRM107	2457T [pMP7604; Tc^R]	This study
RMA723	2457T *ΔrmlD*::Km^R	(Van Den Bosch *et al.*, 1997)
RMA2041	2457T *ΔicsA*::Tc^R	(Van Den Bosch & Morona, 2003)
RMA2043	RMA2041 *ΔrmlD*::Km^R	(Van Den Bosch & Morona, 2003)
RMA2159	Virulence plasmid-cured 2457T	Laboratory collection
L. monocytogenes		
DRDC8	Dairy isolate	(Francis & Thomas, 1996)

[#]Km^R, Kanamycin resistant; Tc^R, Tetracycline resistant

3.3.4 Reverse transfection and HeLa cell lysate preparation

DNM2 siRNA (L004007-00-0005) and siRNA controls (Non-targeting Pool; D-001810-10-05, siGLO Green Transfection Indicator; D-001630-01-05) were purchased from Thermo Scientific. siRNAs were transfected with DharmaFECT 3 Transfection Reagent (T-2003-03) and DharmaFECT Cell Culture Reagent (DCCR; B-004500-100), also purchased from Thermo Scientific. Reverse transfection of HeLa cells (Human, cervical, epithelial cells ATCC #CCL-70) were carried out based on a method by Thermo Scientific. siRNA were prepared as a 5 µM stock and the final concentration used was 50 nM.

HeLa cells were transfected as follows. 12 µL siRNA, 6 µL DharmaFect 3 and 282 µL DCCR were mixed and transferred to a single well in a 12 well tray (Tray 1) and was incubated for 40 min at RT. For each siRNA, two wells were prepared. After 40 min, 2.5×10^5 HeLa cells in 0.9 mL MEM, 10% FCS were added to each well. The tray was incubated overnight at 37°C, 5% CO_2. HeLa cells were re-transfected on day 2. 12 µL siRNA, 6 µL DharmaFect 3 and 282 µL DCCR were mixed and transferred to a single well in a 12 well tray (Tray 2) and was incubated for 40 min at RT. HeLa cells from the one well that was transfected the day before (Tray 1) were trypsinised (110 µL 0.1% [w/v] trypsin/0.02% [w/v] EDTA/PBS) and resuspended in 190 µL MEM, 10% FCS. The trypsinised HeLa cells were combined with 600 µL MEM, 10% FCS and were added to the DCCR mixture in Tray 2. The tray was incubated overnight at 37°C, 5% CO_2. On day 3, HeLa cell lysate extracts were prepared as described by Qualmann and Kelly (2000) with some modifications. Re-transfected HeLa monolayers from two wells of a 12-well tray were washed with PBS for 15 - 20 min, dislodged with 110 µL trypsin and resuspended in 190 µL PBS. The cells were pelleted by centrifugation (3,500 rpm, 5 min, RT, Eppendorf 5415R) and the pellet was resuspended in 80 µL in 0.1 % (v/v) Triton X-100 in lysis buffer A (10 mM HEPES pH 7.4, 150 mM NaCl, 1 mM EGTA, 0.1 mM $MgCl_2$) supplemented with protease inhibitors (5 µg/mL pepstatin, 10 µg/mL aprotinin, 10 µg/mL chymostatin, 1 mM PMSF). The cells were lysed at 4°C for 30 min and were pelleted by centrifugation (25,000 rpm, 30 min, 4°C, Beckman OptimaTM MAX-UP Ultracentrifuge). The supernatant was collected and mixed with 80 µL 2× Sample buffer (0.125 M Tris-HCl, pH 6.8, 4% [w/v] SDS, 20% [v/v] glycerol, 10% [v/v] β-mercaptoethanol, 0.04% [w/v] Bromophenol blue), and stored at -20°C. Samples were heated at 100°C for 5 min prior to SDS-PAGE.

3.3.5 SDS-PAGE and Western immunoblotting

SDS-PAGE (12% acrylamide gel) and Western immunoblotting were carried out as described previously (May & Morona, 2008). Molecular weight markers used were BenchMark™ Pre-Stained Protein Ladder (Invitrogen).

3.3.6 Plaque assay

Plaque assays were performed with HeLa cells as described previously (Oaks *et al.*, 1985) with modifications. 1.2×10^6 HeLa cells were seeded in six-well trays in minimal essential medium (MEM), 10% FCS, 1% penicillin/streptomycin. Cells were grown to confluence overnight and were washed twice with Dulbecco's modified Eagle medium (DMEM) prior to inoculation. 2.5×10^4 mid-exponential phase bacteria were added to each well. Trays were incubated at 37°C, 5% CO_2 and were rocked gently every 15 min to spread the inoculum evenly across the well. At 90 min post-infection, the inoculum was aspirated. 3 mL of the first overlay (DMEM, 5% FCS, 20 µg/mL gentamicin, 0.5% (w/v) agarose [Seakem ME]) was added to each well. Dynasore or DMSO were added and were swirled to ensure even distribution. The second overlay (DMEM, 5% FCS, 20 µg/mL gentamicin, 0.5% (w/v) agarose, 0.1% (w/v) Neutral Red solution [Gibco BRL]) was added 48 h post-infection and plaques were imaged 6 h later. All observable plaques were counted and the diameter was measured for each condition in each experiment. At least 25 plaques were measured for each condition.

3.3.7 Infectious focus assay

HeLa cells were transfected prior to infectious focus assay as per "***Reverse transfection***" (Section 3.3.4). On day 3, the infectious focus assay was carried out. Transfected HeLa cells were washed twice with DMEM prior to inoculation. 5×10^4 mid-exponential phase bacteria expressing mCherry were added to each well. Trays were incubated at 37°C, 5% CO_2 and were rocked every 15 min to spread the inoculum evenly across the well. At 90 min post-infection, the inoculum was aspirated. 1.5 mL of DMEM (phenol red-free) (31053-028; Life Technologies), 1 mM sodium pyruvate, 5% FCS, 20 µg/mL gentamicin, 2 mM IPTG was added to each well. 24 h later the infectious foci were imaged with an Olympus IX-70 microscope using a 10× objective. The filter set used was DA/FI/TX-3X-A-OMF (Semrock).

Fluorescence and phase contrast images were captured and false colour merged with the Metamorph software programme (Version 7.7.3.0, Molecular Devices). The area of the infectious focus i.e. area where mCherry was expressed, was outlined and measured with Metamorph. All observable infectious foci were counted and the area was measured for each condition in each experiment. At least 20 infectious foci were measured for each condition.

3.3.8 Invasion assay and IF microscopy

HeLa cells (8×10^4) were seeded onto sterile glass cover slips in 24-well trays in MEM, 10% FCS, 1% penicillin/streptomycin. For transfected HeLa cells, refer to "***Reverse transfection***" (Section 3.3.4). The following modifications were made. On day 1, one well was prepared for each siRNA. On day 2, the siRNA:DharmaFect3:DCCR mixture was halved. 80% of the HeLa cells that had been transfected on day 1 were reseeded in Tray 2. Cells were grown to semi-confluence overnight, washed twice with Dulbecco's PBS (D-PBS) and once with MEM, 10% FCS. 4 x 10^7 mid-exponential phase bacteria were added to each well and subsequently centrifuged (2,000 rpm, 7 min, Heraeus Labofuge 400 R) onto HeLa cells. After 1 h incubation at 37°C, 5% CO_2, the infected cells were washed thrice with D-PBS and incubated with 0.5 mL MEM containing 40 µg/mL of gentamicin for a further 1.5 h. Infected cells were washed thrice in D-PBS, fixed in 3.7% (v/v) formalin for 15 min, incubated with 50 mM NH_4Cl in D-PBS for 10 min, followed by permeabilisation with 0.1% Triton X-100 (v/v) for 5 min. After blocking in 10% FCS in PBS, the infected cells were incubated at 37°C for 30 min with the desired primary antibody. After washing in PBS, coverslips were incubated with either Alexa Fluor 594-conjugated donkey anti-rabbit or Alexa 594-conjugated donkey anti-mouse secondary antibody (Molecular Probes) (1:100). F-actin was visualised by staining with Alexa Fluor 488-conjugated phalloidin (2 U/mL) and 4',6'-diamidino-2-phenylindole (DAPI) (10 µg/mL) was used to counterstain bacteria and HeLa cell nuclei. Coverslips were mounted on glass slides with Mowiol 4-88 (Calbiochem) containing 1 µg/mL *p*-phenylenediamine (Sigma) and was imaged using a 100× oil immersion objective (Olympus IX-70). The filter set used was DA/FI/TX-3X-A-OMF (Semrock). Fluorescence and phase contrast images were false colour merged using the Metamorph software programme.

3.3.9 Protrusion formation

HeLa cells were seeded, infected and fixed as per "***Invasion assay and IF microscopy***" (Section 3.3.8). HeLa cells were washed twice with 1× Annexin V binding buffer (99902; Biotium) prepared in milliQ (18.2 MΩ·cm) water, mounted on glass slides with the same buffer and were imaged using a 40× oil immersion objective (Olympus IX-70). Protrusion formation was defined as any extensions of bacterial projection(s) (minimum of a full bacterial length) beyond the periphery of the HeLa cell. For each condition in each experiment, a minimum of 100 cells were imaged.

3.3.10 Assay for growth of intracellular bacteria

HeLa cells (8×10^4) were seeded in 24-well trays in MEM, 10% FCS, 1% penicillin/streptomycin. Cells were grown to semi-confluence overnight, washed twice D-PBS and once with MEM, 10% FCS. 4×10^7 mid-exponential phase bacteria were added to each well (multiplicity of infection, moi ~500). The bacteria were centrifuged (2,000 rpm, 7 min, Heraeus Labofuge 400 R) onto HeLa cells. After 1 h incubation at 37°C, 5% CO_2, the infected cells were washed thrice with D-PBS and incubated with 0.5 mL MEM containing 40 µg/mL of gentamicin. At the indicated intervals, monolayers (in duplicate) were washed four times in D-PBS and were lysed with 0.1% (v/v) Triton X-100 in PBS for 5 min and bacteria were enumerated on tryptic soy agar (Gibco) plates.

3.3.11 LDH cytotoxicity assay

HeLa cells (3×10^4) were seeded in 96-well trays in MEM, 10% FCS, 1% penicillin/streptomycin. Cells were grown to confluence overnight and were washed twice with PBS. 50 µL phenol-red free DMEM (31053-028; Life Technologies), 1 mM sodium pyruvate and 3×10^7 mid-exponential phase bacteria (moi ~1000) in 50 µL PBS or PBS were added into each well, where appropriate. The bacteria were centrifuged (2,000 rpm, 7 min, Heraeus Labofuge 400 R) onto HeLa cells. After 1 h incubation at 37°C, 5% CO_2, the infected cells were washed thrice with PBS and incubated with 0.1 mL phenol-red free MEM, 40 µg/mL of gentamicin for 4 h. LDH activity was measured with the Cytotoxicity Detection Kit^{Plus} as per manufacturer's instructions (Roche). The percentage of LDH released was

calculated with the following formula: ((experimental LDH release − spontaneous LDH release)/(maximal LDH − spontaneous LDH release)) × 100.

3.3.12 Ethics statement

The use of animals in this study has been approved by the University of Adelaide Animal Ethics Committee (Project number: S-2012-90). All animals used were handled in compliance with the Australian code of practice for the care and use of animals for scientific purposes, 7th edition (2004).

3.3.13 Mouse Sereny test

The mouse Sereny test (Murayama *et al.*, 1986) was carried out as follows. Male Balb/c mice (20 - 22g) were inoculated with 2.5×10^7 or 5×10^8 CFU bacteria in 5 μL of bacterial suspension (in PBS) into the right eye; the left eye served as a diluent control. To ascertain the impact of dynasore on ocular infection, mice were injected intraperitoneal (IP) with drug at a dose rate of 30 mg/kg, at t = -1, +6, +23 and +30 h with respect to infection at 0 h. Keratoconjunctivitis was evaluated at specific time points after inoculation and scored on a scale ranging from 0 (no infection), 1 (mild keratoconjunctivitis where the eye lid is slightly swollen), 2 (severe keratoconjunctivitis where the eye is half closed) and 3 (fully developed keratoconjunctivitis where the eye is completely closed).

Ethics concerns regarding the *in vivo* use of DMSO prompted us to adopt a different vehicle, NMP/PEG, which is made up of 1 part *N*-methyl-2-pyrrolidione (NMP) and 9 parts polyethylene glycol 300 (PEG300), for *in vivo* studies designed to assess the impact of dynasore in this model. *In vitro* studies showed that plaque formation by *S. flexneri* strain 2457T was comparable using either diluent (Figure 3.S1A - B). A preliminary mouse study showed that for injections of vehicle (Figure 3.S1C) or dynasore (Figure 3.S1D) resulted in comparable (~5%) weight loss.

3.3.14 Sectioning and H&E staining of mouse eyes and eyelids

For histopathological observations, the infected and uninfected eyes (together with eyelids) were removed and fixed in 4% buffered formaldehyde overnight before embedding in

paraffin. Sections were prepared and stained with hematoxylin plus eosin by the Ophthalmic Research Laboratories, Centre for Neurological Diseases, Adelaide, Australia.

3.3.15 Statistical analysis

Statistical analysis was carried out using GraphPad Prism 6. Results are expressed as means ± SEM of data obtained in independent experiments. Statistical differences between two groups were determined with a two-tailed unpaired *t*-test. Statistical differences between three or more groups were determined with a one-way ANOVA followed by Tukey's or Dunnett's multi comparison post hoc test. Statistical significance was set at $p < 0.05$.

3.4 Results

3.4.1 Dynamin II is important for *S. flexneri* cell-to-cell spreading but not protrusion formation

We investigated if the process of cell-to-cell spreading was dependent on dynamin II, a component of endocytosis. The effects of dynasore, a dynamin II inhibitor, and dynamin II siRNA on plaque formation by *S. flexneri* were determined. HeLa monolayers infected with *S. flexneri* were treated with increasing concentrations of dynasore or with the DMSO vehicle alone. Treatment with 80 μM dynasore reduced plaque diameter (*$p < 0.05$) and addition of 120 μM dynasore abolished plaque formation altogether (Figure 3.1A - C). *S. flexneri* entry into HeLa cells and intracellular growth were not affected (Figure 3.S2 and Figure 3.S3). We also investigated if dynamin II is important for *Listeria* cell-to-cell spreading. HeLa monolayers infected with *Listeria* were treated with the DMSO control or increasing concentrations of dynasore. The plaque diameter of *Listeria*-infected HeLa cells treated with 80 and 120 μM dynasore were significantly reduced (*$p < 0.05$) (Figure 3.1A and 3.1D). No difference in plaque diameter was observed between 80 μM and 120 μM dynasore.

To investigate the effect of dynamin II depletion on *S. flexneri* cell-to-cell spreading, HeLa cells were transfected with dynamin II siRNA and an infectious foci assay was carried out. Western immunoblots of HeLa cell lysates two days post-siRNA treatment showed ~95% reduction in dynamin II levels (Figure 3.2A). *S. flexneri* formed infectious foci on HeLa cells treated with dynamin II siRNA with a reduced foci area but not foci counts when compared to HeLa cells treated with the negative control siRNA (*$p < 0.05$) (Figure 3.2B - D). Therefore dynamin II inhibition with dynasore as well as siRNA knockdown reduced *Shigella* cell-to-cell spreading.

Next we investigated if dynamin II is involved *S. flexneri* protrusion formation, which may account for the reduction in plaque formation. HeLa monolayers infected with *S. flexneri* were treated with the DMSO control or 80 μM dynasore and the percentage of infected cells with one or more bacteria protrusions were enumerated by counting >100 cells in each experiment (Figure 3.3). 66.33 ± 1.35% of infected HeLa cells had one or more protrusions. Protrusion formation was not affected by the DMSO control (67.42 ± 1.25%) or 80 μM

dynasore (63.12 ± 1.43%). It should be noted that while our assessment of the effect of dynasore on plaque formation used confluent cells, and its effect on protrusion formation used semi confluent cells; this approach to study cell-to-cell spreading has previously been reported by others (Ambrosi *et al.*, 2012; Bishai *et al.*, 2012; Egile *et al.*, 1997; Heindl *et al.*, 2009; Prunier *et al.*, 2007; Sandlin *et al.*, 1996).

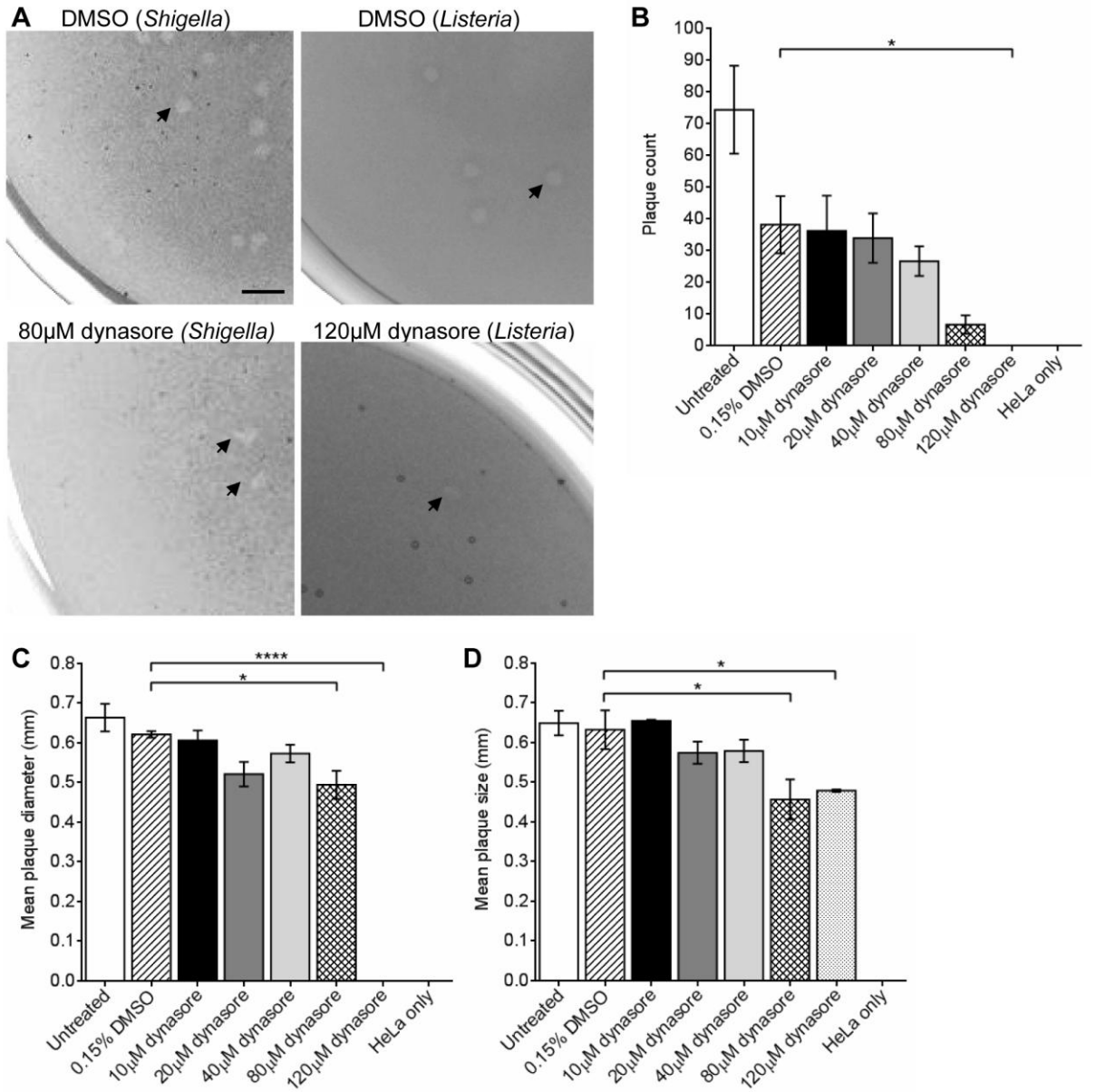

Figure 3.1 Dynamin II inhibition with dynasore reduces *S. flexneri* 2457T plaque counts and plaque size.

HeLa cells were infected with either *S. flexneri* 2457T or *Listeria* in a plaque assay using a 6-well tray as described in the Methods section. Plaque formation was performed in the presence of increasing concentrations of dynasore or the vehicle, 0.15% DMSO. (A) Wells were stained with Neutral Red to makes plaques more visible. Scale bar = 2 mm. (B) The total plaque counts or (C) mean plaque diameters from each well infected with *Shigella* were calculated. (D) Mean plaque diameters from each well infected with *Listeria* were calculated. Data are represented as mean ± SEM of independent experiments ($n = 4$ for *Shigella* and $n = 3$ for *Listeria*), analysed with one-way ANOVA ($p < 0.0001$), followed by Tukey's post hoc test (*$p < 0.05$, ****$p < 0.0001$).

Figure 3.2 Transfection of HeLa cells with dynamin II siRNA reduces *S. flexneri* MLRM107 foci counts and foci area.

HeLa cells were either mock transfected or transfected with control or dynamin II siRNA for 24 h, trypsinised and re-transfected for further 24 h. (A) HeLa cell extracts were probed with anti-dynamin. GAPDH was used as a loading control. (B - D) Post-transfection, HeLa cells were infected with *S. flexneri* MLRM107 in an infectious focus assay using a 12-well tray as described in the Methods section. Infectious foci were imaged 24 h post-gentamicin treatment. Images shown are overlay of an image taken with phase contrast and TxRed filter (10× magnification). The area of the infectious foci i.e. area where mCherry was expressed, is outlined. Scale bar = 0.1 mm. (C) The total foci counts from one well or (D) mean foci area from one well were calculated. Data are represented as mean ± SEM of independent experiments (n = 3). For total foci count analysed with one-way ANOVA, $p > 0.05$. Mean foci area was analysed with one-way ANOVA ($p = 0.0027$), followed by Tukey's post hoc test ($^*p < 0.05$).

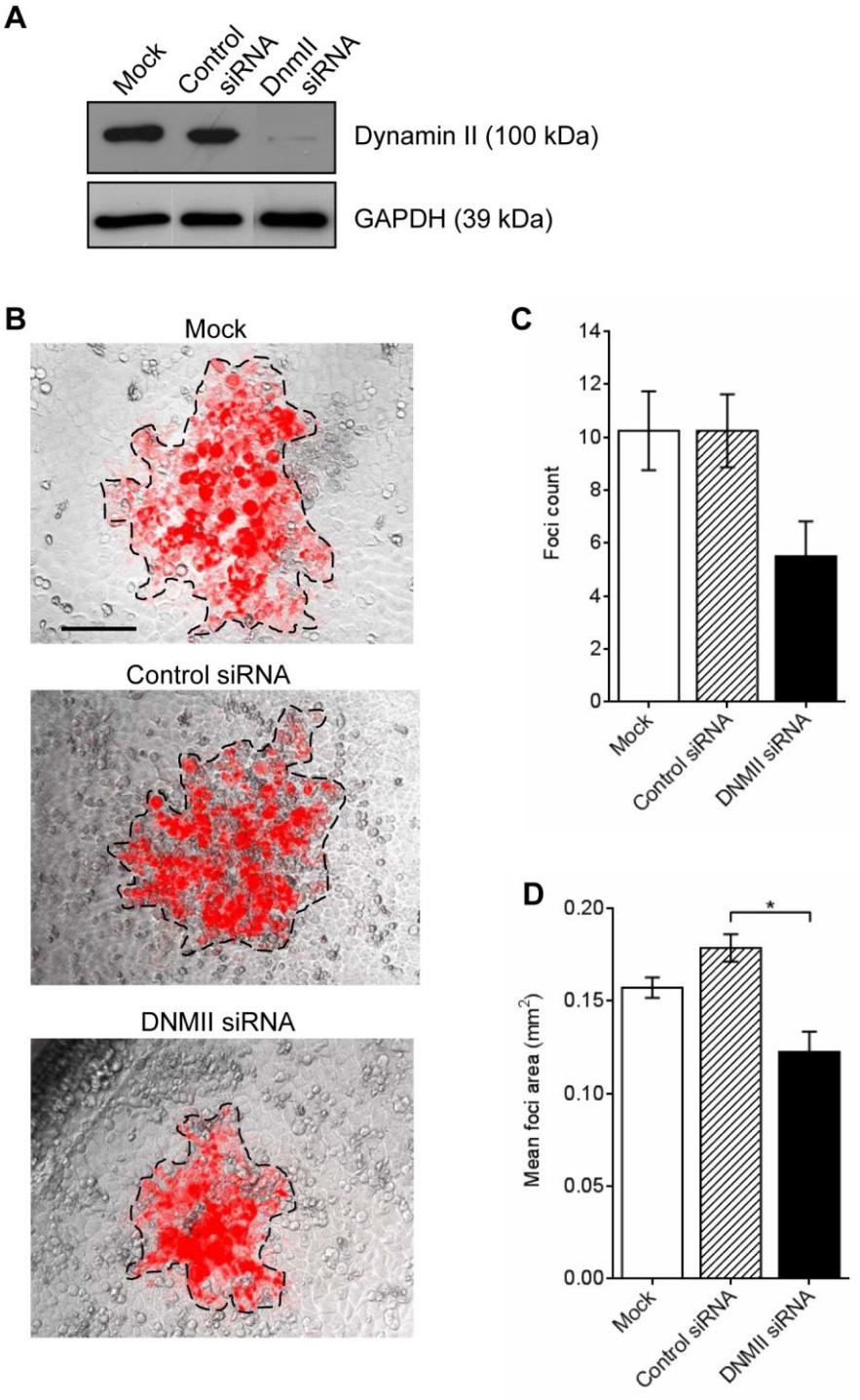
A
Mock
Control siRNA
DnmII siRNA
Dynamin II (100 kDa)
GAPDH (39 kDa)
B
Mock
Control siRNA
DNMII siRNA
C
Foci count
14
12
10
8
6
4
2
0
Mock
Control siRNA
DNMII siRNA
D
Mean foci area (mm2)
0.20
0.15
0.10
0.05
0.00
*
Mock
Control siRNA
DNMII siRNA

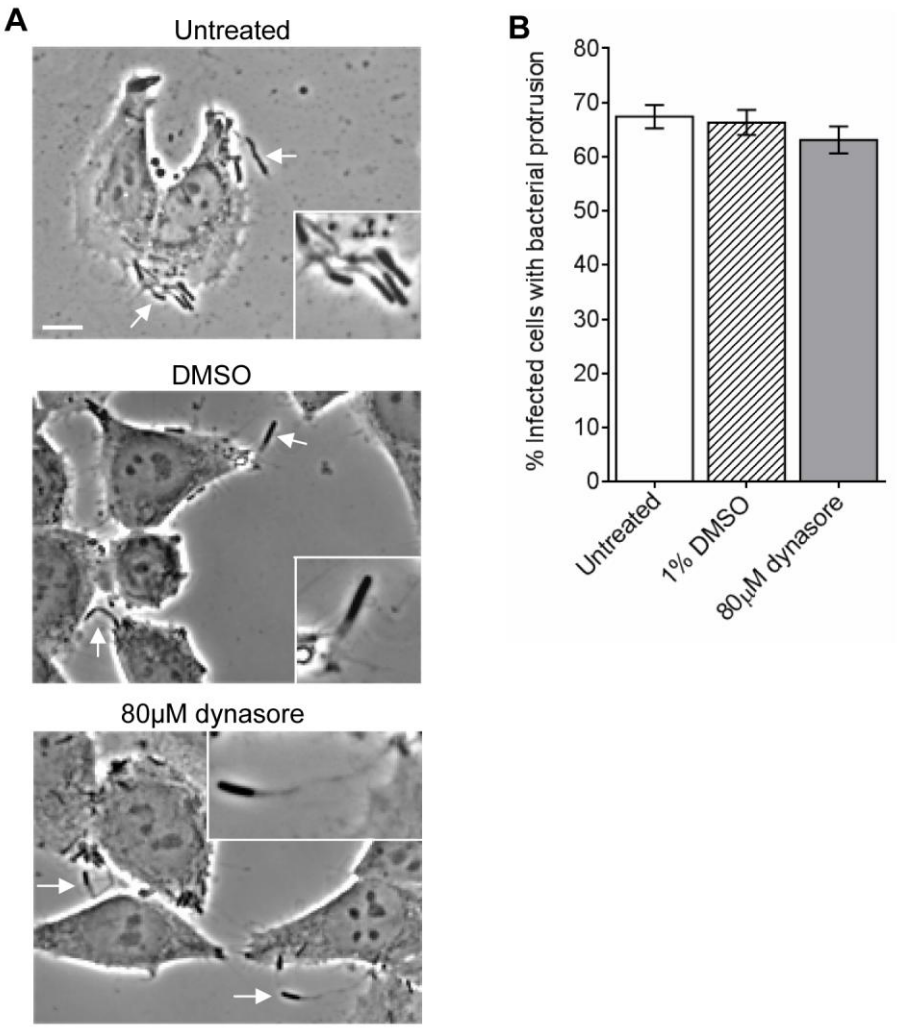

Figure 3.3 *S. flexneri* 2457T protrusion formation is not affected by dynasore.

HeLa cells were infected with *S. flexneri* 2457T for 1 h in a 24-well tray. HeLa cells were washed thrice with D-PBS and incubated with MEM containing 40 μg/mL of gentamicin (t = 0) to exclude extracellular bacteria. Concurrently HeLa cells were treated with 80 μM dynasore or DMSO for 1.5 h. At t = 1.5, HeLa cells were fixed to observe bacteria protrusions. (A) Infected HeLa cells were imaged at 40× magnification. Scale bar = 10 μm. The arrows indicate protrusion formation. Insert shows 2× enlargement of the indicated region. (B) The percentage of infected cells with bacteria protrusion(s) were enumerated by counting >100 cells in three independent experiments. Data are represented as mean ± SEM of independent experiments (n = 3), analysed with one-way ANOVA (p > 0.05).

3.4.2 Dynamin II is localised to the F-actin tail and protrusions of *S. flexneri*, adjacent to N-WASP

The polarly localised *S. flexneri* IcsA protein interacts with host proteins such as N-WASP and Arp2/3 complex to initiate actin polymerisation to form an actin tail which imparts motility to the bacteria (Goldberg *et al.*, 1993; Goldberg, 2001; Suzuki *et al.*, 1998). We investigated dynamin II localisation in *S. flexneri* infected HeLa cells by IF microscopy. Dynamin II was localised to the *S. flexneri* F-actin tail and/or protrusion (Figure 3.4A). F-actin labelling with FITC-phalloidin does not readily distinguish F-actin tails from protrusion formation as both architectures appear as long F-actin structures behind one pole of the bacteria. We observed 109 infected HeLa cells, and found that 150 out of 158 (95%) of *S. flexneri* F-actin tails and/or protrusions were localised with dynamin II. Treatment with DMSO and 80 µM dynasore did not affect dynamin II localisation (Figure 3.4B - C). In 104 infected HeLa cells treated with 80 µM dynasore, 143 out of 154 *S. flexneri* (93%) F-actin tails and/or protrusions were localised with dynamin II. Similarly in 109 infected HeLa cells treated with the DMSO control, 152 out of 159 *S. flexneri* (96%) F-actin tails and/or protrusions were localised with dynamin II. These results suggest dynamin II interaction at the *S. flexneri* F-actin tail and/or protrusion does not require the activity of its GTPase domain. In dynamin II siRNA-transfected HeLa cells, a reduction in cellular dynamin II protein levels was observed, as expected. Reduction of dynamin II protein level did not affect dynamin II localisation to the bacteria F-actin tail (Figure 3.4D).

In R-LPS strains, IcsA polar localisation and ABM is affected but the bacteria can still invade host cells (Sandlin *et al.*, 1995). The R-LPS strain can form F-actin tails, albeit infrequently. The F-actin tails are also shortened and distorted (Van Den Bosch *et al.*, 1997). Similarly *S. flexneri icsA* mutants in either the smooth or rough LPS (R-LPS) background can invade HeLa cells. In the R-LPS strain dynamin II is recruited to *S. flexneri* F-actin tail (Figure 3.4E) but no recruitment was observed for the Δ*icsA* mutant strains (Figure 3.4F - G). This suggests that dynamin II may interact with the F-actin tail since F-actin *de novo* synthesis is dependent on IcsA. Alternately dynamin II could also be interacting indirectly with the F-actin tail through other proteins such as N-WASP which are found at the *S. flexneri* bacterial surface (Suzuki *et al.*, 2002). HeLa cells infected with *S. flexneri* were labelled with anti-N-WASP and anti-dynamin (Figure 3.S4). N-WASP is located immediately at the pole of

S. flexneri (Figure 3.S4A), forming a cap. Dynamin II labelling also resembles a cap at the *S. flexneri* pole (Figure 3.S4B) and is adjacent to the N-WASP cap with a seemingly small area of overlap (Figure 3.S4C - D).

Figure 3.4 Dynamin II is localised to the *S. flexneri* 2457T F-actin tails and protrusions.

HeLa cells were infected with *S. flexneri* 2457T in an invasion assay as described in the Methods section. Bacteria and HeLa nuclei were stained with DAPI (blue), F-actin was stained with FITC-phalloidin (green) and dynamin II was stained with anti-dynamin and Alexa Fluor 594-conjugated secondary antibody (red). Images were taken at 100× magnification. Scale bar = 10 μm. (A) - (D) HeLa cells were treated with DMSO, dynasore or were transfected with dynamin II siRNA and were infected with *S. flexneri* 2457T; (A) Untreated; (B) 1% DMSO; (C) 80 μM dynasore; (D) Dynamin II siRNA-transfected HeLa cells. (E) - (G) HeLa cells were infected and treated as above with *S. flexneri* control stains; (E) RMA723 (R-LPS - Δ*rmlD*); (F) RMA2041 (Δ*icsA*); (G) RMA2043 (Δ*icsA* Δ*rmlD*). The arrows indicate dynamin II localisation at comet tails or protrusions. Insert shows 2× enlargement of the indicated region. The experiment was repeated twice and representative images are shown.

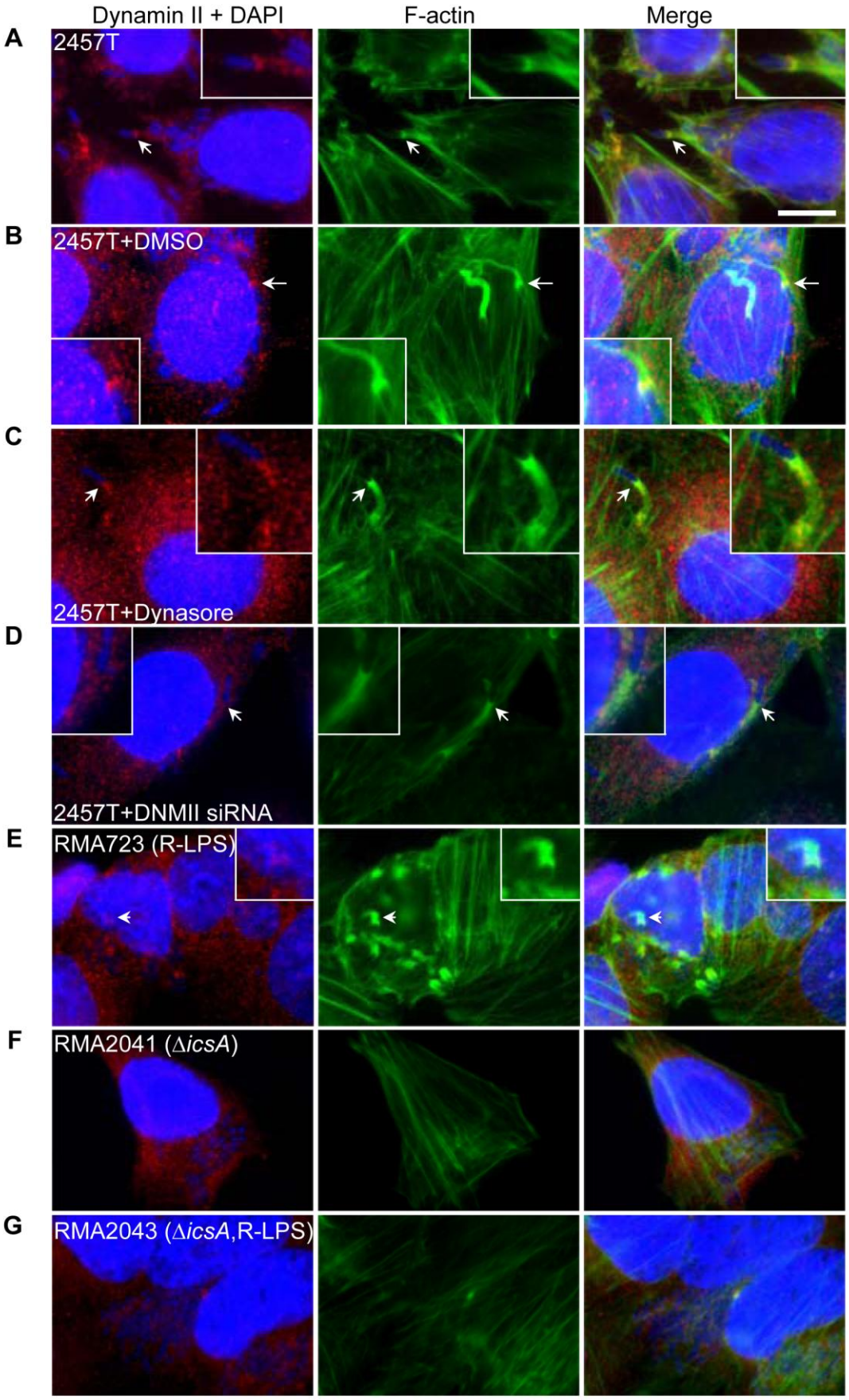
Dynamin II + DAPI
F-actin
Merge
A
2457T
B
2457T+DMSO
C
2457T+Dynasore
D
2457T+DNMII siRNA
E
RMA723 (R-LPS)
F
RMA2041 (ΔicsA)
G
RMA2043 (ΔicsA,R-LPS)

3.4.3 Effect of dynasore on *S. flexneri* infection of mice

We next investigated the possible *in vivo* relevance of the observed association between dynamin II and *S. flexneri* spreading. A mouse Sereny test was established and used to determine whether ocular infection by *S. flexneri* could be inhibited by the administration of dynasore. In initial studies, mice were infected with 5×10^8 CFU WT *S. flexneri* 2457T in the right eye and the left eye was used as the control (Figure 3.S5A). At 24, 48 and 72 h, scores between 0 and 3 were given depending on the severity of the inflammation. Histology was carried out to compare sections prepared from eyes with scores of 0 (left eye PBS control) and 3 (fully developed keratoconjunctivitis). No inflammation was observed as expected in the PBS control (Figure 3.S5B, left image). In the *Shigella*-infected eye, desquamation and degeneration of the palpebral conjunctiva and fornix epithelial were observed as well as infiltration of polymorphonuclear leukocytes into the epithelial layers (Figure 3.S5B, right image).

Mice were infected with WT, Δ*icsA* or virulence plasmid negative (VP^-) *S. flexneri* strains which are virulent, attenuated or are completely avirulent, respectively, to establish suitable controls. Mice infected with the Δ*icsA* or VP^- strains did not develop any observable inflammation (Figure 3.S5C). Mice infected with WT *S. flexneri* developed a strong inflammatory response with a score of ≥2.5. The inflammation peaked at 24 and 30 h with four out of six mice developing strong inflammatory reaction. Over the next two days, the inflammation slowly resolved with two out of six mice developing a strong inflammatory response (score of 3) (Figure 3.S5D). Mice were also weighed on D0 and D3 of the experiment. Mice infected with the avirulent VP^- strain did not lose weight, however mice infected with either WT or Δ*icsA* strains had comparable weight loss (~6 - 9%) (Figure 3.S5E).

In the first *in vivo* study with dynasore, mice were infected with 5×10^8 CFU *S. flexneri* 2457T in the right eye ($t = 0$) and were injected IP with dynasore (30 mg/kg) or vehicle at t = -1, 6, 23 and 30 h. The mice in both groups developed ocular inflammation at a similar rate and the Sereny scores were similar (Figure 3.5A - B). Mice in both groups also had ruffled fur and were often reluctant to move, suggesting that the combination of *Shigella* infection and injection of NMP/PEG (alone or in combination with dynasore) was detrimental to the mice. Mice injected with NMP/PEG lost 15% of their weight during the course of the infection,

which was significantly higher than that observed in infected mice not receiving injections (Figure 3.S5E) or in uninfected mice injected with the vehicle or dynasore (Figure 3.S1C - D). Mice injected with vehicle only also lost more weight (14.49 ± 1.63%) compared to mice injected with dynasore (8.29 ± 2.01%) (*$p < 0.05$) (Figure 3.5C).

The experiment was repeated with a second group of mice since the first group had varied Sereny scores at respective time points. Mice were infected with 5×10^8 CFU *S. flexneri* 2457T in the right eye ($t = 0$) and were IP injected with dynasore (30 mg/kg) or the vehicle at $t = -1$, 6, 23 and 30 h and were weighed daily. Mice developed the ocular inflammation at the same rate and there was no difference in Sereny scores (Figure 3.6A - B). Mice injected with dynasore lost significantly less weight compared to mice treated with the vehicle alone on D1 (4.39 ± 0.76% vs. 8.77 ± 0.71%, **$p < 0.01$) and D2 (7.71 ± 1.21% vs. 12.52 ± 1.53%, *$p < 0.05$) (Figure 3.6C). Weight loss which was previously observed on D3 in the first experiment (Figure 3.5C) was not observed in the second group of mice. The latter group of mice collectively had less variations in their Sereny scores (Figure 3.6A), which could explain why the weight differences were only observed on D1 and D2. Nonetheless these studies suggest that dynasore provided a protective effect against weight loss associated with *S. flexneri* infection.

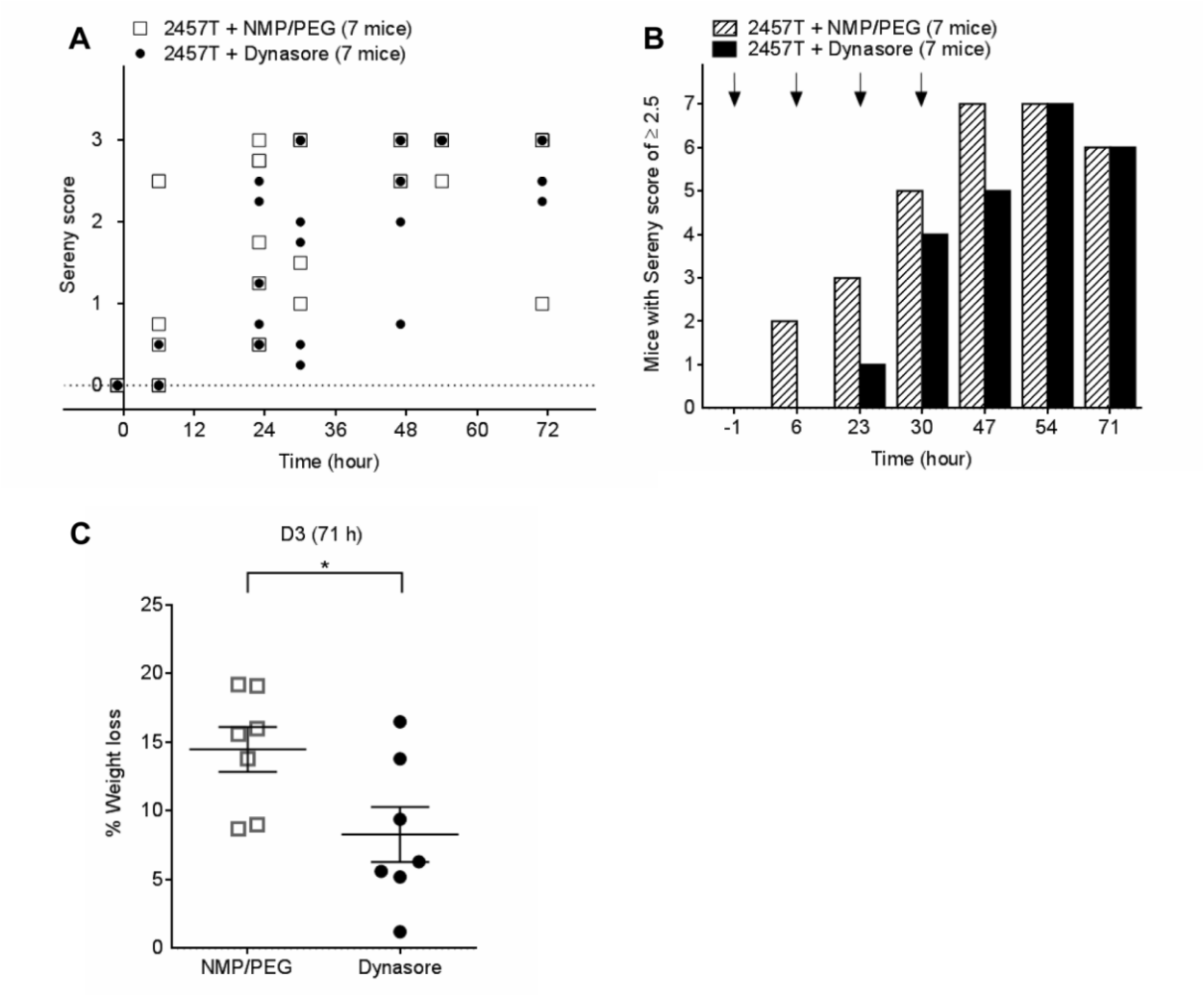

Figure 3.5 Dynasore protects mice against weight loss resulting from *S. flexneri* 2457T ocular infection (Experiment 1).

(A) Sereny scores of mice infected with 5×10^8 CFU *S. flexneri* 2457T at $t = 0$ and IP injected with either 100 µL of 5.5 mg/mL of dynasore in NMP/PEG (30 mg/kg) or 100 µL NMP/PEG at $t = -1$, 7, 23, 30 h post-inoculation. Each symbol represents one or more mice. (B) The total number of mice with a Sereny score of ≥2.5 was calculated and plotted as a bar graph for each time point. Arrows indicate injection with dynasore or NMP/PEG alone. (C) The percentage weight loss for each mouse on D3 was calculated. Data are represented as mean ± SEM (Student's *t*-test, $*p < 0.05$).

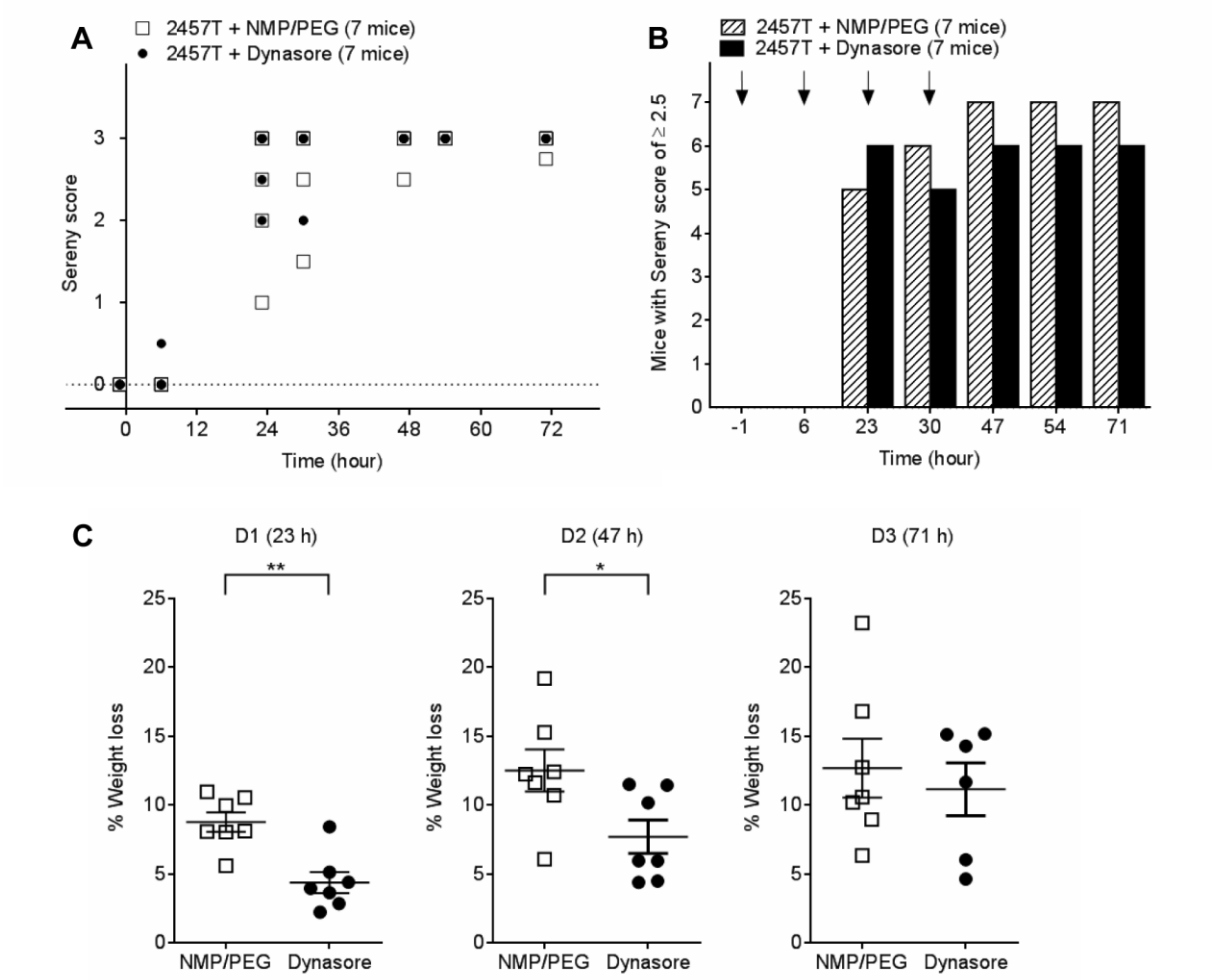

Figure 3.6 Dynasore protects mice against weight loss resulting from *S. flexneri* 2457T ocular infection (Experiment 2).

(A) Sereny scores of mice infected with 5×10^8 CFU *S. flexneri* 2457T at $t = 0$ and IP injected with either 100 µL of 5.5 mg/mL of dynasore in NMP/PEG (30 mg/kg) or 100 µL NMP/PEG at $t = -1$, 7, 23, 30 h post-inoculation. Each symbol represents one or more mice. (B) The total number of mice with a Sereny score of ≥2.5 was calculated and plotted as a bar graph for each time point. Arrows indicate injection with dynasore or NMP/PEG alone. (C) The percentage weight loss for each mouse on D1, D2 and D3 were calculated. Data are represented as mean ± SEM (Student's *t*-test, *$p < 0.05$, **$p < 0.01$).

3.4.4 Effect of dynasore on mice infected with a low inoculum of *S. flexneri* 2457T

Since dynasore treatment reduced weight loss associated with *Shigella* infection but not the extent of ocular inflammation, further studies were performed using a reduced *Shigella* dose. Mice were infected with 2.5×10^7 CFU *S. flexneri* 2457T and were weighed on D0 and D3 (Figure 3.7A - C). The mice developed inflammation at a slightly slower rate compared to the higher *Shigella* dose (Figure 3.S5C - D); the inflammation peaked at 54 h with three out of six mice developing an inflammation with a score of ≥2.5 (Figure 3.7A - B). The mice lost an average of 4% of their body weight (Figure 3.7C).

In a second study with the same lower challenge dose, mice were given injection of dynasore (30 mg/kg) or vehicle at t = -1, 6, 23 and 30 h. Mice in both groups developed ocular inflammation at a similar rate and no difference in Sereny scores was observed (Figure 3.7D - E). Similar to the high dose infection, dynasore significantly protected mice against weight loss associated with *Shigella* infection when compared to the vehicle group on D1 (4.81 ± 1.68% vs. 8.75 ± 0.55%, $*p < 0.05$) and D2 (6.85 ± 1.82% vs. 12.46 ± 0.67%, $*p < 0.05$) (Figure 3.7F). The group of mice in this study had ruffled fur and displayed reduced mobility similar to the mice in the higher challenge dose which were give dynasore or vehicle injection.

In the ocular infection model, dynasore afforded significant protection against weight loss but did not reduce ocular inflammation. In contrast, mice infected with Δ*icsA* (RMA2041) had similar weight loss to 2457T (Figure 3.S5E) but no ocular inflammation was observed (Figure 3.S5C), suggesting that dynasore is not preventing *S. flexneri* cell-to-cell spreading *in vivo.*

3.4.5 Effect of dynasore on *S. flexneri*-induced HeLa cell death

Since dynasore did not seem to affect *S. flexneri* cell-to-cell spreading and ameliorate inflammation *in vivo*, we sought to determine if dynasore could be targeting TTSS effectors encoded on the VP (Buchrieser *et al.*, 2000), thus reducing the cytotoxic effects of the TTSS effectors, using an *in vitro* cytotoxicity assay. Previously IpaB and MxiA, both TTSS effectors, have been reported to play a role in weight loss during *S. flexneri* infection

(Buchrieser *et al.*, 2000; Suzuki *et al.*, 2006). HeLa cells were infected with WT, Δ*icsA* or VP^{-} *S. flexneri* strains and LDH release was measured (Figure 3.S6). HeLa cells infected with the VP^{-} had very little cell death (2.34 ± 0.53%), comparable to the uninfected HeLa cells (5.78 ± 2.99%). In contrast, HeLa cells infected with WT and Δ*icsA* strains had 40.2 ± 2.37% and 42.04 ± 2.79% cell death, respectively. Therefore in the absence of *icsA*, the bacteria still retained significant cytotoxicity presumable due the presence of TTSS effectors encoded by the VP. The weight loss observed mice infected with the Δ*icsA* strain in this study (Figure 3.S5E) could be partly attributed to the cytotoxicity from the TTSS effectors.

Next we treated HeLa cells with increasing concentrations of dynasore or with the DMSO vehicle alone (Figure 3.8). No differences in LDH release was observed between dynasore and DMSO in uninfected HeLa cells. *S. flexneri*-induced HeLa cytotoxicity was significantly reduced in the presence of 120 μM (28.72 ± 4.30%) and 160 μM dynasore (26.1 ± 3.63%) compared to DMSO-treated cells (47.73 ± 2.84%, $*p < 0.05$), suggesting dynasore reduces *S. flexneri* induced cytotoxicity *in vitro* and may explain the weight loss protection observed *in vivo*.

Figure 3.7 Dynasore protects mice against weight loss from *S. flexneri* 2457T ocular infection (reduced bacterial challenge).

(A) Sereny scores of mice infected with 2.5×10^7 CFU *S. flexneri* 2457T from 0 - 71 h post-inoculation. Each symbol represents one or more mice. (B) The total number of mice with a Sereny score of ≥2.5 was calculated and plotted as a bar graph for each time point. (C) The percentage weight loss for each mouse on D3 was calculated. (D) Sereny scores of mice infected with 2.5×10^7 CFU *S. flexneri* 2457T at $t = 0$ and IP injected with either 100 µL of 5.5 mg/mL of dynasore in NMP/PEG (30 mg/kg) or 100 µL NMP/PEG at $t = -1, 7, 23, 30$ h post-inoculation. Each symbol represents at least one mouse. (E) The total number of mice with a Sereny score of ≥2.5 was calculated and plotted as a bar graph for each time point. Arrows indicate injection with dynasore or NMP/PEG alone. (F) The percentage weight loss for each mouse on D1, D2 and D3 were calculated. Data are represented as mean ± SEM (Student's *t*-test, $*p < 0.05$).

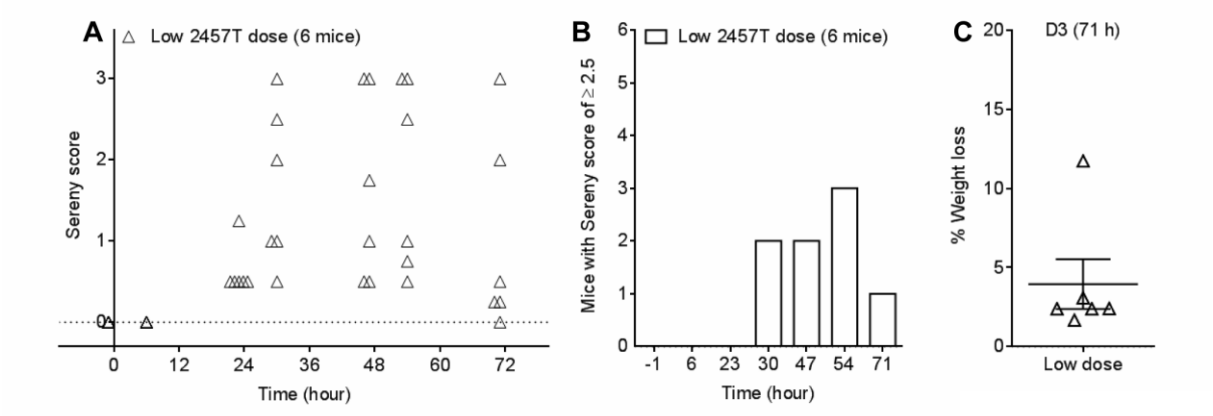
A
Low 2457T dose (6 mice)
Sereny score
Time (hour)
B
Low 2457T dose (6 mice)
Mice with Sereny score of ≥ 2.5
Time (hour)
C
D3 (71 h)
% Weight loss
Low dose

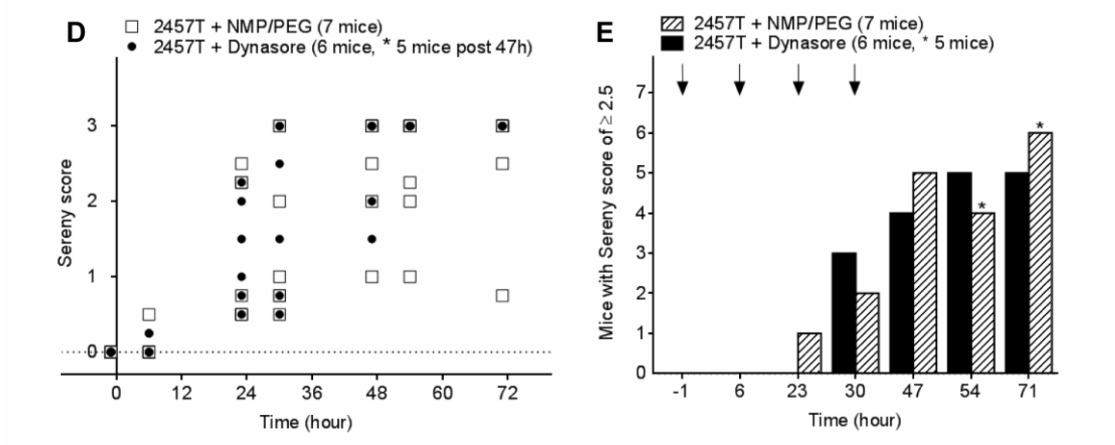
D
2457T + NMP/PEG (7 mice)
2457T + Dynasore (6 mice, * 5 mice post 47h)
Sereny score
Time (hour)
E
2457T + NMP/PEG (7 mice)
2457T + Dynasore (6 mice, * 5 mice)
Mice with Sereny score of ≥ 2.5
Time (hour)

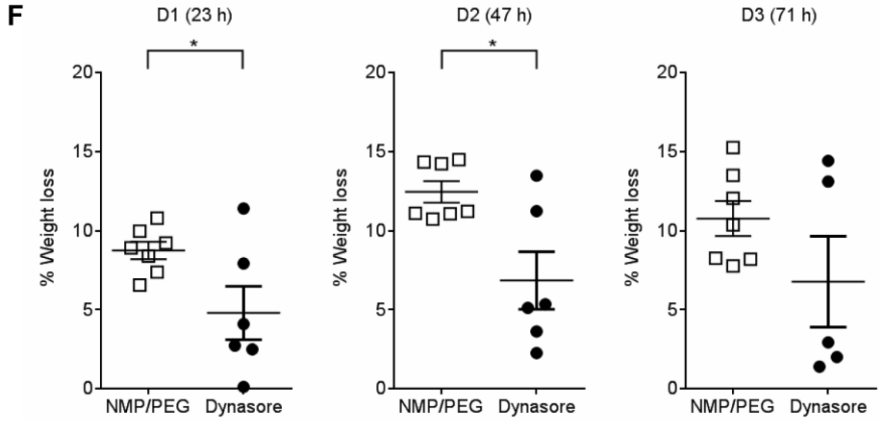
F
D1 (23 h)
D2 (47 h)
D3 (71 h)
% Weight loss
NMP/PEG
Dynasore

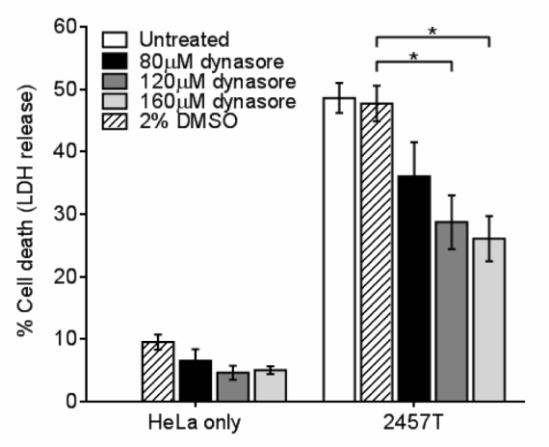

Figure 3.8 Dynasore reduces HeLa cell death during *S. flexneri* 2457T infection.

HeLa cells were infected with *S. flexneri* 2457T in a 96-well tray as described in the Methods section. LDH release was measured in the presence of dynasore or DMSO. Data are represented as mean ± SEM of independent experiments (n = 3), analysed with one-way ANOVA (p = 0.0043), followed by Tukey's post hoc test (*p < 0.05). No differences in LDH release were observed in the presence of dynasore or DMSO in the absence of bacterial infection.

3.5 Discussion

Shigella infection remains a significant problem in developing countries. In this study we have identified a potential intervention strategy by targeting dynamin II, a key component of the clathrin-mediated pathway. Previously dynamin II was shown to be important for *Shigella* engulfment, but not protrusion into the neighbouring cell (Fukumatsu *et al.*, 2012). In this study the role of dynamin II in facilitating *Shigella* cell-to-cell spreading was explored with a well described dynamin II inhibitor, dynasore, as well as by siRNA knockdown.

Inhibition of the dynamin II GTPase activity with dynasore as well as depletion of dynamin II with siRNA knockdown significantly reduced *S. flexneri* plaque size. A reduction in plaque formation could be attributed to a lack of protrusion formation. However *S. flexneri* protrusion formation was not affected by dynasore, which suggests that dynamin II and hence endocytosis is critical for *S. flexneri* entry into neighbouring cell and not exit from the initially infected cell. These results are in agreement with recently reported findings by Fukumatsu *et al.* (2012), where the involvement of dynamin II, as well components of the of the clathrin-mediated endocytic pathway have been shown to be important for *S. flexneri* cell-to-cell spreading and pseudopodia formation. Dynamin II was also reported to accumulate around bacteria containing pseudopodia (Fukumatsu *et al.*, 2012).

Inhibition of dynasore reduced *Listeria* plaque formation to a lesser extent since plaque formation was still observed when HeLa cells were treated with 120 μM dynasore. At the same dynasore concentration, plaque formation by *Shigella* was abolished. These results suggest *Listeria* relies less on dynamin II during cell-to-cell spreading. Previously dynamin II had been shown to associate with the *Listeria* comet tail, although the role of the protein was not explored (Lee & De Camilli, 2002). Recently Fukumatsu *et al.* (2012) reported that clathrin-mediated endocytosis is not the primary pathway utilised by *Listeria* during intercellular spreading. Since dynamin II is a critical component of clathrin-mediated endocytosis, dynamin II may localise non-specifically to the *Listeria* F-actin tail or have other unexplored functions.

S. flexneri lateral spreading is dependent on the bacteria's IcsA protein, a polarly localised outer membrane protein. IcsA is predominantly expressed on the old pole, i.e. the pole that was present before cellular division which gives rise to new daughter poles (Goldberg *et al.*,

1993). IcsA interacts with host proteins such as N-WASP, which recruits the Arp2/3 complex to initiate F-actin polymerisation, allowing the bacteria to spread intracellularly and between cell to cell (Goldberg *et al.*, 1993; Goldberg, 2001; Suzuki *et al.*, 1998). In the absence of IcsA, F-actin tails and subsequent protrusion formation is abolished. The lack of dynamin II recruitment to the Δ*icsA* mutants suggests that dynamin II associates with the F-actin tail as reported for *Listeria* (Lee & De Camilli, 2002). The lack of dynamin II involvement in protrusion formation however, also suggests that its interaction with F-actin tail could be non-specific. Actin binding proteins such as Nck has been shown to associate non-specifically with the *S. flexneri* F-actin tail (Moreau *et al.*, 2000). Alternately dynamin II could play a minor role in membrane remodelling. BAR domain proteins, such as syndapin and sorting nexin 9 (SNX9), interact with N-WASP and dynamin (Qualmann & Kelly, 2000; Shin *et al.*, 2008). Double labelling with anti-N-WASP and anti-dynamin revealed that dynamin II is localised adjacent to N-WASP at the *S. flexneri* old pole. Some overlap of N-WASP and dynamin II labelling was observed.

Mice were initially with challenged the WT, Δ*icsA* and VP^{-} *S. flexneri* strains to establish suitable controls. IcsA is important for *Shigella* cell-to-cell spreading and absence of the protein prevented the bacteria from disseminating further as no inflammation was observed. However, the Δ*icsA* strain can still invade the epithelial cells and have TTSS proteins encoded on the VP such as OspG that can interfere with the host signalling pathways to prevent clearance of the bacteria (Ashida *et al.*, 2011c). Previously it was reported that Balb/c mice inoculated intranasally with 2×10^7 and 2×10^8 CFU Δ*icsA* (Δ*virG*) mutant lost >20% of their body weight 5 days post-inoculation (Suzuki *et al.*, 2006). Similarly, we found that the Δ*icsA* strain still retained significant virulence as measured by weight loss in the ocular infection model used in this study. In a rectal model, guinea pigs inoculated with 1×10^9 CFU *S. flexneri* 2a (strain 2457T and YSH6000) and *S. flexneri* 5a (M90T) lost ~20% of their body weight. No weight loss was observed in guinea pigs inoculated with 2457T VP^{-} strain (Shim *et al.*, 2007). It was also reported that piglets that were orally challenged with 5×10^9 CFU *S. dysenteriae* type 1 expressing the Shiga toxin lost considerable amount of weight. Weight lost was not observed in piglets inoculated with the attenuated Shiga toxin negative strain (Jeong *et al.*, 2010). Weight loss during *S. flexneri* 2a infection has also been reported in other animal models of infection (Barman *et al.*, 2011; Rabbani *et al.*, 1995; Yang *et al.*, 2014).

Mice were challenged with low and high doses of *S. flexneri* 2457T and treated with dynasore to determine if this drug could delay the progression of *Shigella* infection *in vivo*. Mice infected with the low dose *S. flexneri* lost less weight compared to mice infected with the high bacterial dose. Dynasore afforded significant protection against weight loss for both challenge doses but did not reduce ocular inflammation. In comparison, mice infected with Δ*icsA* (RMA2041) had similar weight loss to 2457T but no ocular inflammation was observed. Hence weight loss during *S. flexneri* infection is unrelated to cell-to-cell spreading. The *in vivo* data from this study is summarised in Table 3.2.

We investigated if dynasore could be targeting or inhibiting TTSS effectors encoded on the VP. Addition of 120 μM dynasore reduced *S. flexneri*-induced HeLa cell death by ~39% compared to DMSO-treated cells. The Δ*icsA* mutant strain exhibited similar cytotoxicity to the WT strain, suggesting the HeLa cell death observed is not due to cell-to-cell spreading. Dynasore's ability to reduce *S. flexneri*-induced HeLa cytotoxicity *in vitro* could explain the reduction in weight loss in mice, even though ocular inflammation was not decreased. Previously Balb/c mice inoculated intranasally with 2×10^8 CFU Δ*ipaB* mutant had comparable body weight compared to saline-treated mice. Furthermore the Δ*ipaB* mutant had no cytotoxic effects, as measured by LDH release in mouse J774 macrophages (Suzuki *et al.*, 2006). Invasion plasmid antigen B (IpaB) is a secreted TTSS protein and has recently been shown to induce cell death of macrophages by disrupting ion homeostasis within endosomal compartments leading to subsequent Caspase-1 activated cell death (pyroptosis) (Senerovic *et al.*, 2012). In a recent report adult B6 mice infected with *S. flexneri* YSH6000 lost 25% of their body weight 72 h after initial infection. Mice infected with a *mxiA::Tn5* insertion mutant (strain S325) did not have any appreciable weight loss (Yang *et al.*, 2014). MxiA is a key structural protein of the TTSS and *mxiA* mutants are avirulent (Abrusci *et al.*, 2013; Yang *et al.*, 2014).

Limitations in this study include the dosage of dynasore and the drug carrier used. In the *in vivo* experiments mice were given four dynasore injections during the course of infection. It is possible that the drug did not reach an effective concentration *in vivo*. The NMP/PEG carrier did not result in significant toxicity alone but the combination of NMP/PEG and the *Shigella* infection was detrimental to the mice. This limited the number of dynasore injections that could be administered during the infection. Nonetheless these results suggest that

dynamin II inhibition may be a novel intervention strategy for preventing *Shigella* dissemination. The use of a different carrier solvent, increased or prolonged dynasore dosage and a different administration route may improve the efficacy of dynasore. Dynasore also inhibits the GTPase activity of Drp1 (Dynamin-related protein 1), a mitochondrial dynamin, which regulates mitochondrial fission (Macia *et al.*, 2006; Smirnova *et al.*, 1998). Since dynasore inhibits both dynamin II and Drp1, a role for Drp1 in preventing weight loss in mice during *S. flexneri* infection cannot be ruled out. We are currently investigating this possibility (Chapter 4).

In conclusion, dynamin II is a critical component of *Shigella* cell-to-cell spreading. Our data suggest that the process of *Shigella* cell-to-cell spreading relies in part on components important for endocytosis. Furthermore dynamin II inhibition with dynasore or a similar compound could provide a potential intervention strategy to dampen *Shigella* dissemination. The effect of dynasore on TTSS-induced cell death is currently being investigated.

Table 3.2 Summary of Sereny test. Mice were inoculated with 5×10^8 CFU bacteria where applicable.

Strain / treatment	Sereny score[a]	Mean (SD) % weight loss[b]	Figure
WT (2457T)	0.25 - 3 (D3)	6.00 (2.52) (*n* = 6)	3.S5
Δ*icsA* (RMA2041)	0 (D3)	8.88 (6.37) (*n* = 4)	3.S5
VP^- (RMA2159)	0 (D3)	-0.35 (1.93) (*n* = 4)	3.S5
NMP/PEG (no infection)	N/A (D3)	6.29 (0.68) (*n* = 6)	3.S1
NMP/PEG + Dynasore (no infection)	N/A (D3)	4.44 (3.44) (*n* = 6)	3.S1
2457T + NMP/PEG (Expt 2)	2.5 - 3 (D2)	12.52 (4.04) (*n* = 7)	3.6
2457T + NMP/PEG + Dynasore (Expt 2)	3 (D2)	7.72 (3.21) (*n* = 7)	3.6

[a]Sereny scores are between 0 - 3, recorded on D2 or D3

[b]% Mean weight loss on D2 or D3 (see Sereny scores) compared to D0

N/A Not applicable

3.6 Acknowledgements

We are grateful to the reviewer for their comments and suggestions, and to Dr Arindam Dey (James Cook University) for assistance with statistical analysis. We thank Dr Guido V. Bloemberg (Universität Zürich) for plasmid pMP7604, Dr Connor Thomas (University of Adelaide) for the *Listeria* strain and Luisa Van Den Bosch for preliminary work on dynasore. We thank Mark Daymon and Sofie Kogoj from the Ophthalmic Research Laboratories, Centre for Neurological Diseases, Adelaide, Australia for assistance with tissue embedding, sectioning and staining.

3.7 Supplementary data

Figure 3.S1 1:9 NMP/PEG as a vehicle for dynasore.

(A - B) HeLa cells were infected with *S. flexneri* 2457T in a plaque assay using a 6-well tray as described in the Methods section. Plaque formation was performed in the presence of dynasore dissolved in either DMSO or NMP/PEG. (A) The total plaque counts or (B) mean plaque diameters from each well from independent experiments were calculated. Data are represented as mean ± SEM of independent experiments (n = 3), analysed with one-way ANOVA ($p < 0.0001$), followed by Tukey's post hoc test (*$p < 0.05$, **$p < 0.01$, ***$p < 0.001$, ****$p < 0.0001$). Mice were not adversely affected by IP injection with either (C) 100 µL NMP/PEG or (D) 100 µL 5.5 mg/mL of dynasore in NMP/PEG (30 mg/kg) at t = 0, 7, 24, 31 h in the absence of bacterial inoculation. Each symbol represents one mouse. Data are represented as mean ± SEM, analysed with one-way ANOVA ($p = 0.0241$ for NMP/PEG and $p = 0.4529$ for dynasore in NMP/PEG). Tukey's post hoc test was carried out for NMP/PEG (*$p < 0.05$).

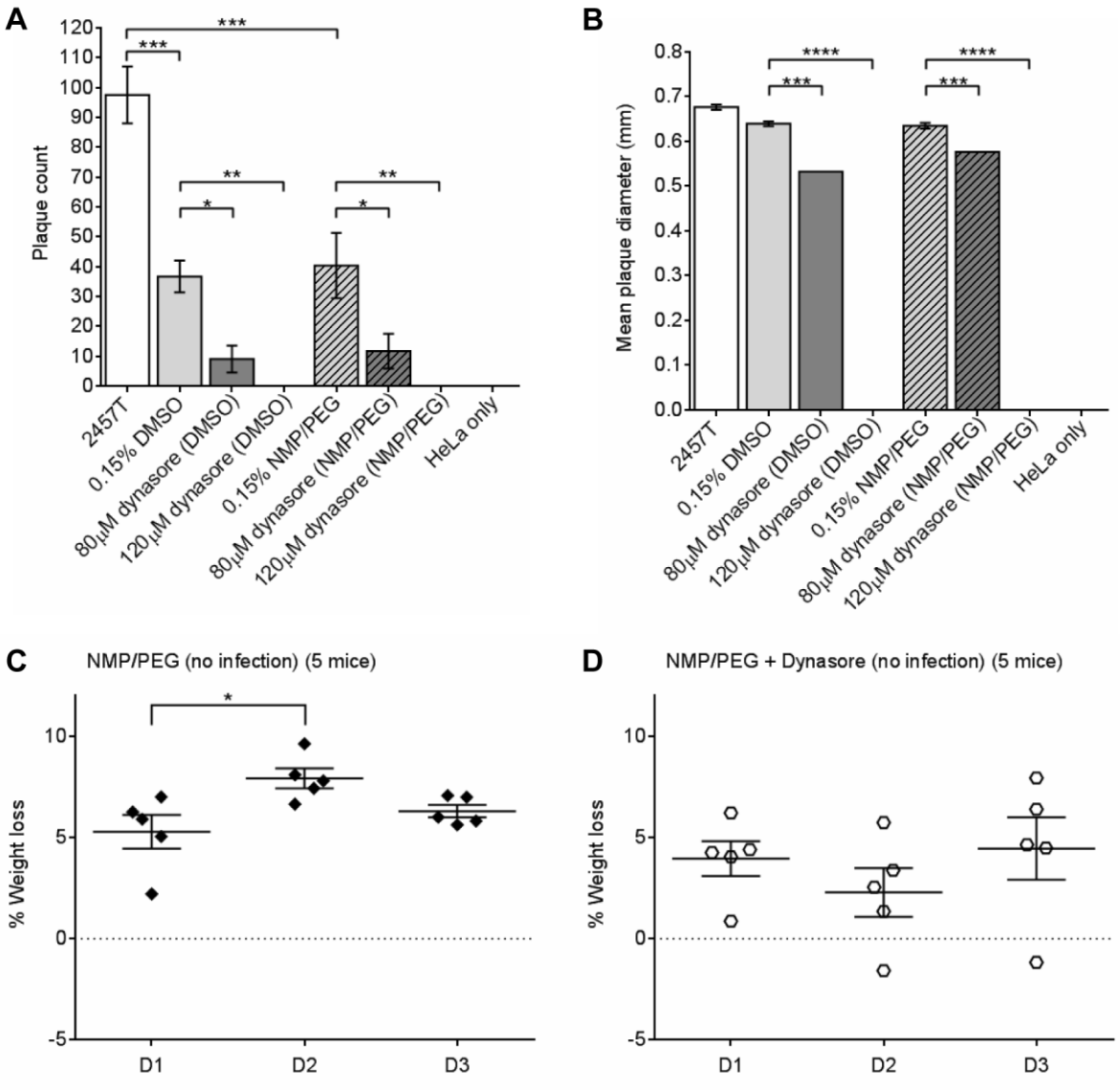
A
Plaque count
120
110
100
90
80
70
60
50
40
30
20
10
0
***
***
**
*
**
*
2457T
0.15% DMSO
80μM dynasore (DMSO)
120μM dynasore (DMSO)
0.15% NMP/PEG
80μM dynasore (NMP/PEG)
120μM dynasore (NMP/PEG)
HeLa only
B
Mean plaque diameter (mm)
0.8
0.7
0.6
0.5
0.4
0.3
0.2
0.1
0.0
****
***
****
***
2457T
0.15% DMSO
80μM dynasore (DMSO)
120μM dynasore (DMSO)
0.15% NMP/PEG
80μM dynasore (NMP/PEG)
120μM dynasore (NMP/PEG)
HeLa only
C
NMP/PEG (no infection) (5 mice)
% Weight loss
10
5
0
-5
*
D1
D2
D3
D
NMP/PEG + Dynasore (no infection) (5 mice)
% Weight loss
10
5
0
-5
D1
D2
D3

Figure 3.S2 Intracellular growth of *S. flexneri* 2457T in HeLa cells is not affected by dynasore.

HeLa cells were infected with *S. flexneri* 2457T for 1 h in a 24-well tray. HeLa cells were washed thrice with D-PBS and incubated with MEM containing 40 µg/mL of gentamicin (t = 0) to exclude extracellular bacteria. Concurrently HeLa cells were treated with 80 µM dynasore or DMSO. For each condition, two wells were prepared for each time point (t = 1, 2, 4 and 6 h). At each interval, HeLa cells were washed, followed by lysis with 0.1% Triton-X 100 to recover intracellular bacteria. Data are represented as mean from three independent experiments.

Figure 3.S3 *S. flexneri* 2457T entry into HeLa cells is not affected by dynasore.

HeLa cells were infected with *S. flexneri* 2457T for 1 h in a 24-well tray. Concurrently HeLa cells were treated with 80 µM dynasore or DMSO. For each condition, two wells were prepared. After the 1 h invasion, HeLa cells were washed thrice with D-PBS and incubated with MEM containing 40 µg/mL of gentamicin to exclude extracellular bacteria. After 2 h, HeLa cells were washed, followed by lysis with 0.1% Triton-X 100 to recover intracellular bacteria. Data are represented as mean from three independent experiments.

Figure 3.S4 Dynamin II is localised adjacent to N-WASP at *S. flexneri* 2457T pole.

HeLa cells were infected with *S. flexneri* 2457T in an invasion assay as described in the Methods section. Bacteria and HeLa nuclei were stained with DAPI (blue), N-WASP was stained with anti-N-WASP and Alexa Fluor 488-conjugated secondary antibody (green); and dynamin II was stained with anti-dynamin and Alexa Fluor 594-conjugated secondary antibody (red). Images were taken at 100× magnification. Scale bar = 10 µm. (A) - (C) The white arrows indicate protrusions. Insert shows 2× enlargement of the indicated region. Bacteria are outlined with white dotted lines. (D) The bacteria indicated with the white arrow are enlarged 6×. The thin arrowhead points to N-WASP and the thick arrowhead points to dynamin II. The yellow arrows point to areas of N-WASP and dynamin II overlap. The experiment was repeated twice and representative images are shown.

Figure 3.S2

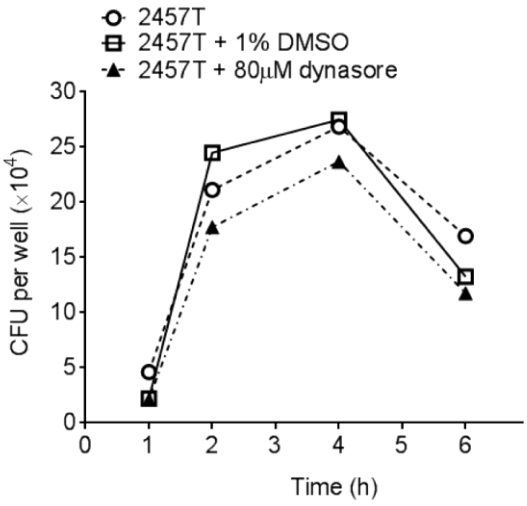

Figure 3.S3

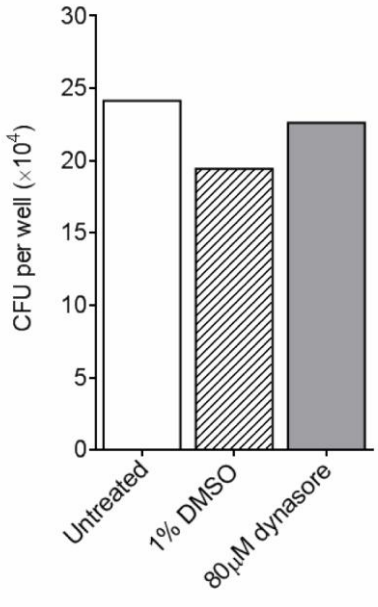

Figure 3.S4

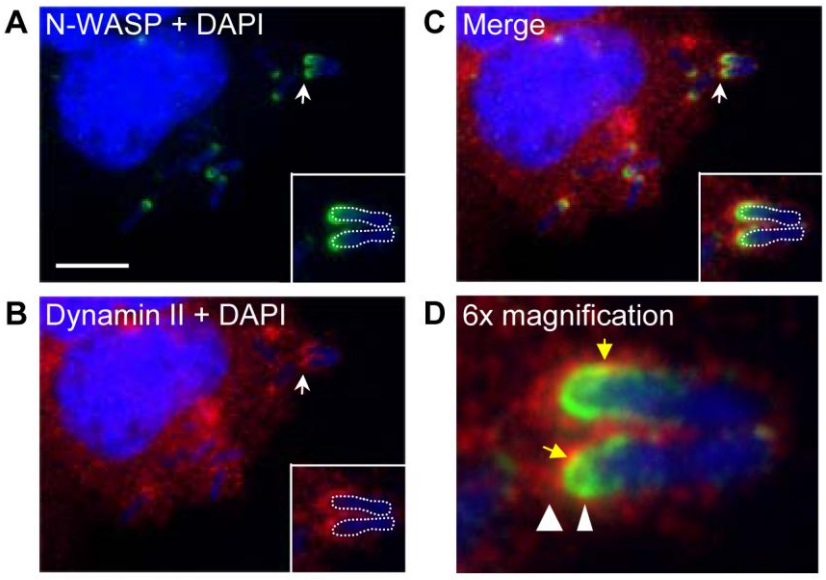

Figure 3.S5 Establishment of a mouse Sereny test to measure keratoconjunctivitis caused by *S. flexneri* 2457T.

(A) The left eye was inoculated with LB broth (control) and the right eye was inoculated with 5×10^8 CFU WT *S. flexneri* 2457T. Mouse keratoconjunctival inflammation was defined as follows: a score of 1 is defined as mild keratoconjunctivitis where the eye lid is slightly swollen, a score of 2 is defined as severe keratoconjunctivitis where the eye is half closed, and a score of 3 is defined as fully developed keratoconjunctivitis where the eye is completely closed. (B) Histology of fornix *(F)*, palpebral conjunctiva *(C)* and cornea *(Cor)* of the control eye (left - LB) and *S. flexneri*-infected eye with a Sereny score of 3 (right - 2457T). Polymorphonuclear leukocytes are infiltrating into the epithelial layer of the fornix (◀) and submucosal area of the conjunctiva and cornea (⬅) (60× magnification). (C - E) Mouse Sereny test with 5×10^8 CFU *S. flexneri* 2457T, Δ*icsA* (RMA2041) and virulence plasmid negative strain (VP^-) (RMA2159). (C) Sereny scores of mice infected with *S. flexneri* 2457T, RMA2041 and RMA2159 from 0 - 71 h post-infection. Each symbol represents one mouse. (D) The total number of mice with a Sereny score of ≥2.5 was calculated and plotted as a bar graph for each time point. (E) The percentage weight loss for each mouse on D3 was calculated. Data are represented as mean ± SEM, analysed with one-way ANOVA ($p = 0.0171$), followed by Dunnett's post hoc test with comparison to the mean of the VP^- strain ($^*p < 0.05$).

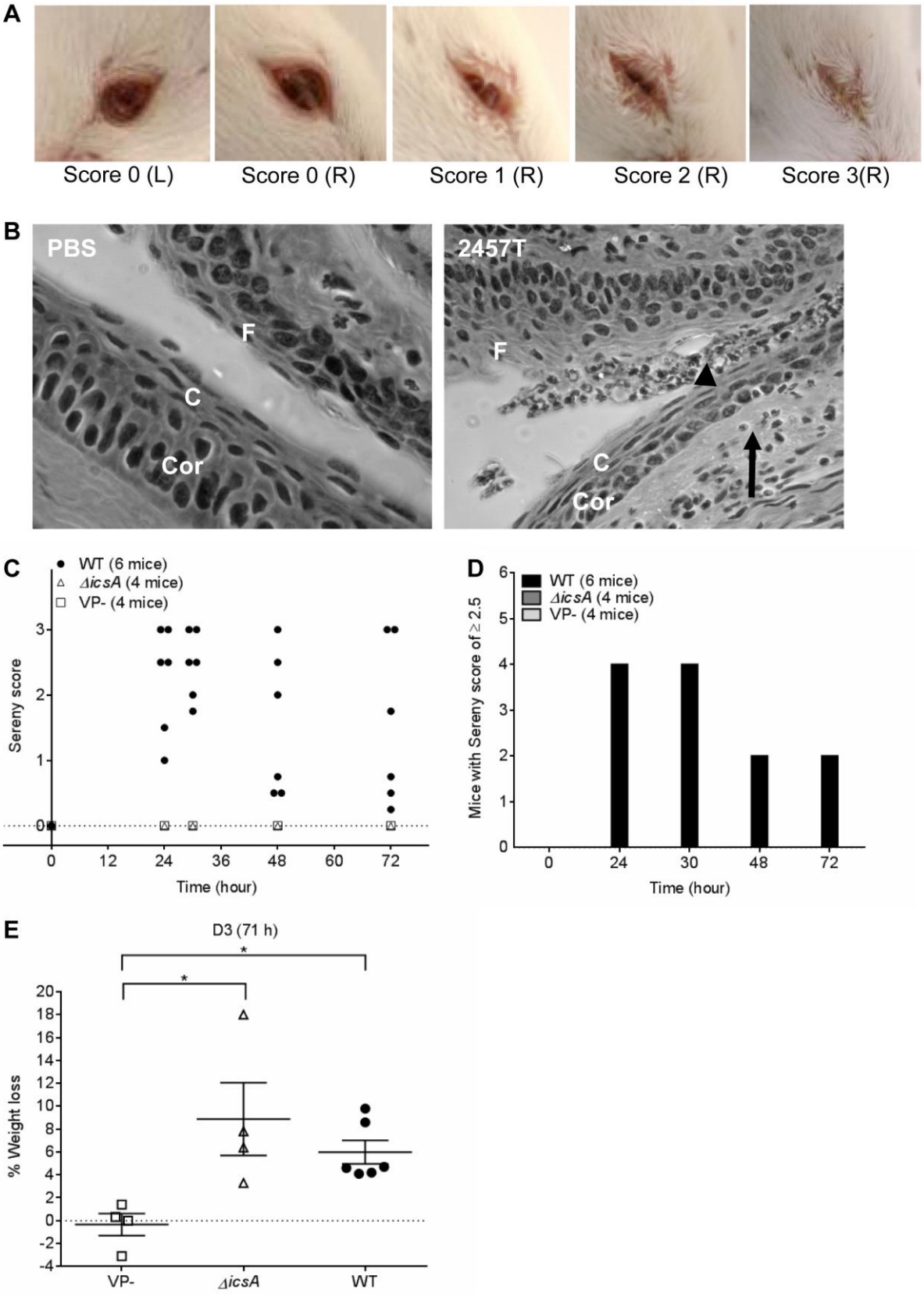
A
Score 0 (L)
Score 0 (R)
Score 1 (R)
Score 2 (R)
Score 3(R)
B
PBS
F
C
Cor
2457T
F
C
Cor
C
WT (6 mice)
ΔicsA (4 mice)
VP- (4 mice)
Sereny score
Time (hour)
D
WT (6 mice)
ΔicsA (4 mice)
VP- (4 mice)
Mice with Sereny score of ≥ 2.5
Time (hour)
E
D3 (71 h)
% Weight loss
VP-
ΔicsA
WT

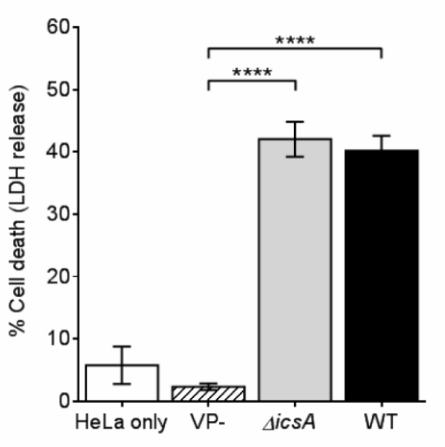

Figure 3.S6 HeLa cell death during *S. flexneri* 2457T and Δ*icsA* infection.

HeLa cells were infected with *S. flexneri* 2457T, Δ*icsA* (RMA2041) and virulence plasmid negative strain (VP^{-}) (RMA2159) in a 96-well tray and LDH release was measured as described in the Methods section. Data are represented as mean ± SEM of independent experiments ($n = 3$), analysed with one-way ANOVA ($p < 0.0001$), followed by Tukey's post hoc test (****$p < 0.0001$).

ꕥ CHAPTER 4 ꕥ

DYNAMIN-RELATED PROTEIN DRP1 AND MITOCHONDRIA ARE IMPORTANT FOR *Shigella flexneri* INFECTION

Dynamin-related protein Drp1 and mitochondria are important for *Shigella flexneri* infection

Mabel Lum and Renato Morona

School of Molecular and Biomedical Science, University of Adelaide, Adelaide, South Australia, Australia

Lum M & Morona R (2014). Dynamin-related protein Drp1 and mitochondria are important for *Shigella flexneri* infection.
***Int J Med Microbiol* 304, 530-541.**

STATEMENT OF AUTHORSHIP

Title of Paper	Dynamin-related protein Drp1 and mitochondria are important for *Shigella flexneri* infection
Publication Status	○ Published ○ Accepted for Publication ○ Submitted for Publication ○ Publication Style
Publication Details	Lum M & Morona R (2014). Dynamin-related protein Drp1 and mitochondria are important for *Shigella flexneri* infection. *Int J Med Microbiol* 304, 530-541.

Author Contributions

By signing the Statement of Authorship, each author certifies that their stated contribution to the publication is accurate and that permission is granted for the publication to be included in the candidate's thesis.

Name of Principal Author (Candidate)	Mabel Yuen Teng Lum		
Contribution to the Paper	Performed all experiments, performed analysis on all samples, interpreted data, wrote manuscript and acted as corresponding author.		
Signature		Date	

Name of Co-Author	Renato Morona		
Contribution to the Paper	Supervised development of work, helped in data interpretation, helped to evaluate and edit the manuscript.		
Signature		Date	

Chapter 4: Dynamin-related protein Drp1 and mitochondria are important for *Shigella flexneri* infection

4.1 Abstract

Shigella infection in epithelial cells induces cell death which is accompanied by mitochondrial dysfunction. In this study the role of the mitochondrial fission protein, Drp1, during *Shigella* infection in HeLa cells was examined. Significant lactate dehydrogenase (LDH) release was detected in the culture supernatant when HeLa cells were infected with *Shigella* at a high multiplicity of infection. Drp1 inhibition with Mdivi-1 and siRNA knockdown significantly reduced LDH release. HeLa cell death was also accompanied by mitochondrial fragmentation. Tubular mitochondrial networks were partially restored when Drp1 was depleted with either siRNA or inhibited with Mdivi-1. Surprisingly either Mdivi-1 treatment or Drp1 siRNA-depletion of HeLa cells also reduced *Shigella* plaque formation. The effect of Mdivi-1 on *Shigella* infection was assessed using the murine Sereny model; however it had no impact on ocular inflammation. Overall our results suggest that Drp1 and the mitochondria play important roles during *Shigella* infection.

4.2 Introduction

Shigella flexneri is the causative agent of bacillary dysentery (shigellosis) and is a significant human pathogen due to its high morbidity among children <5 years in developing countries (Bardhan *et al.*, 2010). The key pathogenic features of *Shigella* include cell death induction in myeloid immune cells and circumventing cell death in colonic epithelial cells, the site of *Shigella* infection. *Shigella* also interact with host proteins to initiate *de novo* actin synthesis to facilitate its intra- and intercellular spread to disseminate within the colon.

Post-ingestion of contaminated food and water, *Shigella* initially invade the host intestinal epithelium via microfold cells and induce pyroptosis of the resident macrophages in the follicle associated epithelium by activating ICE protease-activating factor-dependent (IPAF/NLRC4) and apoptosis-associated speck-like protein containing caspase recruitment domain (ASC) inflammasome (Senerovic *et al.*, 2012; Suzuki *et al.*, 2007). Subsequent caspase-1 activation releases interleukin-1β and interleukin-18, resulting in strong inflammatory responses and magnified innate responses, respectively (Sansonetti *et al.*, 2000). Another form of necrotic cell death induced in macrophage is pyronecrosis, which is independent of caspase-1 activation and releases another proinflammatory factor, HMGB1 (high-mobility group box 1 protein) (Willingham *et al.*, 2007).

Following macrophage pyroptosis, *Shigella* are released into the basolateral compartment and invade enterocytes via the type three secretion system (TTSS), followed by lysis of the endocytic vacuole and replication in the cytoplasm (Cossart & Sansonetti, 2004; Sansonetti *et al.*, 1986). The polarly localised *Shigella* IcsA protein interacts with the host Neural Wiskott-Aldrich syndrome protein (N-WASP) and Arp2/3 complex to initiate F-actin nucleation and polymerisation, leading to actin-based motility which allows the bacterium to spread within the cytoplasm and also laterally via protrusion formation into the adjacent cells (Bernardini *et al.*, 1989; Lett *et al.*, 1989; Makino *et al.*, 1986). After escaping from the double membrane vacuole, subsequent cycles of infection are initiated (Schuch *et al.*, 1999). Proteins localised at the enterocyte tight junctions and adherens junctions facilitate *Shigella* protrusion formation and may associate directly with the *Shigella* actin tail (Bishai *et al.*, 2012; Kadurugamuwa *et al.*, 1991; Sansonetti *et al.*, 1994). *Shigella* invasion and dissemination is also dependent on ATP release by connexin 26 and formins, Dia1 and Dia2, which can initiate

de novo actin polymerisation and cross-link actin filaments (Heindl *et al.*, 2009; Tran Van Nhieu *et al.*, 2003). Components of the clathrin-mediated endocytosis pathway also facilitate *Shigella* entry into the adjacent cell (Fukumatsu *et al.*, 2012; Lum *et al.*, 2013).

Eliminating infected enterocytes prevents *Shigella* from propagating and disseminating into uninfected cells (Ashida *et al.*, 2011a). However *Shigella* is able to delay cell death by manipulating host signalling pathways. Depending on the experimental conditions such as host cell type, time of infection and multiplicity of infection (moi), apoptotic and necrotic cell death have been observed during *Shigella* infection. Apoptosis is a non-inflammatory cell death which is activated by mitochondria and death receptor-mediated pathways characterised by caspase activation, DNA fragmentation, cell shrinkage, membrane blebbing and mitochondrial permeability (Lamkanfi & Dixit, 2010), whereas necrosis is characterised by nuclear swelling, membrane rupture and spillage of cellular contents into the environment resulting in inflammatory conditions. Absence of caspase activation, reactive oxygen species (ROS) production, lysosomal destabilisation, calpain release and ATP depletion are also observed (Golstein & Kroemer, 2007; Vandenabeele *et al.*, 2010).

S*higella* infection in HeLa cells induces an early genotoxic stress (Bergounioux *et al.*, 2012). The tumour suppressor protein p53, an inducer of apoptosis, is normally stabilised during genotoxic response. However p53 is rapidly degraded by calpain, through degradation of the calpain protease inhibitor, calpastatin, by the *Shigella* VirA TTSS effector (Bergounioux *et al.*, 2012). Calpain activation inadvertently activates the necrosis pathway which restricts *Shigella* intracellular growth (Bergounioux *et al.*, 2012). In the colonic HCT116 cells, the slow degradation of p53 shifts the executing pathway from necrosis to apoptosis (Bergounioux *et al.*, 2012). In HaCat (immortalised keratinocytes) cells, the *Shigella* TTSS effector, OspC3, targets the p19 subunit of Caspase-4 to delay necrotic cell death (Kobayashi *et al.*, 2013). *In vivo* the Δ*ospC3* mutant exacerbates colonic inflammation in guinea pigs (Kobayashi *et al.*, 2013). In HeLa cells and mouse embryonic fibroblasts (MEFs), pro-survival Nod1/NF-κB/Bcl-2 signalling is activated to counteract the necrotic pathway mediated by Bnip3, a regulator of mitochondrial permeability transition, during *Shigella* infection (Carneiro *et al.*, 2009). In staurosporine (STS)-induced apoptosis in HeLa cells, the *Shigella* Spa15 (TTSS) effector prevented caspase-3 activation (Faherty & Maurelli, 2009). *Shigella* infection in HeLa cells and in an *ex vivo* colonic epithelial cell model

reportedly triggered apoptosis via caspase-9 and caspase-3 activation (Lembo-Fazio *et al.*, 2011). Furthermore *gadd45a* (stress sensor growth arrest and DNA damage 45a), a stress-inducible gene, was also upregulated *in vitro* and *ex vivo* (Lembo-Fazio *et al.*, 2011).

Mitochondrial fission is an important downstream event for intrinsic apoptotic and programmed necrosis signalling pathways (Otera *et al.*, 2013). Mitochondrial constriction is initially mediated by the endoplasmic reticulum and actin (Friedman *et al.*, 2011; Korobova *et al.*, 2013). Dimeric or tetrameric cytosolic dynamin-related protein 1 (Drp1, also known as dynamin-1-like protein) is then recruited to fission sites on the mitochondria to its receptor, Mff (Otera *et al.*, 2010). In the presence of GTP, Drp1 self-assembly stimulates GTP hydrolysis and formation of higher order structures as foci at the mitochondrial fission sites (Smirnova *et al.*, 2001). Oligomerised Drp1 wraps around the mitochondria and following GTP hydrolysis, the mitochondrial membrane is severed (Smirnova *et al.*, 2001). Drp1 assembly on the mitochondria is inhibited by the small molecule inhibitor, *m*itochondrial *div*ision *i*nhibitor-*1* (Mdivi-1), through interactions with an allosteric site which does not affect its GTPase activity (Cassidy-Stone *et al.*, 2008). Mdivi-1 has therapeutic effects in various animal models of non-infectious diseases (Ferrari *et al.*, 2011; Ong *et al.*, 2010; Tang *et al.*, 2013).

Previously we reported that dynasore, an inhibitor of dynamin II and Drp1 GTPase activity, affected *Shigella* cell-to-cell spreading and *Shigella*-induced cytotoxicity in HeLa cells. Furthermore dynasore also protected mice from weight loss in an ocular infection model even though inflammation was not reduced (Lum *et al.*, 2013) (Chapter 3). We decided to investigate if Drp1 contributed to the observations we made earlier. In this study HeLa cells were infected with *Shigella* at a moi of 500 and 1000. During *Shigella* infection, lactate dehydrogenase (LDH) was released into the culture supernatant. HeLa cells treated with a pan-caspase inhibitor did not reduce LDH release and caspase-3 was not activated, suggesting *Shigella* induces non-apoptotic cell death under these conditions. Drp1 inhibition with Mdivi-1 and Drp1 depletion with siRNA reduced LDH release. Mitochondrial fragmentation was also observed in *Shigella*-infected HeLa cells and was partially restored when HeLa cells were either treated with Mdivi-1 or when Drp1 was depleted with siRNA. Unexpectedly *Shigella* plaque formation was reduced in Mdivi-1-treated HeLa cells. This was also observed in HeLa cells knockdown with Drp1 siRNA, suggesting maintaining mitochondria structure is

important for efficient cell-to-cell spreading. A murine Sereny test was used to determine if Mdivi-1 could reduce keratoconjunctivitis or protect mice from weight loss due to *Shigella* infection. Mdivi-1 treatment did not reduce ocular inflammation but did protect mice from weight loss in the first 24 h only. These results suggest Drp1 and the mitochondria are critical for *Shigella* infection.

4.3 Materials and methods

4.3.1 Bacterial strains and growth media

The strains used in this study are listed in Table 4.1. *S. flexneri* strains were grown from a Congo Red positive colony as described previously (Morona *et al.*, 2003) and were routinely cultured in Luria Bertani (LB) broth and on LB agar. Virulence plasmid-cured (VP^-) derivative of WT *S. flexneri* strain was isolated on Congo Red agar as white colonies and re-streaked until pure (Morona & Van Den Bosch, 2003). Bacteria were grown in media for 16 h with aeration, subcultured 1/20 and then grown with aeration to mid-exponential growth phase for 1.5 h at 37°C. Where appropriate, media were supplemented with tetracycline (4 or 10 μg/mL).

Table 4.1 Bacterial strains and plasmids

Strain	Relevant characteristics[#]	Reference or source
S. flexneri		
2457T	*S. flexneri* 2a wild type	Laboratory collection
MLRM107	2457T [pMP7604; Tc^R]	(Lum *et al.*, 2013) (Chapter 3)
RMA2159	Virulence plasmid-cured 2457T	Laboratory collection

[#]Tc^R, Tetracycline resistant

4.3.2 Chemicals and antibodies

IM-54 (5 mM stock - ALX-430137; Enzo Life Sciences), Mdivi-1 (50 mM stock - M0199; Sigma-Aldrich, BML-CM127; Enzo Life Sciences), Necrostatin-1 (100 mM stock - N9037; Sigma-Aldrich), Necrostatin-7 (20 mM stock - ALX-430-170; Enzo Life Sciences), Necrosulfonamide (20 mM stock - N388600; Toronto Research Chemicals), NecroX-2 (5 mM stock - ALX-430-166; Enzo Life Sciences), NecroX-5 (5 mM stock - ALX-430-167; Enzo Life Sciences), Staurosporine (10 mM stock - 00025, Biotium), Z-FA-fmk (20 mM stock - 550411; BD Biosciences) and Z-VAD-fmk (20 mM stock - Merck Calbiochem; 627610) were

prepared in dimethyl sulfoxide (DMSO) (D2650; Sigma-Aldrich) for *in vitro* studies. For *in vivo* studies, Mdivi-1 was dissolved in a formulation containing *N*-methyl-2-pyrrolidone (NMP/Pharmasolve; Ashland ISP) and polyethylene glycol 300 (PEG300; Sigma-Aldrich) (1 part NMP to 9 parts PEG300). Mdivi-1 was prepared as a 22 mg/mL stock and diluted 1/4 (5.5 mg/mL) with NMP/PEG before injection into mice. Mouse anti-DLP1 antibody (611112; BD Biosciences) and rabbit anti-GAPDH antibody (600-401-A33; Rockland Immunochemicals, Inc.) were used at 1:100 and 1:3000 for Western immunoblotting, respectively. For immunofluorescence (IF) microscopy, rabbit anti-active (cleaved) caspase-3 antibody (AB3623; Merck Milipore), anti-DLP1 antibody, Alexa 594-conjugated donkey anti-mouse secondary antibody and Alexa Fluor 594-conjugated donkey anti-rabbit antibody (Molecular Probes) were used at 1:100.

4.3.3 Reverse transfection and HeLa cell lysate preparation

DNM1L siRNA (L012092-00-0005) and siRNA controls (Non-targeting Pool; D-001810-10-05, siGLO Green Transfection Indicator; D-001630-01-05) were purchased from Thermo Scientific. siRNAs were transfected with DharmaFECT 3 Transfection Reagent (T-2003-03) and DharmaFECT Cell Culture Reagent (DCCR; B-004500-100), also purchased from Thermo Scientific. Reverse transfection of HeLa cells (Human, cervical, epithelial cells ATCC #CCL-70) were carried out based on a method by Thermo Scientific. siRNA were prepared as a 5 µM stock and the final concentration used was 50 nM. HeLa cells were transfected and cell lysates were prepared as described previously (Lum *et al.*, 2013).

4.3.4 SDS-PAGE and Western immunoblotting

SDS-PAGE (12% acrylamide gel) and Western immunoblotting were carried out as described previously (Lum *et al.*, 2013). Molecular weight markers used were BenchMark™ Pre-Stained Protein Ladder (Invitrogen).

4.3.5 Plaque assay

Plaque assays were performed with HeLa cells as described previously (Oaks *et al.*, 1985) with modifications. HeLa cells were transfected in 12-well trays prior to plaque assay as described previously (Lum *et al.*, 2013). On day 4, the plaque assay was carried out when the cells reached confluency. HeLa cells were washed twice with Dulbecco's modified Eagle

medium (DMEM) prior to inoculation. 5×10^4 mid-exponential phase bacteria were added to each well. Trays were incubated at 37°C, 5% CO_2 and were rocked gently every 15 min to spread the inoculum evenly across the well. At 90 min post-infection, the inoculum was aspirated. 0.5 mL of the first overlay (DMEM, 5% FCS, 20 µg/mL gentamicin, 0.5% (w/v) agarose [Seakem ME]) was added to each well. The second overlay (DMEM, 5% FCS, 20 µg/mL gentamicin, 0.5% (w/v) agarose, 0.1% (w/v) Neutral Red solution [Gibco BRL]) was added 24 h post-infection and plaques were imaged 6 h later. All observable plaques were counted and the diameter was measured for each condition in each experiment. At least 50 plaques were measured for each condition.

4.3.6 Infectious focus assay

1.2×10^6 HeLa cells were seeded in six-well trays in minimal essential medium (MEM), 10% FCS, 1% penicillin/streptomycin. Cells were grown to confluence overnight and were washed twice with DMEM prior to inoculation. 5×10^4 mid-exponential phase bacteria expressing mCherry were added to each well. Trays were incubated at 37°C, 5% CO_2 and were rocked every 15 min to spread the inoculum evenly across the well. At 90 min post-infection, the inoculum was aspirated. 1.5 mL of DMEM (phenol red-free) (31053-028; Life Technologies), 1 mM sodium pyruvate, 5% FCS, 20 µg/mL gentamicin, 2 mM IPTG was added to each well. Mdivi-1 or DMSO were added and were swirled to ensure even distribution. 24 h later the infectious foci were imaged with an Olympus IX-70 microscope using a 10× objective. The filter set used was DA/FI/TX-3X-A-OMF (Semrock). Fluorescence and phase contrast images were captured and false colour merged with the Metamorph software programme (Version 7.7.3.0, Molecular Devices). The area of the infectious focus, i.e. area where mCherry was expressed, was outlined and measured with Metamorph. All observable infectious foci were counted and the area was measured for each condition in each experiment. At least 5 infectious foci were measured for each condition.

4.3.7 Invasion assay and IF microscopy

HeLa cells (8×10^4) were seeded onto sterile glass cover slips in 24-well trays in MEM, 10% FCS, 1% penicillin/streptomycin. For transfected cells, HeLa cells were transfected as described previously (Lum *et al.*, 2013). Cells were grown to semi-confluence overnight, washed twice with Dulbecco's PBS (D-PBS) and once with MEM, 10% FCS. 4×10^7 mid-

exponential phase bacteria were added to each well and subsequently centrifuged (2,000 rpm, 7 min, Heraeus Labofuge 400 R) onto HeLa cells. After 1 h incubation at 37°C, 5% CO_2, the infected cells were washed thrice with D-PBS and incubated with 0.5 mL MEM containing 40 µg/mL of gentamicin for a further 1.5 h (or 3.5 h for labelling with anti-activated caspase-3). Infected cells were washed thrice in D-PBS, fixed in 3.7% (v/v) formalin for 15 min, incubated with 50 mM NH_4Cl in D-PBS for 10 min, followed by permeabilisation with 0.1% Triton X-100 (v/v) for 5 min. After blocking in 10% FCS in PBS, the infected cells were incubated at 37°C for 30 min with the desired primary antibody. After washing in PBS, coverslips were incubated with either Alexa Fluor 594-conjugated donkey anti-mouse or Alexa 594-conjugated donkey anti-rabbit secondary antibody (Molecular Probes) (1:100). F-actin was visualised by staining with Alexa Fluor 488-conjugated phalloidin (2 U/mL) and 4',6'-diamidino-2-phenylindole (DAPI) (10 µg/mL) was used to counterstain bacteria and HeLa cell nuclei. Coverslips were mounted on glass slides with Mowiol 4-88 (Calbiochem) containing 1 µg/mL *p*-phenylenediamine (Sigma) and was imaged using a 100× oil immersion objective (Olympus IX-70). The filter set used was DA/FI/TX-3X-A-OMF (Semrock). Fluorescence and phase contrast images were false colour merged using the Metamorph software programme.

4.3.8 MitoTracker® Red CMXRos labelling

HeLa cells were seeded and infected as described in "***Invasion assay and IF microscopy***" (Section 4.3.7). The infected cells were washed thrice with D-PBS and incubated with 0.5 mL MEM containing 40 µg/mL of gentamicin for 2 h 55 min. The media was removed and replaced with pre-warmed 400 nM MitoTracker® Red CMXRos (Invitrogen) in MEM, 40 µg/mL gentamicin for 35 min. HeLa cells were washed thrice with pre-warmed D-PBS, fixed in pre-warmed 3.7% (v/v) formalin for 15 min, followed by three washes with pre-warmed PBS. Bacteria and HeLa cell nuclei were stained with 10 µg/mL DAPI in MQ water for 1.5 min at RT, followed by two washes with pre-warmed PBS and one wash with pre-warmed mQ water. Cover slips were mounted and imaged using a 100× oil immersion objective as described in "***Invasion assay and IF microscopy***" (Section 4.3.7).

4.3.9 Protrusion formation

HeLa cells were seeded, infected and fixed as per "***Invasion assay and IF microscopy***" (Section 4.3.7). HeLa cells were washed twice with 1× Annexin V binding buffer (99902; Biotium) prepared in milliQ (18.2 MΩ·cm) water, mounted on glass slides with the same buffer and were imaged using a 40× oil immersion objective (Olympus IX-70). Protrusion formation was defined as any extensions of bacterial projection(s) (minimum of a full bacterial length) beyond the periphery of the HeLa cell. For each condition in each experiment, a minimum of 100 cells were imaged.

4.3.10 Assay for growth of intracellular bacteria

HeLa cells (8×10^4) were seeded in 24-well trays in MEM, 10% FCS, 1% penicillin/streptomycin. Cells were grown to semi-confluence overnight, washed twice with D-PBS and once with MEM, 10% FCS. 4×10^7 mid-exponential phase bacteria were added to each well (moi 500) and were centrifuged (2,000 rpm, 7 min, Heraeus Labofuge 400 R) onto HeLa cells. After 1 h incubation at 37°C, 5% CO_2, the infected cells were washed thrice with D-PBS and incubated with 0.5 mL MEM containing 40 µg/mL of gentamicin. At the indicated intervals, monolayers (in duplicate) were washed four times in D-PBS and were lysed with 0.1% (v/v) Triton X-100 in PBS for 5 min and bacteria were enumerated on tryptic soy agar (Gibco) plates.

4.3.11 LDH cytotoxicity assay

HeLa cells (3×10^4) were seeded in 96-well trays in MEM, 10% FCS, 1% penicillin/streptomycin. Cells were grown to confluence overnight and were washed twice with PBS. 50 µL phenol-red free DMEM, 1 mM sodium pyruvate and 3×10^7 mid-exponential phase bacteria (moi 1000) in 50 µL PBS or PBS were added into each well, where appropriate. The bacteria were centrifuged (2,000 rpm, 7 min, Heraeus Labofuge 400 R) onto HeLa cells. After 1 h incubation at 37°C, 5% CO_2, the infected cells were washed thrice with PBS and incubated with 0.1 mL phenol-red free MEM, 40 µg/mL of gentamicin for 4 h. LDH activity was measured with the Cytotoxicity Detection Kit^{Plus} as per manufacturer's instructions (Roche). The percentage of LDH released was calculated with the following

formula: ((experimental LDH release − spontaneous LDH release) / (maximal LDH − spontaneous LDH release)) × 100.

4.3.12 Ethics statement

The use of animals in this study has been approved by the University of Adelaide Animal Ethics Committee (Project number: S-2012-90). All animals used were handled in compliance with the Australian code of practice for the care and use of animals for scientific purposes, 7th edition (2004).

4.3.13 Mouse Sereny test

The mouse Sereny test (Murayama *et al.*, 1986) was carried out as described previously (Lum *et al.*, 2013). Male Balb/c mice (20 - 22g) were inoculated with 2.5×10^7 CFU bacteria in 5 μL of bacterial suspension (in PBS) into the right eye; the left eye served as a diluent control. To ascertain the impact of Mdivi-1 on ocular infection, mice were injected intraperitoneally (IP) with drug at a dose rate of 30 mg/kg, at t = -1, +6, +23 and +30 h with respect to infection at 0 h. Keratoconjunctivitis was evaluated at specific time points after inoculation and scored on a scale ranging from 0 (no infection), 1 (mild keratoconjunctivitis where the eye lid is slightly swollen), 2 (severe keratoconjunctivitis where the eye is half closed) and 3 (fully developed keratoconjunctivitis where the eye is completely closed). Due to an ethics concern with the *in vivo* use of DMSO, Mdivi-1 was prepared in NMP/PEG, which is made up of 1 part *N*-methyl-2-pyrrolidone (NMP) and 9 parts polyethylene glycol 300 (PEG300). A preliminary mouse study showed that this dosing regime resulted in ~10% weight loss over a period of 72 h (Figure 4.S1).

4.3.14 Statistical analysis

Statistical analysis was carried out using GraphPad Prism 6. Results are expressed as means ± SEM of data obtained in independent experiments. Statistical differences between two groups were determined with a two-tailed unpaired *t*-test. Statistical differences between three or more groups were determined with a one-way ANOVA followed by Tukey's multi comparison post hoc test. Statistical significance was set at $p < 0.05$.

4.4 Results

4.4.1 *S. flexneri* induces Drp1-mediated cell death in HeLa cells

In a preliminary experiment, we investigated the effects of *S. flexneri* moi on LDH release. HeLa monolayers were infected with WT or virulence plasmid-cured (VP^-) *S. flexneri* at moi ranging from 1 to 1000 (Figure 4.S2). HeLa cells infected with WT *Shigella* at moi of ≥100 had significantly higher LDH release compared to the VP^- strain. Moi of 500 and 1000 was used in this study to reflect the experimental conditions used previously (Lum *et al.*, 2013) (Chapter 3). No difference in LDH release was observed between moi 500 and 1000 (Figure 4.S2).

Recently we reported that dynasore, a non-competitive, reversible inhibitor of dynamin II and Drp1 GTPase activity, significantly reduced *S. flexneri*-induced cytotoxicity in HeLa cells (Lum *et al.*, 2013) (Chapter 3). The efficacy of dynasore was also tested in a murine ocular infection model. Mice treated with dynasore lost significantly less weight compared to mice treated with the NMP/PEG vehicle, however no improvement in ocular inflammation was observed. These results prompted us to examine the role of Drp1, if any, during *S. flexneri* pathogenesis. We initially investigated if *S. flexneri*-induced HeLa cytotoxicity was mediated by the mitochondrial fission protein, Drp1. The effects of Mdivi-1, a Drp1 inhibitor, and Drp1 siRNA on LDH release were determined. HeLa monolayers infected with *S. flexneri* (moi 1000) were treated with increasing concentrations of Mdivi-1 or with the DMSO control alone. *Shigella*-infected DMSO-treated HeLa cells released high levels of LDH (43.68 ± 0.85%) (Figure 4.1A). In HeLa cells treated with 50 μM Mdivi-1, LDH release was significantly reduced (32.70 ± 0.47%) and further reduction was observed with 100 μM Mdivi-1 treatment (24.06 ± 2.70) (Figure 4.1A). To investigate the effect of Drp1 depletion on *S. flexneri*-induced cytotoxicity, HeLa cells were transfected with Drp1 siRNA and LDH release by infected cells was measured. Western immunoblots of HeLa cell lysates two days post-siRNA treatment showed no detectable Drp1 levels (Figure 4.1B). LDH release induced by *S. flexneri* was significantly reduced in HeLa cells treated with Drp1 siRNA ($*p < 0.05$) (Figure 4.1C).

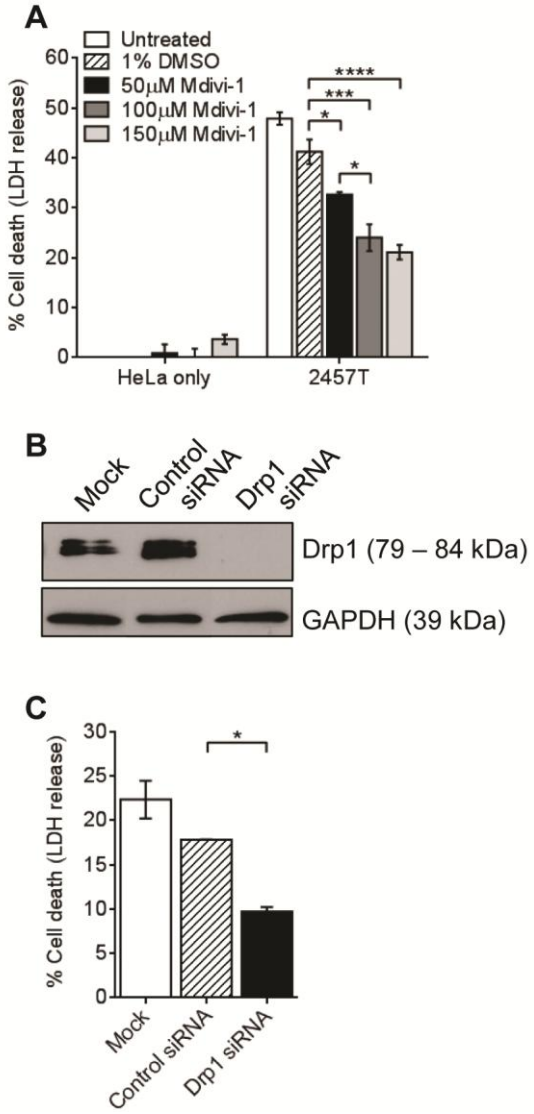

Figure 4.1 Drp1 mediates *S. flexneri* 2457T-induced HeLa cell death.

(A) HeLa cells were infected with *S. flexneri* 2457T (moi 1000) in a 96-well tray for 1 h, followed by incubation with MEM containing 40 µg/mL of gentamicin to exclude extracellular bacteria for 4 h as described in the Methods section. LDH release was measured in the presence of DMSO or Mdivi-1. Data are represented as mean ± SEM of independent experiments (n = 3), analysed with one-way ANOVA ($p < 0.0001$), followed by Tukey's post hoc test (*$p < 0.05$, ***$p < 0.001$, ****$p < 0.0001$). No differences in LDH release were observed in the presence of Mdivi-1 or DMSO in the absence of bacterial infection. (B - C) HeLa cells were either mock transfected or transfected with control or Drp1 siRNA for 24 h, trypsinised and re-transfected for further 24 h. (B) HeLa cell extracts were probed with anti-Drp1. GAPDH was used as a loading control. (C) Post-transfection, HeLa cells were infected with *S. flexneri* 2457T in a 96-well tray as described in (A). Data are represented as mean ± SEM of independent experiments (n = 2), analysed with one-way ANOVA (p = 0.0129), followed by Tukey's post hoc test (*$p < 0.05$).

4.4.2 *S. flexneri* induces non-apoptotic cell death in HeLa cells

Since Drp1 has been implicated in both apoptosis and necrosis, we determined if components of the apoptotic or necrotic cell death pathways were involved. Uninfected HeLa monolayers were treated with the DMSO control or positive control agents; staurosporine (STS) to induce apoptosis, or 0.01% Triton X-100 to induce necrosis (Kwon *et al.*, 2011) (Figure 4.2A). LDH release was observed in HeLa cells treated with 0.01% Triton X-100 but not STS. The effects of Z-VAD-fmk, a pan-caspase inhibitor and its inactive analogue, Z-FA-fmk, on LDH release during *S.flexneri* infection were determined. HeLa monolayers infected with *S. flexneri* were treated with increasing concentrations of Z-VAD-fmk or Z-FA-fmk or the DMSO control. No reduction in LDH release was observed (Figure 4.2B - C). Caspase-3 cleavage is indicative of apoptosis activation (Reed, 2000). We investigated activated caspase-3 localisation in untreated, DMSO-treated, STS-treated and *S. flexneri*-infected (moi 500) HeLa cells (Figure 4.S3). Activated caspase-3 was only observed in HeLa cells treated with STS (Figure 4.S3C). Nuclear and cell shrinkage was also observed. Therefore *S. flexneri* infection induced non-apoptotic cell death in HeLa cells. Since LDH release was observed when HeLa cells were treated with Triton X-100 and not STS, we reasoned that the cell death pathway activated during *Shigell*a infection under the conditions used is most likely necrosis.

Next we investigated if components of the programmed necrosis pathway are important during *S. flexneri*-infection. Necrostatin-1 is an allosteric inhibitor of receptor-interacting serine/threonine-protein kinase 1 (RIP1) (Degterev *et al.*, 2008); necrostatin-7 targets an unknown effector in the programmed necrosis pathway (Zheng *et al.*, 2008); and necrosulfonamide covalently modifies mixed lineage kinase domain-like protein (MLKL) to prevent downstream necrosis activation (Sun *et al.*, 2012). HeLa monolayers infected with *S. flexneri* (moi 1000) were treated with increasing concentrations of necrostatin-1 or necrostatin-7 or necrosulfonamide or with the DMSO control alone. No reduction in LDH release was observed (Figure 4.2D - F). We also investigated if *S. flexneri*-induced cell death was a result of oxidative stress. IM-54 inhibits hydrogen peroxide-induced necrosis (Dodo *et al.*, 2005), and NecroX-2 and -5 are mitochondria-targeted ROS and nitrogen oxidative species (NOS) scavengers (Kim *et al.*, 2010). HeLa monolayers infected with *S. flexneri* (moi 1000) were treated with increasing concentrations of IM-54 or NecroX-2 or -5 or with the DMSO control alone. No reduction in LDH release was observed (Figure 4.2G - H). Hence *S.*

flexneri-induced cell death in HeLa cells is unlikely a consequent of oxidative stress and is unlikely activated via the RIP1/MLKL programmed necrosis pathway.

4.4.3 *S. flexneri* infection induces mitochondrial fragmentation

Next we investigated the effects of *S. flexneri* infection on mitochondria of HeLa cells by IF microscopy. In uninfected and DMSO-treated HeLa cells, the mitochondrial network is long and tubular (Figure 4.3A - B). When mitochondrial division is inhibited, tubular mitochondrial networks becomes interconnected to form net-like structures, or collapse into perinuclear structures (Smirnova *et al.*, 1998; Smirnova *et al.*, 2001). HeLa cells treated with the Drp1 inhibitor, Mdivi-1, had degenerate perinuclear mitochondrial structures (Figure 4.3C). HeLa cells were either untreated, treated with DMSO or treated with Mdivi-1, and were infected with *S. flexneri* (moi 500) for 3.5 h. Infected HeLa cells treated with Mdivi-1 had significantly reduced mitochondrial fragmentation (17.26 ± 1.26%) compared to untreated (33.49 ± 3.40%) or DMSO-treated (30.88 ± 1.63%) HeLa cells (Figure 4.3D - G). High bacterial loads were also observed in *Shigella*-infected HeLa cells regardless of treatment (Figure 4.3D - F).

The effect of Drp1 depletion on mitochondrial fragmentation during *S. flexneri* infection was determined. HeLa cells were mock transfected or transfected with either negative siRNA or Drp1 siRNA, and were infected with *S. flexneri* (moi 500) for 3.5 h. Drp1-depleted HeLa cells had significantly reduced mitochondrial fragmentation (15.94 ± 2.55%) compared with mock-transfected (27.65 ± 0.38%) or negative siRNA-treated (27.88 ± 0.10%) HeLa cells during *Shigella* infection (Figure 4.4). No differences in bacterial loads were observed in infected cells regardless of treatment. Therefore *S. flexneri* infection in HeLa cells increased Drp1-dependent mitochondrial fragmentation.

Figure 4.2 *S. flexneri* 2457T induces non-apoptotic cell death in HeLa cells.

HeLa cells were infected with *S. flexneri* 2457T (moi 1000) in a 96-well tray for 1 h, followed by incubation with MEM containing 40 µg/mL of gentamicin to exclude extracellular bacteria for 4 h as described in the Methods section. LDH release was measured in the presence of DMSO or (A) Staurosporine (STS) or 0.01% Triton X-100, (B) Z-VAD-fmk, (C) Z-FA-fmk, (D) Necrostatin-1, (E) Necrostatin-7, (F) Necrosulfonamide, (G) IM-54, (H) NecroX-2 or NecroX-5. Data are represented as mean ± SEM of independent experiments ($n = 3$). (B) - (H) were analysed with one-way ANOVA ($p = 0.0495$ for Z-VAD-fmk, $p > 0.05$ for Z-FA-fmk, $p = 0.0073$ for Necrostatin-1, $p = 0.0458$ for Necrostatin-7, $p > 0.05$ for Necrosulfonamide, $p = 0.0193$ for IM-54, and $p > 0.05$ for NecroX-2 and NecroX-5), followed by Tukey's post hoc test. No differences in LDH release were observed in the presence of the specific chemicals or DMSO in the absence of bacterial infection.

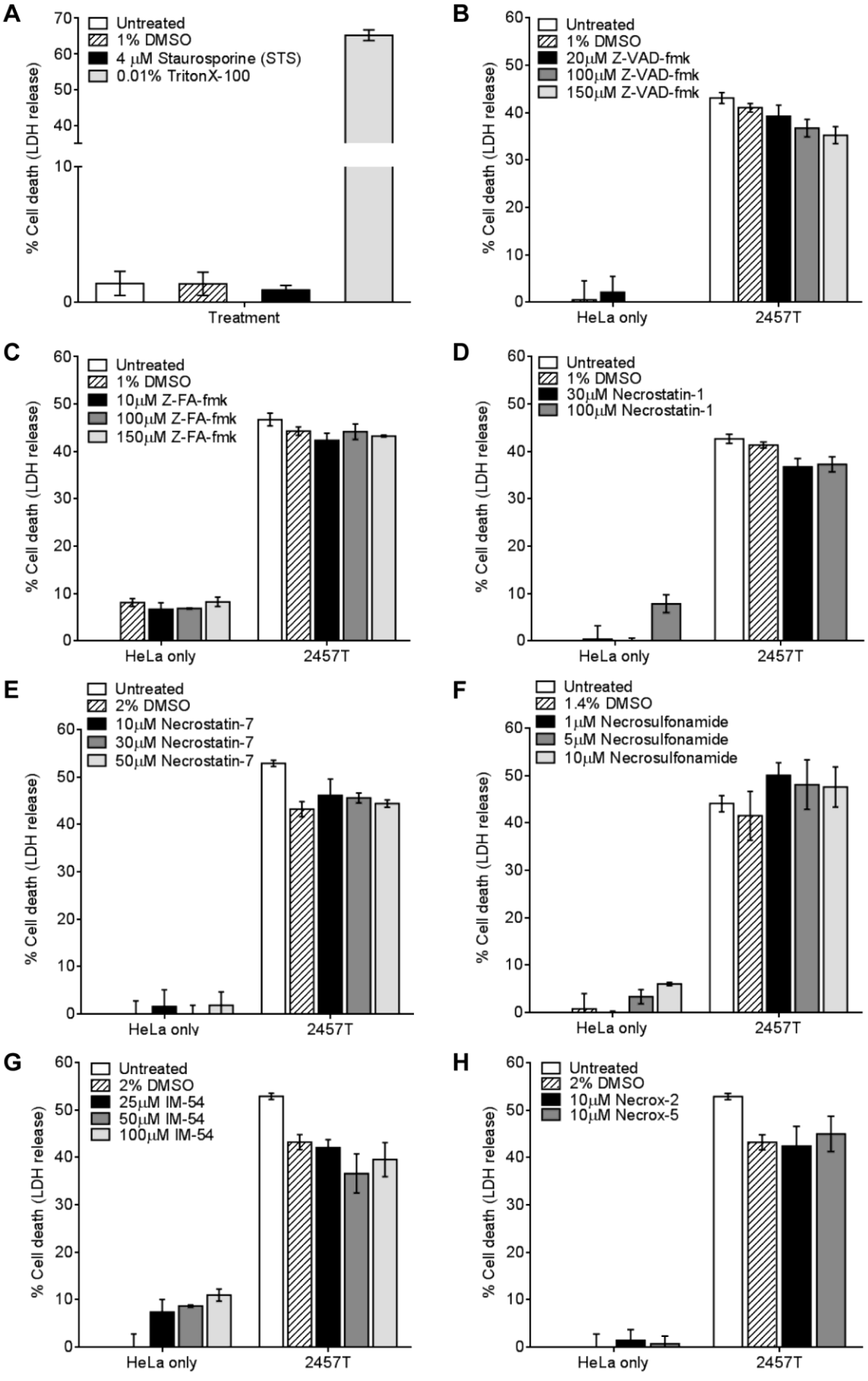
A
Untreated
1% DMSO
4 μM Staurosporine (STS)
0.01% TritonX-100
% Cell death (LDH release)
Treatment
B
Untreated
1% DMSO
20μM Z-VAD-fmk
100μM Z-VAD-fmk
150μM Z-VAD-fmk
% Cell death (LDH release)
HeLa only
2457T
C
Untreated
1% DMSO
10μM Z-FA-fmk
100μM Z-FA-fmk
150μM Z-FA-fmk
% Cell death (LDH release)
HeLa only
2457T
D
Untreated
1% DMSO
30μM Necrostatin-1
100μM Necrostatin-1
% Cell death (LDH release)
HeLa only
2457T
E
Untreated
2% DMSO
10μM Necrostatin-7
30μM Necrostatin-7
50μM Necrostatin-7
% Cell death (LDH release)
HeLa only
2457T
F
Untreated
1.4% DMSO
1μM Necrosulfonamide
5μM Necrosulfonamide
10μM Necrosulfonamide
% Cell death (LDH release)
HeLa only
2457T
G
Untreated
2% DMSO
25μM IM-54
50μM IM-54
100μM IM-54
% Cell death (LDH release)
HeLa only
2457T
H
Untreated
2% DMSO
10μM Necrox-2
10μM Necrox-5
% Cell death (LDH release)
HeLa only
2457T

Figure 4.3 Drp1 inhibition with Mdivi-1 reduces mitochondrial fragmentation in HeLa cells during *S. flexneri* 2457T infection.

HeLa cells were infected with *S. flexneri* 2457T (moi 500) for 1 h, followed by incubation with MEM containing 40 μg/mL of gentamicin to exclude extracellular bacteria for 3.5 h as described in the Methods section. Bacteria and HeLa nuclei were stained with DAPI and mitochondria was stained with MitoTracker® Red CMXRos. Images were taken at 100× magnification. Scale bar = 10 μm. The last column is 2.5× magnifications of the respective boxed areas in the MitoTracker® Red CMXRos images. (A) - (F) Uninfected or 2457T-infected HeLa cells were treated with DMSO or Mdivi-1; (A) HeLa; (B) HeLa + DMSO; (C) HeLa + 50 μM Mdivi-1; (D) 2457T; (E) 2457T + DMSO ; (F) 2457T + 50 μM Mdivi-1. (G) The percentage of cells with fragmented mitochondria was determined by counting >100 cells in each experiment. Data are represented as mean ± SEM of independent experiments ($n = 2$), analysed with one-way ANOVA ($p = 0.0289$), followed by Tukey's post hoc test ($^*p < 0.05$).

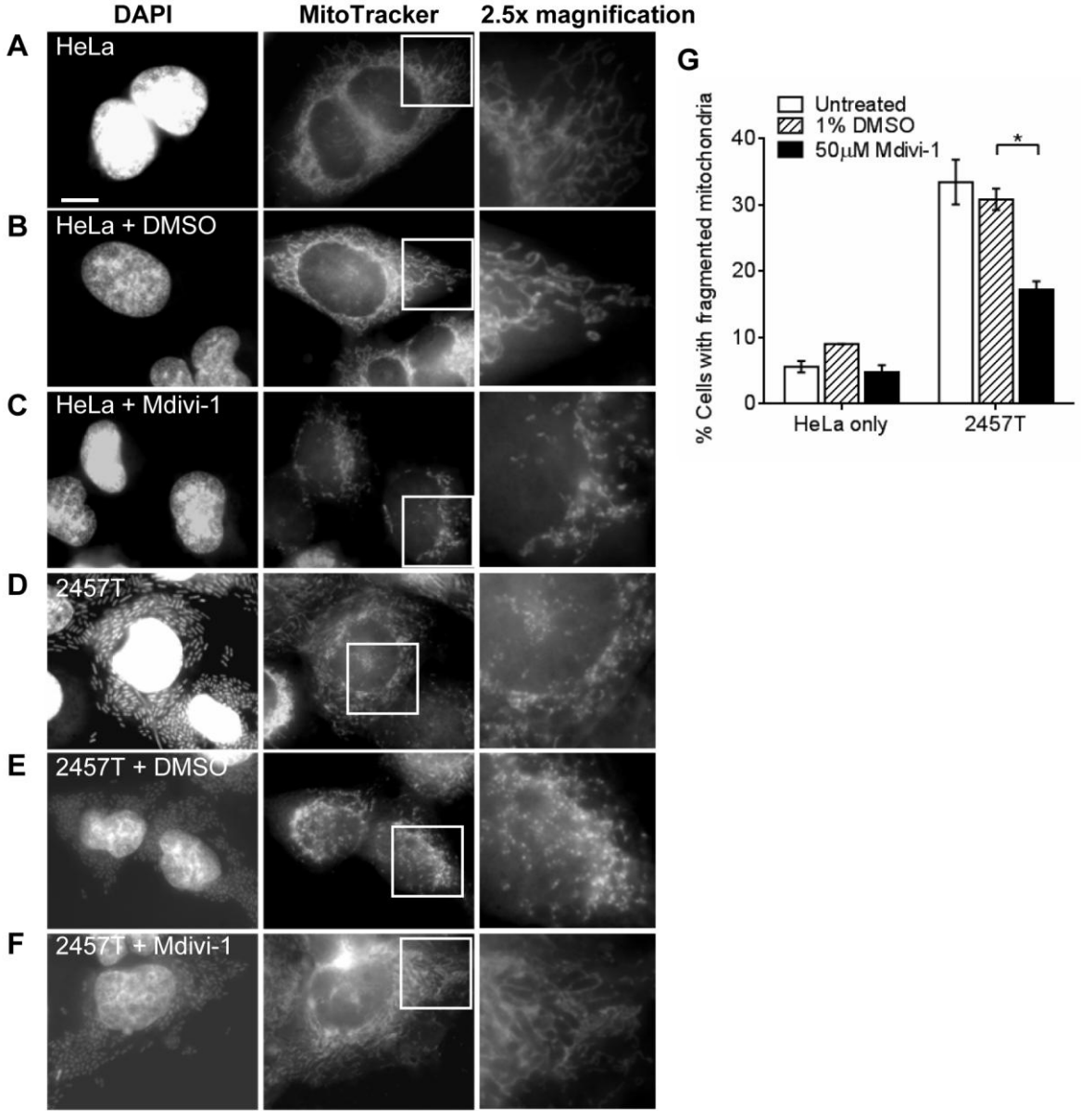
DAPI
MitoTracker
2.5x magnification
A
HeLa
B
HeLa + DMSO
C
HeLa + Mdivi-1
D
2457T
E
2457T + DMSO
F
2457T + Mdivi-1
G
Untreated
1% DMSO
50μM Mdivi-1
% Cells with fragmented mitochondria
40
30
20
10
0
*
HeLa only
2457T

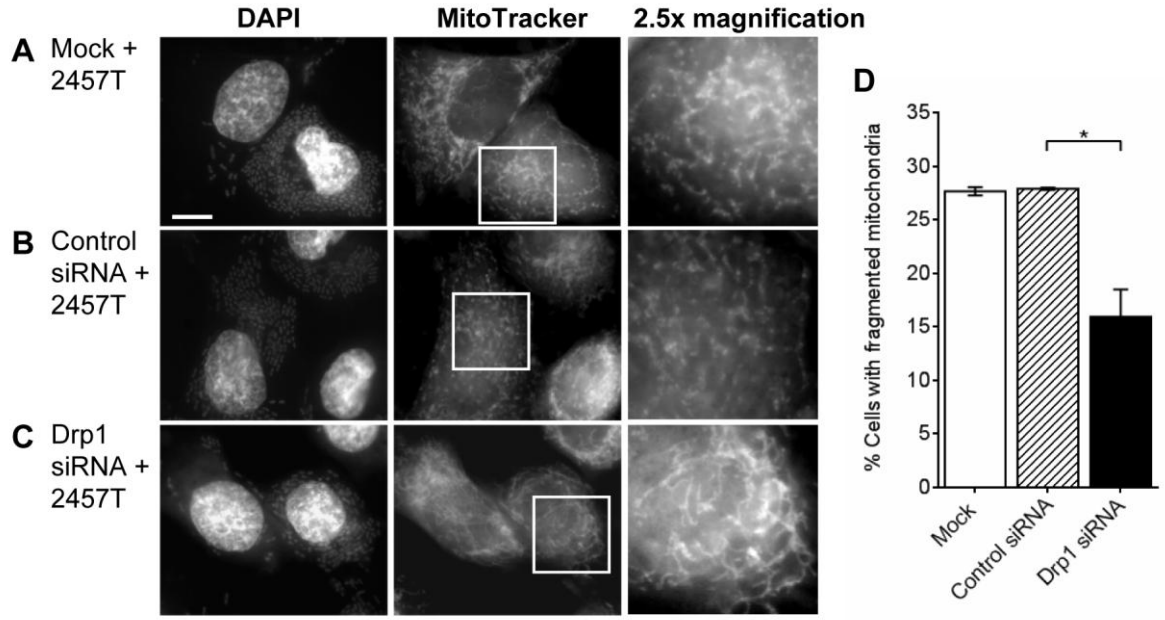

Figure 4.4 Transfection of HeLa cells with Drp1 siRNA reduces mitochondrial fragmentation in HeLa cells during *S. flexneri* 2457T infection.

HeLa cells were either mock transfected or transfected with control or Drp1 siRNA for 24 h, trypsinised and re-transfected for further 24 h. HeLa cells were infected with *S. flexneri* 2457T (moi 500) for 1 h, followed by incubation with MEM containing 40 µg/mL of gentamicin to exclude extracellular bacteria for 3.5 h as described in the Methods section. Bacteria and HeLa nuclei were stained with DAPI and mitochondria was stained with MitoTracker® Red CMXRos. Images were taken at 100× magnification. Scale bar = 10 µm. The last column is 2.5× magnifications of the respective boxed areas in the MitoTracker® Red CMXRos images. (A) - (C) Mock, control siRNA and Drp1 siRNA transfected HeLa cells were infected with 2457T; (A) Mock transfected; (B) Control siRNA; (C) Drp1 siRNA. (D) The percentage of cells with fragmented mitochondria was determined by counting >100 cells in each experiment. Data are represented as mean ± SEM of independent experiments ($n = 2$), analysed with one-way ANOVA ($p < 0.0001$), followed by Tukey's post hoc test (*$p < 0.05$).

4.4.4 Drp1 is important for *S. flexneri* cell-to-cell spreading but not protrusion formation

Dynasore, an inhibitor of dynamin II and Drp1 GTPase, reduced *S. flexneri* cell-to-cell spreading. Dynamin II knockdown with siRNA also significantly affected *S. flexneri* infectious foci formation (Lum *et al.*, 2013) (Chapter 3). We decided to investigate if Drp1 also played a role during *S. flexneri* cell-to-cell spreading. The effects of Mdivi-1 and Drp1 siRNA on infectious focus or plaque formation by *S. flexneri* were determined. Initial experiment showed that Mdivi-1 could not be used in the plaque assay due to precipitation when dissolved in the agar mixture. HeLa monolayers infected with *S. flexneri* (moi 0.1) were treated with increasing concentrations of Mdivi-1 in an infectious focus assay. Treatment with 20 μM Mdivi-1 reduced foci counts and foci area (*$p < 0.05$) (Figure 4.5). To investigate the effect of Drp1 depletion on *S. flexneri* cell-to-cell spreading, HeLa cells were transfected with Drp1 siRNA and plaque assay was carried out. *S. flexneri* formed plaques on HeLa cells treated with Drp1 siRNA with a reduced plaque diameter but not plaque counts when compared to HeLa cells treated with the negative control siRNA (*$p < 0.05$) (Figure 4.6). Therefore Drp1 inhibition with Mdivi-1 as well as siRNA knockdown reduced *Shigella* cell-to-cell spreading.

Reduced or absence of protrusion formation may account for decreased infectious focus and plaque formation. The role of Drp1 in *S. flexneri* protrusion formation was investigated. HeLa monolayers infected with *S. flexneri* were treated with the DMSO control or 50 μM Mdivi-1, and the percentage of infected cells with one or more bacteria protrusions were enumerated by counting >100 cells in each experiment (Figure 4.7). 55.40 ± 1.48% of infected HeLa cells had one or more protrusions. Protrusion formation was not affected by the DMSO control (55.27 ± 2.89%) or 50 μM Mdivi-1 (53.51 ± 0.06%). Reduced *S. flexneri* intracellular growth could also account for the reduction in focus area and plaque size, but no differences in bacterial counts were observed between DMSO and Mdivi-1-treated HeLa cells (Figure 4.S4).

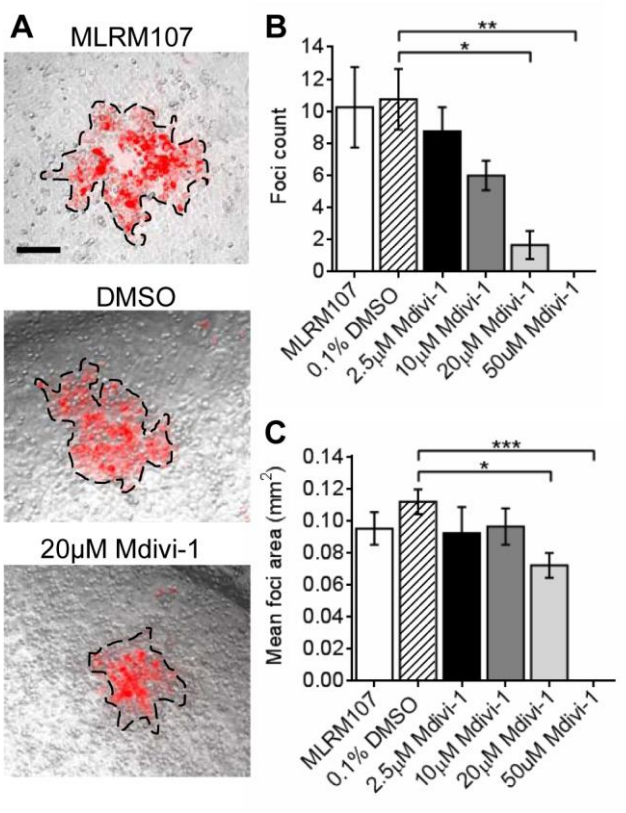

Figure 4.5 Drp1 inhibition with Mdivi-1 reduces *S. flexneri* MLRM107 foci counts and foci area.

HeLa cells were infected with *S. flexneri* MLRM107 in an infectious focus assay using a 12-well tray as described in the Methods section. Infectious foci were imaged 24 h post-gentamicin treatment. (A) Images shown are overlay of an image taken with phase contrast and TxRed filter (10× magnification). The area of the infectious focus i.e. area where mCherry was detected, is outlined. Scale bar = 0.1 mm. (B) The total foci counts from one well or (C) mean foci area from one well were calculated. Data are represented as mean ± SEM of independent experiments (n = 3), analysed with one-way ANOVA (p = 0.0013 for foci counts and p = 0.0003 mean foci area), followed by Tukey's post hoc test (*p < 0.05, **p < 0.01, ***p < 0.001).

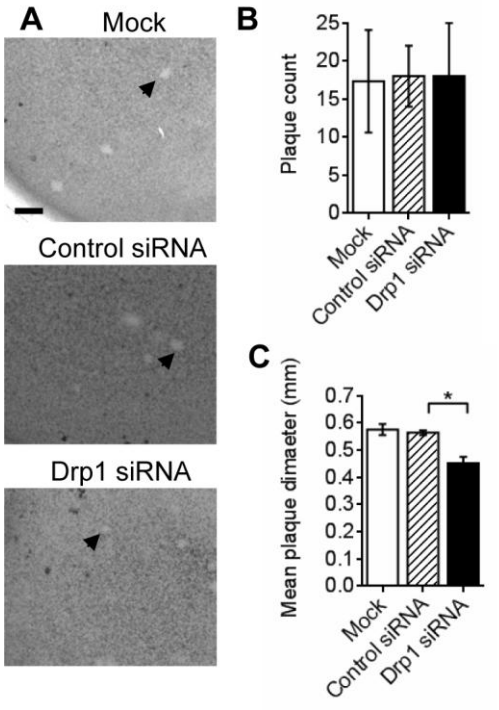

Figure 4.6 HeLa cells transfected with Drp1 siRNA reduces *S. flexneri* 2457T plaque size.

HeLa cells were either mock transfected or transfected with control or Drp1 siRNA for 24 h, trypsinised and re-transfected for further 24 h. HeLa cells were infected with *S. flexneri* 2457T in a plaque assay using a 6-well tray as described in the Methods section. (A) Wells were stained with Neutral Red to makes plaques more visible. Scale bar = 2 mm. (B) The total plaque counts or (C) mean plaque diameters from each well infected with *Shigella* were calculated. Data are represented as mean ± SEM of independent experiments ($n = 2$), analysed with one-way ANOVA ($p > 0.05$ for plaque counts and $p = 0.0239$ mean plaque diameters), followed by Tukey's post hoc test (*$p < 0.05$).

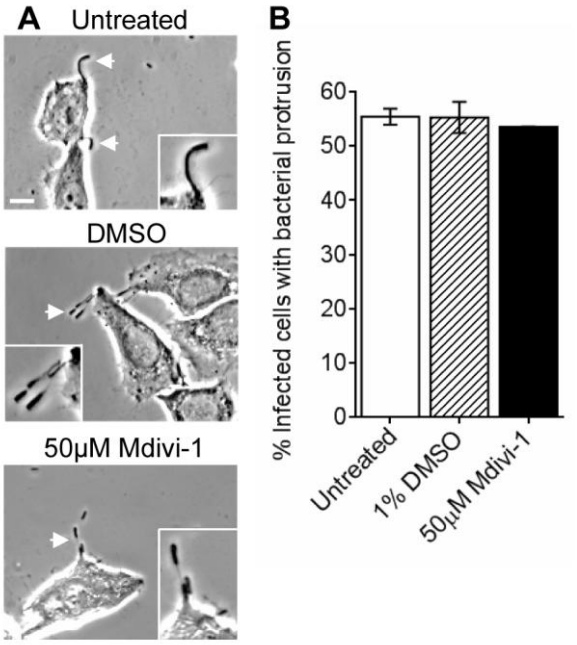

Figure 4.7 *S. flexneri* 2457T protrusion formation is not affected by Mdivi-1.

HeLa cells were infected with *S. flexneri* 2457T for 1 h in a 24-well tray. HeLa cells were washed thrice with D-PBS and incubated with MEM containing 40 μg/mL of gentamicin (t = 0) to exclude extracellular bacteria. Concurrently HeLa cells were treated with 50 μM Mdivi-1 or DMSO for 1.5 h. At t = 1.5, HeLa cells were fixed to observe bacteria protrusions. (A) Infected HeLa cells were imaged at 40× magnification. Scale bar = 10 μm. The arrows indicate protrusion formation. Insert shows 2× enlargement of the indicated region. (B) The percentage of infected cells with bacteria protrusion(s) were enumerated by counting >100 cells in each independent experiment. Data are represented as mean ± SEM of independent experiments (n = 2), analysed with one-way ANOVA (p > 0.05).

4.4.5 Drp1 is not localised to the *S. flexneri* F-actin tails

Host proteins have been shown to associate with *S. flexneri* actin tail (Kadurugamuwa *et al.*, 1991; Lum *et al.*, 2013; Sansonetti *et al.*, 1994). We investigated Drp1 localisation in *S. flexneri*-infected HeLa cells by IF microscopy. Drp1 was not localised to the *S. flexneri* actin tail in untreated, DMSO-treated, Mdivi-1-treated or Drp1 siRNA-treated HeLa cells (Figure 4.8).

4.4.6 Effect of Mdivi-1 on *S. flexneri* infection of mice

We next investigated the possible *in vivo* relevance of the observed association between Drp1 and *S. flexneri* cytotoxicity as well as cell-to-cell spreading. A mouse Sereny test we established previously (Lum *et al.*, 2013) (Chapter 3) was used to determine whether ocular infection by *S. flexneri* could be inhibited by the administration of Mdivi-1. Mice in two groups were injected IP with Mdivi-1 (30 mg/kg) or vehicle at t = -1, 6, 23 and 30 h, and infected with 2.5×10^7 CFU *S. flexneri* 2457T in the right eye (t = 0). The mice in both groups developed ocular inflammation at a similar rate and the Sereny scores were similar (Figure 4.S5A - B). Although a slight effect on weight loss was observed on D1, no differences were observed on D2 and D3 (Figure 4.S5C).

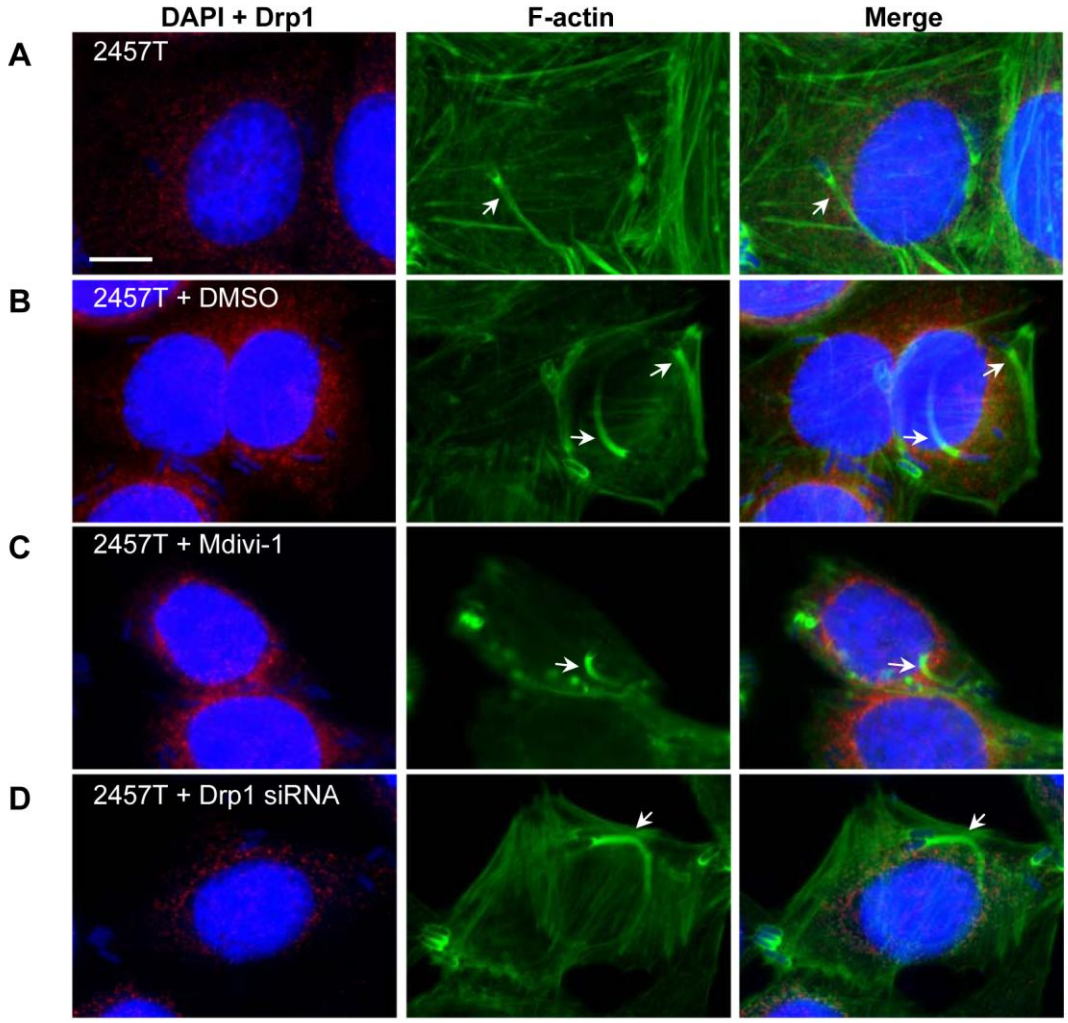

Figure 4.8 Drp1 is not localised to the *S. flexneri* 2457T F-actin tails.

HeLa cells were infected with *S. flexneri* 2457T in an invasion assay as described in the Methods section. Bacteria and HeLa nuclei were stained with DAPI (blue), F-actin was stained with FITC-phalloidin (green) and Drp1 was stained with anti-Drp1 and Alexa Fluor 594-conjugated secondary antibody (red). Images were taken at 100× magnification. Scale bar = 10 μm. (A) - (D) HeLa cells were treated with DMSO, Mdivi-1 or were transfected with Drp1 siRNA and were infected with *S. flexneri* 2457T; (A) Untreated; (B) 1% DMSO; (C) 50 μM Mdivi-1; (D) Drp1 siRNA-transfected HeLa cells. Arrows indicate F-actin comet tails. The experiment was repeated twice and representative images are shown.

4.5 Discussion

Shigella infection in epithelial cells is an interplay between maintaining a replicative niche for *Shigella* and elimination of infected cells to prevent further cell-to-cell spreading, even though cell death and the ensuing inflammation are at considerable cost to the host (Ashida *et al.*, 2011a). During *Shigella* infection, apoptotic (Lembo-Fazio *et al.*, 2011) or necrotic cell death (Bergounioux *et al.*, 2012; Carneiro *et al.*, 2009; Kobayashi *et al.*, 2013) occurs depending on the experimental conditions. In both cases changes to the outer or inner mitochondrial membrane are critical to allow the respective cell death pathways to proceed. In this study we investigated the role of Drp1, the mitochondrial fission protein, during *Shigella* infection in HeLa cells. *Shigella* infection for 4 h at moi 1000 induced high levels of LDH release. Inhibition of Drp1 with Mdivi-1 as well as Drp1 depletion with siRNA significantly reduced HeLa cell cytotoxicity.

Drp1 is recruited to the mitochondria during apoptosis and programmed necrosis. During apoptosis, pro-apoptotic Bax localises to the outer membrane (OM) of the mitochondria and colocalises with Mfn2 and activates Drp1 at fission sites (Wasiak *et al.*, 2007). Following mitochondrial fragmentation, mitochondrial outer membrane permeabilisation (MOMP) and cristae reorganisation, cytochrome *c* is released and caspases are subsequently activated (Frank *et al.*, 2001). Upon programmed necrosis induction by tumour necrosis factor-α (TNF-α), RIP1 and RIP3 interact with MLKL (Wang *et al.*, 2012). The RIP1/RIP3/MLKL complex is translocated to the mitochondria to engage mitochondrial protein phosphatase long variant (PGAM5L) initially and subsequently PGAM5S (PGAM short variant) on the mitochondrial membrane. Drp1 GTPase activity is activated via dephosphorylation at Ser637, likely by both PGAM5L and PGAM5S *in situ* on the mitochondrial OM (Wang *et al.*, 2012). It is speculated Drp1 activation may cause mitochondrial fragmentation resulting in reduced ATP production, ROS generation or other downstream events (Wang *et al.*, 2012).

We next investigated if components of apoptosis or programmed necrosis are activated during *Shigella* infection. HeLa cells treated with STS to induce apoptosis resulted in caspase-3 activation as expected (Nicolier *et al.*, 2009), but no significant LDH release was detected in the culture supernatant. Unsurprisingly pan-caspase inhibition with Z-VAD-fmk or its inactive analogue, Z-FA-fmk, did not affect LDH release in *Shigella*-infected HeLa cells.

Inhibition of programmed necrosis components such RIP1 and MLKL did not reduce LDH release during *Shigella* infection. ROS and NOS inhibitors also had no effect on LDH release. During *Shigella* infection (moi 500, 3.5 h), mitochondrial fragmentation was observed in ~30% of HeLa cells. Mitochondrial fragmentation in infected HeLa cells was halved when Drp1 was inhibited with Mdivi-1 or depleted with siRNA. Previously mitochondrial fragmentation was not observed when HeLa cells were infected with *Shigella* for 1 h at moi 50 (Stavru *et al.*, 2011). In that study t = 1 h refers to the 1 h infection time prior to incubation with 80 μg/mL gentamicin to remove extracellular bacteria. In our study the equivalent time point is t = 0. Collectively data from the previous study and our observations showed during *Shigella* infection, mitochondrial fragmentation occurs at a later time point and/or at a much higher moi. In spite of the high bacterial load, HeLa cells remain intact and alive, similar to observations reported earlier (Mantis *et al.*, 1996).

Overall our results suggest that at high moi, *Shigella* infection induces non-apoptotic HeLa cell death which is mediated by Drp1 and accompanied by mitochondrial fragmentation. Furthermore HeLa cell death induction during *Shigella* infection is also not dependent on the RIP1/MLKL programmed necrosis pathway. Previously hallmarks of necrosis such as loss of mitochondrial inner potential, nuclear and plasma membrane swelling were observed at 8 h post-infection in MEFs infected with *Shigella* (strain M90T) at moi 100 (Carneiro *et al.*, 2009). ROS generation was also observed 10 h post-infection (Carneiro *et al.*, 2009). Consistent with previous finding, ROS scavengers had no effect on LDH release at 4 h post-infection in this study. Mitochondrial swelling was reported in HaCat cells infected with *S. flexneri* strain YSH6000 at moi 25 for 2 h (Kobayashi *et al.*, 2013). Changes to mitochondrial morphology observed previously might now be attributed to Drp1-mediated mitochondrial fragmentation.

Mitochondrial fission during host cell death in other bacterial infections has been reported, although Drp1 involvement is not essential. The pore-forming vacuolating cytotoxin A (VacA) toxin of the gastric pathogen, *Helicobacter pylori*, recruits and activates Drp1 resulting in mitochondrial fission, Bax activation, MOMP and cytochrome *c* release (Jain *et al.*, 2011). Drp1 fission however is not a prerequisite for VacA-mediated MOMP (Jain *et al.*, 2011). Another pore-forming toxin, listeriolysin O (LLO) from *Listeria monocytogenes*, the causative agent of food-borne listeriosis, was reported to fragment mitochondrial networks in

HeLa cells, followed by subsequent decrease in the mitochondrial membrane potential and ATP levels (Stavru *et al.*, 2011). Intriguingly the Drp1 receptor, Mff, is degraded resulting in reduced Drp1 at the mitochondria following *Listeria* infection or LLO treatment, but mitochondrial fission is not disrupted (Stavru *et al.*, 2013). It appears the endoplasmic reticulum and the actin cytoskeleton facilitates mitochondrial fission independently of Drp1, although the exact mechanism is not known.

Earlier we reported dynasore treatment and dynamin II knockdown with siRNA reduced *Shigella* cell-to-cell spreading in HeLa cells (Lum *et al.*, 2013) (Chapter 3). Dynasore is a non-competitive, reversible inhibitor of dynamin II and Drp1 GTPase activity. We decided to investigate Drp1's role, if any, in *Shigella* infectious focus and plaque formation. Drp1 inhibition with Mdivi-1 reduced *Shigella* cell-to-cell spreading in a dose dependant manner and Drp1 knockdown with siRNA also reduced *Shigella* plaque size. Previously Drp1 was reported to co-localise with F-actin stress fibres in Cos-1 cells, an immortalised mammalian fibroblastic cell line (DuBoff *et al.*, 2012). We did not observe any interactions between Drp1 and either the F-actin cytoskeleton or the *Shigella* F-actin tail via IF microscopy in this study. High levels of Drp1 were detected by microscopy in Cos-1 cells (DuBoff *et al.*, 2012), however low levels of Drp1 was observed in HeLa cells in our study. Hence it is possible Drp1 recruitment to HeLa cell F-actin cytoskeleton and/or *Shigella* F-actin tail may not be evident due to technical limitations.

A study in *Potorous tridactylis* kidney epithelial (PtK2) cells showed that *Listeria* cell-to-cell spreading in areas with high mitochondrial density (perinuclear region) had increased mean speed and greater curvature in trajectories compared to areas with low mitochondrial density (cell periphery) (Lacayo & Theriot, 2004). *Listeria* and *Shigella* both mediate actin-based motility for cell-to-cell spreading (Gouin *et al.*, 2005). Inhibition of Drp1 forms net-like mitochondrial networks, which can collapse into perinuclear structures (Smirnova *et al.*, 1998; Smirnova *et al.*, 2001). Hence Mdivi-1 treatment would alter the intracellular milieu of HeLa cells dramatically, such that *Shigella* intracellular speed and movement would be adversely affected. In Mdivi-1-treated cells, F-actin comet tail formation, intracellular bacterial growth and protrusion formation was not affected. Hence *Shigella* protrusion formation is not likely to be dependent on its intracellular motility. Lacoya and Theriot (2004) also observed that MitoTracker Red-labelled mitochondria had loss of fluorescent label post-

Listeria collision, presumably due to loss of mitochondrial integrity and transmembrane potential. In this study, we also noticed on some occasions that MitoTracker Red labelling was more intense in uninfected HeLa cells compared to infected cells.

Since Mdivi-1 was able to reduce *Shigella* cell-to-cell spreading and HeLa cell cytotoxicity, the drug's efficacy was tested *in vivo* in a murine keratoconjunctivitis (Sereny) model we used previously (Lum *et al.*, 2013) (Chapter 3). However Mdivi-1 treatment did not ameliorate conjunctivitis, at least under the dosing protocol used in these studies. Since an Δ*icsA* mutant is not pathogenic in this model (Lum *et al.*, 2013) (Chapter 3), this suggests that Mdivi-1 does not significantly impair intercellular spreading *in vivo*. It is possible that the dosing regime used here was not sufficient to maintain an effective concentration of the drug *in vivo.*

In conclusion, Drp1 and mitochondrial dynamics play important roles in different aspects of *Shigella* pathogenesis. During *Shigella* infection, mitochondrial fission following cell death pathway activation is important to eliminate infected cells. Furthermore loss of mitochondrial networks disrupts *Shigella*'s ability to mediate cell-to-cell spreading. Loss of mitochondrial structure may have altered the intracellular movement of *Shigella*. Although *Shigella* protrusion formation was not affected, the inefficient intracellular movement over an extended period of time in the duration of both the infectious focus and plaque assay may retard *Shigella*'s movement from one cell to the next, resulting in reduced infectious focus area and plaque size. Since the conditions used to study cell death and cell-to-cell spreading differ necessarily in HeLa cell confluency, moi and time of infection, it is difficult to speculate if there are any correlations between cell death, cell-to-cell spreading and mitochondrial structure. Future work should focus on how Drp1 is recruited and activated during *Shigella* infection and if disruption of mitochondrial dynamics would also affect other bacteria which rely on actin-based motility for host dissemination.

4.6 Acknowledgements

We are grateful to Dr. Stephen R. Attridge for assistance with the mouse studies. This work is supported by a Program Grant (565526) from the National Health and Medical Research Council (NHMRC) of Australia. ML was the recipient of the Australian Postgraduate Award from the NHMRC.

4.7 Supplementary data

Figures 4.S1- 4.S5 are supplementary figures of the main text.

Figures 4.S6 - 4.S8 are additional figures not included in the main text.

The data in Figures 4.S6 and 4.S7 show that chemical inhibitors used in the study, in addition to Mdivi-1, did not affect *S. flexneri* 257T intracellular growth and protrusion formation, respectively. The data in Figure 4.S8 shows that Drp1 localisation in HeLa cell was not affected when infected with *S. flexneri* mutant strains defective in cell-to-cell spreading (R-LPS - Δ*rmlD*, RMA723; Δ*icsA*, RMA2041; and Δ*icsA* Δ*rmlD*, RMA2043).

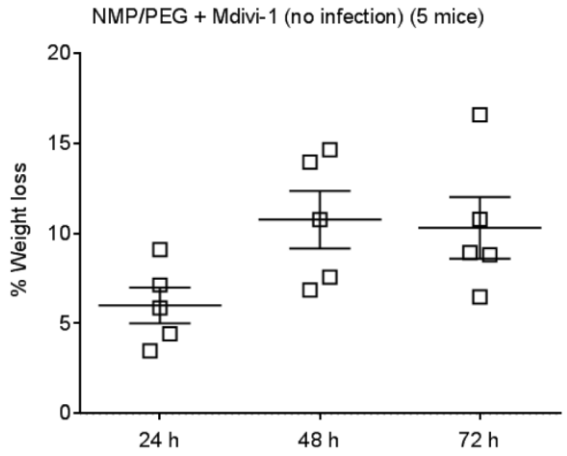

Figure 4.S1 Mdivi-1 injections in 1:9 NMP/PEG results in significant weight loss in mice.

Mice were IP injected with 100 µL 5.5 mg/mL of Mdivi-1 in NMP/PEG (30 mg/kg) at t = 0, 7, 24, 31 h in the absence of bacterial inoculation. Each symbol represents one mouse. Data are represented as mean ± SEM, analysed with one-way ANOVA (p = 0.076).

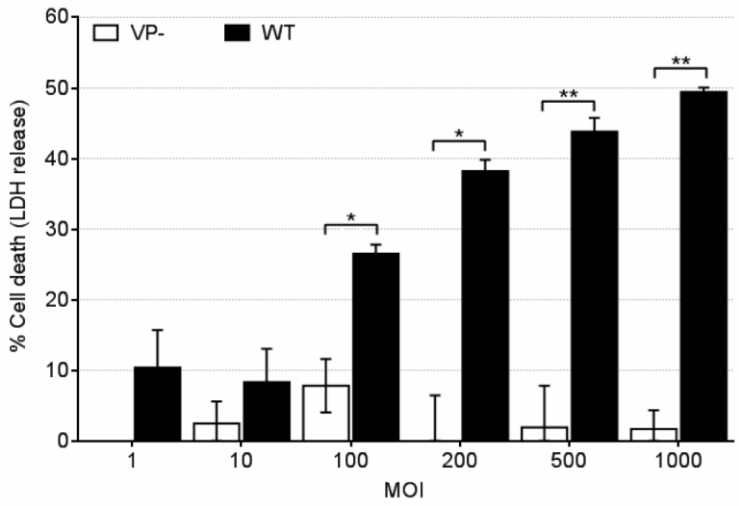

Figure 4.S2 HeLa cells infected with *S. flexneri* 2457T at moi of 100 - 1000 release LDH into culture supernatants.

HeLa cells were infected with WT *S. flexneri* 2457T or virulence plasmid negative strain (VP^-) (RMA2159) in a 96-well tray as described in the Methods section at increasing moi for 1 h, followed by incubation with MEM containing 40 µg/mL of gentamicin to exclude extracellular bacteria for 4 h. Subsequently LDH release was measured. Data are represented as mean ± SEM of independent experiments (n = 2), differences between pair means at the respective moi were analysed with Student's t-test (*p < 0.05, **p < 0.01).

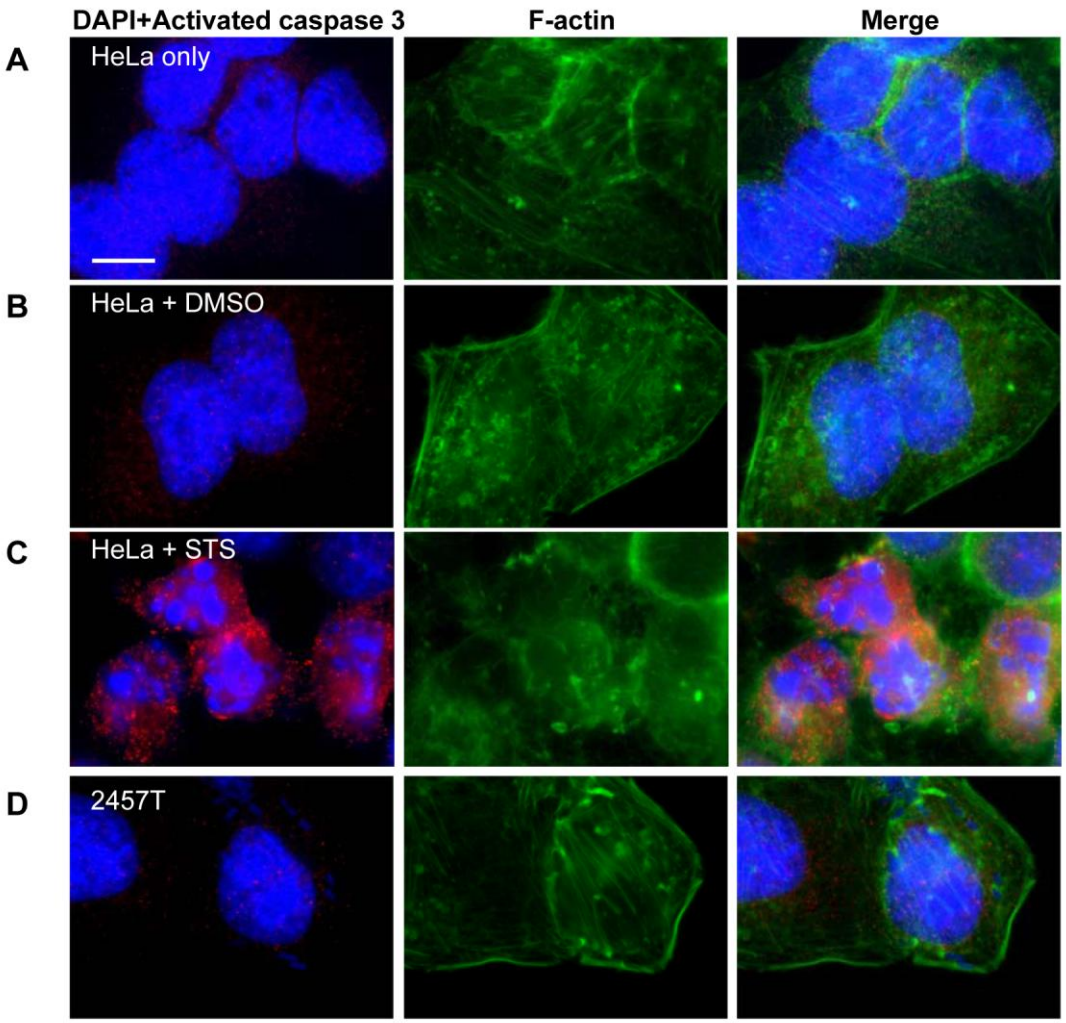

Figure 4.S3 Caspase-3 is not activated during *S. flexneri* 2457T infection in HeLa cells.

HeLa cells were infected with *S. flexneri* 2457T in an invasion assay (moi 500) as described in the Methods section for 1 h, followed by incubation with MEM containing 40 µg/mL of gentamicin (t = 0) to exclude extracellular bacteria for 3.5 h. Concurrently uninfected HeLa cells were treated with DMSO or staurosporine (STS) for 3.5 h. Bacteria and HeLa nuclei were stained with DAPI (blue), F-actin was stained with FITC-phalloidin (green) and cleaved caspase-3 was stained with anti-activated caspase-3 and Alexa Fluor 594-conjugated secondary antibody (red). Images were taken at 100× magnification. Scale bar = 10 µm. (A) - (C) HeLa cells were treated with DMSO or STS or were infected with *S. flexneri* 2457T; (A) Untreated; (B) 1% DMSO; (C) 4 µM STS; (D) 2457T. The experiment was repeated twice and representative images are shown.

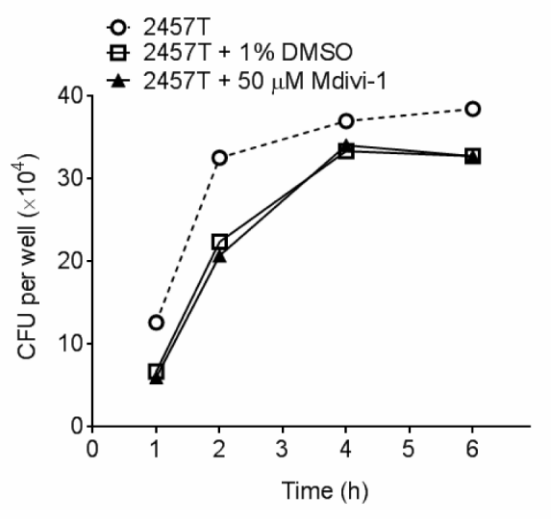

Figure 4.S4 Intracellular growth of *S. flexneri* 2457T in HeLa cells is not affected by Mdivi-1.

HeLa cells were infected with *S. flexneri* 2457T for 1 h in a 24-well tray. HeLa cells were washed thrice with D-PBS and incubated with MEM containing 40 μg/mL of gentamicin (*t* = 0) to exclude extracellular bacteria. Concurrently HeLa cells were treated with 50 μM Mdivi-1 or DMSO. For each condition, two wells were prepared for each time point (*t* = 1, 2, 4 and 6 h). At each interval, HeLa cells were washed, followed by lysis with 0.1% Triton X-100 to recover intracellular bacteria. Data are represented as mean from two-three independent experiments.

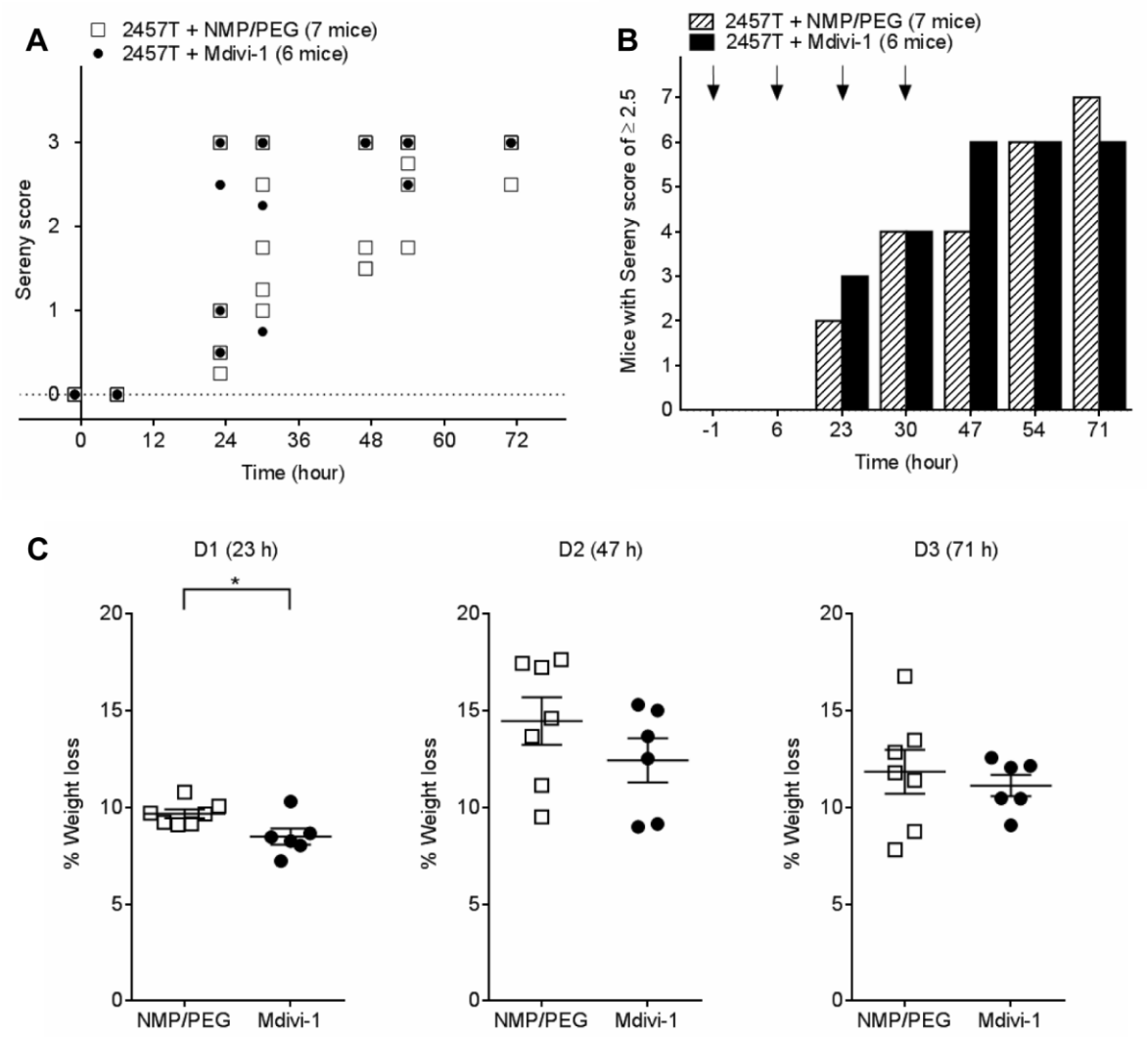

Figure 4.S5 Mdivi-1 protects mice against weight loss from *S. flexneri* 2457T ocular infection.

(A) Sereny scores of mice infected with 2.5×10^7 CFU *S. flexneri* 2457T at $t = 0$ and IP injected with either 100 µL of 5.5 mg/mL of Mdivi-1 in NMP/PEG (30 mg/kg) or 100 µL NMP/PEG at t = -1, 7, 23, 30 h post-inoculation. Each symbol represents at least one mouse. (B) The total number of mice with a Sereny score of ≥2.5 was calculated and plotted as a bar graph for each time point. Arrows indicate injection with Mdivi-1 or NMP/PEG alone. (C) The percentage weight loss for each mouse on D1, D2 and D3 were calculated. Data are represented as mean ± SEM (Student's *t*-test, $*p < 0.05$).

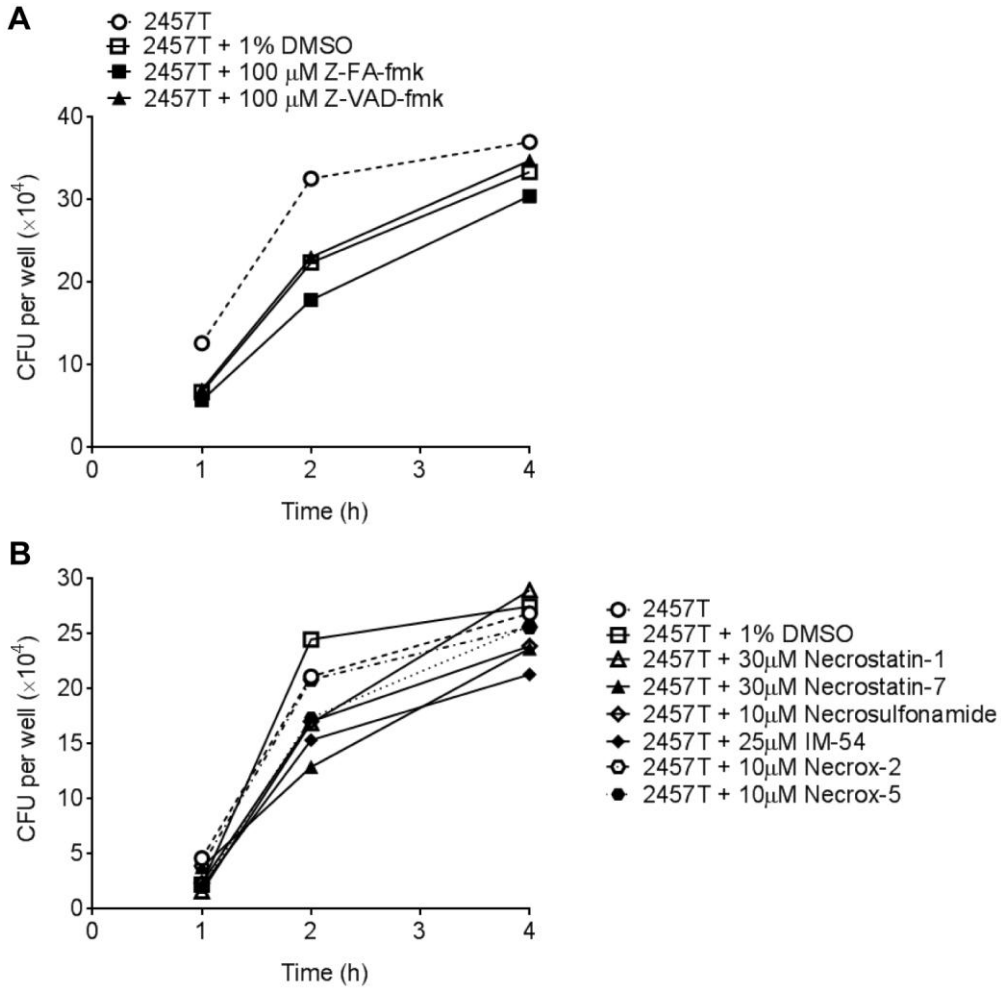

Figure 4.S6 Intracellular growth of *S. flexneri* 2457T in HeLa cells is not affected by inhibitors used in this study.

HeLa cells were infected with *S. flexneri* 2457T for 1 h in a 24-well tray. HeLa cells were washed thrice with D-PBS and incubated with MEM containing 40 μg/mL of gentamicin (*t* = 0) to exclude extracellular bacteria. Concurrently HeLa cells were treated with DMSO or (A) 100 μM Z-VAD-fmk or 100 μM Z-FA-fmk; (B) 30 μM Necrostatin-1 or 30 μM Necrostatin-7 or 10 μM Necrosulfonamide or 25 μM IM-54 or 10 μM Necrox-2 or 30 μM Necrox-5. For each condition, two wells were prepared for each time point (*t* = 1, 2 and 4 h). At each interval, HeLa cells were washed, followed by lysis with 0.1% Triton-X 100 to recover intracellular bacteria. Data are represented as mean from two-three independent experiments.

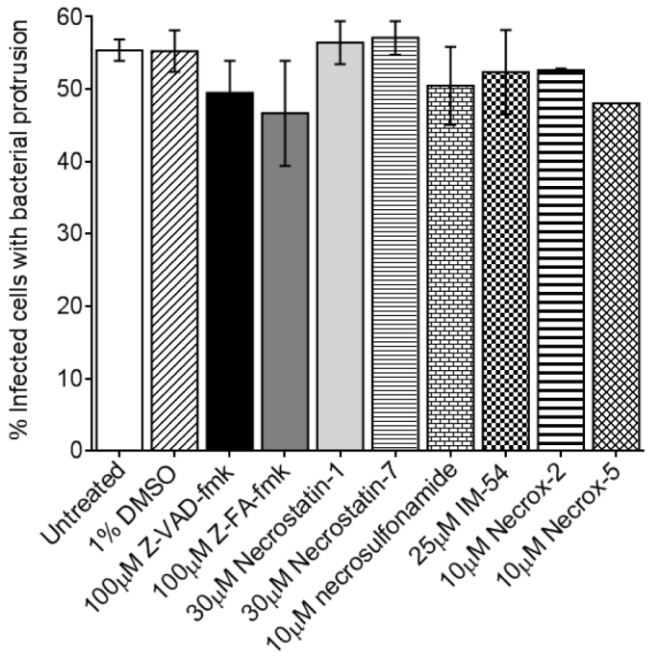

Figure 4.S7 *S. flexneri* 2457T protrusion formation is not affected in the presence of inhibitors used in this chapter.

HeLa cells were infected with *S. flexneri* 2457T for 1 h in a 24-well tray. HeLa cells were washed thrice with D-PBS and incubated with MEM containing 40 μg/mL of gentamicin (t = 0) to exclude extracellular bacteria. Concurrently HeLa cells were treated with 100 μM Z-VAD-fmk, 100 μM Z-FA-fmk, 30 μM Necrostatin-1, 30 μM Necrostatin-7, 10 μM Necrosulfonamide, 25 μM IM-54, 10 μM NecroX-2, 30 μM NecroX-5 or DMSO for 1.5 h. At t = 1.5, HeLa cells were fixed to observe bacteria protrusions. The percentage of infected cells with bacteria protrusion(s) were enumerated by counting >100 cells in two independent experiments. Data are represented as mean ± SEM, analysed with one-way ANOVA (p > 0.05).

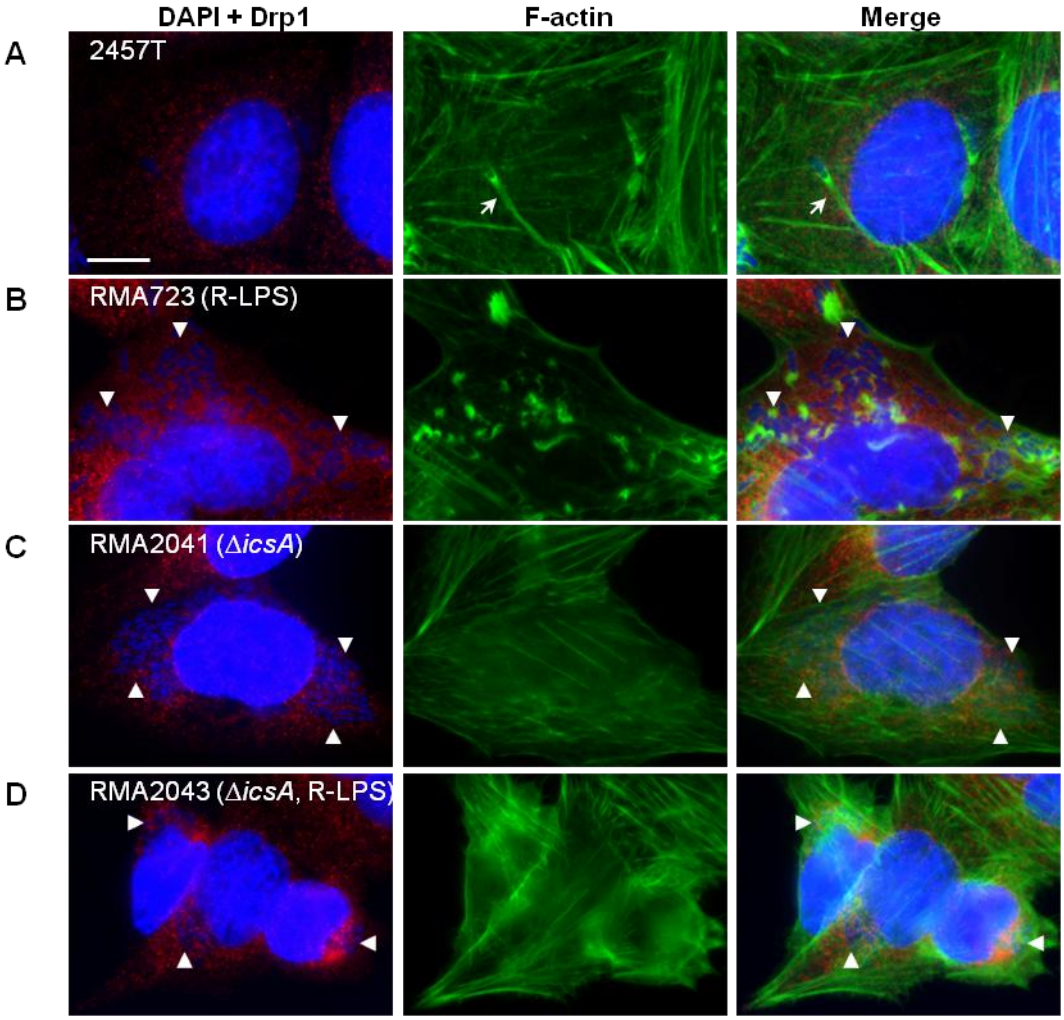

Figure 4.S8 Drp1 localisation in HeLa cells is not affected when infected with *S. flexneri* WT, Δ*icsA* and R-LPS strains.

HeLa cells were infected with *S. flexneri* 2457T in an invasion assay as described in the Methods section. Bacteria and HeLa nuclei were stained with DAPI (blue), F-actin was stained with FITC-phalloidin (green) and Drp1 was stained with anti-Drp1 and Alexa Fluor 594-conjugated secondary antibody (red). Images were taken at 100× magnification. Scale bar = 10 µm. HeLa cells were were infected with *S. flexneri* control strains; (A) 2457T (WT); (B) RMA723 (R-LPS - Δ*rmlD*); (C) RMA2041 (Δ*icsA*); (D) RMA2043 (Δ*icsA* Δ*rmlD*). The experiment was repeated twice and representative images are shown. Arrow indicates F-actin tail and arrowheads indicate bacteria.

ꕥ CHAPTER 5 ꕥ

MYOSIN IIA IS ESSENTIAL FOR *Shigella flexneri* CELL-TO-CELL SPREAD

Myosin IIA is essential for *Shigella flexneri* cell-to-cell spread

Mabel Lum and Renato Morona

School of Molecular and Biomedical Science, University of Adelaide, Adelaide, South Australia, Australia

Lum M & Morona R (2014). Myosin IIA is essential for *Shigella flexneri* cell-to-cell spread. *Pathog Dis*, DOI: 10.1111/2049-632X.12202.

STATEMENT OF AUTHORSHIP

Title of Paper	Myosin IIA is essential for *Shigella flexneri* cell-to-cell spread
Publication Status	○ Published ○ Accepted for Publication ○ Submitted for Publication ○ Publication Style
Publication Details	Lum M & Morona R (2014). Myosin IIA is essential for *Shigella flexneri* cell-to-cell spread. *Pathog Dis*, DOI: 10.1111/2049-632X.12202.

Author Contributions

By signing the Statement of Authorship, each author certifies that their stated contribution to the publication is accurate and that permission is granted for the publication to be included in the candidate's thesis.

Name of Principal Author (Candidate)	Mabel Yuen Teng Lum		
Contribution to the Paper	Performed all experiments, performed analysis on all samples, interpreted data, wrote manuscript and acted as corresponding author.		
Signature		Date	

Name of Co-Author	Renato Morona		
Contribution to the Paper	Supervised development of work, helped in data interpretation, helped to evaluate and edit the manuscript.		
Signature		Date	

Chapter 5: Myosin IIA is essential for *Shigella flexneri* cell-to-cell spread

5.1 Abstract

A key feature of *Shigella* pathogenesis is the ability to spread from cell to cell post-invasion. This is dependent on the bacteria's ability to initiate *de novo* F-actin tail polymerisation, followed by protrusion formation, uptake of bacteria-containing protrusion and finally lysis of the double membrane vacuole in the adjacent cell. In epithelial cells cytoskeletal tension is maintained by the actin-myosin II networks. In this study, the role of myosin II and its specific kinase, myosin light chain kinase (MLCK), during *Shigella* intercellular spreading was investigated in HeLa cells. Inhibition of MLCK and myosin II, as well as myosin IIA knockdown significantly reduced *Shigella* plaque and infectious focus formation. Protrusion formation and intracellular bacterial growth was not affected. Low levels of myosin II were localised to the *Shigella* F-actin tail. HeLa cells were also infected with *Shigella* strains defective in cell-to-cell spreading. Unexpectedly loss of myosin IIA labelling was observed in HeLa cells infected with these mutant strains. This phenomenon was not observed with WT *Shigella* or with the less abundant myosin IIB isoform, suggesting a critical role for myosin IIA.

5.2 Introduction

Shigella flexneri is the causative agent of bacillary dysentery (shigellosis). Post-ingestion, *Shigella* bacteria invade the host intestinal epithelium via microfold cells. Resident macrophages in the follicle-associated epithelium undergo cell death (pyroptosis) induced by *Shigella* through caspase-1 activation, which releases interleukin-1β and interleukin-18 (Sansonetti *et al.*, 2000; Senerovic *et al.*, 2012; Zychlinsky *et al.*, 1992). Interleukin-1β induces a strong inflammatory response and interleukin-18 magnifies innate immune responses (Sansonetti *et al.*, 2000). After *Shigella* are released into the basolateral compartment, *Shigella* invade enterocytes via the type three secretion system, followed by lysis of the endocytic vacuole and replication in the host cytoplasm (Cossart & Sansonetti, 2004; Sansonetti *et al.*, 1986). Concurrently the *Shigella* IcsA (VirG) protein interacts with the host Neural Wiskott-Aldrich syndrome protein (N-WASP) and Arp2/3 complex to initiate *de novo* F-actin nucleation and polymerisation, leading to actin-based motility (ABM) (Bernardini *et al.*, 1989; Rohatgi *et al.*, 1999; Suzuki *et al.*, 1998).

ABM facilitates *Shigella* intracellular movement and intercellular spreading into neighbouring cells via protrusion formation. After escaping from the double membrane vacuole, subsequent cycles of infection are initiated (Schuch *et al.*, 1999). *Shigella* ABM is dependent on IcsA, an outer membrane protein, and lipopolysaccharide (LPS) found on the bacterial surface (Bernardini *et al.*, 1989; Lett *et al.*, 1989; Makino *et al.*, 1986). IcsA is necessary for pathogenesis as Δ*icsA* strains have attenuated virulence in human volunteers and in animal infection models (Kotloff *et al.*, 1996; Makino *et al.*, 1986; Sansonetti *et al.*, 1999). Smooth (WT) *Shigella* strains express the complete LPS molecule, i.e. the lipid A core, core oligosaccharide and O-antigen subunit. In rough LPS strains the O-antigen subunit is absent due to mutations in chromosomal genes encoding LPS synthesis. Rough strains can invade epithelial cells and initiate ABM but have a defect in cell-to-cell spreading (Hong & Payne, 1997; Okamura *et al.*, 1983; Van Den Bosch *et al.*, 1997).

Enterocytes, the site of *Shigella* infection, are polarised colonic epithelial cells characterised by apical junctional complexes, consisting of tight junctions and adherens junctions at the most apical end, which are undercoated with a prominent network of actin-myosin II (actomyosin) ring (Miyoshi & Takai, 2005). For cell-to-cell spreading to occur, the

tensions of the actomyosin ring have to be overcome before disruption of the cellular contacts can take place (Rajabian *et al.*, 2009). *Shigella* engulfment, but not protrusion formation into the neighbouring cell is triggered by phosphoinositide 3-kinase and is dependent upon dynamin II, Epsin-1 and clathrin, components of the clathrin-mediated endocytic pathway (Fukumatsu *et al.*, 2012; Lum *et al.*, 2013). Adherens junction and tight junction components such as L-CAM, α-catenin, β-catenin, α-actinin and vinculin localise to the *Shigella* actin tail during protrusion formation. L-CAM is crucial for cell-to-cell spread as it helps to maintain a tight association between the bacterium and the membrane of the protrusions (Kadurugamuwa *et al.*, 1991; Sansonetti *et al.*, 1994). Knockdown of myosin-X, a component of adherens junctions, resulted in shortened and thickened protrusion stalks which reduced *Shigella*'s ability to form plaques (Bishai *et al.*, 2012). *Shigella* invasion and dissemination is also dependent on ATP release by connexin 26, and formins, Dia1 and Dia2 (Heindl *et al.*, 2009; Tran Van Nhieu *et al.*, 2003). Similar to the Arp2/3 complex, formins initiate *de novo* actin polymerisation but also crosslink actin filaments (Esue *et al.*, 2008).

In an attempt to identify host proteins which are differentially recruited to rough and smooth LPS *Shigella* strains, localisation of various proteins to the F-actin tail and bacterial cells inside infected HeLa cells were carried out by immunofluorescence (IF) microscopy with a panel of antibodies. Curiously it was observed that non-muscle myosin IIA (myosin IIA), but not IIB protein levels were significantly reduced in HeLa cells infected with rough LPS (R-LPS) and Δ*icsA* strains. The involvement of myosin and its specific kinase, myosin light chain kinase (MLCK) has previously been reported at different stages of *Shigella* infection. MLCK and myosin II were previously implicated in *Shigella* cell-to-cell spread in Caco-2 cells (Rathman *et al.*, 2000a). In a later study Mostowy *et al.* (2010) showed that in HeLa cells, myosin II was recruited to the septin cage which entraps intracytosolic *Shigella* without F-actin tails and targets the bacterium to the autophagy pathway for degradation.

In this study, treatment of HeLa cells with MLCK and myosin II inhibitors, as well as siRNA knockdown of myosin IIA heavy chain (*MYH9*) reduced *Shigella* infectious focus and plaque formation. No effect on intracellular bacterial growth and bacteria protrusion formation were observed. Low levels of myosin IIA were also localised to the *Shigella* F-actin tail. Indirect protein quantification with fluorescence labelling showed that myosin IIA, but not IIB protein levels decreased by ~50% in a subpopulation of HeLa cells infected with

Δ*icsA* and R-LPS *Shigella* strains which are defective in cell-to-cell spreading. Furthermore a significantly greater proportion of HeLa cells infected with the *Shigella* Δ*icsA,* R-LPS double mutant had reduced myosin IIA compared to Δ*icsA* or R-LPS-infected HeLa cells, suggesting a synergistic effect between the IcsA and LPS defects.

5.3 Materials and methods

5.3.1 Bacterial strains and growth media

The strains used in this study are listed in Table 1. *S. flexneri* strains were grown from a Congo Red positive colony as described previously (Morona *et al.*, 2003) and were routinely cultured in Luria Bertani (LB) broth and on LB agar. Bacteria were grown in media for 16 h with aeration, subcultured 1/20 and then grown to mid-exponential growth phase by incubation with aeration for 1.5 h at 37°C. Where appropriate, media were supplemented with tetracycline (4 or 10 μg mL^{-1}) or kanamycin (50 μg mL^{-1}).

Table 5.1 Bacterial strains and plasmids

Strain	Relevant characteristics[#]	Reference or source
S. flexneri		
2457T	*S. flexneri* 2a wild type	Laboratory collection
MLRM107	2457T [pMP7604; Tc^R]	(Lum *et al.*, 2013) (Chapter 3)
RMA723	2457T *ΔrmlD*::Km^R	(Van Den Bosch *et al.*, 1997)
RMA2041	2457T *ΔicsA*::Tc^R	(Van Den Bosch & Morona, 2003)
RMA2043	RMA2041 *ΔrmlD*::Km^R	(Van Den Bosch & Morona, 2003)

[#]Km^R, Kanamycin resistant; Tc^R, Tetracycline resistant

5.3.2 Chemicals and antibodies

(-)-Blebbistatin (50 mM stock - 203391; Merck Calbiochem), (+)-blebbistatin (50 mM stock - 203392; Merck Calbiochem), ML-7 (30 mM stock - I2764; Sigma-Aldrich) and ML-9 (100 mM stock - C1172; Sigma-Aldrich) were prepared in dimethyl sulfoxide (DMSO) (D2650; Sigma-Aldrich). Rabbit anti-Myosin IIA (M8064; Sigma-Aldrich) and rabbit anti-GAPDH

antibodies (600-401-A33; Rockland Immunochemicals, Inc.) were used at 1:400 and 1:3000 for Western immunoblotting, respectively. For immunofluorescence (IF) microscopy, rabbit anti-Myosin IIA, rabbit anti-Myosin IIB (M7939; Sigma-Aldrich) and Alexa 594-conjugated donkey anti-rabbit secondary antibodies (Molecular Probes) were used at 1:100.

5.3.3 Reverse transfection and HeLa cell lysate preparation

MYH9 (Myosin IIA) siRNA (L-007668-00-0005) and siRNA controls (Non-targeting Pool; D-001810-10-05, siGLO Green Transfection Indicator; D-001630-01-05) were purchased from Thermo Scientific. siRNAs were transfected with DharmaFECT 3 Transfection Reagent (T-2003-03) and DharmaFECT Cell Culture Reagent (DCCR; B-004500-100), also purchased from Thermo Scientific. Reverse transfection of HeLa cells (Human, cervical, epithelial cells ATCC #CCL-70) were carried out based on a method by Thermo Scientific. siRNA were prepared as a 5 µM stock and the final concentration used was 50 nM. HeLa cells were transfected and HeLa cell lysate were prepared as described previously (Lum *et al.*, 2013).

5.3.4 SDS-PAGE and Western immunoblotting

SDS-PAGE (12% acrylamide gel) and Western immunoblotting were carried out as described previously (Lum *et al.*, 2013). Molecular weight markers used were BenchMark™ Pre-Stained Protein Ladder (Invitrogen).

5.3.5 Plaque assay

Plaque assays were performed with HeLa cells as described previously (Oaks *et al.*, 1985) with modifications. 1.2×10^6 HeLa cells were seeded in six-well trays in minimal essential medium (MEM), 10% FCS, 1% penicillin/streptomycin. Cells were grown to confluence overnight and were washed twice with Dulbecco's modified Eagle medium (DMEM) prior to inoculation. 2.5×10^4 mid-exponential phase bacteria were added to each well. Trays were incubated at 37°C, 5% CO_2 and were rocked gently every 15 min to spread the inoculum evenly across the well. At 90 min post-infection, the inoculum was aspirated. 3 mL of the first overlay (DMEM, 5% FCS, 20 µg mL^{-1} gentamicin, 0.5% (w/v) agarose [Seakem ME]) was added to each well. ML-7, ML-9 or DMSO were added and were swirled to ensure even distribution. The second overlay (DMEM, 5% FCS, 20 µg mL^{-1} gentamicin, 0.5% (w/v) agarose, 0.1% (w/v) Neutral Red solution [Gibco BRL]) was added 48 h post-infection and

plaques were imaged 6 h later. All observable plaques were counted and the diameter was measured for each condition in each experiment. At least 50 plaques were measured for each condition.

5.3.6 Infectious focus assay

1.2×10^6 HeLa cells were seeded in six-well trays in MEM, 10% FCS, 1% penicillin/streptomycin. Cells were grown to confluence overnight and were washed twice with DMEM prior to inoculation. 5×10^4 mid-exponential phase bacteria expressing mCherry were added to each well. Trays were incubated at 37°C, 5% CO_2 and were rocked every 15 min to spread the inoculum evenly across the well. At 90 min post-infection, the inoculum was aspirated. 1.5 mL of DMEM (phenol red-free) (31053-028; Life Technologies), 1 mM sodium pyruvate, 5% FCS, 20 µg mL^{-1} gentamicin, 2 mM IPTG was added to each well. (+)-Blebbistatin, (-)-blebbistatin or DMSO were added and were swirled to ensure even distribution. Twenty-four hours later the infectious foci were imaged with an Olympus IX-70 microscope using a 10× objective. The filter set used was DA/FI/TX-3X-A-OMF (Semrock). Fluorescence and phase contrast images were captured and false colour merged with the Metamorph software program (Version 7.7.3.0, Molecular Devices). The area of the infectious focus, i.e. area where mCherry was expressed, was outlined and measured with Metamorph. All observable infectious foci were counted and the area was measured for each condition in each experiment. At least 15 infectious foci were measured for each condition. The following modifications were made for transfected cells. HeLa cells were transfected prior to infectious focus assay as described previously in 12-well trays (Lum *et al.*, 2013). On day 3, the infectious focus assay was carried out. Transfected HeLa cells were washed twice with DMEM prior to inoculation. 5×10^4 mid-exponential phase bacteria expressing mCherry were added to each well.

5.3.7 Invasion assay and immunofluorescence (IF) microscopy

HeLa cells (8×10^4) were seeded onto sterile glass cover slips in 24-well trays in MEM, 10% FCS, 1% penicillin/streptomycin. For transfected cells, HeLa cells were transfected as described previously (Lum *et al.*, 2013). Cells were grown to semi-confluence overnight, washed twice with Dulbecco's PBS (D-PBS) and once with MEM, 10% FCS. 4×10^7 mid-exponential phase bacteria were added to each well and subsequently centrifuged (2,000 rpm,

7 min, Heraeus Labofuge 400 R) onto HeLa cells. After 1 h incubation at 37°C, 5% CO_2, the infected cells were washed thrice with D-PBS and incubated with 0.5 mL MEM containing 40 µg mL^{-1} gentamicin for a further 1.5 h (or 3.5 h for labelling with anti-activated caspase 3). Infected cells were washed thrice in D-PBS, fixed in 3.7% (v/v) formalin for 15 min, incubated with 50 mM NH_4Cl in D-PBS for 10 min, followed by permeabilisation with 0.1% Triton X-100 (v/v) for 5 min. After blocking in 10% FCS in PBS, the infected cells were incubated at 37°C for 30 min with the desired primary antibody. After washing in PBS, coverslips were incubated with Alexa 594-conjugated donkey anti-rabbit secondary antibody (Molecular Probes) (1:100). F-actin was visualised by staining with Alexa Fluor 488-conjugated phalloidin (2 U mL^{-1}) and 4',6'-diamidino-2-phenylindole (DAPI) (10 µg mL^{-1}) was used to counterstain bacteria and HeLa cell nuclei. Coverslips were mounted on glass slides with Mowiol 4-88 (Calbiochem) containing 1 µg mL^{-1} *p*-phenylenediamine (Sigma) and was imaged using a 100× oil immersion objective (Olympus IX-70). The filter set used was DA/FI/TX-3X-A-OMF (Semrock). Fluorescence and phase contrast images were false colour merged using the Metamorph software program.

5.3.8 Indirect quantification of protein levels by IF

Indirect immunofluorescence was quantified with Metamorph to determine protein levels in bacteria-infected HeLa cells compared to uninfected HeLa cells. *"**Invasion assay and IF microscopy**"* (Section 5.3.7) was carried out as described above. Cells were imaged with a 40× objective. In each image, the maximum fluorescence (100%) was determined by the mean fluorescence of uninfected HeLa cells (2 - 3 cells). Infected and uninfected cells were selected by tracing and the mean fluorescence of the outlined area was determined with Metamorph. HeLa cells exhibited two distinct immunofluorescence staining patterns (high and low) when infected compared to uninfected HeLa cells. In such instances, the HeLa cells were arbitrarily assigned into distinct populations, before the level of fluorescence of the infected cell was determined. The fluorescence of ≥ 100 infected cells for each category was measured for each experiment.

5.3.9 Protrusion formation

HeLa cells were seeded, infected and fixed as per *"**Invasion assay and IF microscopy**"* (Section 5.3.7). HeLa cells were washed twice with 1× Annexin V binding buffer (99902;

Biotium) prepared in milliQ (18.2 MΩ·cm) water, mounted on glass slides with the same buffer and were imaged using a 40× oil immersion phase contrast objective (Olympus IX-70). Protrusion formation was defined as any extensions of bacterial projection(s) (minimum of a full bacterial length) beyond the periphery of the HeLa cell. For each condition in each experiment, a minimum of 100 cells were imaged.

5.3.10 Assay for growth of intracellular bacteria

HeLa cells (8×10^4) were seeded in 24-well trays in MEM, 10% FCS, 1% penicillin/streptomycin. Cells were grown to semi-confluence overnight, washed twice with D-PBS and once with MEM, 10% FCS. 4×10^7 mid-exponential phase bacteria were added to each well (multiplicity of infection ~500). The bacteria were centrifuged (2,000 rpm, 7 min, Heraeus Labofuge 400 R) onto HeLa cells. After 1 h incubation at 37°C, 5% CO_2, the infected cells were washed thrice with D-PBS and incubated with 0.5 mL MEM containing 40 µg mL^{-1} of gentamicin. At the indicated intervals, monolayers (in duplicate) were washed four times in D-PBS and were lysed with 0.1% (v/v) Triton X-100 in PBS for 5 min and bacteria were enumerated on tryptic soy agar (Gibco) plates.

5.3.11 Statistical analysis

Statistical analysis was carried out using GraphPad Prism 6. Results are expressed as means ± SEM of data obtained in independent experiments. Statistical differences between three or more groups were determined with a one-way ANOVA followed by Tukey's or Dunnett's multi comparison post hoc test. Statistical significance was set at $p < 0.05$.

5.4 Results

5.4.1 MLCK and myosin IIA are essential for *S. flexneri* cell-to-cell spreading in HeLa cells

Preliminary data from our laboratory suggested that HeLa cells infected with *Shigella* strains defective in cell-to-cell spreading (Δ*icsA* and R-LPS) strains have significantly reduced myosin IIA, but not IIB protein levels. Hence the study is focused on myosin IIA. ML-7 and ML-9 inhibit the catalytic activity of MLCK by out competing ATP binding, however ML-9 is more potent compared to ML-7 (Saitoh *et al.*, 1987). HeLa monolayers infected with *S. flexneri* were treated with increasing concentrations of ML-7 or ML-9 or with the DMSO vehicle alone (Figure 5.1). ML-7 and ML-9 treatment reduced *Shigella* plaque size (Figure 5.1A, C and E), but not plaque numbers (Figure 5.1B and D). Treatment with 50 μM ML-9 abolished plaque formation altogether (Figure 5.1D).

Blebbistatin exists in two (±) enantiomeric forms. The active (-) enantiomer (Straight *et al.*, 2003) preferentially binds the myosin II active site when ATP has been hydrolysed to the intermediate ADP and phosphate, hence slowing down phosphate release. Blebbistatin binding also locks myosin II in a state which reduces actin binding (Kovacs *et al.*, 2004; Ramamurthy *et al.*, 2004). HeLa monolayers infected with *S. flexneri* were treated with increasing concentrations of (+)-blebbistatin, (-)-blebbistatin or with the DMSO vehicle alone (Figure 5.2A - C). Infectious foci formation was abolished when HeLa cells were treated with 50 μM (-)-blebbistatin (Figure 5.2B). No effect on infectious foci formation was observed with the inactive (+)-enantiomer, as expected (Figure 5.2A - C).

To examine the effect of myosin IIA depletion on *S. flexneri* cell-to-cell spreading, HeLa cells were transfected with myosin IIA (*MYH9*) siRNA and an infectious focus assay was carried out. Western immunoblots of HeLa cells lysates two days post-siRNA treatment showed ~80% reduction in myosin IIA levels (Figure 5.2D). *S. flexneri* formed infectious foci on HeLa cells treated with myosin IIA siRNA with a reduced mean focus area (***$p < 0.001$) (Figure 5.2E and G) but not foci counts (Figure 5.2F) when compared with HeLa cells treated with the negative control siRNA. Therefore myosin II inhibition with (-)-blebbistatin as well

as myosin IIA siRNA knockdown reduced *Shigella* cell-to-cell spreading. Inhibition of MLCK with ML-7 and ML-9 also significantly reduced *Shigella* plaque formation.

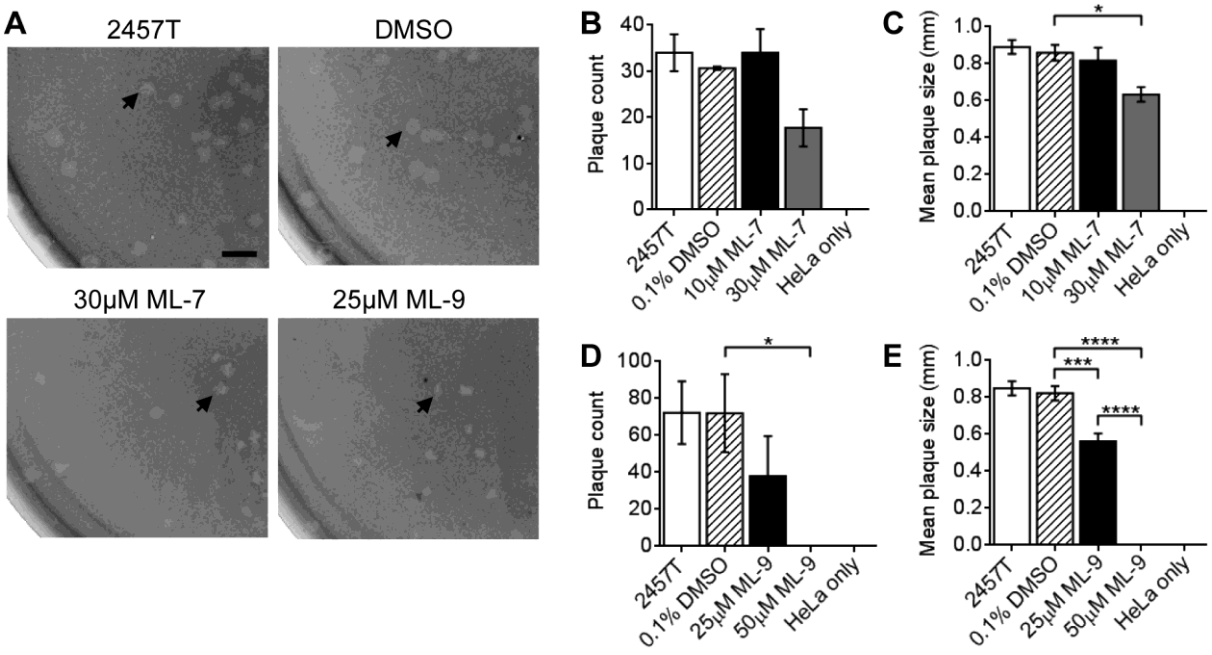

Figure 5.1 MLCK inhibition reduces *S. flexneri* 2457T plaque size.

HeLa cells were infected with *S. flexneri* 2457T in a plaque assay using a 6-well tray as described in the Methods. Plaque formation was performed in the presence of increasing concentrations of ML-7, ML-9 or the vehicle, 0.1 % DMSO. (A) Wells were stained with Neutral Red to makes plaques more visible. Scale bar = 2 mm. (B) The total plaque counts or (C) mean plaque diameters from each well treated with ML-7 and infected with *Shigella* were calculated. (D) The total plaque counts or (E) mean plaque diameters from each well treated with ML-9 and infected with *Shigella* were calculated. Data are represented as mean ± SEM of independent experiments (n = 3), analysed with one-way ANOVA ($p < 0.0001$ for ML-7 plaque counts and mean plaque diameters, $p = 0.0029$ for ML-9 plaque counts and $p < 0.0001$ for ML-9 plaque size), followed by Tukey's post hoc test (*$p < 0.05$, ***$p < 0.001$, ****$p < 0.0001$).

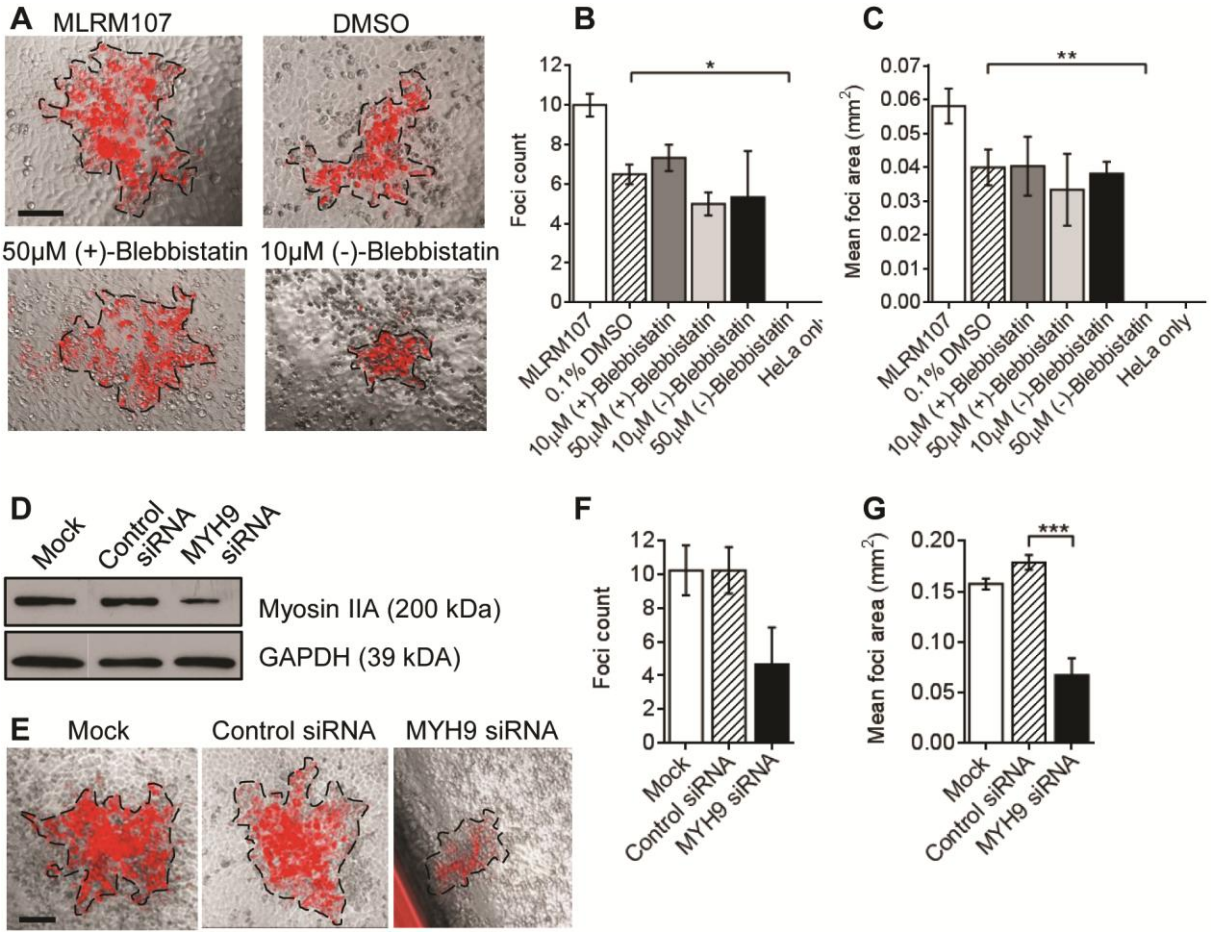

Figure 5.2 Myosin IIA inhibition with (-)-blebbistatin and transfection of HeLa cells with *MYH9* siRNA reduces MLRM107 foci area.

(A) - (C) HeLa cells were infected with *S. flexneri* MLRM107 in an infectious focus assay using a 12-well tray as described in the Methods. Infectious foci were imaged 24 h post-gentamicin treatment. ≥ 15 infectious foci were imaged for each condition. (A) Images shown are overlay of an image taken with phase contrast and TxRed filter (10× magnification). The area of the infection focus i.e. area where mCherry was expressed, is outlined. Scale bar = 0.1 mm. (B) The total foci counts from one well or (C) mean foci area from one well were calculated. Data are represented as mean ± SEM of independent experiments (n = 3), analysed with one-way ANOVA ($p < 0.0001$ for foci counts and mean foci area), followed by Tukey's post hoc test (*$p < 0.05$, **$p < 0.01$). (D) - (G) HeLa cells were either mock transfected or transfected with control or *MYH9* (myosin IIA) siRNA for 24 h, trypsinised and re-transfected for further 24 h. (D) HeLa cell extracts were probed with anti-Myosin IIA. GAPDH was used as a loading control. (E - G) Post-transfection, HeLa cells were infected and infectious foci were imaged as described in (A) - (C). (E) Images shown are overlay of an image taken with phase contrast and TxRed filter (10× magnification). The area of the infection focus i.e. area where mCherry was expressed, is outlined. Scale bar = 0.1 mm. (F) The total foci counts from one well or (G) mean foci area from one well were calculated. Data are represented as mean ± SEM of independent experiments (n = 3), analysed with one-way ANOVA ($p > 0.05$ for foci counts and $p = 0.0003$ mean foci area), followed by Tukey's post hoc test (***$p < 0.001$).

5.4.2 MLCK and myosin II inhibitors do not affect bacterial replication and protrusion formation

The inability of *S. flexneri* to form plaques can be attributed to reduced bacterial replication or inability to mediate protrusion formation. Semi-confluent HeLa cells were initially infected with *S. flexneri* to allow bacterial invasion into HeLa cells before treatment with ML-7, ML-9 and (-)-blebbistatin. The number of intracellular bacteria was calculated at 1, 2, 4 and 6 h post-incubation in gentamicin, which kills extracellular bacteria. As shown in Figure 5.3A, HeLa cells treated with DMSO or MLCK or myosin II inhibitors had no adverse effect on the rate of intracellular replication.

Bacterial protrusion formation was also determined in HeLa cells treated with MLCK and myosin inhibitors. Semi-confluent HeLa cells were initially infected with *S. flexneri* to allow bacterial invasion into HeLa cells before treatment with ML-7, ML-9 and (-)-blebbistatin for 1.5 h. HeLa cells treated with DMSO or MLCK or myosin II inhibitors formed protrusions similar to untreated HeLa cells (Figure 5.3C). No differences in % infected HeLa cells with bacterial protrusion were observed (Figure 5.3B).

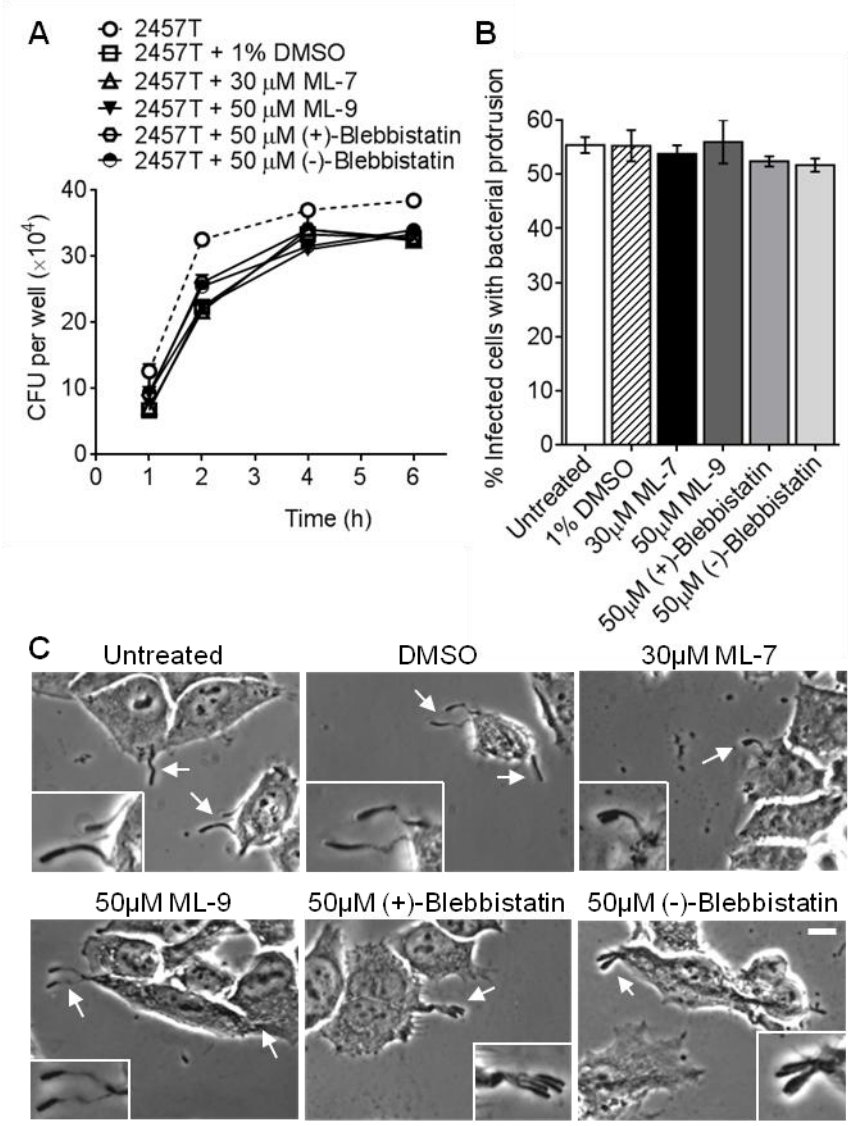

Figure 5.3 *S. flexneri* 2457T intracellular growth and protrusion formation in HeLa cells are not affected by of ML-7, ML-9, (+)-blebbistatin and (-)-blebbistatin.

HeLa cells were infected with *S. flexneri* 2457T for 1 h in a 24-well tray. HeLa cells were washed thrice with D-PBS and incubated with MEM containing 40 μg mL^{-1} of gentamicin (t = 0) to exclude extracellular bacteria. Concurrently HeLa cells were treated with 30 μM ML-7, 50 μM ML-9, 50 μM (+)-blebbistatin, 50 μM (-)-blebbistatin or DMSO. (A) To determine bacterial intracellular growth, two wells were prepared for each time point (t = 1, 2, 4 and 6 h) for each condition. At each interval, HeLa cells were washed, followed by lysis with 0.1% Triton X-100 to recover intracellular bacteria. Data are represented as mean from two-three independent experiments. (B - C) At t = 1.5, HeLa cells were fixed to observe bacteria protrusions. (B) The percentage of infected cells with bacteria protrusion(s) were enumerated by counting >100 cells in each independent experiment. Data are represented as mean ± SEM of independent experiments (n = 2), analysed with one-way ANOVA (p > 0.05). (C) Infected HeLa cells were imaged at 40× magnification. Scale bar = 10 μm. The arrows indicate protrusion formation. Insert shows 2× enlargement of the indicated region.

5.4.3 Myosin IIA is localised to the *S. flexneri* F-actin tail

The *S. flexneri* IcsA protein is localised at the old pole of the bacteria and interacts with the host N-WASP, which in turn recruits the Arp2/3 complex to initiate actin polymerisation. The F-actin tail that is formed imparts motility to the bacteria (Goldberg *et al.*, 1993; Goldberg, 2001; Suzuki *et al.*, 1998). The localisation of myosin IIA in *S. flexneri*-infected HeLa cells was investigated with IF microscopy. In untreated HeLa cells, myosin IIA is localised at the cytoplasm, cortex and stress fibers, and co-localises with the *S. flexneri* F-actin tail (Figure 5.4A). This was similarly observed when HeLa cells were treated with DMSO and infected with *S. flexneri* tail (Figure 5.4B). Treatment of infected HeLa cells with MLCK inhibitors, ML-7 and ML-9, did not affect myosin IIA localisation to bacterial F-actin tail tail (Figure 5.4C and D).

HeLa cells were also treated with the myosin II inhibitor, blebbistatin. As expected treatment with the inactive (+) enantiomer did not affect myosin II localisation to the bacteria F-actin tail tail (Figure 5.4E). Treatment with (-)-blebbistatin resulted in loss of stress fibres integrity and exaggerated membrane ruffling tail (Figure 5.4F). In myosin IIA siRNA-transfected cells, a reduction in cellular myosin IIA protein levels was observed, as expected tail (Figure 5.4G). Myosin II inhibition with (-)-blebbistatin and siRNA knockdown did not affect *S. flexneri* F-actin tail formation nor myosin IIA localisation to F-actin tail tail (Figure 5.4F and G). The frequency of *S. flexneri* comet tail formation also did not differ between untreated cells, *MYH9* siRNA-transfected cells and cells treated with DMSO, ML-7, ML-9 or both enantiomers of blebbistatin (data not shown). Hence F-actin tail formation is not dependent on either MLCK or myosin IIA.

Figure 5.4 Myosin IIA is localised to the *S. flexneri* 2457T F-actin tail and is not affected by MLCK and myosin II inhibitors.

HeLa cells were infected with *S. flexneri* 2457T in an invasion assay as described in the Methods. Bacteria and HeLa nuclei were stained with DAPI (blue), F-actin was stained with FITC-phalloidin (green) and myosin IIA was stained with anti-myosin IIA and Alexa Fluor 594-conjugated secondary antibody (red). Images were taken at 100× magnification. Scale bar = 10 μm. HeLa cells were treated with DMSO, ML-7, ML-9, (+)-blebbistatin, (-)-blebbistatin or were transfected with *MYH9* siRNA and were infected with *S. flexneri* 2457T; (A) Untreated; (B) 1% DMSO; (C) 30 μM ML-7; (D) 50 μM ML-9; (E) 50 μM (+)-blebbistatin; (F) 50 μM (-)-blebbistatin; (G) *MYH9* siRNA-transfected HeLa cells. Arrowheads indicate myosin IIA localisation at F-actin comet tails. Insert shows 1.5× enlargement of the indicated region. The experiment was repeated twice and representative images are shown.

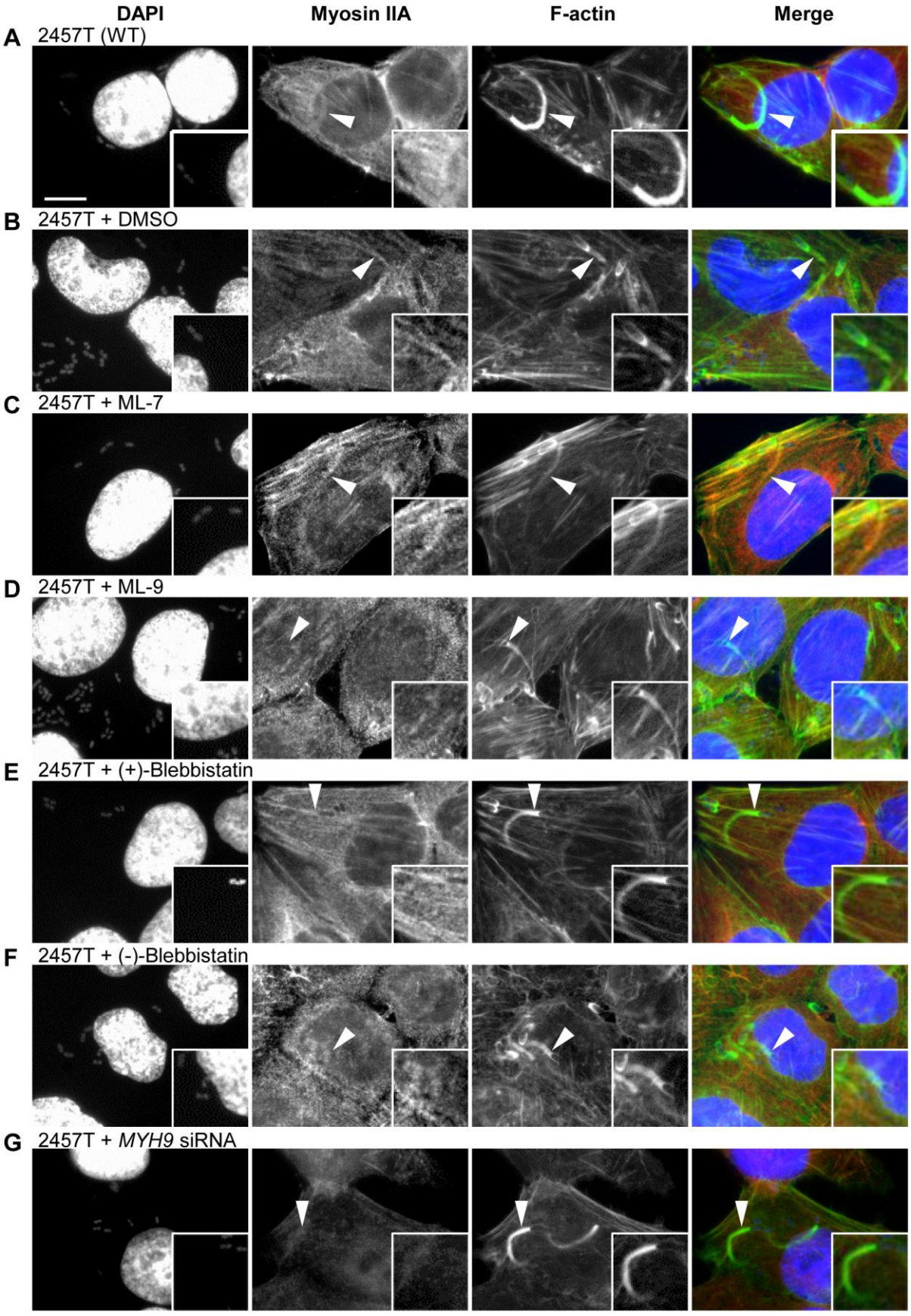
DAPI
Myosin IIA
F-actin
Merge
A
2457T (WT)
B
2457T + DMSO
C
2457T + ML-7
D
2457T + ML-9
E
2457T + (+)-Blebbistatin
F
2457T + (-)-Blebbistatin
G
2457T + MYH9 siRNA

5.4.4 Two distinct myosin IIA staining patterns are observed in HeLa cells infected with *S. flexneri* R-LPS and Δ*icsA* strains

IcsA and LPS are important for *S. flexneri* cell-to-cell spreading. In R-LPS strains, IcsA polar localisation and ABM is affected, but bacteria can still invade cells (Sandlin *et al.*, 1995; Van Den Bosch *et al.*, 1997). R-LPS strains also form F-actin tails, albeit infrequently and are shortened and distorted (Van Den Bosch *et al.*, 1997). *S. flexneri* Δ*icsA* strains can invade cells but do not form F-actin tails and hence are defective in cell-to-cell spreading (Goldberg & Theriot, 1995; Van Den Bosch & Morona, 2003). The localisation of myosin IIA in HeLa cells infected with Δ*icsA* and R-LPS strains was investigated with IF microscopy. While myosin IIA was observed in infected HeLa cells, the level of staining observed varied greatly between WT *S. flexneri*, R-LPS, Δ*icsA* or Δ*icsA*, R-LPS-infected HeLa cells (Figure 5.5A).

The relative myosin IIA fluorescence of infected HeLa cells was quantified by comparing myosin IIA staining intensity in infected HeLa cells relative to the mean staining intensity of two to three uninfected HeLa cells within the same image. The maximum intensity of uninfected HeLa cells was set at 100% (Figure 5.5E). In HeLa cells infected with WT *S. flexneri* 2457T, myosin IIA staining did not differ from uninfected HeLa cells (90.59 ± 6.79 %) (Figure 5.5A and E). HeLa cells infected with *S. flexneri* R-LPS (RMA723) had more intracellular bacteria in the cytoplasm (Figure 5.5B - column 1) compared to the WT strain (Figure 5.5A - column 1), presumably due to intercellular spreading defects. As seen in Figure 5.5B (column 2), two different myosin IIA staining was observed. Infected HeLa cells either had similar myosin IIA protein levels compared to the WT 2475T infected-HeLa cells or had uniform loss of myosin IIA from the cytoplasm, cortex and stress fibers. These cells were marked with ‡. The myosin IIA fluorescence of the two distinct cell populations [RMA723 and RMA723 (Lo - low myosin IIA protein levels)] was measured from 200 cells from two independent experiments and differed significantly (89.69 ± 3.97% vs 47.00 ± 1.43%, ***$p <$ 0.001). The overall percentage of RMA723-infected cells with low myosin II protein levels was 25.30 ± 0.44% (Figure 5.5F).

Significant bacterial clumping was observed in HeLa cells infected with *S. flexneri* Δ*icsA* strain (Figure 5.5C - column 1) compared to HeLa cells infected with the R-LPS strain (Figure 5.5B, column 1). Individual bacterium could not be distinguished due to the overcrowding of bacteria in the HeLa cell cytoplasm (Figure 5.5C - column 1). This was

expected since Δ*icsA* mutants are deficient in cell-to-cell spreading. Similar to HeLa cells infected with the *S. flexneri* R-LPS strain, two distinct myosin IIA staining profiles were observed in HeLa cells infected with the Δ*icsA* strain (Figure 5.5C - column 2). Infected HeLa cells with low myosin IIA staining were similarly marked with ‡ [RMA2041 (Lo)] and the mean myosin IIA intensity of this infected HeLa population was 54.43 ± 1.18%, which was significantly lower than RMA2041-infected HeLa cells with unaffected myosin IIA protein levels (91.36 ± 6.93%, $^{**}p < 0.001$). The overall percentage of RMA2041 (Δ*icsA*)-infected cells with low myosin II protein levels was 30.31 ± 0.72%, which was not significantly different from that of RMA723 (R-LPS)-infected cells (Figure 5.5F).

HeLa cells were infected with *S. flexneri* Δ*icsA*, R-LPS double mutant (RMA2043) to investigate if there were any synergistic effect between the Δ*icsA* and R-LPS mutants (Figure 5.5D). Similar to HeLa cells infected with the Δ*icsA* strain (Figure 5.5C - column 1), individual bacterium could not be distinguished due to significant bacterial clumping in the HeLa cytosol (Figure 5.5D - column 1). Two distinct myosin IIA staining profiles were also observed in RMA2043-infected HeLa cells (Figure 5.5D - column 2), similar to the R-LPS and Δ*icsA* mutants (Figure 5.5B and C, column 2). The difference in mean myosin IIA labelling intensity between RMA2043-infected HeLa cells with no loss of myosin IIA staining and infected HeLa cells with significant reduction in myosin IIA protein levels [RMA2043 (Lo)] was 82.27 ± 0.14% and 49.25 ± 0.14% ($^{**}p < 0.001$), respectively. Hence, no further reduction in myosin IIA protein levels was observed when both IcsA and LPS were mutated. No differences in F-actin cytoskeletal staining were observed between infected HeLa cells with typical or reduced myosin IIA protein levels (Figure 5.5D, column 3). The overall percentage of RMA2043 (Δ*icsA*, R-LPS)-infected cells with low myosin II protein levels was 43.97 ± 4.11%, which was higher ($^{*}p < 0.05$) than RMA723 (R-LPS) and RMA2041 (Δ*icsA*)-infected cells (Figure 5.5F). The increased frequency of infected HeLa cells with reduced myosin IIA staining in the double mutant suggests the mutations had a synergistic effect.

It is unclear how and why myosin IIA protein levels are decreased when infected with *S. flexneri* mutants defective in cell-to-cell spreading. The number of *S. flexneri* bacteria within the infected HeLa cell does not appear to be the distinguishing difference as bacterial loads appears to be similar between the two cell populations in either *S. flexneri* R-LPS, Δ*icsA* or Δ*icsA*, R-LPS-infected HeLa cells (Figure 5.5B - D, column 1). Furthermore no changes to

the cell shape or actin cytoskeleton is observed in spite of the reduced myosin IIA protein levels (Figure 5.5B - D, column 3). The HeLa cell line used in this study also expresses myosin IIB (Betapudi, 2010). Myosin IIB localisation in HeLa cells during *S. flexneri* infection was investigated by IF microscopy (Figure 5.6). Myosin IIB staining was similar to myosin IIA, but is more pronounced at the stress fibres. HeLa cells were infected with *S. flexneri* 2457T (WT), RMA723 (R-LPS), RMA2041 (Δ*icsA*) or RMA2043 (Δ*icsA*, R-LPS) and myosin IIB localisation was examined (Figure 5.6). Similar levels of myosin IIB staining were observed in both infected and uninfected HeLa cells. It appears the distinctive myosin II staining in *S. flexneri* R-LPS or Δ*icsA*-infected HeLa cells is specific for isoform IIA.

Figure 5.5 Myosin IIA protein levels are significantly reduced when infected with R-LPS and Δ*icsA S. flexneri* strains.

HeLa cells were infected with *S. flexneri* strains; (A) 2457T; (B) RMA723 (Δ*rmlD* - R-LPS); (C) RMA2041 (Δ*icsA*); (D) RMA2043 (Δ*icsA* Δ*rmlD*); in an invasion assay as described in the Methods. Bacteria and HeLa nuclei were stained with DAPI (blue), F-actin was stained with FITC-phalloidin (green) and myosin IIA was stained with anti-myosin IIA and Alexa Fluor 594-conjugated secondary antibody (red). Images were taken at 40× magnification. Scale bar = 20 μm. Infected HeLa cells are outlined. Infected HeLa cells with reduced myosin IIA labelling are marked with ‡. (E) The % myosin IIA labelling intensity of infected HeLa cells were compared with uninfected HeLa cells (set at 100%) in each individual image. In instances where infected HeLa cells have marked reduction in myosin IIA immunofluorescence, the infected HeLa cells are grouped into a separate category marked as (Lo = low) of the respective strains. The mean % myosin IIA labelling intensity of infected HeLa cells were determined by measuring ≥ 100 infected HeLa cells in each independent experiment for each category. Data are represented as mean ± SEM of independent experiments (n = 2), analysed with one-way ANOVA ($p < 0.0001$), followed by Tukey's post hoc test (**$p < 0.01$, ***$p < 0.001$). (F) The % infected HeLa cells with low myosin IIA immunofluorescence was determined from the IF images analysed. Data are represented as mean ± SEM of independent experiments (n = 2), analysed with one-way ANOVA ($p < 0.0001$), followed by Tukey's post hoc test (*$p < 0.05$).

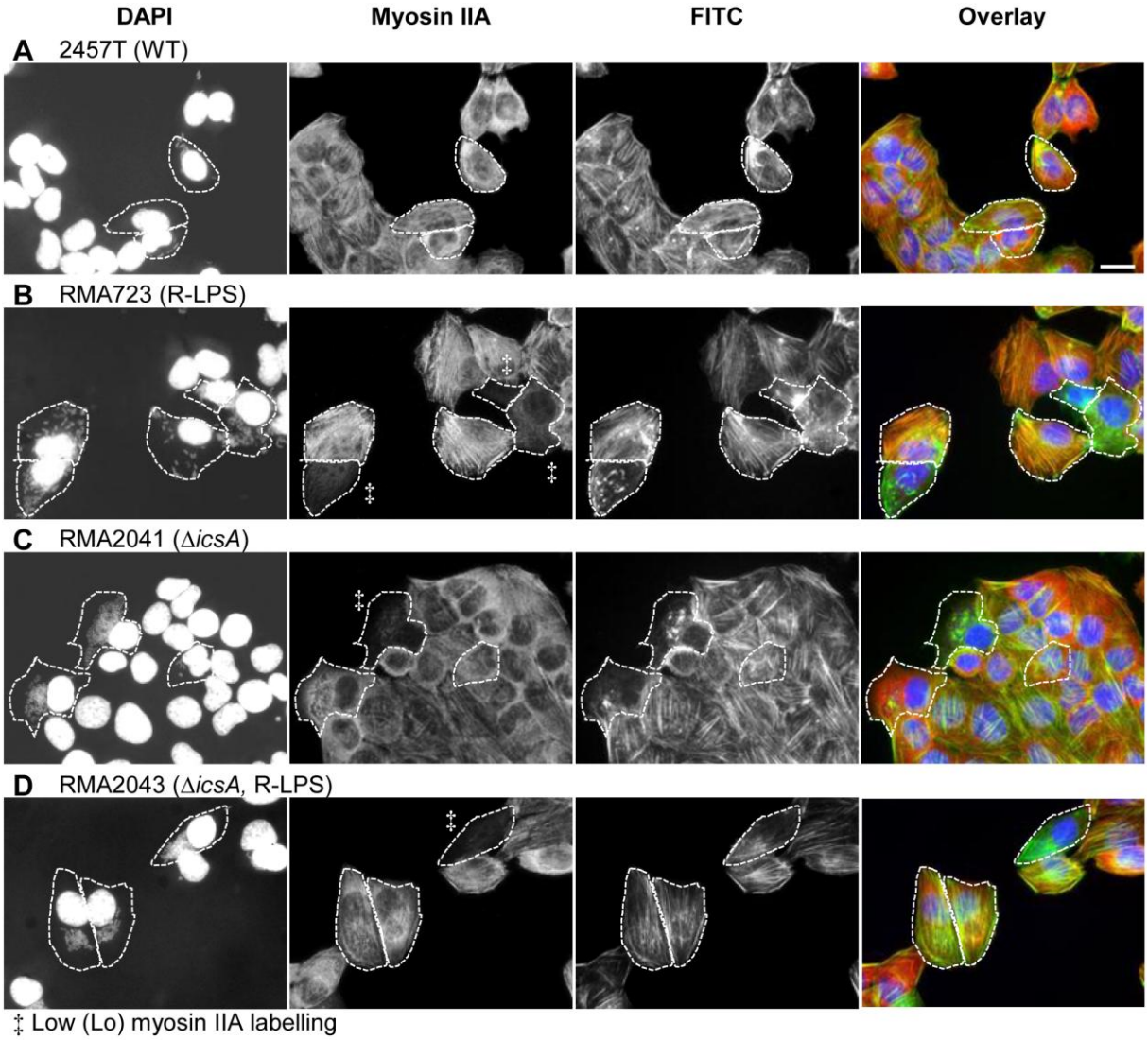
DAPI
Myosin IIA
FITC
Overlay
A 2457T (WT)
B RMA723 (R-LPS)
C RMA2041 (ΔicsA)
D RMA2043 (ΔicsA, R-LPS)
‡ Low (Lo) myosin IIA labelling

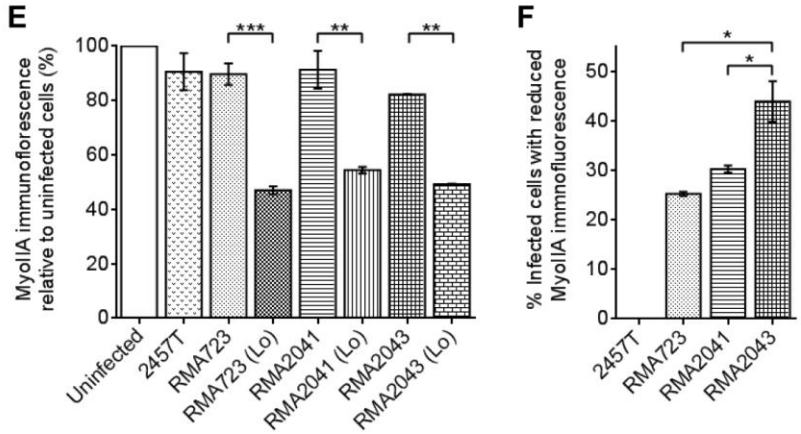
E
MyoIIA immunofloresecence relative to uninfected cells (%)
100
80
60
40
20
0
***
**
**
Uninfected
2457T
RMA723
RMA723 (Lo)
RMA2041
RMA2041 (Lo)
RMA2043
RMA2043 (Lo)

F
% Infected cells with reduced MyoIIA immnofluorescence
50
40
30
20
10
0
*
*
2457T
RMA723
RMA2041
RMA2043

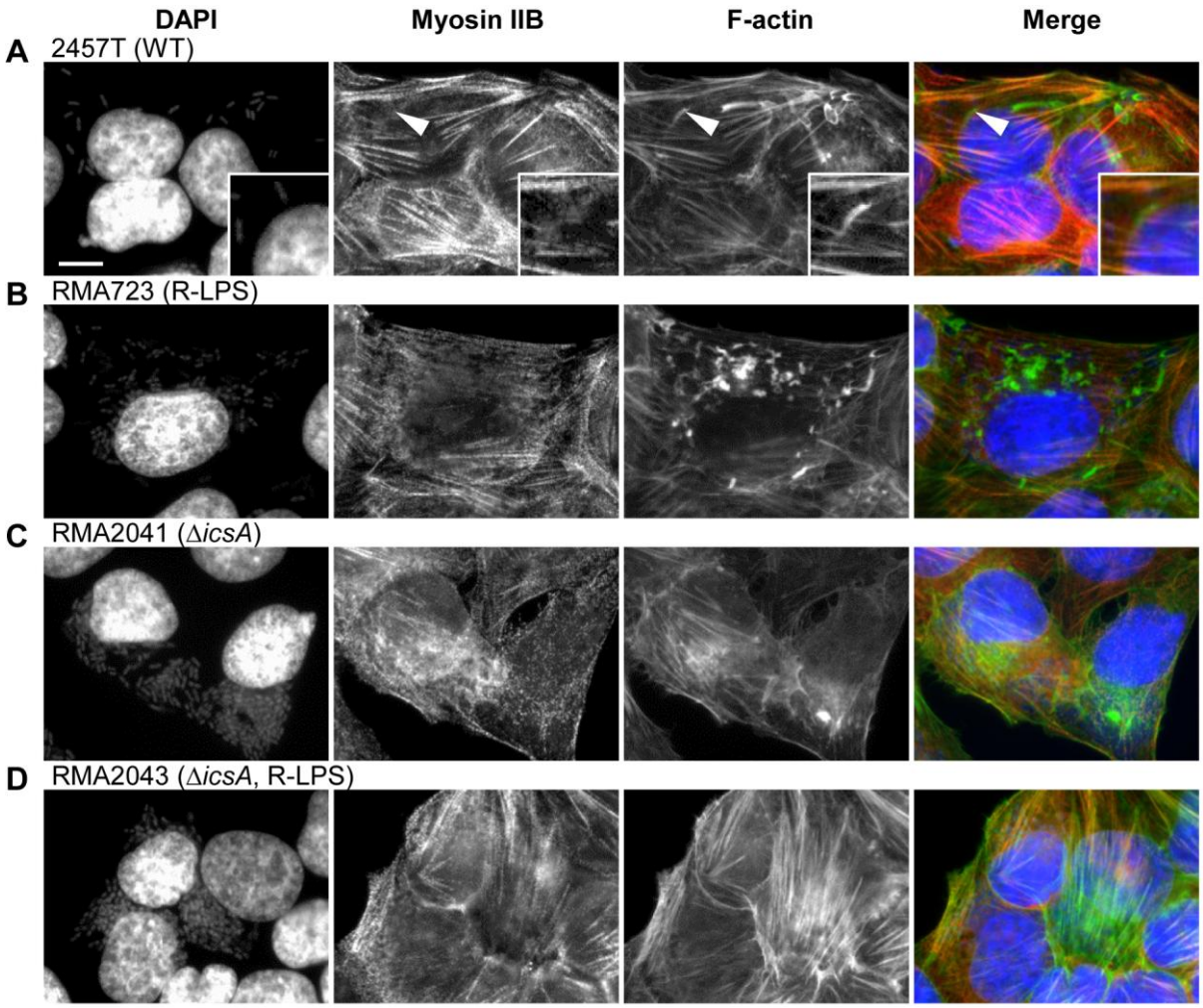

Figure 5.6 Myosin IIB protein levels are not affected when infected with R-LPS and Δ*icsA S. flexneri* strains.

HeLa cells were infected with *S. flexneri* strains; (A) 2457T; (B) RMA723 (Δ*rmlD* - R-LPS); (C) RMA2041 (Δ*icsA*); (D) RMA2043 (Δ*icsA* Δ*rmlD*); in an invasion assay as described in the Methods. Bacteria and HeLa nuclei were stained with DAPI (blue), F-actin was stained with FITC-phalloidin (green) and myosin IIB was stained with anti-myosin IIB and Alexa Fluor 594-conjugated secondary antibody (red). Images were taken at 100× magnification. Scale bar = 10 μm. Arrowheads indicate myosin IIB localisation at the F-actin comet tails. Insert shows 2× enlargement of the indicated region. The experiment was repeated twice and representative images are shown.

5.5 Discussion

In an attempt to differentiate host proteins which are recruited to rough and smooth *Shigella* strains, we observed that myosin IIA but not IIB protein levels were significantly reduced in HeLa cells infected with R-LPS and Δ*icsA* strains. Previously inhibition of myosin II and its specific kinase, MLCK, reportedly reduced the size of *Shigella* foci of infection in Caco-2 cells (Rathman *et al.*, 2000a). In a separate study, Mostowy *et al.* (2010) showed that in HeLa cells, myosin II was recruited to the septin cage which entraps intracytosolic *Shigella* without F-actin tails and targets the bacterium to the autophagy pathway for degradation. In this study the contribution of myosin IIA and MLCK during *Shigella* cell-to-cell spreading in HeLa cells was investigated with inhibitors and siRNA knockdown. The differences between myosin IIA and IIB labelling in *S. flexneri* R-LPS and Δ*icsA*-infected HeLa cells was also investigated.

Shigella intercellular spreading in host cells is dependent on its ability to initiate *de novo* F-actin tail polymerisation, protrusion formation into neighbouring cells, engulfment of protrusions and lysis of the double membrane vacuole, and is dependent on both *Shigella* and host proteins. In eukaryotic cells, the cortical tension is maintained by the actin-myosin II (actomyosin) network (Pasternak *et al.*, 1989) which is important for various processes such as lamellipodia formation (Betapudi, 2010) and maintaining cell morphology (Eliott *et al.*, 1993; Even-Ram *et al.*, 2007; Wei & Adelstein, 2000). Phosphorylation of myosin II regulatory light chain by a number of kinases, including MLCK and Rho-activated kinase activate myosin II ATPase activity, filament formation and contractile activity *in vitro* and *in vivo* (Conti *et al.*, 2008; Conti & Adelstein, 2008). Mammalian cells express three myosin II isoforms, IIA, IIB and IIC; however in spite high degree of similarity in sequence identity and structural conservation, myosin II isoforms differ in enzymatic properties and subcellular localisation (Conti *et al.*, 2008; Maupin *et al.*, 1994). The isoforms also have distinct and redundant roles depending on the specific cellular processes (Betapudi, 2010; Kelley *et al.*, 1996; Kolega, 1998; Wang *et al.*, 2011).

Inhibition of MLCK and myosin II catalytic activity with ML-7, ML-9 and (-)-blebbistatin significantly reduced *Shigella* intercellular spreading. Knockdown of myosin IIA with siRNA similarly affected *Shigella* cell-to-cell spreading. Myosin IIA knockdown was not complete as

low levels of the protein was detected with Western immunoblotting. Nonetheless myosin IIA inhibition reduced *Shigella* infectious focus area by > 60%. These results also suggest myosin IIB is unable to rescue myosin IIA function and that myosin IIA's role in *Shigella* cell-to-cell spreading is specific. These results are in agreement with previous findings that showed MLCK involvement during *Shigella* intercellular spreading in polarised Caco-2 cells (Rathman *et al.*, 2000a). The authors also provided indirect evident for myosin II involvement (Rathman *et al.*, 2000a).

The inability to form plaques or infectious foci could be attributed to either reduced bacterial motility or lack of protrusion formation. *Shigella* F-actin tail formation occurred at a similar frequency to untreated cells. Furthermore *Shigella* protrusion formation in semi-confluent HeLa cells was also not significantly affected. This was in contrast to the previous report in confluent Caco-2 cells where ML-7 inhibited *Shigella* protrusion formation as detected by transmission electron microscopy. In the few protrusions that were observed, *Shigella* bacteria were not tightly associated with the protruding membrane (Rathman *et al.*, 2000a). While that study primarily used Caco-2 cells, the authors also used semi-confluent HeLa cells to observe F-actin tail formation in the presence of ML-7. Both *Shigella* F-actin tail and protrusion formation were observed and were not significantly different from untreated, infected HeLa cells in that study, as we also observed (Rathman *et al.*, 2000a). No differences in *Shigella* viable cell counts were observed for ML-7, ML-9 and (-)-blebbistatin-treated HeLa cells, suggesting *Shigella* growth is unaffected. Hence the most likely explanation for reduced *Shigella* plaque or foci formation in the absence of MLCK and myosin II is likely due to a defect in the uptake of bacteria-containing protrusion into the neighbouring cells.

In Mostowy *et al.* (2010)'s study, myosin II depletion with siRNA increased the number of *Shigella*-infected cells 4 h 40 min post-infection when observed with quantitative microscopy. Similar results were observed by flow cytometry when Caco-2 cells were treated with the myosin II inhibitor, blebbistatin (Mostowy *et al.*, 2010). To rule out the possibility that myosin II inactivation increased *Shigella* cell-to-cell spread independently of septin caging, blebbistatin treatment was repeated with *Listeria monocytogenes*-infected Caco-2 cells (Mostowy *et al.*, 2010). *Listeria* also relies on F-actin tail formation for cell-to-cell spread (Gouin *et al.*, 2005), but septin caging was not observed under similar experimental

conditions (Mostowy *et al.*, 2010). Blebbistatin treatment did not increase, and even slightly reduced the number of *Listeria*-infected Caco-2 cells and it was inferred loss of myosin II does not affect *Shigella* cell-to-cell spread and that inactivation of septin caging alone was responsible for the increase in *Shigella* intercellular spreading.

The conclusion in reference to the role of myosin II and *Shigella* cell-to-cell spreading from Mostowy *et al.* (2010)'s study would appear contradictory to our findings and that of Rathman *et al.* (2000a). The main issue with using *Listeria* as an alternative model is that myosin II and MLCK are not required for *Listeria* cell-to-cell spread regardless of septin caging. This has been demonstrated by various groups in *Potorous tridactylis* kidney (PtK2) cells (Cramer & Mitchison, 1995), Caco-2 cells (Rathman *et al.*, 2000a) and Caco-2 BBE1 cells (Rajabian *et al.*, 2009). Hence the role of myosin II in *Shigella* intercellular spreading during septin caging of non-motile *Shigella*-infected HeLa cells requires further investigation. It is likely myosin II plays different roles during different stages of *Shigella* infection. Myosin II interaction with septin initially helps to target a subset of non-motile *Shigella* for destruction via autophagy. *Shigella* bacteria which have successfully initiated F-actin tail undergo replication and subsequently form protrusions into the neighbouring cells, whereby myosin II facilitates uptake of the bacterium. Depending on the experimental conditions, myosin II inhibition would result in different outcomes. In Mostowy *et al.* (2010)'s study, the number of infected cells was determined out 4 h 40 min post-infection whereas plaque and infectious focus formation are typically measured 24 - 48 h post-infection.

The *Shigella* IcsA outer membrane protein is localised to the old pole, ie the pole which exists prior to cellular division which gives rise to new daughter poles (Goldberg *et al.*, 1993). IcsA polar localisation is also dependent on LPS. Shortening of LPS O-antigen chain length has revealed IcsA expression on the lateral surface of *Shigella* (Morona & Van Den Bosch, 2003). Hence LPS may act to mask IcsA on the lateral regions to reinforce polar localisation. Alterations of LPS O-antigen chain length also affect ABM and *Shigella* plaque formation adversely (Morona *et al.*, 2003). In infected HeLa cells, myosin IIA and IIB were found at *Shigella* F-actin tail. However only myosin IIA protein levels in HeLa cells were significantly reduced (~50%) when infected with *Shigella* Δ*icsA* and R-LPS strains. This was observed in ~25 - 30% of infected cells. No further decrease in myosin IIA labelling was observed when cells were infected with the Δ*icsA*, R-LPS double mutant, although the proportion of cells

with reduced myosin IIA was almost doubled. This suggests that there might be some synergistic effects between Δ*icsA* and R-LPS mutations, although it is unclear how this interaction may occur. *Shigella* Δ*icsA* and R-LPS strains are defective in cell-to-cell spreading and over time, bacterial clumps accumulate within the HeLa cell cytoplasm. The uniform loss of myosin IIA could be partly attributed to the increased bacterial loads in HeLa cells. However infected cells with similar bacterial numbers can have either similar or decreased myosin IIA protein levels compared to uninfected neighbouring HeLa cells (Figure 5.5). Nonetheless the increased bacterial load in the cytoplasm may trigger activation of an undefined signalling pathway which in turn decreases myosin IIA levels.

In addition to its role in *Shigella* cell-to-cell spreading, recent studies implicate myosin II in the pathogenesis of several important bacterial pathogens such as *Chlamydia*, *Salmonella* and *Helicobacter*. In *Chlamydia,* myosin IIA and IIB are required for extrusion egress following chlamydial development within a vacuole in the host. In the absence of myosin IIA and IIB activation, lytic egress is favoured (Lutter *et al.*, 2013). The balance between lytic and extrusion egress mechanism is achieved in response to cellular signalling pathways and external environmental stimuli (Lutter *et al.*, 2013). In *Salmonella,* the bacterial SopB protein mediates myosin IIA-dependent contractility, forming stress-fibre like structures which is thought to facilitate *Salmonella* entry into the host cell (Hänisch *et al.*, 2011). Additionally myosin IIB induces cytoskeletal rearrangements around the *Salmonella*-containing vacuole (SCV) in the host cell, which may act to restrain bacterial growth and regulate bacterial virulence (Odendall *et al.*, 2012). Myosin IIA has also been reported to facilitate positioning of the SCV at the host nucleus (Wasylnka *et al.*, 2008). In *Helicobacter*, increased myosin II activity resulted in subsequent loss of gastric mucosal tight junction barrier integrity which may contribute to the predisposition of gastric cancer development (Posselt *et al.*, 2013). In non-polarised gastric epithelial cells, inhibition of myosin II activity affected the rear retraction of the cell resulting in significantly altered cell shape (Lu *et al.*, 2009), which may contribute to gastric carcinoma invasion and metastasis (Argent *et al.*, 2004; Azuma *et al.*, 2004; Basso *et al.*, 2008). Hence myosin IIA and IIB play diverse roles during pathogenesis of different intracellular pathogens, which is distinct from its role in *Shigella* intercellular spread. In some cases, only one of the myosin II isoform is required suggesting myosin II specificity.

Although we initially set out to identify host proteins which are differentially localised to *Shigella* smooth and rough strains, it was unexpectedly observed that *Shigella* strains defective in cell-to-cell spreading had reduced myosin IIA, but not IIB protein levels in a proportion of infected HeLa cells, suggesting specificity between the two isoforms. This was not surprising since myosin II isoforms have been reported to play different roles within the same cell type (Betapudi, 2010; Maupin *et al.*, 1994). Furthermore different myosin II isoforms are also targeted by bacteria at different stages of infection, as in the case of *Salmonella*.

We also show that MLCK and myosin IIA inhibition significantly affected *Shigella* plaque formation but no effect on intracellular growth and protrusion formation was observed. Low levels of myosin IIA was detected in the *Shigella* F-actin tails. We hypothesize that the reduced plaque formation could be a defect in the uptake of bacteria-containing protrusion in the neighbouring cells. Previously components of the clathrin mediated endocytic pathway including dynamin, clathrin and Epsin-1 was shown to mediate bacterial uptake in the neighbouring cells (Fukumatsu *et al.*, 2012; Lum *et al.*, 2013). It is possible myosin IIA may interact with components of the endocytic pathway to facilitate uptake of bacteria-containing protrusions. Perhaps the loss of *icsA* or LPS O-antigen affected *Shigella* cell-to-cell spreading which led to downstream effects including bacterial overcrowding of HeLa cell cytoplasm, which in turn affected myosin IIA expression.

5.6 Acknowledgements

We thank Luisa Van Den Bosch for preliminary work on myosin IIA. This work is supported by a Program Grant (565526) from the National Health and Medical Research Council (NHMRC) of Australia. ML was the recipient of the Australian Postgraduate Award from the NHMRC. The authors declare that they have no conflict of interest.

ꕥ Chapter 6 ꕥ

Overall Discussion and Conclusions

Chapter 6: Overall Discussion and Conclusions

6.1 Introduction

To date, *Shigella* infection remains a significant human pathogen due to high morbidity in children <5 years in developing countries although deaths resulting from shigellosis have significantly reduced, possibly due to unrestricted access to antibiotics, improved nutrition and a reduction in bacterial virulence (Bardhan *et al.*, 2010). In the Australian state of New South Wales, reports have emerged suggesting *Shigella* infection is on the rise among gay couples due to the practice of rimming, a variation of the faecal-oral route transmission (Badorrek, 2014). In previous years *Shigella* outbreaks from similar practices have been reported in the states of Victoria and Queensland (Badorrek, 2008). Since *Shigella* is largely a preventable disease in developed countries, it is unlikely shigellosis will pose significant health risks.

Shigella bacteria have co-evolved with its human host for a long time and hence are adept at exploiting host proteins to further its dissemination, and to evade host defences. In this thesis, two key features of shigellosis, cell-to-cell spreading and induction of epithelial cell death, were investigated. The host proteins investigated were dynamin II (Chapter 3), Drp1 (Chapter 4) and myosin IIA (Chapter 5). Dynamin II, Drp1 and myosin IIA are usually cytoplasmic but are recruited to the plasma membrane, mitochondria and cortical actin, respectively, to carry out their specific roles. Below is an overview of the outcomes of this thesis and further discussion points not included in the individual Results and Discussion chapters.

6.2 Discussion

6.2.1 Role of dynamin II, Drp1 and myosin IIA

The main body of this work was to study the contribution of dynamin II, Drp1 and myosin IIA in *Shigella* cell-to-cell spreading. Dynamin II was initially chosen as it was hypothesised that the process of cell-to-cell spreading may require components of endocytosis and/or exocytosis. Dynamin II is important for *Shigella* and *Listeria* cell-to-cell spread, and is also localised to the *Shigella* F-actin tail (Chapter 3). During the course of this study, various components of the clathrin-mediated endocytic pathway was shown to facilitate *Shigella* cell-to-cell spread (Fukumatsu *et al.*, 2012). Furthermore it appears *Shigella* prefer to translocate into the neighbouring cell at tricellular junctions, i.e. TJs where three cells meet. This contrasted with *Listeria* which depended less on the clathrin-mediated endocytic pathway and preferentially translocate at TJs where two cells meet (bicellular junctions) (Fukumatsu *et al.*, 2012). The dynamin II inhibitor, dynasore, was also tested *in vivo* in the murine Sereny model and some protection against weight loss as a result for *Shigella* infection was observed. However there was no improvement in keratoconjunctivitis.

Since dynasore was reported to inhibit Drp1 (Cassidy-Stone *et al.*, 2008), the protein was included in the study. Drp1 maintains the homeostatic state of the mitochondria by facilitating mitochondrial fission (Smirnova *et al.*, 1998; Smirnova *et al.*, 2001). Unexpectedly Drp1 inhibition with dynasore and siRNA knockdown reduced plaque formation (Chapter 4). Unlike dynamin II, Drp1 was not recruited to the *Shigella* F-actin tail. While Drp1 is not likely to affect *Shigella* cell-to-cell spreading directly, the loss of mitochondrial dynamics highlights the importance of maintaining the internal landscape of the cell to facilitate bacterial ABM and subsequent cell-to-cell spread. Even though differences in *Listeria* movement in the subcellular environment of the host cell was reported previously (Lacayo & Theriot, 2004), the outcomes of this work showed clearly that extreme changes within the subcellular architecture is not favourable for bacterial cell-to-cell spread. Previously microtubule degradation by the secreted *Shigella* TTSS effector, VirA, was reported to facilitate bacteria invasion into the cell and subsequent *Shigella* intra- and intercellular movement (Yoshida *et al.*, 2002; Yoshida *et al.*, 2006). It was suggested VirA has cysteine protease-like properties allowing the bacteria to degrade microtubules (Yoshida *et al.*, 2006),

however subsequent crystallographic studies by Davis *et al.* (2008) and Germane *et al.* (2008) showed that VirA has no protease activity, but plays a role in invasion as reported earlier (Yoshida *et al.*, 2002). Recently Burnaevskiy *et al.* (2013) reported that VirA and IpaJ (also a TTSS effector) induces Golgi fragmentation, but *Shigella* ABM was not affected. The role of VirA and Golgi in *Shigella* cell-to-cell spread was not determined (Burnaevskiy *et al.*, 2013).

Mitochondrial fission is also a crucial downstream event following intrinsic apoptosis (Frank *et al.*, 2001; Wasiak *et al.*, 2007) and programmed necrosis pathway activation (Wang *et al.*, 2012). In previous studies the involvement of mitochondria in *Shigella*-induced epithelial cell death has been observed. Biochemical and morphological changes to the mitochondria were noted, albeit under different experimental conditions (Bergounioux *et al.*, 2012; Carneiro *et al.*, 2009; Kobayashi *et al.*, 2013; Lembo-Fazio *et al.*, 2011). The finding that Drp1 inhibition reduces *Shigella*-induced epithelial cell death and restores mitochondrial structure may be the common factor underlying these observations. Although the results from this study suggest a critical role for Drp1 during *Shigella*-induced cell death, the same was not observed for other pathogens such as *L. monocytogenes* (Stavru *et al.*, 2011; Stavru *et al.*, 2013) and *H. pylori* (Jain *et al.*, 2011). For these pathogens, the bacterial factor responsible for the changes in mitochondria during infection has been identified. This is in contrast with *Shigella* infection. To date, the possible *Shigella* effector(s) which may act to trigger epithelial cell death has yet to be identified. On the contrary the *Shigella* OspC3 TTSS effector was reported to delay necrotic cell death *in vitro* and dampen colonic inflammation in guinea pigs (Kobayashi *et al.*, 2013). Hence *Shigella* infection in the host cells presents a complex interplay between maintaining a replicative niche and the host's response in favouring inflammation to retard *Shigella*'s dissemination.

The third host protein included in this study is myosin IIA. Myosin IIA was identified when host protein localisation was compared between *S. flexneri* WT and mutant strains. The results from this work suggest myosin IIA, but not IIB, is critical for *Shigella* plaque formation. Furthermore myosin IIB cannot compensate for myosin IIA depletion (Chapter 5). Previously myosin II and its specific kinase, MLCK, were implicated in *Shigella* cell-to-cell spreading (Rathman *et al.*, 2000a). Another study also reported that intracytosolic *Shigella* can be prevented from intercellular spreading when the bacteria are encased in septin cages (Mostowy *et al.*, 2010). Actin, myosin II and phosphorylated MLCK co-localised with the

septin cage in non-motile bacteria (Mostowy *et al.*, 2010). Collectively the outcomes from Rathman *et al.* (2000a), Mostowy *et al.* (2010) and this study suggest myosin II have two distinct roles during *Shigella* infection. The first is to facilitate caging of *Shigella* bacteria via interactions with septin and secondly to facilitate *Shigella* cell-to-cell spreading at the membrane, although the exact mechanism has not been elucidated. In contrast, myosin II and MLCK are not required for *Listeria* cell-to-cell spreading (Cramer & Mitchison, 1995; Rajabian *et al.*, 2009; Rathman *et al.*, 2000a). In fact (-)-blebbistatin treatment of Caco-2 BBE1 cells rescued the protrusion formation defect of the *Listeria* Δ*inlC* mutant (Rajabian *et al.*, 2009). Hence while *Shigella* and *Listeria* both share similarities in the ability to exploit host proteins for ABM, host proteins involved in subsequent events differ.

Recently it was reported that myosin II inhibition significantly increased mitochondrial length, hinting at a possible role for myosin II in mitochondrial fission (DuBoff *et al.*, 2012; Korobova *et al.*, 2014). Myosin IIA and IIB knockdown with siRNA also reduced Drp1 recruitment to fission sites on the mitochondria in U2OS human osteosarcoma cells (Korobova *et al.*, 2014). Loss of Drp1 recruitment was also observed in *Drosophila* neuron mitochondria when the *Drosophila* homologues of the mammalian myosin II heavy chain and regulatory light chain, Zipper (zip) and spaghetti squash (sqh), respectively, were mutated (DuBoff *et al.*, 2012). In this study HeLa cells were treated with the DMSO control, ML-7, ML-9, (+)-blebbistatin or (-)-blebbistatin and were infected with *S. flexneri* 2457T. No differences in LDH release were observed between the DMSO treatment and inhibition of MLCK (ML-7 and ML-9) or myosin II [(-)-blebbistatin] (data not shown). The LDH assay was not repeated with siRNA knockdown of myosin IIA. Since myosin II and MLCK inhibition did not reduce LDH release following *S. flexneri* infection, myosin II may not have a role in Drp1-mediated mitochondrial fission following cell death pathway activation; however this remains to be investigated.

6.2.2 Alternative therapeutic approaches to improve shigellosis symptoms

Non-antibiotic therapeutic approaches to treatment of shigellosis have been investigated in several studies. One of these approaches is the addition of cooked green banana to diets of children infected with *Shigella*. Green banana is rich in amylase resistant starch, which is subsequently fermented by colonic bacteria into short chain fatty acids such as acetate,

propionate, butyrate (Topping & Clifton, 2001). These fatty acids are the major source of metabolic energy for the colonocytes. In a study by Rabbani *et al.* (2009), children aged 6 to 60 months with severe bloody dysentery caused by *Shigella* infection had significantly cleared faecal blood and reduced number of stools/day when given a rice-based diet with cooked green banana compared to the control group. Levels of acetate, propionate and butyrate were also higher in the treatment group (Rabbani *et al.*, 2009). Previously addition of green banana to regular diet of children enhanced recovery from persistent diarrhoea, and improved intestinal mucosal integrity and nutrient absorption (Rabbani *et al.*, 2001; Rabbani *et al.*, 2004). *In vitro* butyrate, in particular, decreased cytokines and NF-κB expression (Hase *et al.*, 2002), inhibited NF-κB (Augenlicht *et al.*, 2002; Segain *et al.*, 2000) and induced expression of an endogenous antimicrobial peptide (CAP 18) during *Shigella* infection (Raqib *et al.*, 2006). Recently Chang *et al.* (2014) reported that *n*-butyrate expressed by commensal bacteria in the gut renders resident macrophages hyporesponsive to commensal bacteria. Hence during *Shigella* infection, the increased butyrate availability from ingestion of green banana may dampen macrophage immune responses, thus limiting damage to the colonic epithelium. Consequently treatments that affect the interaction of *Shigella* with host cells might be beneficial in treating shigellosis. In this doctoral work, dynasore (Chapter 3) and Mdivi-1 (Chapter 4) did not significantly improve *Shigella*-induced inflammation in the murine Sereny model, but some protection against weight loss was observed, suggesting the use of small molecule inhibitors may be developed in future to ameliorate the symptoms associated with shigellosis by interfering with host proteins essential for *Shigella* pathogenesis.

The use of dynasore and Mdivi-1 as potential therapeutics has been tested in various experimental models of human diseases. Dynasore is a potent inhibitor of the clathrin-mediated endocytosis pathway and has been shown to effectively improve atherosclerosis in the aortic endothelium of hypercholesterolemic mutant mice by inhibiting endocytosis of cell surface transforming growth factor beta (TGFβ) cytokine. Consequently formation of hetero-oligomeric TGFβ receptor complexes at the plasma membrane was enhanced, resulting in the upregulation of TGFβ-induced signalling and cellular responses (Chen *et al.*, 2009). Dyngo4a, a structural analogue of dynasore, protected rat hemidiaphragm from botulinum/A heavy chain binding domain-induced paralysis by blocking endocytosis of the botulinum neurotoxin

(Harper *et al.*, 2011). In a another study, it was reported that pretreatment of mouse bladders with dynasore inhibited uropathogenic *E. coli* uptake (endoctytosis) into the umbrella cells found at the epithelium of the urinary bladder (Terada *et al.*, 2009). Dynasore inhibition of Drp1-mediated mitochondrial fission during ischemia/reperfusion injury in Langendorff perfused mouse hearts also protected cardiac lusitropy and limited cell damage through a mechanism that maintains mitochondrial morphology and intracellular ATP in stressed cells (Gao *et al.*, 2013).

Mdivi-1 inhibition of Drp1-mediated apoptotic pathway has been reported to have protective effects in animal models of ischemia/reperfusion in the heart (Ong *et al.*, 2010), retina (Park *et al.*, 2011), kidney (Brooks *et al.*, 2009), cerebrum (Zhang *et al.*, 2013) and hippocampal neuron (Xie *et al.*, 2013). Other studies on the protective effects of Mdivi-1 have been reported in animal models of neuropathic pain (Ferrari *et al.*, 2011), pulmonary hypertension (Marsboom *et al.*, 2012), lung cancer (Rehman *et al.*, 2012), pressure overload-induced heart failure (Givvimani *et al.*, 2012), cardiac hypertrophy (Chang *et al.*, 2013) and epilepsy (Qiu *et al.*, 2013). Hence loss of Drp1 function and regulation contributes to many pathophysiological conditions. On the whole these studies suggest small molecule inhibitors have potential therapeutic benefits.

6.3 Conclusions

In conclusion, the work from this thesis has identified Drp1 as a host factor important for *Shigella*-induced epithelial cell death (Chapter 4). It was also demonstrated clearly for the first time that an intact mitochondrial network is essential for efficient *Shigella* intercellular spreading (Chapter 4). The outcomes from this thesis also provided further evidence for the involvement of dynamin II in *Shigella* cell-to-cell spread (Chapter 3). Although dynasore-treatment did not improve inflammation resulting from *Shigella* infection, it did afford some protection against weight loss during the course of infection. Future work should consider the use of small molecule inhibitors to target host proteins as an alternative avenue to ameliorate shigellosis symptoms. Another key finding is that myosin IIA, but not IIB, is important for *Shigella* cell-to-cell spread. Moreover myosin IIA levels are significantly reduced in HeLa cells when infected *Shigella* strains defective in cell-to-cell spread, although the exact mechanism has yet to be identified (Chapter 5).

BIBLIOGRAPHY

Abrusci P, Vergara-Irigaray M, Johnson S & other authors (2013). Architecture of the major component of the type III secretion system export apparatus. *Nat Struct Mol Biol* 20, 99-104.

Al Mamun AA, Tominaga A & Enomoto M (1996). Detection and characterization of the flagellar master operon in the four *Shigella* subgroups. *J Bacteriol* 178, 3722-3726.

Ambrosi C, Pompili M, Scribano D, Zagaglia C, Ripa S & Nicoletti M (2012). Outer membrane protein A (OmpA): a new player in *Shigella flexneri* protrusion formation and inter-cellular spreading. *PLoS One* 7, e49625.

Arbibe L, Kim DW, Batsche E, Pedron T, Mateescu B, Muchardt C, Parsot C & Sansonetti PJ (2007). An injected bacterial effector targets chromatin access for transcription factor NF-κB to alter transcription of host genes involved in immune responses. *Nat Immunol* 8, 47-56.

Argent RH, Kidd M, Owen RJ, Thomas RJ, Limb MC & Atherton JC (2004). Determinants and consequences of different levels of CagA phosphorylation for clinical isolates of *Helicobacter pylori*. *Gastroenterology* 127, 514-523.

Ashida H, Toyotome T, Nagai T & Sasakawa C (2007). *Shigella* chromosomal IpaH proteins are secreted via the type III secretion system and act as effectors. *Mol Microbiol* 63, 680-693.

Ashida H, Kim M, Schmidt-Supprian M, Ma A, Ogawa M & Sasakawa C (2010). A bacterial E3 ubiquitin ligase IpaH9.8 targets NEMO/IKKγ to dampen the host NF-κB-mediated inflammatory response. *Nat Cell Biol* 12, 66-73.

Ashida H, Mimuro H, Ogawa M, Kobayashi T, Sanada T, Kim M & Sasakawa C (2011a). Cell death and infection: a double-edged sword for host and pathogen survival. *J Cell Biol* 195, 931-942.

Ashida H, Ogawa M, Kim M, Suzuki S, Sanada T, Punginelli C, Mimuro H & Sasakawa C (2011b). *Shigella* deploy multiple countermeasures against host innate immune responses. *Curr Opin Microbiol* 14, 16-23.

Ashida H, Ogawa M, Mimuro H, Kobayashi T, Sanada T & Sasakawa C (2011c). *Shigella* are versatile mucosal pathogens that circumvent the host innate immune system. *Curr Opin Immunol* 23, 448-455.

Ashida H, Nakano H & Sasakawa C (2013). *Shigella* IpaH0722 E3 ubiquitin ligase effector targets TRAF2 to inhibit PKC-NF-κB activity in invaded epithelial cells. *PLoS Pathog* 9, e1003409.

Aspenström P (2005). The verprolin family of proteins: regulators of cell morphogenesis and endocytosis. *FEBS Lett* 579, 5253-5259.

Augenlicht LH, Mariadason JM, Wilson A, Arango D, Yang W, Heerdt BG & Velcich A (2002). Short Chain Fatty Acids and Colon Cancer. *J Nutr* 132, 3804S-3808S.

Azuma T, Yamazaki S, Yamakawa A & other authors (2004). Association between diversity in the Src homology 2 domain-containing tyrosine phosphatase binding site of *Helicobacter pylori* CagA protein and gastric atrophy and cancer. *J Infect Dis* 189, 820-827.

Badorrek M (2008). *Shigella Outbreak Among Gay Men in Sydney*, ACON, NSW. Accessed February 28, 2014 at http://www.acon.org.au/about-acon/Newsroom/Media-Releases/2008/31.

Badorrek M (2014). *Shigella Increase Prompts Mardi Gras Concern*, ACON, NSW. Accessed February 28, 2014 at http://www.acon.org.au/about-acon/Newsroom/Media-Releases/2013/71#.

Baker SJ, Gunn JS & Morona R (1999). The *Salmonella typhi* melittin resistance gene *pqaB* affects intracellular growth in PMA-differentiated U937 cells, polymyxin B resistance and lipopolysaccharide. *Microbiology* 145, 367-378.

Bardhan P, Faruque A, Naheed A & Sack D (2010). Decrease in Shigellosis-related deaths without *Shigella* spp.-specific interventions, Asia. *Emerg Infect Dis* 16, 1718-1723.

Barman S, Saha DR, Ramamurthy T & Koley H (2011). Development of a new guinea-pig model of shigellosis. *FEMS Immunol Med Microbiol* 62, 304-314.

Barry EM, Pasetti MF, Sztein MB, Fasano A, Kotloff KL & Levine MM (2013). Progress and pitfalls in *Shigella* vaccine research. *Nat Rev Gastroenterol Hepatol* 10, 245-255.

Bârzu S, Benjelloun-Touimi Z, Phalipon A, Sansonetti P & Parsot C (1997). Functional analysis of the *Shigella flexneri* IpaC invasin by insertional mutagenesis. *Infect Immun* 65, 1599-1605.

Basso D, Zambon CF, Letley DP & other authors (2008). Clinical relevance of *Helicobacter pylori cagA* and *vacA* gene polymorphisms. *Gastroenterology* 135, 91-99.

Bereiter-Hahn J (1990). Behavior of mitochondria in the living cell. *Int Rev Cytol* 122, 1-63.

Bergounioux J, Elisee R, Prunier A-L, Donnadieu F, Sperandio B, Sansonetti P & Arbibe L (2012). Calpain activation by the *Shigella flexneri* effector VirA regulates key steps in the formation and life of the bacterium's epithelial niche. *Cell Host & Microbe* 11, 240-252.

Bergsbaken T, Fink SL & Cookson BT (2009). Pyroptosis: host cell death and inflammation. *Nat Rev Microbiol* 7, 99-109.

Bernardini ML, Mounier J, d'Hauteville H, Coquis-Rondon M & Sansonetti PJ (1989). Identification of *icsA*, a plasmid locus of *Shigella flexneri* that governs bacterial intra- and intercellular spread through interaction with F-actin. *Proc Natl Acad Sci U S A* 86, 3867-3871.

Betapudi V (2010). Myosin II motor proteins with different functions determine the fate of lamellipodia extension during cell spreading. *PLoS One* 5, e8560.

Bishai EA, Sidhu GS, Li W, Dhillon J, Bohil AB, Cheney RE, Hartwig JH & Southwick FS (2012). Myosin-X facilitates *Shigella*-induced membrane protrusions and cell-to-cell spread. *Cell Microbiol* 15, 353–367.

Brandon LD & Goldberg MB (2001). Periplasmic Transit and Disulfide Bond Formation of the Autotransported *Shigella* Protein IcsA. *J Bacteriol* 183, 951-958.

Brandon LD, Goehring N, Janakiraman A, Yan AW, Wu T, Beckwith J & Goldberg MB (2003). IcsA, a polarly localized autotransporter with an atypical signal peptide, uses the Sec apparatus for secretion, although the Sec apparatus is circumferentially distributed. *Mol Microbiol* 50, 45-60.

Brooks C, Wei Q, Cho SG & Dong Z (2009). Regulation of mitochondrial dynamics in acute kidney injury in cell culture and rodent models. *J Clin Invest* 119, 1275-1285.

Brundage RA, Smith GA, Camilli A, Theriot JA & Portnoy DA (1993). Expression and phosphorylation of the *Listeria monocytogenes* ActA protein in mammalian cells. *Proc Natl Acad Sci U S A* 90, 11890-11894.

Buchrieser C, Glaser P, Rusniok C, Nedjari H, D'Hauteville H, Kunst F, Sansonetti P & Parsot C (2000). The virulence plasmid pWR100 and the repertoire of proteins secreted by the type III secretion apparatus of *Shigella flexneri*. *Mol Microbiol* 38, 760-771.

Burger KNJ, Demel RA, Schmid SL & de Kruijff B (2000). Dynamin is membrane-active: lipid insertion is induced by phosphoinositides and phosphatidic acid. *Biochem* 39, 12485-12493.

Burnaevskiy N, Fox TG, Plymire DA, Ertelt JM, Weigele BA, Selyunin AS, Way SS, Patrie SM & Alto NM (2013). Proteolytic elimination of *N*-myristoyl modifications by the *Shigella* virulence factor IpaJ. *Nature* 496, 106-109.

Burton EA, Oliver TN & Pendergast AM (2005). Abl kinases regulate actin comet tail elongation via an N-WASP-dependent pathway. *Mol Cell Biol* 25, 8834-8843.

Cameron LA, Svitkina TM, Vignjevic D, Theriot JA & Borisy GG (2001). Dendritic organization of actin comet tails. *Curr Biol* 11, 130-135.

Cao H, Garcia F & McNiven MA (1998). Differential distribution of dynamin isoforms in mammalian cells. *Mol Biol Cell* 9, 2595-2609.

Capaldo CT, Farkas AE & Nusrat A (2014). Epithelial adhesive junctions. *F1000 Prime Rep* 6, 1.

Carayol N & Tran Van Nhieu G (2013). Tips and tricks about *Shigella* invasion of epithelial cells. *Curr Opin Microbiol* 16, 32-37.

Carlsson F & Brown EJ (2006). Actin-based motility of intracellular bacteria, and polarized surface distribution of the bacterial effector molecules. *J Cell Physiol* 209, 288-296.

Carneiro LAM, Travassos LH, Soares F & other authors (2009). *Shigella* induces mitochondrial dysfunction and cell death in nonmyleoid cells. *Cell Host & Microbe* 5, 123-136.

Cassidy-Stone A, Chipuk JE, Ingerman E & other authors (2008). Chemical inhibition of the mitochondrial division dynamin reveals its role in Bax/Bak-dependent mitochondrial outer membrane permeabilization. *Dev Cell* 14, 193-204.

Chang PV, Hao L, Offermanns S & Medzhitov R (2014). The microbial metabolite butyrate regulates intestinal macrophage function via histone deacetylase inhibition. *Proc Natl Acad Sci U S A* 111, 2247-2252.

Chang YW, Chang YT, Wang Q, Lin JJ, Chen YJ & Chen CC (2013). Quantitative phosphoproteomic study of pressure-overloaded mouse heart reveals dynamin-related protein 1 as a modulator of cardiac hypertrophy. *Mol Cell Proteomics* 12, 3094-3107.

Chappie JS, Acharya S, Leonard M, Schmid SL & Dyda F (2010). G domain dimerization controls dynamin's assembly-stimulated GTPase activity. *Nature* 465, 435-440.

Chappie JS, Mears JA, Fang S, Leonard M, Schmid SL, Milligan RA, Hinshaw JE & Dyda F (2011). A pseudoatomic model of the dynamin polymer identifies a hydrolysis-dependent powerstroke. *Cell* 147, 209-222.

Charles M, Pérez M, Kobil JH & Goldberg MB (2001). Polar targeting of *Shigella* virulence factor IcsA in Enterobacteriacae and *Vibrio*. *Proc Natl Acad Sci U S A* 98, 9871-9876.

Chen C-L, Hou W-H, Liu I-H, Hsiao G, Huang SS & Huang JS (2009). Inhibitors of clathrin-dependent endocytosis enhance TGFβ signaling and responses. *J Cell Sci* 122, 1863-1871.

Clark CS & Maurelli AT (2007). *Shigella flexneri* inhibits staurosporine-induced apoptosis in epithelial cells. *Infect Immun* 75, 2531-2539.

Conti M, Kawamoto S & Adelstein R (2008). Nonmuscle myosin II. In *Myosins: A Superfamily of Molecular Motors*, pp. 223-264. Edited by L. Coluccio. Dordrecht: Springer.

Conti MA & Adelstein RS (2008). Nonmuscle myosin II moves in new directions. *J Cell Sci* 121, 11-18.

Cossart P & Sansonetti PJ (2004). Bacterial invasion: The paradigms of enteroinvasive pathogens. *Science* 304, 242-248.

Cossart P & Toledo-Arana A (2008). *Listeria monocytogenes*, a unique model in infection biology: an overview. *Microbes Infect* 10, 1041-1050.

Cramer LP & Mitchison TJ (1995). Myosin is involved in postmitotic cell spreading. *J Cell Biol* 131, 179-189.

d'Hauteville H, Dufourcq Lagelouse R, Nato F & Sansonetti P (1996). Lack of cleavage of IcsA in *Shigella flexneri* causes aberrant movement and allows demonstration of a cross-reactive eukaryotic protein. *Infect Immun* 64, 511-517.

Dabiri GA, Sanger JM, Portnoy DA & Southwick FS (1990). *Listeria monocytogenes* moves rapidly through the host-cell cytoplasm by inducing directional actin assembly. *Proc Natl Acad Sci U S A* 87, 6068-6072.

Davis J, Wang J, Tropea JE, Zhang D, Dauter Z, Waugh DS & Wlodawer A (2008). Novel fold of VirA, a type III secretion system effector protein from *Shigella flexneri*. *Protein Sci* 17, 2167-2173.

Degterev A, Hitomi J, Germscheid M & other authors (2008). Identification of RIP1 kinase as a specific cellular target of necrostatins. *Nat Chem Biol* 4, 313-321.

Dodo K, Katoh M, Shimizu T, Takahashi M & Sodeoka M (2005). Inhibition of hydrogen peroxide-induced necrotic cell death with 3-amino-2-indolylmaleimide derivatives. *Bioorg Med Chem Lett* 15, 3114-3118.

Dragoi AM, Talman AM & Agaisse H (2013). Bruton's tyrosine kinase regulates *Shigella flexneri* dissemination in HT-29 intestinal cells. *Infect Immun* 81, 598-607.

Drevets DA & Bronze MS (2008). *Listeria monocytogenes:* epidemiology, human disease, and mechanisms of brain invasion. *FEMS Immunol Med Mic* 53, 151-165.

DuBoff B, Götz J & Feany Mel B (2012). Tau promotes neurodegeneration via DRP1 mislocalization in vivo. *Neuron* 75, 618-632.

DuPont HL, Levine MM, Hornick RB & Formal SB (1989). Inoculum size in shigellosis and implications for expected mode of transmission. *J Infect Dis* 159, 1126-1128.

Egile C, d'Hauteville H, Parsot C & Sansonetti PJ (1997). SopA, the outer membrane protease responsible for polar localization of IcsA in *Shigella flexneri*. *Mol Microbiol* 23, 1063-1073.

Egile C, Loisel TP, Laurent V, Li R, Pantaloni D, Sansonetti PJ & Carlier MF (1999). Activation of the CDC42 effector N-WASP by the *Shigella flexneri* IcsA protein promotes actin nucleation by Arp2/3 complex and bacterial actin-based motility. *J Cell Biol* 146, 1319-1332.

Eliott S, Joss GH, Spudich A & Williams KL (1993). Patterns in *Dictyostelium discoideum*: the role of myosin II in the transition from the unicellular to the multicellular phase. *J Cell Sci* 104, 457-466.

Esue O, Harris ES, Higgs HN & Wirtz D (2008). The filamentous actin cross-linking/bundling activity of mammalian formins. *J Mol Biol* 384, 324-334.

Even-Ram S, Doyle AD, Conti MA, Matsumoto K, Adelstein RS & Yamada KM (2007). Myosin IIA regulates cell motility and actomyosin-microtubule crosstalk. *Nat Cell Biol* 9, 299-309.

Faelber K, Posor Y, Gao S, Held M, Roske Y, Schulze D, Haucke V, Noe F & Daumke O (2011). Crystal structure of nucleotide-free dynamin. *Nature* 477, 556-560.

Faherty CS & Maurelli AT (2009). Spa15 of *Shigella flexneri* is secreted through the type III secretion system and prevents staurosporine-induced apoptosis. *Infect Immun* 77, 5281-5290.

Fasano A, Noriega FR, Liao FM, Wang W & Levine MM (1997). Effect of shigella enterotoxin 1 (ShET1) on rabbit intestine in vitro and in vivo. *Gut* 40, 505-511.

Ferguson KM, Lemmon MA, Schlessinger J & Sigler PB (1994). Crystal structure at 2.2 Å resolution of the pleckstrin homology domain from human dynamin. *Cell* 79, 199-209.

Ferguson SM & De Camilli P (2012). Dynamin, a membrane-remodelling GTPase. *Nat Rev Mol Cell Biol* 13, 75-88.

Fernandez-Prada CM, Hoover DL, Tall BD & Venkatesan MM (1997). Human monocyte-derived macrophages infected with virulent *Shigella flexneri* in vitro undergo a rapid cytolytic event similar to oncosis but not apoptosis. *Infect Immun* 65, 1486-1496.

Ferrari LF, Chum A, Bogen O, Reichling DB & Levine JD (2011). Role of Drp1, a key mitochondrial fission protein, in neuropathic pain. *J Neurosci* 31, 11404-11410.

Fixen KR, Janakiraman A, Garrity S, Slade DJ, Gray AN, Karahan N, Hochschild A & Goldberg MB (2012). Genetic reporter system for positioning of proteins at the bacterial pole. *MBio* 3, e00251-11.

Ford MGJ, Jenni S & Nunnari J (2011). The crystal structure of dynamin. *Nature* 477, 561-566.

Foster RA, Carlin NI, Majcher M, Tabor H, Ng LK & Widmalm G (2011). Structural elucidation of the O-antigen of the *Shigella flexneri* provisional serotype 88-893: structural and serological similarities with *S. flexneri* provisional serotype Y394 (1c). *Carbohydr Res* 346, 872-876.

Francis MS & Thomas CJ (1996). Effect of multiplicity of infection on *Listeria monocytogenes* pathogenicity for HeLa and Caco-2 cell lines. *J Med Microbiol* 45, 323-330.

Frank S, Gaume B, Bergmann-Leitner ES, Leitner WW, Robert EG, Catez F, Smith CL & Youle RJ (2001). The role of dynamin-related protein 1, a mediator of mitochondrial fission, in apoptosis. *Dev Cell* 1, 515-525.

Friedman JR, Lackner LL, West M, DiBenedetto JR, Nunnari J & Voeltz GK (2011). ER tubules mark sites of mitochondrial division. *Science* 334, 358-362.

Fröhlich C, Grabiger S, Schwefel D, Faelber K, Rosenbaum E, Mears J, Rocks O & Daumke O (2013). Structural insights into oligomerization and mitochondrial remodelling of dynamin 1-like protein. *EMBO J* 32, 1280-1292.

Fukuda I, Suzuki T, Munakata H, Hayashi N, Katayama E, Yoshikawa M & Sasakawa C (1995). Cleavage of *Shigella* surface protein VirG occurs at a specific site, but the secretion is not essential for intracellular spreading. *J Bacteriol* 177, 1719-1726.

Fukumatsu M, Ogawa M, Arakawa S, Suzuki M, Nakayama K, Shimizu S, Kim M, Mimuro H & Sasakawa C (2012). *Shigella* targets epithelial tricellular junctions and uses a noncanonical clathrin-dependent endocytic pathway to spread between cells. *Cell Host Microbe* 11, 325-336.

Galluzzi L, Vitale I, Abrams JM & other authors (2012). Molecular definitions of cell death subroutines: recommendations of the Nomenclature Committee on Cell Death 2012. *Cell Death Differ* 19, 107-120.

Gao D, Zhang L, Dhillon R, Hong T-T, Shaw RM & Zhu J (2013). Dynasore protects mitochondria and improves cardiac lusitropy in langendorff perfused mouse heart. *PLoS One* 8, e60967.

Germane KL, Ohi R, Goldberg MB & Spiller BW (2008). Structural and functional studies indicate that *Shigella* VirA is not a protease and does not directly destabilize microtubules. *Biochemistry* 47, 10241-10243.

Girardin SE, Boneca IG, Carneiro LAM & other authors (2003). Nod1 detects a unique muropeptide from Gram-negative bacterial peptidoglycan. *Science* 300, 1584-1587.

Givvimani S, Munjal C, Tyagi N, Sen U, Metreveli N & Tyagi SC (2012). Mitochondrial division/mitophagy inhibitor (Mdivi) ameliorates pressure overload induced heart failure. *PLoS One* 7, e32388.

Goldberg MB, Barzu O, Parsot C & Sansonetti PJ (1993). Unipolar localization and ATPase activity of IcsA, a *Shigella flexneri* protein involved in intracellular movement. *J Bacteriol* 175, 2189-2196.

Goldberg MB (1994). Cleavage of the *Shigella* surface protein IcsA (VirG): intention or accident? *Trends Microbiol* 2, 35-36.

Goldberg MB & Theriot JA (1995). *Shigella flexneri* surface protein IcsA is sufficient to direct actin-based motility. *Proc Natl Acad Sci U S A* 92, 6572-6576.

Goldberg MB (2001). Actin-based motility of intracellular microbial pathogens. *Microbiol Mol Biol Rev* 65, 595-626.

Goley ED & Welch MD (2006). The ARP2/3 complex: an actin nucleator comes of age. *Nat Rev Mol Cell Biol* 7, 713-726.

Golstein P & Kroemer G (2007). Cell death by necrosis: towards a molecular definition. *Trends Biochem Sci* 32, 37-43.

Gouin E, Gantelet H, Egile C, Lasa I, Ohayon H, Villiers V, Gounon P, Sansonetti PJ & Cossart P (1999). A comparative study of the actin-based motilities of the pathogenic bacteria *Listeria monocytogenes*, *Shigella flexneri* and *Rickettsia conorii*. *J Cell Sci* 112, 1697-1708.

Gouin E, Welch MD & Cossart P (2005). Actin-based motility of intracellular pathogens. *Curr Opin Microbiol* 8, 35-45.

Grabowicz M (2010). Biogenesis of *Shigella flexneri* IcsA protein: *PhD dissertation, University of Adelaide, Australia*.

Gray AN, Li Z, Henderson-Frost J & Goldberg MB (2014). Biogenesis of YidC cytoplasmic membrane substrates is required for positioning of autotransporter IcsA at future poles. *J Bacteriol* 196, 624-632.

Haglund CM & Welch MD (2011). Pathogens and polymers: Microbe-host interactions illuminate the cytoskeleton. *J Cell Biol* 195, 7-17.

Hänisch J, Kölm R, Wozniczka M, Bumann D, Rottner K & Stradal TEB (2011). Activation of a RhoA/Myosin II-dependent but Arp2/3 complex-independent pathway facilitates *Salmonella* invasion. *Cell Host & Microbe* 9, 273-285.

Harper CB, Martin S, Nguyen TH & other authors (2011). Dynamin Inhibition blocks botulinum neurotoxin type A endocytosis in neurons and delays botulism. *J Biol Chem* 286, 35966-35976.

Hartsock A & Nelson WJ (2008). Adherens and tight junctions: Structure, function and connections to the actin cytoskeleton. *BBA-Biomembranes* 1778, 660-669.

Hase K, Eckmann L, Leopard JD, Varki N & Kagnoff MF (2002). Cell differentiation is a key determinant of cathelicidin LL-37/human cationic antimicrobial protein 18 expression by human colon epithelium. *Infect Immun* 70, 953-063.

Heindl JE, Saran I, Yi C-r, Lesser CF & Goldberg MB (2009). Requirement for formin-induced actin polymerization during spread of *Shigella*. *Infect Immun* 78, 193-203.

Heissler SM & Manstein DJ (2013). Nonmuscle myosin-2: mix and match. *Cell Mol Life Sci* 70, 1-21.

High N, Mounier J, Prévost MC & Sansonetti PJ (1992). IpaB of *Shigella flexneri* causes entry into epithelial cells and escape from the phagocytic vacuole. *EMBO J* 11, 1991-1999.

Hilbi H, Moss JE, Hersh D & other authors (1998). *Shigella*-induced Apoptosis Is Dependent on Caspase-1 Which Binds to IpaB. *J Biol Chem* 273, 32895-32900.

Hong M & Payne SM (1997). Effect of mutations in *Shigella flexneri* chromosomal and plasmid-encoded lipopolysaccharide genes on invasion and serum resistance. *Mol Microbiol* 24, 779-791.

Ingersoll M, Groisman EA & Zychlinsky A (2002). Pathogenicity islands of *Shigella*. *Curr Top Microbiol Immunol* 264, 49-65.

Ito H, Kido N, Arakawa Y, Ohta M, Sugiyama T & Kato N (1991). Possible mechanisms underlying the slow lactose fermentation phenotype in *Shigella* spp. *Appl Environ Microbiol* 57, 2912-2917.

Jain P, Luo Z-Q & Blanke SR (2011). *Helicobacter pylori* vacuolating cytotoxin A (VacA) engages the mitochondrial fission machinery to induce host cell death. *Proc Natl Acad Sci U S A* 108, 16032-16037.

Jain S & Goldberg MB (2007). Requirement for YaeT in the outer membrane assembly of autotransporter proteins. *J Bacteriol* 189, 5393-5398.

Jennison AV & Verma NK (2004). *Shigella flexneri* infection: pathogenesis and vaccine development. *FEMS Microbiol Rev* 28, 43-58.

Jeong KI, Zhang Q, Nunnari J & Tzipori S (2010). A piglet model of acute gastroenteritis induced by *Shigella dysenteriae* Type 1. *J Infect Dis* 201, 903-911.

Jin Q, Yuan Z, Xu J & other authors (2002). Genome sequence of *Shigella flexneri* 2a: insights into pathogenicity through comparison with genomes of *Escherichia coli* K12 and O157. *Nucleic Acids Res* 30, 4432-4441.

Kadurugamuwa JL, Rohde M, Wehland J & Timmis KN (1991). Intercellular spread of *Shigella flexneri* through a monolayer mediated by membranous protrusions and associated with reorganization of the cytoskeletal protein vinculin. *Infect Immun* 59, 3463-3471.

Kamio Y & Nikaido H (1976). Outer membrane of *Salmonella typhimurium* - Accessibility of phospholipid head groups to phospholipase c and cyanogen-bromide activated dextran in external medium. *Biochemistry* 15, 2561-2570.

Kelley CA, Sellers JR, Gard DL, Bui D, Adelstein RS & Baines IC (1996). *Xenopus* nonmuscle myosin heavy chain isoforms have different subcellular localizations and enzymatic activities. *J Cell Biol* 134, 675-687.

Kessels MM, Engqvist-Goldstein AEY, Drubin DG & Qualmann B (2001). Mammalian Abp1, a signal-responsive F-actin-binding protein, links the actin cytoskeleton to endocytosis via the GTPase dynamin. *J Cell Biol* 153, 351-366.

Khalid S, Bond PJ, Carpenter T & Sansom MS (2008). OmpA: gating and dynamics via molecular dynamics simulations. *BBA* 1778, 1871-1880.

Kim DW, Lenzen G, Page AL, Legrain P, Sansonetti PJ & Parsot C (2005). The *Shigella flexneri* effector OspG interferes with innate immune responses by targeting ubiquitin-conjugating enzymes. *Proc Natl Acad Sci U S A* 102, 14046-14051.

Kim HJ, Koo SY, Ahn BH & other authors (2010). NecroX as a novel class of mitochondrial reactive oxygen species and $ONOO^-$ scavenger. *Arch Pharm Res* 33, 1813-1823.

Kobayashi T, Ogawa M, Sanada T & other authors (2013). The *Shigella* OspC3 effector inhibits Caspase-4, antagonizes inflammatory cell death, and promotes epithelial infection. *Cell Host & Microbe* 13, 570-583.

Kocks C, Gouin E, Tabouret M, Berche P, Ohayon H & Cossart P (1992). *L. monocytogenes*-induced actin assembly requires the *actA* gene product, a surface protein. *Cell* 68, 521-531.

Kocks C, Marchand JB, Gouin E, d'Hauteville H, Sansonetti PJ, Carlier MF & Cossart P (1995). The unrelated surface proteins ActA of *Listeria monocytogenes* and IcsA of *Shigella flexneri* are sufficient to confer actin-based motility on *Listeria innocua* and *Escherichia coli* respectively. *Mol Microbiol* 18, 413-423.

Kolega J (1998). Cytoplasmic dynamics of myosin IIA and IIB: spatial 'sorting' of isoforms in locomoting cells. *J Cell Sci* 111, 2085-2095.

Korobova F, Ramabhadran V & Higgs HN (2013). An actin-dependent step in mitochondrial fission mediated by the ER-associated formin INF2. *Science* 339, 464-467.

Korobova F, Gauvin TJ & Higgs HN (2014). A role for myosin II in mammalian mitochondrial fission. *Curr Biol* 24, 409-414.

Koterski JF, Nahvi M, Venkatesan MM & Haimovich B (2005). Virulent *Shigella flexneri* causes damage to mitochondria and triggers necrosis in infected human monocyte-derived macrophages. *Infect Immun* 73, 504-513.

Kotloff KL, Noriega F, Losonsky GA, Sztein MB, Wasserman SS, Nataro JP & Levine MM (1996). Safety, immunogenicity, and transmissibility in humans of CVD 1203, a live oral *Shigella flexneri* 2a vaccine candidate attenuated by deletions in *aroA* and *virG*. *Infect Immun* 64, 4542-4548.

Kotloff KL, Taylor DN, Sztein MB & other authors (2002). Phase I evaluation of Δ*virG Shigella sonnei* live, attenuated, oral vaccine strain WRSS1 in healthy adults. *Infect Immun* 70, 2016-2021.

Kovacs M, Toth J, Hetenyi C, Malnasi-Csizmadia A & Sellers JR (2004). Mechanism of blebbistatin inhibition of myosin II. *J Biol Chem* 279, 35557-35563.

Krendel M & Mooseker MS (2005). Myosins: Tails (and heads) of functional diversity. *Physiol* 20, 239-251.

Krishnan S & Prasadarao NV (2012). Outer membrane protein A and OprF: versatile roles in Gram-negative bacterial infections. *FEBS J* 279, 919-931.

Kwon CH, Wheeldon I, Kachouie NN, Lee SH, Bae H, Sant S, Fukuda J, Kang JW & Khademhosseini A (2011). Drug-eluting microarrays for cell-based screening of chemical-induced apoptosis. *Anal Chem* 83, 4118-4125.

Lacayo CI & Theriot JA (2004). *Listeria monocytogenes* actin-based motility varies depending on subcellular location: a kinematic probe for cytoarchitecture. *Mol Biol Cell* 15, 2164-2175.

Lagendijk EL, Validov S, Lamers GEM, De Weert S & Bloemberg GV (2010). Genetic tools for tagging Gram-negative bacteria with mCherry for visualization *in vitro* and in natural habitats, biofilm and pathogenicity studies. *FEMS Microbiol Lett* 305, 81-90.

Lamkanfi M & Dixit VM (2010). Manipulation of host cell death pathways during microbial infections. *Cell Host & Microbe* 8, 44-54.

Lan R & Reeves PR (2002). *Escherichia coli* in disguise: molecular origins of *Shigella*. *Microbes Infect* 4, 1125-1132.

Lasa I, Gouin E, Goethals M, Vancompernolle K, David V, Vandekerckhove J & Cossart P (1997). Identification of two regions in the N-terminal domain of ActA involved in the actin comet tail formation by *Listeria monocytogenes*. *EMBO J* 16, 1531-1540.

Lee E & De Camilli P (2002). Dynamin at actin tails. *Proc Natl Acad Sci U S A* 99, 161-166.

Legros F, Lombès A, Frachon P & Rojo M (2002). Mitochondrial fusion in human cells is efficient, requires the inner membrane potential, and is mediated by mitofusins. *Mol Biol Cell* 13, 4343-4354.

Lembo-Fazio L, Nigro G, Noel G, Rossi G, Chiara F, Tsilingiri K, Rescigno M, Rasola A & Bernardini ML (2011). Gadd45α activity is the principal effector of *Shigella* mitochondria-dependent epithelial cell death *in vitro* and *ex vivo*. *Cell Death & Dis* 2, e122.

Lett MC, Sasakawa C, Okada N, Sakai T, Makino S, Yamada M, Komatsu K & Yoshikawa M (1989). *virG,* a plasmid-coded virulence gene of *Shigella flexneri*: identification of the *virG* protein and determination of the complete coding sequence. *J Bacteriol* 171, 353-359.

Leung Y, Ally S & Goldberg MB (2008). Bacterial Actin Assembly Requires Toca-1 to Relieve N-WASP Autoinhibition. *Cell Host & Microbe* 3, 39-47.

Levine MM, Kotloff KL, Barry EM, Pasetti MF & Sztein MB (2007). Clinical trials of *Shigella* vaccines: two steps forward and one step back on a long, hard road. *Nat Rev Microbiol* 5, 540-553.

Liu KC, Jacobs DT, Dunn BD, Fanning AS & Cheney RE (2012). Myosin-X functions in polarized epithelial cells. *Mol Biol Cell* 23, 1675-1687.

Loisel TP, Boujemaa R, Pantaloni D & Carlier MF (1999). Reconstitution of actin-based motility of *Listeria* and *Shigella* using pure proteins. *Nature* 401, 613-616.

Lommel S, Benesch S, Rottner K, Franz T, Wehland J & Kühn R (2001). Actin pedestal formation by enteropathogenic *Escherichia coli* and intracellular motility of *Shigella flexneri* are abolished in N-WASP-defective cells. *EMBO reports* 2, 850-857.

Low HH & Löwe J (2010). Dynamin architecture — from monomer to polymer. *Curr Opin Struct Biol* 20, 791-798.

Lu H, Murata-Kamiya N, Saito Y & Hatakeyama M (2009). Role of partitioning-defective 1/microtubule affinity-regulating kinases in the morphogenetic activity of *Helicobacter pylori* CagA. *J Biol Chem* 284, 23024-23036.

Lum M, Attridge SR & Morona R (2013). Impact of dynasore an inhibitor of dynamin II on *Shigella flexneri* infection. *PLoS One* 8, e84975.

Lutter EI, Barger AC, Nair V & Hackstadt T (2013). *Chlamydia trachomatis* inclusion membrane protein CT228 recruits elements of the myosin phosphatase pathway to regulate release mechanisms. *Cell Reports* 3, 1921-1931.

Macia E, Ehrlich M, Massol R, Boucrot E, Brunner C & Kirchhausen T (2006). Dynasore, a cell-permeable inhibitor of dynamin. *Dev Cell* 10, 839-850.

Makino S, Sasakawa C, Kamata K, Kurata T & Yoshikawa M (1986). A genetic determinant required for continuous reinfection of adjacent cells on large plasmid in *S. flexneri* 2a. *Cell* 46, 551-555.

Malinverni JC & Silhavy TJ (2009). An ABC transport system that maintains lipid asymmetry in the Gram-negative outer membrane. *Proc Natl Acad Sci U S A* 106, 8009-8014.

Man AL, Prieto-Garcia ME & Nicoletti C (2004). Improving M cell mediated transport across mucosal barriers: do certain bacteria hold the keys? *Immunology* 113, 15-22.

Mantis N, Prévost MC & Sansonetti P (1996). Analysis of epithelial cell stress response during infection by *Shigella flexneri*. *Infect Immun* 64, 2474-2482.

Marsboom G, Toth PT, Ryan JJ & other authors (2012). Dynamin-related protein 1-mediated mitochondrial mitotic fission permits hyperproliferation of vascular smooth muscle cells and offers a novel therapeutic target in pulmonary hypertension. *Circ Res* 110, 1484-1497.

Maupin P, Phillips CL, Adelstein RS & Pollard TD (1994). Differential localization of myosin-II isozymes in human cultured cells and blood cells. *J Cell Sci* 107, 3077-3090.

May KL & Morona R (2008). Mutagenesis of the *Shigella flexneri* autotransporter IcsA reveals novel functional regions involved in IcsA biogenesis and recruitment of host neural Wiscott-Aldrich syndrome protein. *J Bacteriol* 190, 4666-4676.

McCluskey A, Daniel JA, Hadzic G & other authors (2013). Building a better dynasore: The dyngo compounds potently inhibit dynamin and endocytosis. *Traffic* 14, 1272-1289.

McMahon HT & Boucrot E (2011). Molecular mechanism and physiological functions of clathrin-mediated endocytosis. *Nat Rev Mol Cell Biol* 12, 517-533.

McNiven MA, Kim L, Krueger EW, Orth JD, Cao H & Wong TW (2000). Regulated interactions between dynamin and the actin-binding protein cortactin modulate cell shape. *J Cell Biol* 151, 187-198.

Miki H, Miura K & Takenawa T (1996). N-WASP, a novel actin-depolymerizing protein, regulates the cortical cytoskeletal rearrangement in a PIP2-dependent manner downstream of tyrosine kinases. *EMBO J* 15, 5326-5335.

Miki H & Takenawa T (2003). Regulation of actin dynamics by WASP family proteins. *J Biochem* 134, 309-313.

Mimuro H, Suzuki T, Suetsugu S, Miki H, Takenawa T & Sasakawa C (2000). Profilin is required for sustaining efficient intra- and intercellular spreading of *Shigella flexneri*. *J Biol Chem* 275, 28893-28901.

Miyoshi J & Takai Y (2005). Molecular perspective on tight-junction assembly and epithelial polarity. *Adv Drug Deliv Rev* 57, 815-855.

Moreau V, Frischknecht F, Reckmann I, Vincentelli R, Rabut G, Stewart D & Way M (2000). A complex of N-WASP and WIP integrates signalling cascades that lead to actin polymerization. *Nat Cell Biol* 2, 441-448.

Morona R, Van Den Bosch L & Manning PA (1995). Molecular, genetic, and topological characterization of O-antigen chain length regulation in *Shigella flexneri*. *J Bacteriol* 177, 1059-1068.

Morona R, Daniels C & Van Den Bosch L (2003). Genetic modulation of *Shigella flexneri* 2a lipopolysaccharide O antigen modal chain length reveals that it has been optimized for virulence. *Microbiol* 149, 925-939.

Morona R & Van Den Bosch L (2003). Lipopolysaccharide O antigen chains mask IcsA (VirG) in *Shigella flexneri*. *FEMS Microbiol Lett* 221, 173-180.

Morona R, Purins L, Tocilj A, Matte A & Cygler M (2009). Sequence-structure relationships in polysaccharide co-polymerase (PCP) proteins. *Trends Biochem Sci* 34, 78-84.

Mostowy S, Bonazzi M, Hamon MA & other authors (2010). Entrapment of intracytosolic bacteria by septin cage-like structures. *Cell Host & Microbe* 8, 433-444.

Muhlberg AB, Warnock DE & Schmid SL (1997). Domain structure and intramolecular regulation of dynamin GTPase. *EMBO J* 16, 6676-6683.

Muhlradt PF & Golecki JR (1975). Asymmetrical distribution and artifactual reorientation of lipopolysaccharide in the outer membrane bilayer of *Salmonella typhimurium*. *Eur J Biochem* 51, 343-352.

Mullins RD, Heuser JA & Pollard TD (1998). The interaction of Arp2/3 complex with actin: Nucleation, high affinity pointed end capping, and formation of branching networks of filaments. *Proc Natl Acad Sci U S A* 95, 6181-6186.

Murayama SY, Sakai T, Makino S, Kurata T, Sasakawa C & Yoshikawa M (1986). The use of mice in the Sereny test as a virulence assay of Shigellae and enteroinvasive *Escherichia coli*. *Infect Immun* 51, 696-698.

Nakanishi S, Kakita S, Takahashi I & other authors (1992). Wortmannin, a microbial product inhibitor of myosin light chain kinase. *J Biol Chem* 267, 2157-2163.

Nataro JP, Seriwatana J, Fasano A, Maneval DR, Guers LD, Noriega F, Dubovsky F, Levine MM & Morris JG, Jr. (1995). Identification and cloning of a novel plasmid-encoded enterotoxin of enteroinvasive *Escherichia coli* and *Shigella* strains. *Infect Immun* 63, 4721-4728.

Nicholson-Dykstra S, Higgs HN & Harris ES (2005). Actin dynamics: growth from dendritic branches. *Curr Biol* 15, R346-R357.

Nicolier M, Decrion-Barthod A-Z, Launay S, Prétet J-L & Mougin C (2009). Spatiotemporal activation of caspase-dependent and -independent pathways in staurosporine-induced apoptosis of p53wt and p53mt human cervical carcinoma cells. *Biol Cell* 101, 455-467.

Nikaido H (2003). Molecular basis of bacterial outer membrane permeability revisited. *Microbiol Mol Biol Rev* 67, 593-656.

Niyogi SK (2005). Shigellosis. *J Microbiol* 43, 133-143.

Nonaka T, Kuwae A, Sasakawa C & Imajoh-Ohmi S (1999). *Shigella flexneri* YSH6000 induces two types of cell death, apoptosis and oncosis, in the differentiated human monoblastic cell line U937. *FEMS Microbiol Lett* 174, 89-95.

Oaks EV, Wingfield ME & Formal SB (1985). Plaque formation by virulent *Shigella flexneri*. *Infect Immun* 48, 124-129.

Odendall C, Rolhion N, Förster A, Poh J, Lamont Douglas J, Liu M, Freemont Paul S, Catling Andrew D & Holden David W (2012). The *Salmonella* Kinase SteC targets the MAP kinase MEK to regulate the host actin cytoskeleton. *Cell Host & Microbe* 12, 657-668.

Ogawa H, Nakamura A & Nakaya R (1968). Cinemicrographic study of tissue cell cultures infected with *Shigella flexneri*. *Jpn J Med Sci Biol* 21, 259-273.

Okada N, Sasakawa C, Tobe T, Yamada M, Nagai S, Talukder KA, Komatsu K, Kanegasaki S & Yoshikawa M (1991). Virulence-associated chromosomal loci of *Shigella flexneri* identified by random Tn*5* insertion mutagenesis. *Mol Microbiol* 5, 187-195.

Okamura N, Nagai T, Nakaya R, Kondo S, Murakami M & Hisatsune K (1983). HeLa cell invasiveness and O antigen of *Shigella flexneri* as separate and prerequisite attributes of virulence to evoke keratoconjunctivitis in guinea pigs. *Infect Immun* 39, 505-513.

Okuda J, Toyotome T, Kataoka N, Ohno M, Abe H, Shimura Y, Seyedarabi A, Pickersgill R & Sasakawa C (2005). *Shigella* effector IpaH9.8 binds to a splicing factor U2AF(35) to modulate host immune responses. *Biochem Biophys Res Commun* 333, 531-539.

Olichon A, Baricault L, Gas N, Guillou E, Valette A, Belenguer P & Lenaers G (2003). Loss of OPA1 perturbates the mitochondrial inner membrane structure and integrity, leading to cytochrome c release and apoptosis. *J Biol Chem* 278, 7743-7746.

Ong SB, Subrayan S, Lim SY, Yellon DM, Davidson SM & Hausenloy DJ (2010). Inhibiting mitochondrial fission protects the heart against ischemia/reperfusion injury. *Circulation* 121, 2012-2022.

Oshima A (2014). Structure and closure of connexin gap junction channels. *FEBS Lett* 588, 1230-1237.

Ostap EM (2002). 2,3-Butanedione monoxime (BDM) as a myosin inhibitor. *J Muscle Res Cell Motil* 23, 305-308.

Otera H, Wang C, Cleland MM, Setoguchi K, Yokota S, Youle RJ & Mihara K (2010). Mff is an essential factor for mitochondrial recruitment of Drp1 during mitochondrial fission in mammalian cells. *J Cell Biol* 191, 1141-1158.

Otera H, Ishihara N & Mihara K (2013). New insights into the function and regulation of mitochondrial fission. *BBA-Mol Cell Res* 1833, 1256-1268.

Paciello I, Silipo A, Lembo-Fazio L & other authors (2013). Intracellular *Shigella* remodels its LPS to dampen the innate immune recognition and evade inflammasome activation. *Proc Natl Acad Sci U S A* 110, E4345-4354.

Pantaloni D & Carlier MF (1993). How profilin promotes actin filament assembly in the presence of thymosin β4. *Cell* 75, 1007-1014.

Pantaloni D, Clainche CL & Carlier M-F (2001). Mechanism of actin-based motility. *Science* 292, 1502-1506.

Park SW, Kim KY, Lindsey JD, Dai Y, Heo H, Nguyen DH, Ellisman MH, Weinreb RN & Ju WK (2011). A selective inhibitor of drp1, mdivi-1, increases retinal ganglion cell survival in acute ischemic mouse retina. *Invest Ophthalmol Vis Sci* 52, 2837-2843.

Pasternak C, Spudich JA & Elson EL (1989). Capping of surface receptors and concomitant cortical tension are generated by conventional myosin. *Nature* 341, 549-551.

Pedron T, Thibault C & Sansonetti PJ (2003). The invasive phenotype of *Shigella flexneri* directs a distinct gene expression pattern in the human intestinal epithelial cell line Caco-2. *J Biol Chem* 278, 33878-33886.

Perdomo JJ, Gounon P & Sansonetti PJ (1994). Polymorphonuclear leukocyte transmigration promotes invasion of colonic epithelial monolayer by *Shigella flexneri*. *J Clin Invest* 93, 633-643.

Philpott DJ, Yamaoka S, Israel A & Sansonetti PJ (2000). Invasive *Shigella flexneri* activates NF-κB through a lipopolysaccharide-dependent innate intracellular response and leads to IL-8 expression in epithelial cells. *J Immunol* 165, 903-914.

Picking WL, Nishioka H, Hearn PD, Baxter MA, Harrington AT, Blocker A & Picking WD (2005). IpaD of *Shigella flexneri* is independently required for regulation of Ipa protein secretion and efficient insertion of IpaB and IpaC into host membranes. *Infect Immun* 73, 1432-1440.

Pore D, Chowdhury P, Mahata N, Pal A, Yamasaki S, Mahalanabis D & Chakrabarti MK (2009). Purification and characterization of an immunogenic outer membrane protein of *Shigella flexneri* 2a. *Vaccine* 27, 5855-5864.

Pore D, Mahata N, Pal A & Chakrabarti MK (2011). Outer membrane protein A (OmpA) of *Shigella flexneri* 2a, induces protective immune response in a mouse model. *PLoS One* 6, e22663.

Pore D, Mahata N & Chakrabarti MK (2012). Outer membrane protein A (OmpA) of *Shigella flexneri* 2a links innate and adaptive immunity in a TLR2-dependent manner and involvement of IL-12 and nitric oxide. *J Biol Chem* 287, 12589-12601.

Pore D & Chakrabarti MK (2013). Outer membrane protein A (OmpA) from *Shigella flexneri* 2a: A promising subunit vaccine candidate. *Vaccine* 31, 3644-3650.

Posselt G, Backert S & Wessler S (2013). The functional interplay of *Helicobacter pylori* factors with gastric epithelial cells induces a multi-step process in pathogenesis. *Cell Commun Signal* 11, 77.

Prévost MC, Lesourd M, Arpin M, Vernel F, Mounier J, Hellio R & Sansonetti PJ (1992). Unipolar reorganization of F-actin layer at bacterial division and bundling of actin filaments by plastin correlate with movement of *Shigella flexneri* within HeLa cells. *Infect Immun* 60, 4088-4099.

Prunier A-L, Schuch R, Fernández RE, Mumy KL, Kohler H, McCormick BA & Maurelli AT (2007). *nadA* and *nadB* of *Shigella flexneri* 5a are antivirulence loci responsible for the synthesis of quinolinate, a small molecule inhibitor of *Shigella* pathogenicity. *Microbiology* 153, 2363-2372.

Pupo GM, Lan R & Reeves PR (2000). Multiple independent origins of *Shigella* clones of *Escherichia coli* and convergent evolution of many of their characteristics. *Proc Natl Acad Sci U S A* 97, 10567-10572.

Qiu X, Cao L, Yang X, Zhao X, Liu X, Han Y, Xue Y, Jiang H & Chi Z (2013). Role of mitochondrial fission in neuronal injury in pilocarpine-induced epileptic rats. *Neuroscience* 245, 157-165.

Qualmann B & Kelly RB (2000). Syndapin isoforms participate in receptor-mediated endocytosis and actin organization. *J Cell Biol* 148, 1047-1062.

Qualmann B & Kessels MM (2002). Endocytosis and the cytoskeleton. *Int Rev Cytol* 220, 93-144.

Rabbani GH, Albert MJ, Rahman H, Islam M, Mahalanabis D, Kabir I, Alam K & Ansaruzzaman M (1995). Development of an improved animal model of shigellosis in the adult rabbit by colonic infection with *Shigella flexneri* 2a. *Infect Immun* 63, 4350-4357.

Rabbani GH, Teka T, Zaman B, Majid N, Khatun M & Fuchs GJ (2001). Clinical studies in persistent diarrhea: dietary management with green banana or pectin in Bangladeshi children. *Gastroenterology* 121, 554-560.

Rabbani GH, Teka T, Saha SK, Zaman B, Majid N, Khatun M, Wahed MA & Fuchs GJ (2004). Green banana and pectin improve small intestinal permeability and reduce fluid loss in Bangladeshi children with persistent diarrhea. *Dig Dis Sci* 49, 475-484.

Rabbani GH, Ahmed S, Hossain I, Islam R, Marni F, Akhtar M & Majid N (2009). Green banana reduces clinical severity of childhood shigellosis: a double-blind, randomized, controlled clinical trial. *Pediatr Infect Dis J* 28, 420-425.

Rafelski SM & Theriot JA (2006). Mechanism of polarization of *Listeria monocytogenes* surface protein ActA. *Mol Microbiol* 59, 1262-1279.

Rajabian T, Gavicherla B, Heisig M, Muller-Altrock S, Goebel W, Gray-Owen SD & Ireton K (2009). The bacterial virulence factor InlC perturbs apical cell junctions and promotes cell-to-cell spread of *Listeria*. *Nat Cell Biol* 11, 1212-1218.

Rajakumar K, Jost BH, Sasakawa C, Okada N, Yoshikawa M & Adler B (1994). Nucleotide sequence of the rhamnose biosynthetic operon of *Shigella flexneri* 2a and role of lipopolysaccharide in virulence. *J Bacteriol* 176, 2362-2373.

Ramamurthy B, Yengo CM, Straight AF, Mitchison TJ & Sweeney HL (2004). Kinetic mechanism of blebbistatin inhibition of nonmuscle myosin IIb. *Biochemistry* 43, 14832-14839.

Ranallo RT, Fonseka S, Boren TL, Bedford LA, Kaminski RW, Thakkar S & Venkatesan MM (2012). Two live attenuated *Shigella flexneri* 2a strains WRSf2G12 and WRSf2G15: A new combination of gene deletions for 2nd generation live attenuated vaccine candidates. *Vaccine* 30, 5159-5171.

Ranieri M, Brajkovic S, Riboldi G, Ronchi D, Rizzo F, Bresolin N, Corti S & Comi GP (2013). Mitochondrial fusion proteins and human diseases. *Neurol Res Int* 2013, 293893.

Raqib R, Sarker P, Bergman P & other authors (2006). Improved outcome in shigellosis associated with butyrate induction of an endogenous peptide antibiotic. *Proc Natl Acad Sci U S A* 103, 9178-9183.

Rathman M, de Lanerolle P, Ohayon H, Gounon P & Sansonetti P (2000a). Myosin light chain kinase plays an essential role in *S. flexneri* dissemination. *J Cell Sci* 113, 3375-3386.

Rathman M, Jouirhi N, Allaoui A, Sansonetti P, Parsot C & Tran Van Nhieu G (2000b). The development of a FACS-based strategy for the isolation of *Shigella flexneri* mutants that are deficient in intercellular spread. *Mol Microbiol* 35, 974-990.

Reed JC (2000). Mechanisms of apoptosis. *Am J Pathol* 157, 1415-1430.

Rehman J, Zhang HJ, Toth PT & other authors (2012). Inhibition of mitochondrial fission prevents cell cycle progression in lung cancer. *FASEB J* 26, 2175-2186.

Robbins JR, Monack D, McCallum SJ, Vegas A, Pham E, Goldberg MB & Theriot JA (2001). The making of a gradient: IcsA (VirG) polarity in *Shigella flexneri*. *Mol Microbiol* 41, 861-872.

Robinson RC, Turbedsky K, Kaiser DA, Marchand J-B, Higgs HN, Choe S & Pollard TD (2001). Crystal structure of Arp2/3 complex. *Science* 294, 1679-1684.

Rohatgi R, Ma L, Miki H, Lopez M, Kirchhausen T, Takenawa T & Kirschner MW (1999). The interaction between N-WASP and the Arp2/3 complex links Cdc42-dependent signals to actin assembly. *Cell* 97, 221-231.

Saitoh M, Ishikawa T, Matsushima S, Naka M & Hidaka H (1987). Selective inhibition of catalytic activity of smooth muscle myosin light chain kinase. *J Biol Chem* 262, 7796-7801.

Sakaguchi T, Köhler H, Gu X, McCormick BA & Reinecker H-C (2002). *Shigella flexneri* regulates tight junction-associated proteins in human intestinal epithelial cells. *Cell Microbiol* 4, 367-381.

Sanada T, Kim M, Mimuro H & other authors (2012). The *Shigella flexneri* effector OspI deamidates UBC13 to dampen the inflammatory response. *Nature* 483, 623-626.

Sandlin RC, Lampel KA, Keasler SP, Goldberg MB, Stolzer AL & Maurelli AT (1995). Avirulence of rough mutants of *Shigella flexneri*: requirement of O antigen for correct unipolar localization of IcsA in the bacterial outer membrane. *Infect Immun* 63, 229-237.

Sandlin RC, Goldberg MB & Maurelli AT (1996). Effect of O side-chain length and composition on the virulence of *Shigella flexneri* 2a. *Mol Microbiol* 22, 63-73.

Sansonetti PJ, Ryter A, Clerc P, Maurelli AT & Mounier J (1986). Multiplication of *Shigella flexneri* within HeLa cells: lysis of the phagocytic vacuole and plasmid-mediated contact hemolysis. *Infect Immun* 51, 461-469.

Sansonetti PJ, Arondel J, Fontaine A, d'Hauteville H & Bernardini ML (1991). *Omp*B (osmo-regulation) and *ics*A (cell-to-cell spread) mutants of *Shigella flexneri*: vaccine candidates and probes to study the pathogenesis of shigellosis. *Vaccine* 9, 416-422.

Sansonetti PJ, Mounier J, Prévost MC & Mege RM (1994). Cadherin expression is required for the spread of *Shigella flexneri* between epithelial cells. *Cell* 76, 829-839.

Sansonetti PJ, Arondel J, Cantey JR, Prévost MC & Huerre M (1996). Infection of rabbit Peyer's patches by *Shigella flexneri*: effect of adhesive or invasive bacterial phenotypes on follicle-associated epithelium. *Infect Immun* 64, 2752-2764.

Sansonetti PJ, Arondel J, Huerre M, Harada A & Matsushima K (1999). Interleukin-8 controls bacterial transepithelial translocation at the cost of epithelial destruction in experimental shigellosis. *Infect Immun* 67, 1471-1480.

Sansonetti PJ, Phalipon A, Arondel J, Thirumalai K, Banerjee S, Akira S, Takeda K & Zychlinsky A (2000). Caspase-1 activation of IL-1β and IL-18 are essential for *Shigella flexneri*-induced inflammation. *Immunity* 12, 581-590.

Santapaola D, Del Chierico F, Petrucca A, Uzzau S, Casalino M, Colonna B, Sessa R, Berlutti F & Nicoletti M (2006). Apyrase, the product of the virulence plasmid-encoded *phoN2* (*apy*) gene of *Shigella flexneri*, is necessary for proper unipolar IcsA localization and for efficient intercellular spread. *J Bacteriol* 188, 1620-1627.

Schroeder GN & Hilbi H (2008). Molecular pathogenesis of *Shigella* spp.: Controlling host cell signaling, invasion, and death by type III secretion. *Clin Microbiol Rev* 21, 134-156.

Schuch R, Sandlin RC & Maurelli AT (1999). A system for identifying post-invasion functions of invasion genes: requirements for the Mxi-Spa type III secretion pathway of *Shigella flexneri* in intercellular dissemination. *Mol Microbiol* 34, 675-689.

Scribano D, Petrucca A, Pompili M & other authors (2014). Polar Localization of PhoN2, a Periplasmic Virulence-Associated Factor of *Shigella flexneri*, Is Required for Proper IcsA Exposition at the Old Bacterial Pole. *PLoS One* 9, e90230.

Segain J-P, de la Blétière DR, Bourreille A & other authors (2000). Butyrate inhibits inflammatory responses through NF-κB inhibition: implications for Crohn's disease. *Gut* 47, 397-403.

Senerovic L, Tsunoda SP, Goosmann C, Brinkmann V, Zychlinsky A, Meissner F & Kolbe M (2012). Spontaneous formation of IpaB ion channels in host cell membranes reveals how *Shigella* induces pyroptosis in macrophages. *Cell Death Dis* 3, e384.

Sereny B (1957). Experimental keratoconjunctivitis shigellosa. *Acta Microbiol Acad Sci Hung* 4, 367-376.

Shere KD, Sallustio S, Manessis A, D'Aversa TG & Goldberg MB (1997). Disruption of IcsP, the major *Shigella* protease that cleaves IcsA, accelerates actin-based motility. *Mol Microbiol* 25, 451-462.

Shim DH, Suzuki T, Chang SY, Park SM, Sansonetti PJ, Sasakawa C & Kweon MN (2007). New animal model of shigellosis in the Guinea pig: its usefulness for protective efficacy studies. *J Immunol* 178, 2476-2482.

Shin N, Ahn N, Chang-Ileto B, Park J, Takei K, Ahn S-G, Kim S-A, Di Paolo G & Chang S (2008). SNX9 regulates tubular invagination of the plasma membrane through interaction with actin cytoskeleton and dynamin 2. *J Cell Sci* 121, 1252-1263.

Simmons DA (1993). Genetic and biosynthetic aspects of *Shigella flexneri* O-specific lipopolysaccharides. *Biochem Soc Trans* 21, 58S.

Singer M & Sansonetti PJ (2004). IL-8 is a key chemokine regulating neutrophil recruitment in a new mouse model of *Shigella*-induced colitis. *J Immunol* 173, 4197-4206.

Skoble J, Portnoy DA & Welch MD (2000). Three regions within ActA promote Arp2/3 complex-mediated actin nucleation and *Listeria monocytogenes* motility. *J Cell Biol* 150, 527-538.

Smirnova E, Shurland D-L, Ryazantsev SN & van der Bliek AM (1998). A human dynamin-related protein controls the distribution of mitochondria. *J Cell Biol* 143, 351-358.

Smirnova E, Griparic L, Shurland D-L & van der Bliek AM (2001). Dynamin-related protein Drp1 is required for mitochondrial division in mammalian cells. *Mol Biol Cell* 12, 2245-2256.

Smith GA, Portnoy DA & Theriot JA (1995). Asymmetric distribution of the *Listeria monocytogenes* ActA protein is required and sufficient to direct actin-based motility. *Mol Microbiol* 17, 945-951.

Smith SG, Mahon V, Lambert MA & Fagan RP (2007). A molecular Swiss army knife: OmpA structure, function and expression. *FEMS Microbiol Lett* 273, 1-11.

Snapper SB, Takeshima F, Anton I & other authors (2001). N-WASP deficiency reveals distinct pathways for cell surface projections and microbial actin-based motility. *Nat Cell Biol* 3, 897-904.

Stavru F, Bouillaud F, Sartori A, Ricquier D & Cossart P (2011). *Listeria monocytogenes* transiently alters mitochondrial dynamics during infection. *Proc Natl Acad Sci U S A* 108, 3612-3617.

Stavru F, Palmer AE, Wang C, Youle RJ & Cossart P (2013). Atypical mitochondrial fission upon bacterial infection. *Proc Natl Acad Sci U S A* 110, 16003-16008.

Steinhauer J, Agha R, Pham T, Varga AW & Goldberg MB (1999). The unipolar *Shigella* surface protein IcsA is targeted directly to the bacterial old pole: IcsP cleavage of IcsA occurs over the entire bacterial surface. *Mol Microbiol* 32, 367-377.

Stevens JM, Galyov EE & Stevens MP (2006). Actin-dependent movement of bacterial pathogens. *Nat Rev Micro* 4, 91-101.

Straight AF, Cheung A, Limouze J, Chen I, Westwood NJ, Sellers JR & Mitchison TJ (2003). Dissecting temporal and spatial control of cytokinesis with a myosin II Inhibitor. *Science* 299, 1743-1747.

Sun L, Wang H, Wang Z & other authors (2012). Mixed lineage kinase domain-like protein mediates necrosis signaling downstream of RIP3 kinase. *Cell* 148, 213-227.

Sun Q, Lan R, Wang J & other authors (2013). Identification and characterization of a novel *Shigella flexneri* serotype Yv in China. *PLoS One* 8, e70238.

Suzuki T, Murai T, Fukuda I, Tobe T, Yoshikawa M & Sasakawa C (1994). Identification and characterization of a chromosomal virulence gene, *vacJ*, required for intercellular spreading of *Shigella flexneri*. *Mol Microbiol* 11, 31-41.

Suzuki T, Lett M-C & Sasakawa C (1995). Extracellular transport of VirG protein in *Shigella*. *J Biol Chem* 270, 30874-30880.

Suzuki T, Saga S & Sasakawa C (1996). Functional analysis of *Shigella* VirG domains essential for interaction with vinculin and actin-based motility. *J Biol Chem* 271, 21878-21885.

Suzuki T, Miki H, Takenawa T & Sasakawa C (1998). Neural Wiskott-Aldrich syndrome protein is implicated in the actin-based motility of *Shigella flexneri*. *EMBO J* 17, 2767-2776.

Suzuki T, Mimuro H, Suetsugu S, Miki H, Takenawa T & Sasakawa C (2002). Neural Wiskott-Aldrich syndrome protein (N-WASP) is the specific ligand for *Shigella* VirG among the WASP family and determines the host cell type allowing actin-based spreading. *Cell Microbiol* 4, 223-233.

Suzuki T, Nakanishi K, Tsutsui H, Iwai H, Akira S, Inohara N, Chamaillard M, Nuñez G & Sasakawa C (2005). A novel Caspase-1/Toll-like Receptor 4-independent pathway of cell death induced by cytosolic *Shigella* in infected macrophages. *J Biol Chem* 280, 14042-14050.

Suzuki T, Yoshikawa Y, Ashida H, Iwai H, Toyotome T, Matsui H & Sasakawa C (2006). High vaccine efficacy against shigellosis of recombinant noninvasive *Shigella* mutant that expresses *Yersinia* invasin. *J Immunol* 177, 4709-4717.

Suzuki T, Franchi L, Toma C & other authors (2007). Differential regulation of caspase-1 activation, pyroptosis, and autophagy via Ipaf and ASC in *Shigella*-infected macrophages. *PLoS Pathog* 3, e111.

Tang WX, Wu WH, Qiu HY, Bo H & Huang SM (2013). Amelioration of rhabdomyolysis-induced renal mitochondrial injury and apoptosis through suppression of Drp-1 translocation. *J Nephrol* 26, 1073-1082.

Teh MY & Morona R (2013). Identification of *Shigella flexneri* IcsA residues affecting interaction with N-WASP, and evidence for IcsA-IcsA co-operative interaction. *PLoS One* 8, e55152.

Terada N, Ohno N, Saitoh S & other authors (2009). Involvement of dynamin-2 in formation of discoid vesicles in urinary bladder umbrella cells. *Cell Tissue Res* 337, 91-102.

Theriot JA (2000). The polymerization motor. *Traffic* 1, 19-28.

Tilney L & Portnoy D (1989). Actin filaments and the growth, movement, and spread of the intracellular bacterial parasite, *Listeria monocytogenes*. *J Cell Biol* 109, 1597-1608.

Tilney L, DeRosier D & Tilney M (1992). How *Listeria* exploits host cell actin to form its own cytoskeleton. I. Formation of a tail and how that tail might be involved in movement. *J Cell Biol* 118, 71-81.

Tominaga A, Lan R & Reeves PR (2005). Evolutionary changes of the *flhDC* flagellar master operon in *Shigella* strains. *J Bacteriol* 187, 4295-4302.

Topping DL & Clifton PM (2001). Short-chain fatty acids and human colonic function: roles of resistant starch and nonstarch polysaccharides. *Physiol Rev* 81, 1031-1064.

Tran ENH, Doyle MT & Morona R (2013). LPS unmasking of *Shigella flexneri* reveals preferential localisation of tagged outer membrane protease IcsP to septa and new poles. *PLoS One* 8, e70508.

Tran ENH (2007). Molecular characterisation of *Shigella flexneri* outer membrane protease IcsP: *PhD dissertation, University of Adelaide, Australia*.

Tran Van Nhieu G, Clair C, Bruzzone R, Mesnil M, Sansonetti P & Combettes L (2003). Connexin-dependent inter-cellular communication increases invasion and dissemination of *Shigella* in epithelial cells. *Nat Cell Biol* 5, 720-726.

Van Den Bosch L, Manning PA & Morona R (1997). Regulation of O-antigen chain length is required for *Shigella flexneri* virulence. *Mol Microbiol* 23, 765-775.

Van Den Bosch L & Morona R (2003). The actin-based motility defect of a *Shigella flexneri rmlD* rough LPS mutant is not due to loss of IcsA polarity. *Microb Pathog* 35, 11-18.

Vandenabeele P, Galluzzi L, Vanden Berghe T & Kroemer G (2010). Molecular mechanisms of necroptosis: an ordered cellular explosion. *Nat Rev Mol Cell Biol* 11, 700-714.

Wang A, Ma X, Conti MA & Adelstein RS (2011). Distinct and redundant roles of the non-muscle myosin II isoforms and functional domains. *Biochem Soc Trans* 39, 1131-1135.

Wang Y (1985). Exchange of actin subunits at the leading edge of living fibroblasts: possible role of treadmilling. *J Cell Biol* 101, 597-602.

Wang Z, Jiang H, Chen S, Du F & Wang X (2012). The mitochondrial phosphatase PGAM5 functions at the convergence point of multiple necrotic death pathways. *Cell* 148, 228-243.

Wasiak S, Zunino R & McBride HM (2007). Bax/Bak promote sumoylation of DRP1 and its stable association with mitochondria during apoptotic cell death. *J Cell Biol* 177, 439-450.

Wassef JS, Keren DF & Mailloux JL (1989). Role of M cells in initial antigen uptake and in ulcer formation in the rabbit intestinal loop model of shigellosis. *Infect Immun* 57, 858-863.

Wasylnka JA, Bakowski MA, Szeto J, Ohlson MB, Trimble WS, Miller SI & Brumell JH (2008). Role for Myosin II in regulating positioning of *Salmonella*-containing vacuoles and intracellular replication. *Infect Immun* 76, 2722-2735.

Waterman SR & Small PL (1996). Identification of σ^S-dependent genes associated with the stationary-phase acid-resistance phenotype of *Shigella flexneri*. *Mol Microbiol* 21, 925-940.

Wei J, Goldberg MB, Burland V & other authors (2003). Complete genome sequence and comparative genomics of *Shigella flexneri* serotype 2a strain 2457T. *Infect Immun* 71, 2775-2786.

Wei Q & Adelstein RS (2000). Conditional expression of a truncated fragment of nonmuscle myosin II-A alters cell shape but not cytokinesis in HeLa cells. *Mol Biol Cell* 11, 3617-3627.

Welch MD, DePace AH, Verma S, Iwamatsu A & Mitchison TJ (1997a). The human Arp2/3 complex is composed of evolutionarily conserved subunits and is localized to cellular regions of dynamic actin filament assembly. *J Cell Biol* 138, 375-384.

Welch MD, Iwamatsu A & Mitchison TJ (1997b). Actin polymerization is induced by Arp2/3 protein complex at the surface of *Listeria monocytogenes*. *Nature* 385, 265-269.

Welch MD & Way M (2013). Arp2/3-mediated actin-based motility: A tail of pathogen abuse. *Cell Host & Microbe* 14, 242-255.

Willingham SB, Bergstralh DT, O'Connor W & other authors (2007). Microbial pathogen-induced necrotic cell death mediated by the inflammasome components CIAS1/cryopyrin/NLRP3 and ASC. *Cell Host Microbe* 2, 147-159.

Xie N, Wang C, Lian Y, Zhang H, Wu C & Zhang Q (2013). A selective inhibitor of Drp1, mdivi-1, protects against cell death of hippocampal neurons in pilocarpine-induced seizures in rats. *Neurosci Lett* 545, 64-68.

Yang F, Yang J, Zhang X & other authors (2005). Genome dynamics and diversity of *Shigella* species, the etiologic agents of bacillary dysentery. *Nucl Acids Res* 33, 6445-6458.

Yang J-Y, Lee S-N, Chang S-Y, Ko H-J, Ryu S & Kweon M-N (2014). A mouse model of shigellosis by intraperitoneal infection. *J Infect Dis* 209, 203-215.

Yoshida S, Katayama E, Kuwae A, Mimuro H, Suzuki T & Sasakawa C (2002). *Shigella* deliver an effector protein to trigger host microtubule destabilization, which promotes Rac1 activity and efficient bacterial internalization. *EMBO J* 21, 2923-2935.

Yoshida S, Handa Y, Suzuki T, Ogawa M, Suzuki M, Tamai A, Abe A, Katayama E & Sasakawa C (2006). Microtubule-severing activity of *Shigella* is pivotal for intercellular spreading. *Science* 314, 985-989.

Zakharian E & Reusch RN (2005). Kinetics of folding of *Escherichia coli* OmpA from narrow to large pore conformation in a planar bilayer. *Biochemistry* 44, 6701-6707.

Zalevsky J, Grigorova I & Mullins RD (2001). Activation of the Arp2/3 complex by the *Listeria* ActA protein. *J Biol Chem* 276, 3468-3475.

Zeile WL, Purich DL & Southwick FS (1996). Recognition of two classes of oligoproline sequences in profilin-mediated acceleration of actin-based *Shigella* motility. *J Cell Biol* 133, 49-59.

Zettl M & Way M (2002). The WH1 and EVH1 domains of WASP and Ena/VASP family members bind distinct sequence motifs. *Curr Biol* 12, 1617-1622.

Zhang L, Ding X, Cui J & other authors (2012). Cysteine methylation disrupts ubiquitin-chain sensing in NF-κB activation. *Nature* 481, 204-208.

Zhang X, Yan H, Yuan Y & other authors (2013). Cerebral ischemia-reperfusion-induced autophagy protects against neuronal injury by mitochondrial clearance. *Autophagy* 9, 1321-1333.

Zheng W, Degterev A, Hsu E, Yuan J & Yuan C (2008). Structure-activity relationship study of a novel necroptosis inhibitor, necrostatin-7. *Bioorg Med Chem Lett* 18, 4932-4935.

Zychlinsky A, Prévost MC & Sansonetti PJ (1992). *Shigella flexneri* induces apoptosis in infected macrophages. *Nature* 358, 167-169.

Zychlinsky A, Kenny B, Menard R, Prévost MC, Holland IB & Sansonetti PJ (1994). IpaB mediates macrophage apoptosis induced by *Shigella flexneri*. *Mol Microbiol* 11, 619-627.

Zychlinsky A, Thirumalai K, Arondel J, Cantey JR, Aliprantis AO & Sansonetti PJ (1996). In vivo apoptosis in *Shigella flexneri* infections. *Infect Immun* 64, 5357-5365.